Fundamental studies of poly(ethylene glycol-*b*-caprolactone) block copolymer self-assembly in water

by

Khandokar Sadique Faisal

Bachelor of Pharmacy, Master of Pharmacy (Pharmaceutical Technology)

Submitted in total fulfilment of the requirements of the degree of

Doctor of Philosophy

May 2019

School of Pharmacy and Medical Sciences

Division of Health Sciences

University of South Australia

Imagination is more important than knowledge. - Albert Einstein

Preface

This thesis consists of six chapters that cover the background of the research, all experimental procedures, data analysis and discussion.

Chapter 1 provides a brief overview of the background related to this work, which includes the origin of self-assembly and drug delivery systems. It also covers the fundamentals of polymeric aggregate drug delivery systems and their application. A brief discussion about polymer synthesis and characterisation is also included, which provides a basis to develop more effective synthetic procedures in this study. In addition, this chapter also provides a description of the different characterisation techniques used in this study, which is aimed at helping the reader to understand the application of those techniques in later chapters.

In chapter 2, the synthesis of poly(ethylene glycol-*b*-caprolactone) (PEG-*b*-PCL) block copolymers is reported and discussed in detail. Building on previously reported procedures, extensive optimisation was conducted to ensure the preparation of well-defined polymers with precise structures. This chapter also includes extensive characterisation of the synthesised copolymers, and evidence for their purity.

Chapter 3 covers the synthesis and characterisation of aggregates prepared from different PEG-*b*-PCL block copolymers, and provides a detailed discussion and interpretation of the parameters that regulate self-assembly of PEG-*b*-PCL copolymers. In this chapter, self-assembly of PEG-*b*-PCL was characterised using nuclear magnetic resonance (NMR) spectroscopy, dynamic light scattering (DLS) and small-angle X-ray scattering (SAXS). The results indicate that despite the fundamental differences between these techniques, they provide complementary information in most cases.

In Chapter 4, the thermal characteristics of PEG-*b*-PCL block copolymers and their aggregates are discussed. The results demonstrate that the polymer microstructure plays a critical role in controlling the melting and crystallisation behaviour of the polymers. In addition, self-assembly of the polymers was found to significantly effect the thermal behaviour of polymers when compared to their non-aggregated form.

In Chapter 5, the self-assembly of block copolymers in the presence of drugs is reported and discussed. The drug-loaded aggregates were characterised using the same approach applied in Chapter 3. The results indicate that polymer self-assembly in the presence of the drugs is a complex process, and depends on the nature of the drug and the polymer microstructure to control the mechanism of aggregation. In addition, the level of drug loading also plays an important role.

In chapter 6, general conclusions have been drawn based on the experiments, data analysis and discussion from the previous chapters. The overall results show that the characteristics of the self-assembly system are significantly effected by the polymer microstructure and the presence of drugs. However, it cannot be concluded that this study will define other polymer systems, and further theoretical and experimental work needs to be conducted to establish a generalisable model for micelle drug delivery systems.

Abstract

Amphiphilic polymers are being considered as next-generation tools in drug delivery due to their unique ability to form different types of nanoscale drug delivery devices. In particular, poly(ethylene glycol-*b*-caprolactone) (PEG-*b*-PCL) copolymers have been extensively studied in drug delivery due to their biodegradability and biocompatibility, and their propensity to form micelles in aqueous media due to their amphiphilic nature, which enables the encapsulation of hydrophobic drugs in the core. Whilst many studies have been focused on investigating the *ex vivo* or *in vivo* effects of polymeric drug delivery systems, there is limited understanding of the polymeric self-assembly process and how variation in the polymer microstructure influences their aggregation. A complete understanding of the parameters that influence self-assembly will allow the logical design of drug delivery systems with optimal characteristics (e.g., size, shape, stability, encapsulation capacity).

Therefore, in this work, a large family of well-defined PEG-*b*-PCL copolymers was prepared to allow a systematic study of the effect of polymer microstructure on self-assembly in aqueous media; in particular, the molecular weight and ratio (PCL:PEG) between the hydrophilic and hydrophobic blocks. A unique feature of this study was the application of pulsed-gradient stimulated-echo (PGSTE) NMR spectroscopy to characterise the self-assembly systems, which provides unique insights into the aggregate structure, which complements conventional dynamic light scattering (DLS) analysis.

The aggregate structure and stability were found to be controlled by the molecular weight ratio between the PCL and PEG blocks. At lower PCL:PEG molecular weight ratios, the self-assembled aggregates were unstable, showing a broad polydisperse nature in both NMR spectroscopy and DLS analysis. As the ratio was increased, stable and well-defined micelles were formed. Diffusion NMR spectroscopy proved to be a valuable tool to study the polymeric aggregate system. SAXS analysis of the aggregates revealed a transition of the aggregate shape from cylinder to ellipsoid as the PCL:PEG ratio increases or PEG molecular weight increases.

In addition, self-assembly of the PEG-*b*-PCL copolymers was investigated in the presence of drug molecules, with the aim of understanding how the drug characteristics and loading influence the self-assembly process for polymers with different microstructures. In this study, two model drugs were used – gossypol (very hydrophobic) and phloretin (slightly hydrophobic) – to investigate the effect of the drugs on the polymeric self-assembly.

Interestingly, several mechanisms of self-assembly were evident depending on the polymer microstructure, supporting simulations conducted by others. At lower PCL:PEG molecular weight ratios aggregation was governed by the nature of the drug, and it was hypothesised that poor interactions between the PCL block and drug due to the short length of PCL led to the formation of drug clusters that act as a nucleus for self-assembly. However, as the PCL:PEG molecular weight ratio is increased, and the PCL block favours interaction between PCL and the drug, aggregation occurs via a co-aggregation mechanism of the drug and polymer. Further, the drug loading also influences the self-assembly mechanism, as at higher drug loadings aggregation occurs via a combination of nucleation and co-aggregation. However, it is evident that more studies are needed to understand the self-assembly process fully.

Another important consideration for the development of drug delivery system systems is the morphology (e.g., crystallinity) of the polymer chains in the aggregate state, as this can affect the stability, dissolution, degradation and drug-release kinetics. Therefore, the morphology of the PEG-*b*-PCL copolymer aggregate was investigated using thermal and X-ray diffraction techniques and compared to the bulk polymer and polymer blends, that showed that the copolymers in the aggregates possessed a distinctly different morphology.

Table of Contents

Abstract…….. i

Table of contents…… iii

List of Tables…… ix

List of Figures…….. xi

List of Schemes……. xxi

List of Abbreviations…… xxii

Declaration…….. xxvi

Acknowledgement…….. xxvii

Chapter 1: Introduction and Theory

Introduction

1.1 Self-assembly drug delivery systems 1

1.1.1 Origins of self-assemblies 1

1.1.2 Classification of the self-assemblies 2

1.1.3 Fabrication of drug delivery systems 4

1.1.3.1 Liposomes

1.1.3.2 Polymeric micelles

1.1.3.3 Other self-assembly based drug delivery systems

1.1.4 Overview of amphiphilic polymer self-assembly 10

1.1.2.1 Amphiphilic polymers and their self-assembly in the aqueous systems

1.1.2.2 Factors affecting micelle formation from block copolymers

Theory

1.2 Thermodynamics of micelle formation 14

1.3 Characterisation of the micellar systems 18

1.3.1 Analysis of micelles by light scattering techniques 18

1.3.1.1 Fundamental aspects of light scattering techniques

1.3.1.2 Static light scattering (SLS)

1.3.1.3 Dynamic light Scattering (DLS)

1.3.1.4 Application of light scattering techniques

1.3.2 Analysis of micelles by nuclear magnetic resonance (NMR) spectroscopy 25

1.3.2.1 Fundamental aspects of diffusion NMR spectroscopy

1.3.2.2 Application of diffusion NMR studies

1.4 Synthesis and Characterisation of amphiphilic polymers 31

1.4.1 Controlled polymer synthesis 31

1.4.2 Ring-opening polymerisation (ROP) 32

1.4.2.1 Radical ROP

1.4.2.2 Cationic ROP

1.4.2.3 Anionic ROP

1.4.2.4 Kinetics of ROP

1.4.3 Synthesis of PEG-*b*-PCL copolymers 36
1.4.3.1 Synthesis of PEG
1.4.3.2 Synthesis of PCL
1.4.4 PEG-*b*-PCL copolymer characterisations 42
1.4.4.1 Thermal analysis of polymers
1.4.4.2 Structural analysis of polymers
1.4.5 Applications of PEG-*b*-PCL copolymers 45
1.5 Aims and objective of the thesis 47
1.5.1 Aims of the study 47
1.5.2 Research objectives 47
1.6 References 49

Chapter 2: Synthesis and characterisation of poly(ethylene glycol-*b*-caprolactone) block copolymers
2.1 Results and Discussion 77
2.1.1 Synthesis of PEG-*b*-PCL copolymers 77
2.1.1.1 Synthesis of PEG-b-PCL copolymers using solvents
2.1.1.2 Synthesis of PEG_2PCL_y copolymers series
2.1.1.3 Synthesis of PEG_5PCL_y copolymers series
2.1.1.4 Synthesis of $PEG_{10}PCL_y$ copolymers series
2.2 Conclusion 100
2.3 Experimental 101
2.3.1 Materials 101
2.3.2 Characterisation of PEG-*b*-PCL copolymers 101
2.3.3 Synthesis of PEG-*b*-PCL copolymers 102
2.4 References 104

Chapter 3: Relationship between molecular structure and self-assembly of poly(ethylene glycol-*b*-caprolactone) copolymers in aqueous solution

3.1 Results and Discussion 107

3.1.1 Synthesis and characterisation of PEG-*b*-PCL copolymers 107

3.1.2 Correlating PEG-*b*-PCL microstructure to self-assembly behaviours 107

3.1.2.1 PGSTE NMR spectroscopy of self-assembled PEG-b-PCL copolymer aggregates

3.1.2.2 DLS analysis of self-assembled PEG-b-PCL copolymer aggregates

3.1.2.3 SAXS analysis of self-assembled PEG-b-PCL copolymer aggregates

3.1.2.4 Correlation of NMR spectroscopy, DLS and SAXS data, and interpretation of trends in copolymer self-assembly

3.2 Conclusion 128

3.3 Experimental 129

3.3.1 Materials 129

3.3.2 Methods 129

3.3.2.1 Synthesis of PEG-b-PCL copolymers

3.3.2.2 Self-assembly of PEG-b-PCL copolymers in water

3.3.3 Characterisation of PEG-*b*-PCL copolymer aggregate solutions 130

3.3.2.1 PGSTE NMR measurements of PEG-b-PCL copolymer aggregate solutions

3.3.2.2 DLS analysis of PEG-b-PCL copolymer aggregate solutions

3.3.2.3 SAXS analysis of PEG-b-PCL copolymer aggregate solutions

3.4 References 133

Chapter 4: Effect of poly(ethylene glycol-*b*-caprolactone) microstructure and self-assembly on the morphology and thermal characteristics

4.1 Results and Discussion 138

4.1.1 Synthesis and characterisation of PEG-*b*-PCL copolymers 138

4.1.2 Thermal characterisation of PEG-*b*-PCL copolymers 138

4.1.2.1 Thermal characterisation of PEG and PCL homopolymers

4.1.2.2 Thermal characterisation of PEG and PCL homopolymer blends

4.1.2.3 Thermal characterisation of PEG-b-PCL copolymers

4.1.2.4 Thermal characterisation of lyophilised PEG-b-PCL copolymer aggregates

4.2 Conclusion 167

4.3 Experimental 168

4.3.1 Synthesis and characterisation of PEG-*b*-PCL copolymers 168

4.3.2 Preparation of PEG-*b*-PCL copolymer aggregates and their lyophilisation 168

4.3.3 DSC analysis of PEG-*b*-PCL copolymers and aggregate powders 168

4.3.4 WXRD analysis of PEG-*b*-PCL copolymers and aggregate powders

4.4 References 170

Chapter 5: Application of NMR spectroscopy for studying the formation of drug-loaded micelles from poly(ethylene glycol-*b*-caprolactone) copolymers

5.1 Results and Discussion 174

5.1.1 Synthesis and characterisation of PEG-*b*-PCL copolymers 174

5.1.2 Synthesis of drug-loaded polymeric aggregates from PEG-*b*-PCL copolymers 174

5.1.3 Factors effecting the self-assembly PEG-*b*-PCL copolymers in the presence of drugs 175

5.2 Conclusion 200

5.3 Experimental 201

5.3.1 Materials 201

5.3.2 Synthesis and characterisation of PEG-*b*-PCL copolymers 201

5.3.3 Formulation of drug-loaded aggregates from PEG-*b*-PCL copolymers 201

5.3.4 Determination of drug loading efficiency in polymeric aggregates 202
5.3.5 Analysis of drug-loaded aggregate using PGSTE NMR spectroscopy 202
5.3.6 DLS analysis of the polymer aggregate solutions 203
5.4 References 204
Chapter 6: Conclusions and future work 206
Appendices

List of Tables

Chapter 1

Table 1.1: Different static and dynamic self-assembly systems and their applications.

Table 1.2: Different self-assembly systems classified according to the self-assembled structure**.**

Table 1.3: Examples of some nanoscale DDS formed through the self-assembly of amphiphilic polymers.

Table 1.4: Liposomal DDSs products in different stages of clinical development.

Table 1.5: Different techniques used to prepare micelles, including applications as DDSs.

Table 1.6: Recent examples of polymeric micellar-based DDSs for the treatment of cancers.

Table 1.7: Polymeric micelle DDSs in different stages of clinical development.

Table 1.8: Drug-polymer conjugates at different stages of clinical development.

Table 1.9: Examples of dendrimers used as DDSs.

Table 1.10: Application of light scattering techniques for the characterisation of polymer systems.

Table 1.11: Catalysts used in ROP of caprolactone.

Table 1.12: Conditions used for the synthesis of PEG-b-PCL block copolymers and their molecular weight characteristics

Table 1.13: Examples of PEG-*b*-PCL block copolymers as drug delivery systems.

Chapter 2

Table 2.1: Composition and molecular weight characteristics of PEG macroinitiators and PEG-*b*-PCL block copolymers.

Table 2.2: PCL homopolymer in copolymer after precipitation in different binary mixtures of EtOAc and DEE, as determined from GPC.

Chapter 4

Table 4.1: Thermal properties of PEG and PCL homopolymers determined via DSC (n = 3) from the first and second heating/cooling cycles. Thermal properties include T_m and T_c, and the associated enthalpy changes (ΔH_m and ΔH_c respectively).

Table 4.2: Thermal properties of PEG and PCL homopolymers, and PEG/PCL physical blend 1:1 (%w/w) determined via DSC (n = 3) from the first and second heating/cooling cycles. Thermal properties include the T_m and T_c and the associated enthalpy changes (ΔH_m and ΔH_c, respectively).

Chapter 5

Table 5:1: Drug loading efficiency of aggregates prepared using from the PEG_5PCL_y copolymers series.

Table 5.2: Description of aggregate formulation used in the study.

List of Figures

Chapter 1

Figure 1.1: Illustration of light scattering by a particle, showing how the incidence light is scattered from a particle at a scattering angle that depends on the dimension of the particle.

Figure 1.2: Illustration of particle size dependency on light scattering, showing that small particles are responsible for '*non-isotropic emissions*' and large particle demonstrate '*isotropic scattering*.'

Figure 1.3: Illustration showing the basic components required for a static light scattering experiment; the detector can be moved to different angles to detect scattering intensity at different angles.

Figure 1.4: Illustration of a Zimm plot for the molecular weight determination of a particle showing the Rayleigh ratio ($\frac{Kc}{R}$) value for solutions with different particle concentrations as determined by multi-angle static light scattering.

Figure 1.5: Illustrative correlation function measured by DLS for a polystyrene particle dispersion in water, determined to have a R_h of 20 nm. The plot was an output from the Zetasizer (Malvern) software.

Figure 1.6: A schematic representation of a PGSE pulse sequence measuring diffusion in solution. Two gradient pulse of the same magnitude (g) are applied at Δ time interval to determine the signal attenuation due to translational motion of the particle.

Figure 1.7: A schematic representation of the PGSTE sequence. The PGSTE sequence consists of a second $\pi/2$ RF pulse which prevents the loss of NMR signal due to transverse relaxation.

Chapter 2

Figure 2.1: GPC DRI chromatograms following the a) formation of PEG-*b*-PCL copolymers over time from the polymerisation of caprolactone from a PEG_2 macroinitiator, and b) the relative decrease in the caprolactone monomer peak at 24, 48 and 72 h. The shift in the copolymer peak to lower retention volumes with increasing polymerisation time is an indication of an increase in the copolymer molecular weight, while the decrease in intensity of the caprolactone peak is consistent with a decrease in concentration as it is consumed in the polymerisation. Normalisation was conducted relative to the copolymer peak height for each sample.

Figure 2.2: Illustration showing the mechanistic detail of intermolecular chain-transfer and intramolecular back-biting and their influence on a typical GPC DRI chromatogram. Chain-transfer leads to the formation of lower and higher molecular weight copolymer chains and intramolecular back-biting forms a lower molecular weight copolymer chain and a cyclic homopolymer, resulting in an increase in dispersity, observed as a broadening of the polymer peak in the GPC chromatogram.

Figure 2.3: a) Normalised GPC DRI chromatograms following the ROP of caprolactone from the PEG_2 macroinitiator at different timepoints and; b) monomer conversion and pseudo-first-order kinetics plot for the polymerisation and the dotted line represents the first-order kinetics. Normalisation was conducted relative to the copolymer peak height for each sample.

Figure 2.4: a) Normalised GPC DRI chromatograms for ROP of caprolactone from the PEG_2 macroinitiator at various timepoints and b) M_n and $Đ$ of the copolymers over time for the polymerisation (M_n determined from ^{1}H NMR spectroscopy and $Đ$ from GPC analysis). Normalisation was conducted relative to the copolymer peak height for each sample.

Figure 2.5: ^{1}H NMR spectra ($CDCl_3$, 298 K) following the ROP of caprolactone from the PEG_2 macroinitiator at various timepoints. Labels a and a* indicate the methylene proton signals from the monomer and polymer, respectively. Integral values are shown under each signal and are relative to the PEG signal integral value.

Figure 2.6: Monomer conversion and pseudo first-order kinetic plot for the ROP of caprolactone from the PEG_2 macroinitiator. Monomer conversion was calculated from NMR spectroscopy by comparing the relative integration of signals corresponding to the monomer and polymer (**Figure 2.5**).

Figure 2.7: Normalised GPC DRI chromatograms of the isolated PEG_2PCL_y copolymer series. A clear shift towards lower retention volumes is observed, indicative of the formation of larger PCL blocks and higher molecular weight copolymers. Normalisation was conducted relative to the copolymer peak height for each sample.

Figure 2.8: ^1H NMR spectra ($CDCl_3$, 298 K) of the purified PEG_2PCL_y block copolymer series. The M_n values of PCL block was calculated from the ratio of the integral values of the methylene protons for PEG (δ_H = 3.64 ppm) and the methylene protons adjacent to the ester group in PCL (δ_H = 4.06 ppm).

Figure 2.9: ^1H NMR spectra ($CDCl_3$, 298 K) following the ROP of caprolactone from the PEG_5 macroinitiator at various timepoints. Labels a and a* indicate the methylene proton signals from the monomer and polymer, respectively.

Figure 2.10: Monomer conversion and pseudo-first-order kinetic plot for the ROP of caprolactone from the PEG_5 macroinitiator. Monomer conversion was calculated from ^1H NMR spectroscopy by comparing the relative integration of signals corresponding to the monomer and polymer (**Figure 2.9**).

Figure 2.11: a) Normalised GPC DRI chromatograms for ROP of caprolactone from the PEG_5 macroinitiator at various timepoints and b) M_n and $Đ$ values over time for the polymerisation (M_n was determined from ^1H NMR spectroscopy and $Đ$ from GPC analysis). Normalisation was conducted relative to the copolymer peak height for each sample.

Figure 2.12: Normalised GPC DRI chromatograms of the insoluble component obtained from precipitation of the crude PEG_5PCL_5 copolymer in different solvents. A slight reduction in the intensity of the peak at 28 mL corresponding to the PCL homopolymer was observed for hexane and DEE, indicating the partial fraction of the PCL homopolymer impurities. Normalisation was conducted relative to the copolymer peak height for each sample.

Figure 2.13: Normalised GPC DRI chromatograms of crude PEG_5PCL_5 polymer before and after precipitation in 30 % v/v EtOAc in DEE. A reduction in the peak at a retention volume of 28 mL indicates the removal of the PCL homopolymer. Normalisation was conducted relative to the copolymer peak height for each sample.

Figure 2.14: ^1H NMR spectra ($CDCl_3$, 298 K) of the purified PEG_5PCL_y block copolymer series. The M_n values of PCL block was calculated from the ratio of the integral values of the methylene protons for PEG (δ_H = 3.64 ppm) and the methylene protons adjacent to the ester group in PCL (δ_H = 4.06 ppm).

Figure 2.15: Normalised GPC DRI chromatograms of the purified PEG_5PCL_y copolymer series. A clear shift of the peaks with time to higher retention volumes confirmed the successful synthesis of the block copolymers. Normalisation was conducted relative to the copolymer peak height for each sample.

Figure 2.16: Monomer conversion and pseudo-first-order kinetics plot for the polymerisation of caprolactone from the PEG_{10} macroinitiator. Monomer conversion was calculated from NMR spectroscopy by comparing the relative integration of signals corresponding to the monomer and polymer.

Figure 2.17: a) Normalised GPC DRI chromatograms for ROP of caprolactone from the PEG_{10} macroinitiator at various timepoints and b) M_n and $Đ$ values over time for the polymerisation (M_n determined from ^{1}H NMR spectroscopy and $Đ$ from GPC analysis). Normalisation was conducted relative to the copolymer peak height for each sample.

Figure 2.18: ^{1}H NMR spectra ($CDCl_3$, 298 K) of the purified $PEG_{10}PCL_y$ block copolymer series. The M_n values of PCL block was calculated from the ratio of the integral values of the methylene protons for PEG (δ_H = 3.64 ppm) and the methylene protons adjacent to the ester group in PCL (δ_H = 4.06 ppm).

Figure 2.19: Normalised GPC DRI chromatograms of the purified $PEG_{10}PCL_y$ copolymer series. A clear shift of the peaks with time to higher retention volumes confirmed the successful synthesis of the block copolymers. Normalisation was conducted relative to the copolymer peak height for each sample.

Chapter 3

Figure 3.1: a) PGSTE NMR signal intensity decay profile and b) *D* distributions for the methylene protons of the PEG backbone (δ_H = 3.6 ppm) of the PEG_2 (blue), PEG_5 (green) and PEG_{10} (yellow) homopolymers in D_2O.

Figure 3.2: ^{1}H NMR of a) PEG_5 homopolymer in D_2O solution; b) $PEG_5PCL_{2.4}$ copolymer in chloroform ($CDCl_3$) solution; c) $PEG_5PCL_{2.4}$ copolymer in D_2O solution. PEG and PCL characteristic peaks from PEG-*b*-PCL copolymer in D_2O solution are broad comparing to $CDCl_3$ solution indicates polymer individual polymer units are experiencing slightly different environment from each other.

Figure 3.3: An illustration of the hypothetical layered aggregate structure. An aggregate structure was hypothesised that consisted of five distinct regions (i) the outer corona which is completely hydrated by the solvent; (ii) the inner corona which is well hydrated and adjacent to the boundary layer; (iii) the boundary layer, where the core and corona meet and is partially hydrated (the movement of polymer here is restricted); (iv) outer core which is adjacent to the boundary layer, and; (v) the deep core which is totally segregated from the solvent and the aqueous surroundings.

Figure 3.4: *D* distribution for the PEG (red) and PCL (blue) blocks of a) PEG_2 homopolymer and PEG_2PCL_y copolymers series; b) PEG_5 homopolymer and PEG_5PCL_y copolymers series; c) PEG_{10} homopolymer and $PEG_{10}PCL_y$ copolymers series in D_2O.

Figure 3.5: Mean (marker) and standard deviation (error bars) of $\langle D \rangle$ measured on three separate self-assembled samples for each PEG_xPCL_y copolymer, plotted against PCL:PEG ratio. The green and red symbols represent the $\langle D \rangle$ of PEG and PCL blocks, respectively, whereas the diamond, square and circle symbols correspond to the PEG_2PCL_y, PEG_5PCL_y and $PEG_{10}PCL_y$ copolymers series, respectively.

Figure 3.6: DLS analysis of particle size distribution of aggregates synthesised from PEG_xPCL_y polymers series. The bimodal characteristic at lower PCL:PEG ratio indicates a polydisperse system.

Figure 3.7: DLS analysis of the particle size distribution of $PEG_2PCL_{0.4}$ polymer solution in chloroform. The bimodal characteristic indicates DLS analysis of unimer is not providing the correct information about the system, as it should be monomodal.

Figure 3.8: Mean (marker) and standard deviation (error bars) of PDI measured on three separate samples made for each PEG_xPCL_y composition, plotted against PCL:PEG ratios.

Figure 3.9: SAXS scattering profile of aggregates synthesised from PEG_xPCL_y polymer series. Illustrations at the bottom left of each scattering profile show proposed morphology of each aggregate.

Figure 3.10: Aggregate structure determined for the PEG_xPCL_y block copolymer in water via SAXS analysis. A clear transition of a cylinder to ellipsoid shape is observed in PEG_5PCL_y and $PEG_{10}PCL_y$ copolymers series.

Figure 3.11: Radius of aggregates as determined by SAXS analysis versus the PCL:PEG ratios for the copolymers. For cylindrical and ellipsoidal aggregates the diameter and polar radii, respectively, are presented.

Figure 3.12: Phase diagram of the aggregate system for the PEG_xPCL_y block copolymer systems at different PCL:PEG ratios. A clear transition between unimer to stable aggregate system as PCL:PEG ratio increased.

Chapter 4

Figure 4.1: DSC thermograms of PEG (M_n = 2, 5 and 10 kDa) and PCL (M_n = 2 kDa) homopolymers showing the first heating, first cooling and second heating profiles (ramp rate 10 °C /min). The melting behaviour of the PCL homopolymer is different between the first and second heating cycles due to the erosion of the polymers thermal history.

Figure 4.2: DSC thermograms of the PEG_2 and PCL_2 homopolymers and PEG_2/PCL_2 physical blend 1:1 (%w/w) showing the first heating, first cooling and second heating profiles (ramp rate 10 ºC/min). The reduction of the PEG T_c in the first cooling cycle of the blend indicates that PCL influences the crystallisation of PEG, which is supported by the observed decrease in the PEG T_m in the second heating cycle.

Figure 4.3: DSC thermograms of the PEG_5 and PCL_2 homopolymers and PEG_5/PCL_2 physical blend 1:1 (%w/w) showing the first heating, first cooling and second heating profiles (ramp rate 10 ºC/min). The blend does not appear to have a significant impact on the melting or crystallisation of the PCL component; however, a slight decrease in the PEG melting and crystallisation temperatures is observed, indicating fractional crystallisation has occurred.

Figure 4.4: DSC thermograms of the PEG_{10} and PCL_2 homopolymers, and PEG_{10}/PCL_2 physical blend 1:1 (%w/w) showing the first heating, first cooling and second heating profiles (ramp rate 10 ºC/min). The blend does not appear to have a significant impact on the melting or crystallisation of the PCL component; however, a slight decrease in the PEG melting and crystallisation temperatures is observed, indicating fractional crystallisation has occurred.

Figure 4.5: DSC thermograms of PEG_2 and PCL_2 homopolymers, PEG_2PCL_2 physical blend 1:1 (%w/w), and $PEG_2PCL_{1.8}$ block copolymer showing the first heating, first cooling and second heating profiles (ramp rate 10 ºC /min). The $PEG_2PCL_{1.8}$ copolymer displays significantly different behaviour to the homopolymers and the blend, with only a sharp T_c on the first cooling cycle and a distinct T_m peak on the second heating.

Figure 4.6: T_m and ΔH_m of the PEG_2PCL_y copolymer series recorded during the first heating cycle, with increasing PCL:PEG ratios (n = 3). The T_m and ΔH_m of the copolymers were found to be less than that of the PEG homopolymer.

Figure 4.7: T_c and ΔH_c of the PEG_2PCL_y copolymer series obtained from the first cooling cycle, with increasing PCL:PEG ratio (n = 3). The T_c and ΔH_c of the copolymers were found to be less than that of the PEG homopolymer.

Figure 4.8: DSC thermograms of PEG, PEG_2 and PCL_2 homopolymers, and the PEG_2PCL_y copolymers series obtained during the first cooling cycle (ramp rate 10 ºC /min). Minimal variation in the T_c was observed with different PCL:PEG ratios.

Figure 4.9: Stacked WXRD patterns of the PEG_2 and PCL_2 homopolymers recorded at 25 °C, and the PEG_2PCL_y block copolymers recorded at room temperature (25 °C), in the molten state (80 °C) and near to the T_c upon cooling.

Figure 4.10: DSC thermograms of the PEG_2 and PCL_2 homopolymers, and the PEG_2PCL_y block copolymer series, showing the second heating profiles (ramp rate 10 ºC/min). The T_m was found to decrease with increasing PCL:PEG ratio.

Figure 4.11: DSC thermograms of the PEG_5 homopolymer and the PEG_5PCL_y polymer series, showing the first heating, first cooling and second heating profiles (ramp rate 10 ºC/min). The T_m was found to decrease with increasing PCL:PEG ratio. The DSC thermogram of the first cooling cycle shows a bimodal exothermic peak at the highest PCL:PEG ratio.

Figure 4.12: a) T_m and ΔH_m (first heating cycle) values of the PEG_5PCL_y copolymer series as a function of the PCL:PEG ratio (n = 3). b) T_c and ΔH_c (first cooling cycle) of the PEG_5PCL_y copolymer series as a function of the PCL:PEG ratio (n = 3).

Figure 4.13: Stacked WXRD patterns of the PEG_5 and PCL_2 homopolymers recorded at 25 °C, and the PEG_5PCL_y copolymer series at room temperature (25 °C), in the molten state (80 °C) and near the T_c peak or between separate T_c peaks.

Figure 4.14: DSC thermograms of the PEG_{10} homopolymer and the $PEG_{10}PCL_y$ copolymer series showing the first heating, first cooling and second heating profiles (ramp rate 10 °C/min). A gradual decrease in T_c across the series as the PCL:PEG ratio increases is observed, with bimodal crystallisation peaks.

Figure 4.15: a) T_m and ΔH_m of the first heating cycle as a function of the PCL:PEG ratio for the $PEG_{10}PCL_y$ copolymer series (n = 3). b) T_c and ΔH_c of the first cooling cycle as a function of the PCL:PEG ratio for the $PEG_{10}PCL_y$ copolymer series (n = 3).

Figure 4.16: Stacked WXRD patterns of the PEG_5 and PCL_2 homopolymers recorded at 25 °C, and the $PEG_{10}PCL_y$ copolymers series at room temperature (25 °C), in the molten state (80 °C) and near the T_c peak or between separate T_c peaks.

Figure 4.17: Illustration of the solid dispersion formed by lyophilisation of the micelle solution, showing the hypothesised amorphous PEG (blue) continuous phase with PCL(red) cores dispersed therein.

Figure 4.18: DSC thermograms of the PEG_5 and PCL_2 homopolymers, PEG_5/PCL_2 physical blend 1:1 (%w/w), $PEG_5PCL_{2.3}$ block copolymer, and $PEG_2PCL_{2.3}$ block copolymer aggregate (lyophilised powder), showing the first heating profiles (ramp rate 10 °C/min).

Figure 4.19: DSC thermograms of the PEG_2 and PCL_2 homopolymers, and PEG_5PCL_y and PEG_2PCL_y copolymer aggregate (lyophilised powder), showing the first heating profiles (ramp rate 10 °C/min).

Figure 4.20: Illustration showing the proposed structure of PCL in the aggregate core with different PCL lengths (PCL:PEG ratio).

Figure 4.21: DSC thermogram of the $PEG_{10}PCL_{2.5}$ copolymer micelle showing the first heating profile (ramp rate 10 °C/min).

Chapter 5

Figure 5.1: ^1H NMR spectra (D_2O, at 298 K) of blank and drug-loaded (10 wt%) aggregates prepared from the $PEG_5PCL_{9.4}$ copolymer at a concentration of 1 mg/mL. Characteristic peaks corresponding to the PCL block in the aggregates confirm NMR detection of a part of the aggregate core.

Figure 5.2: ^1H NMR spectrum (DMSO-d_6, at 298 K) of Ph.

Figure 5.3: ^1H NMR spectrum (DMSO-d_6, at 298 K) of Gp.

Figure 5.4: Illustration of possible drug distribution in the core of drug-loaded aggregates, showing two potential configurations whereby the drug is either molecularly dispersed within the polymer core, or forms a discretely packed mass within the core.

Figure 5.5: PGSTE NMR signal intensity decay profiles of the PEG methylene proton resonance of blank and drug-loaded aggregate synthesised from the PEG_5PCL_y copolymers series in D_2O (acquired at 25 ºC).

Figure 5.6: Illustration of different types of drug-aggregate systems adapted from Woodhead *et al.*[27] Hydrophobic and hydrophilic blocks are shown in red and blue, respectively, whereas drug molecules are yellow and blue dots represent water molecules.

Figure 5.7: Phase behaviour of solute (e.g. drug)-copolymer-solvent system adapted from Woodhead *et al.*[27] The packing fraction is the total amount of solvent, solute and polymer divided by the volume of the simulation block; in this study solute and polymer amount is constant. A constant polymer amount was used in the simulations, and therefore, the polymer concentration decreases as the packing fraction increases.

Figure 5.8: Mean (marker) and standard deviation (error bars) of $\langle D \rangle$ measured on three separate self-assembled samples for each PEG_5PCL_y copolymer, plotted against PCL:PEG molecular weight ratio. The black square, red circle and blue triangle symbols correspond to the blank, phloretin and gossypol loaded aggregate, respectively.

Figure 5.9: *D* distribution profile determined from PGSTE NMR diffusion of the blank and drug-loaded (10 wt%) self-assemblies, synthesised from $PEG_5PCL_{0.6}$ and $PEG_5PCL_{2.3}$ block copolymers.

Figure 5.10: DLS analysis of blank and drug-loaded (10 wt%) aggregates showing intensity and volume particle size distributions (PSD), prepared using the $PEG_5PCL_{0.6}$ (PCL:PEG 0.1:1) copolymer.

Figure 5.11: *D* distribution profile determined by PGSTE NMR diffusion spectroscopy of drug-loaded (10 wt%) aggregates synthesised from the $PEG_5PCL_{4.2}$ and $PEG_5PCL_{9.4}$ block copolymers.

Figure 5.12: DLS analysis of blank and drug-loaded (10 wt%) aggregates showing intensity and volume PSD, prepared using the $PEG_5PCL_{2.3,}$ $PEG_5PCL_{4.2}$, and $PEG_5PCL_{9.4}$ copolymers.

Figure 5.13: *D* distribution profile determined by PGSTE NMR diffusion studies of the PEG_2 homopolymer, and blank and drug-loaded aggregates prepared using the $PEG_2PCL_{0.4}$ copolymer.

Figure 5.14: *D* distribution profile determined by PGSTE NMR diffusion studies of drug-loaded aggregates (10 wt%) prepared using the $PEG_{10}PCL_{10.7}$ copolymer.

Figure 5.15: DLS analysis of blank and drug-loaded aggregates (10 wt%) showing intensity and volume PSD, prepared using the $PEG_{10}PCL_{10.7}$ (PCL:PEG 1:1) copolymer.

Figure 5.16: ^1H NMR spectra (D_2O, 298 K) of blank and Gp-loaded aggregates prepared from the $PEG_5PCL_{9.4}$ copolymer.

Figure 5.17: Effect of drug-loading on the aggregate structure. An absence of outer core region in aggregate with higher drug loading.

Figure 5.18: *D* distribution profiles determined by PGSTE NMR studies of the drug-loaded aggregates synthesised from $PEG_5CL_{9.4}$ with different drug loadings; a) GP-loaded aggregates, b) Ph-loaded aggregates.

Figure 5.19: DLS analysis of blank and drug-loaded aggregate showing intensity and volume PSD, prepared using the $PEG_5PCL_{9.4}$ copolymer and drug-loadings of 10 and 20 wt%.

Figure 5.20: Proposed nucleation-type mechanism of aggregate formation at different acetone to water ratios. Water has been omitted for clarity.

Figure 5.21: Proposed coaggregation-type mechanism of aggregation at different acetone to water ratios. Water has been omitted for clarity.

Figure 5.22: Mixed model of aggregate formation, at higher drug loading (20 wt%). Water molecules omitted for clarity.

List of Schemes

Chapter 1

Scheme 1.1: ROP of strained cyclic monomers from a propagating polymer chain or macroinitiator.

Scheme 1.2: ROP of a vinyl epoxide monomer via radical addition, ring-opening and the regeneration of a terminal propagating radical.

Scheme 1.3: Synthesis of poly(3-isochromanone) via cationic ROP using triflic acid (TfOH) act as a cationic initiator.

Scheme 1.4: Synthesis of poly(trimethylene carbonate) via anionic ROP. Alkali metal carboxylates, including sodium acetate, sodium benzoate, and sodium sorbate promote the ROP of trimethylene carbonate in the presence of an alcohol initiator.

Scheme 1.5: General scheme showing the synthesis of PEG-*b*-PCL copolymers via ROP of caprolactone, starting from a PEG macroinitiator.

Scheme 1.6: Synthesis of PCL via step-growth condensation polymerisation of the AB-type monomer, 6-hydroxycaproic acid.

Scheme 1.7: Synthesis of PCL via anionic ROP of caprolactone using an alkoxide initiator. Caprolactone ring opens when an anionic initiator (e.g. alkoxide) that attacks the electrophilic carbonyl carbon of the monomer.

Scheme 1.8: Synthesis of PCL via cationic ROP**.** Cationic ROP proceeds via the formation of an activated monomer which is attacked by another monomer through a bimolecular nucleophilic substitution (S_N2) reaction.

Scheme 1.9: Synthesis of PCL via monomer activated ROP. Monomer activated ROP involves the activation of the monomer by a lewis acid catalyst, followed by an attack on the activated monomer by the initiator or a propagating polymer chain.

List of Abbreviations

[I]:[M]:[Cat]	[initator]:[monomer]:[catalyst]
ATRP	Atom transfer radical polymerisation
AFM	Atomic force microscopy
CTAB	Cetyltrimethylammonium bromide
δ_H	Chemical shift in ^{1}H NMR spectrum
$CDCl_3$	Chloroform
Conc.	Concentration
CRP	Controlled radical polymerisation
CAC	Critical aggregation concentration
CMC	Critical micelle concentration
Da	Dalton
DNA	Deoxyribonucleic acid
DEE	Diethyl ether
DRI	Differential refractive index
DSC	Differential scanning calorimetry
DMSO	Dimethyl sulfoxide
DMF	Dimethylformamide
$Đ$	Dispersity
DDS	Drug delivery system
DPC	Drug-polymer conjugate
DP	Degree of polymerisation
DLS	Dynamic light scattering
EPR	Enhanced permeability and retention
EGFR	Epidermal growth factor receptor
EtOAc	Ethyl acetate
EO	Ethylene oxide
GPC	Gel permeation chromatography
T_g	Glass transition temperature
Gp	Gossypol
HMPA	Hexamethylphosphoramide
HDL	High-density lipids
h	Hour

EGF	Human epidermal growth factor
R_h	Hydrodynamic radius
ICM	Isochromanone
K	Kelvin (SI unit of temperature)
k_i	Rate of initiation
R_p	The overall rate of polymerisation
LS	Light scattering
LiCl	Lithium chloride
LDL	Low-density lipids
MAM	Mass action model
MS	Mass spectrometry
MALDI-TOF MS	Matrix-assisted laser desorption ionisation time of flight mass spectrometry
$\langle D \rangle$	Mean self- diffusivity
MSD	Mean square displacement
MeOH	Methanol
mPEG	Methoxy terminated poly(ethylene glycol)
min	Minute
MPS	Mononuclear phagocyte system
MPS	Mononuclear phagocyte system
GM1	Monosialotetrahexosylganglioside
MCR	Multivariate curve resolution
HPMA	*N*-(2-Hydroxypropyl)methacrylamide
NMR	Nuclear magnetic resonance
M_n	Number-average molecular weight
1D	One dimensional
Ph	Phloretin
POM	Polarised optical microscopy
PAA	Poly(acrylic acid)
PDLLA	Poly(D,L-lactide)
PAMAM	Poly(amidoamine)
PDI	Polydispersity index
PEG	Poly(ethylene glycol)

PGA	Poly(glycolic acid)
PLA	Poly(lactic acid)
PLGA	Poly(lactic-*co*-glycolic acid)
PNAM	Poly(*N*-acryloylmorpholine)
PPG	Poly(propylene glycol)
PVP	Poly(vinyl pyrrolidone)
PCL	poly(ε-caprolactone)
PM	Polymeric micelle
PTM	Pseudo-phase transition model
PGSTE	Pulsed field gradient echo
PMMA	Poly(methylmethacrylate)
PGSE	Pulsed field gradient spin-echo
RF	Radiofrequency
R_g	Radius of gyration
RID	refractive index detector
RAFT	Reversible addition fragmentation transfer
ROMP	Ring-opening metathesis polymerisation
ROP	Ring-opening polymerisation
SAMs	Self-assembled monolayers
D	Self-diffusion coefficient
SEC	Size exclusion chromatography
SAXS	Small-angle X-ray diffraction
SLS	Static light scattering
STE	Stimulated-echo sequence
T_c	Temperature of crystallisation
T_m	Temperature of melting
THF	Tetrahydrofuran
k_p	The absolute rate of polymer propagation
k_{app}	The apparent rate constant of polymer propagation
Log P	The log of the partition coefficient
TGA	Thermal gravimetric analysis
TEM	Transmission electron microscopy
M_w	Weight-average molecular weight

WXRD	Wide-angle X-ray diffraction
ε-CL	**ε**-Caprolactone

Declaration

I declare that:

this thesis presents work carried out by myself and does not incorporate without acknowledgement any material previously submitted for a degree or diploma in any university; to the best of my knowledge it does not contain any materials previously published or written by another person except where due reference is made in the text; and all substantive contributions by others to the work presented, including jointly authored publications, is clearly acknowledges.

Khandokar Sadique Faisal

Acknowledgement

I found it most challenging to write acknowledgement as there are so many people that I have to thank and recognise. Above all, I would like to thank my supervisor Dr Anton Blencowe. The thesis would not have been possible without the help, support and patience of him, not to mention his advice and unsurpassed knowledge of polymer chemistry. Similar gratitude goes to my wife Tamima Sumaiya, for her personal support and great patience at all time. My father and mother-in-law, my parents, my brother-in-law have given their unequivocal support throughout, as always, for which my mere expression of thanks likewise not suffice.

I would like to Dr Nathan Williamson for his never-ending assistance and friendship; your passion for science has been my source of insertion for me. Special thanks to kyle, Sarah, Kirsten and Cintya; the informal chat we had regarding science, culture, society, movie was enjoyable. I would also like to acknowledge Dr Paula Facal Marina and Dr Todd Gillam, for their support. I would also like to thank Dr John Denman and Andrew C Robinson for assisting with NMR experiment and XRD. Special thanks go to Paul Andrew, Dr Marta Krasowska, Dr Andrew Clulow, and Professor Gary Bryant for helping me with analysis of my polymer. I would also like to thank Rupal Pradhan, Karen Teague, and Andrew Beck for technical support.

I would like to acknowledge the financial, academic and technical support of the University of South Australia, particularly for my postgraduate scholarship. A special thanks to Associate Professor Craig Williams, Kate Doyle and Professor Susan Hillier for their support during a very crucial moment of my PhD.

Chapter 1
Introduction and Theory

Introduction

1.1 Self-assembly drug delivery systems

1.1.1 Origins of self-assemblies

Nature is one of the greatest scientists because it has two things in abundance, time and resources. Millions of years of natural evolution have provided complex and ingenious solutions, allowing life to thrive in many different forms to face the challenges of the ever-changing environment. Learning from nature, with millions of years' worth of knowledge, provides scientists with great inspiration and a unique starting point for the development of new technological advancements. Nature has taken the simplest building blocks and learnt to combine them, providing nanoscale materials that assemble and function, giving life at the micro and macro scales. In nature, we encounter numerous phenomena, where complex problems have been solved with evolutionary nanotechnology, and it is only relatively recently that scientists have started to venture into the nanoworld to develop nanotechnological solutions.[1] The examples of nanotechnology used in nature are never-ending, but some unique examples would be supplementary to this narrative.

Post-it-notes are used everywhere from the home to the office. When first marketed back in 1990, they were perceived as magical as they had enough adhesive to hold the paper onto a surface, but not so much that it could not be easily removed. However, evolution provided the concept of temporary adhesives millions of years ago. For example, geckos have adhesive pads on their feet which enable them to walk and climb on the smoothest of surfaces (e.g. glass). It has only recently been discovered that the nanostructure of the hairs on their feet provide this unique ability.[2] Understanding nature at the nanoscale makes it possible to translate the unique capabilities of natural systems to human-made technologies; a process termed as 'biomimetics'.

Biomimetic technologies have enormous potential for application from medicine to advanced manufacturing.[3-5] The scope of biomimetic nanotechnologies is so broad it is difficult to discuss them in a single narrative; nevertheless, self-assembly is the molecular level phenomenon common to all biological systems.[6] Self-assembly is the autonomous process of forming organised structures from multiple components in the absence of any external stimuli.[7] The investigation of self-assembly structures is significant for numerous reasons.[8-15] In particular, self-assembly is responsible for protein structure, the storage of genetic information in deoxyribonucleic acid (DNA), and understanding these systems can provide the development of cures to many diseases.[16] For example, Sina *et al.* published a method which enables early detection of cancer using a simple blood test.[17] The study emphasised that the alteration in DNA structure (methylation of the nucleotides) affected not only the biological activity but also the physicochemical properties of the DNA. This alteration affected the self-assembly and aggregation behaviour of DNA, which was translated into a simple diagnostic tool.

Self-assembly is also an important strategy for the formation of nanostructures and is, therefore, a key element in the development of nanotechnologies. A prominent example with direct relevance to the work presented within this thesis is the understanding of how lipids assemble to form cell membranes, which has provided inspiration for the development of amphiphilic molecules and polymers that assemble to form a wide range of different structures (e.g., vesicles, micelles, lamella).

1.1.2 Classification of the self-assemblies

Self-assembly processes can be classified as static or dynamic. In static self-assembly processes, the system forms an ordered state that approaches local or global equilibrium without dissipation of energy.[18] On the other hand, dynamic self-assembly processes will only form ordered states of equilibrium upon dissipation of energy.[7] Examples of static and dynamic self-assembled systems are summarised in **Table 1.1**. Self-assembly systems have also been classified based on components and final self-assembled structures (**Table 1.2**).

Table 1.1: Different static and dynamic self-assembly systems and their applications.

System	Type of self-assembly	Application	Reference
Atomic, ionic and molecular crystals	Static	Materials, optoelectronics	[14]
Phase-separated and ionic layered polymers	Static	Drug delivery	[19]
Self-assembled monolayers (SAMs)	Static	Nanoelectronics, microfabrication	[20]
Bacterial colonies	Dynamic	Study of bacteria and surface interaction	[21]

Table 1.2: Different self-assembly systems classified according to the self-assembled structure.

System	Type of self-assembly	Applications	Reference
Molecular machines	Small molecule	Molecular engine due to rotation caused by self-assembly	[22]
Nanostructures (capsule, cage, box)	Small molecule	Nanomorphology provides unique physicochemical properties, e.g., molecular colour sensing moieties	[23]
Metal-organic frameworks	Coordination self-assembly	Selective sorption and separation of gases, e.g., carbon dioxide, oxygen and acetylene	[24]
Liposomes, vesicles, fibres and tubes	Lipid assembly	Drug delivery, biological model, e.g., cell membranes, biomimicking systems (e.g. photosynthesis)	[25]
Gels and liquid crystals	Assembly of low molecular weight components	Drug delivery and display devices	[26]

1.1.3 Fabrication of drug delivery systems

Compartmentalisation is very common in biological systems, as many biotransformations require specific environmental conditions.[27] In living systems this compartmentalisation is achieved through the formation of phospholipid bilayer membranes. One of the first drug delivery systems (DDS) to be developed were liposomes. Liposomes build on these biological self-assembly processes to allow the compartmentalisation of therapeutics.[28] Using similar self-assembly principles, scientists have also developed polymersomes and micelles as successful DDS using amphiphilic polymers (**Table 1.3**).

Table 1.3: Examples of some nanoscale DDS formed through the self-assembly of amphiphilic polymers.

Polymer	Delivery system	Encapsulated drug	Reference
Poly(ethylene glycol-*b*-D,L-lactic acid) (PEG-*b*-PLGA)	Micelles, nanospheres, nanocapsules, polymersomes	Paclitaxel, antiestrogen, methotrexate	[29–32]
Poly(ethylene glycol-*b*-caprolactone) (PEG-*b*-PCL)	Micelles, nanospheres, polymersomes, nanocapsules	Indomethacin, doxorubicin, dihydrotestosterone	[33–35]
Poly(ethylene glycol-*b*-lactide-*co*-glycolide) (PEG-*b*-PLGA)	Nanospheres, nanocapsules, micelles	Paclitaxel, doxorubicin,	[36,37]
Poly(ethylene oxide-*b*-propylene oxide) (PEO-*b*-PPO)	Micelles	Doxorubicin	[38,39]

1.1.3.1 Liposomes

Liposomes are vesicles formed via the self-assembly of lipids such as phospholipids forming a lipid bilayer that separates an internal aqueous compartment from the bulk aqueous phase. Liposomes can be divided into subclasses based on their lamellarity (uni-, oligo-, and multi-lamellar vesicles), size (small, intermediate, or large) and synthesis technique.[40] Unilamellar liposomes contain a single lipid bilayer and generally have a size between 50 to 250 nm, multilamellar liposomes have several lipid bilayers one inside another and can be several microns in size.[41] For liposomal drug carriers, the hydrophilic aqueous interior or the hydrophobic lipid bilayers can act as the drug reservoirs. Liposomes have several advantages as drug carriers including enhanced solubility of hydrophobic drugs and increased cellular

transportation of therapeutics.[42] Liposome DDSs have been extensively investigated for the delivery of chemotherapeutics, with several products currently in clinical trials or available on the market (**Table 1.4**).[41]

Table 1.4: Liposomal DDSs products in different stages of clinical development.

Stage	Drug	Application	Reference
Marketed	Doxorubicin	Small cell lung cancer	[43]
Approved	Daunorubicin	Kaposi's sarcoma	[44]
Phase II/III	Cisplatin	Head and neck cancer, Lung cancer	[45,46]
	Vincristine	Hodgkin's lymphoma	[47]
	Nistatin	Fungal infections in immuno-suppressed patients	[48]
Phase II	Lurtotecan	Ovarian cancer Head and neck cancer	[48]
	Oxaliplatinanalog	Colorectal cancer	[49]
	Annamycin	Breast cancer	[50]
Phase I	Mitoxantrone	Stomach, liver, ovarian cancers	[49]

One major problem associated with liposome technology is poor blood circulation time due to phagocytosis by the mononuclear phagocyte system (MPS).[51] Interaction with plasma components including high-density lipids (HDL) and low-density lipids (LDL) can result in the rapid release of drugs from liposomes into blood plasma.[41] Several approaches have been investigated to overcome these problems, including modification of the liposome surface with gangliosides (e.g., monosialotetrahexosylganglioside (GM1)) and sialic acid derivatives to mimic properties of erythrocyte membranes.[41] Hydrophilic polymers such as PEG have been used to modify liposome surfaces to increase blood circulation time.[52]

1.1.3.2 Polymeric micelles

Polymeric micelles are composed of amphiphilic block copolymers which self-assemble into nano-sized spherical core-shell structures in aqueous media.[53] Polymeric micelles have a hydrophobic core which can be used as a reservoir for hydrophobic drugs, and a hydrated hydrophilic outer corona (also referred to as the shell) which stabilises the micelle structure and can be conjugated with targeting moieties.[54,55] Examples of polymers that have been used for the hydrophilic component of the block copolymers include PEG, poly(*N*-acryloylmorpholine) (PNAM) and poly(vinyl pyrrolidone) (PVP).[56] PLA, PCL, and PLGA have been used extensively

for the hydrophobic block.[57] The physicochemical characteristics of the copolymers regulate drug loading, biodistribution, cell accumulation and drug release.[58]

In aqueous solutions, amphiphilic block copolymers tend to accumulate at the interfacial boundary to maintain a lower state of free energy.[59] The free energy of the medium increases as the concentration of polymer increases; at a specific concentration, several amphiphiles will assemble into colloidal particles to minimise the free energy. This concentration is called the critical micelle concentration (CMC).[60] If the concentration of the amphiphilic block copolymers remains over the CMC the micelles will be thermodynamically stable.[61] Various techniques have been used to prepare micelles including dialysis, emulsion-solvent evaporation, solid dispersion, lyophilisation and microphase separation (**Table 1.5**). To generate micelle DDSs, the micelles are usually assembled in the presence of the drug such that the drug is incorporated into the hydrophobic core.[53] Recent examples of polymeric micelles continue to demonstrate their utility as potential DDSs in cancer chemotherapy (**Table 1.6**),[64] and as a result of their promising characteristics, several polymeric micellar-based anticancer drug formulations are currently undergoing clinical trials (**Table 1.7**).

Table 1.5: Different techniques used to prepare micelles, including applications as DDSs.

Method of micellisation	**Description of Technique**	**Example Drugs**	**Reference**
Dialysis	Drug and polymer are solubilised in an organic solvent; a small amount of water is added, followed by dialysis in aqueous media to remove the organic solvent.	Doxorubicin	[53]
Microphase separation (solvent evaporation)	Drug and polymer are dissolved in a water-miscible organic solvent that is added to water. The organic solvent is then removed by evaporation.	Gliclazide	[62]
Emulsion solvent evaporation	Drug and polymer are dissolved in a water-immiscible organic solvent and slowly added to an excess of water under vigorous stirring, thus forming an oil-in-water emulsion. The organic solvent is then removed by evaporation.	Paclitaxel	[53]
Lyophilisation	The drug and polymer are dissolved in a mixture of water and organic solvent. Lyophilisation of the solvent results in the formation of drug-polymer micelles.	Paclitaxel	[63]

Table 1.6: Recent examples of polymeric micellar-based DDSs for the treatment of cancers.

Drug	Polymer	Effects	Target	Reference
Doxorubicin	Dextran and PLGA block copolymers	The cellular uptake of the polymeric micelles showed higher toxicity than the free drug, which implies that the micelles may have the potential to overcome drug resistance.	Human cholangiocarcino--ma (HuCCT1)	[65]
Cisplatin	PEG-*b*-poly (glutamic acid) (PGA) copolymers	Higher blood circulation time and higher cellular accumulation via enhanced permeability and retention (EPR) effects resulted in complete tumour regression.	Lewis lung cancer cell	[66]
Doxorubicin	PEG-*b*-PGA copolymers coupled with antibodies	Antibody (C225 against, epidermal growth factor receptor (EGFR)) coupled polymeric micelles demonstrated higher cellular uptake than the free drug.	Vulvar squamous carcinoma A431 cells	[67]
Doxorubicin	Folic acid conjugated PEG-*b*-PLGA copolymers	Conjugated micelles demonstrated significant *in vivo* anticancer activity by inhibiting tumour growth.	Nasopharyngeal epidermal carcinoma cell	[68]

Table 1.7: Polymeric micelle DDs in different stages of clinical development.

Drug	Block copolymer	Phase	Disease	Reference
Genexol-polymeric micelle (PM) (paclitaxel)	PEG-*b*-PLGA	Phase II, III and IV	Metastatic breast cancer	[72]
		Phase II	Advanced urothelial cancer, advanced head and neck cancer, and advanced non-small-cell lung cancer	[73]
		Phase I/II clinical	Ovarian cancer and advanced or metastatic pancreatic cancer	[74]
		Approved	Breast and lung cancer	[75]
Nanoxel-PM (Docetaxel)	PEG-*b*-PLGA	Phase I	Solid tumours	[76]
Nanoplain	PEG-*b*-PGA	Phase I/II	Solid tumours	[77]
Oxaliplatin	PEG-*b*-PGA	Phase I	Lung and breast cancer	[78]
Doxorubicin (NK911)	PEG-*b*-poly(acrylic acid) (PAA)	Phase I/II	Head and neck carcinoma	[79]
Doxorubicin (SP1049C)	PEG-*b*-poly(propylene glycol) (PPG)	Phase II/III	Breast cancer	[80]

1.1.3.3 Other self-assembly based drug delivery systems

Polymeric capsules: Nanocapsules are vesicular systems containing a core-shell structure; a core confined aqueous solution of the drug surrounded by a polymeric membrane or coating.[69] The size of nanocapsules lies between 100-500 nm,[70] and the significant advantage of nanocapsule systems is their high drug loading and release capacity. The main challenges of nanocapsules administration are their poor stability, systemic drug release and poor blood circulation time.[71]

Polymeric nanospheres: Polymeric nanospheres are defined as a matrix of solid colloidal particle containing drug molecules entrapped or encapsulated in the polymeric matrix.[30] Polymeric nanospheres tend to have diameters ranging from 10 to 100 nm.[81,82] Preparation of polymeric nanospheres depends on the polymer used; if particle formation requires polymerisation, emulsion polymerisation or interfacial Polymerisation techniques can be used.[71] Nanospheres may also be prepared from preformed polymers (i.e. biodegradable polymers) using emulsification-solvent evaporation, emulsification-solvent diffusion or salting-out techniques.[61,83] PLA, PGA, PLGA, PCL and poly(methylmethacrylate) (PMMA) have been used due to their biocompatibility.[61]

Drug-polymer conjugates (DPCs): DPCs are drugs that have been conjugated to a polymeric backbone through a cleavable linkage and exhibit a different pharmacokinetic profile compared to the parent drugs.[70] The idea of combining drug molecules with water-soluble polymers to enhance the solubility of drugs was first introduced by Ringsdorf in 1975.[84] DPCs offer several advantages including improved drug solubility, controlled release of drugs, minimal systemic toxicities, increased therapeutic efficacy, higher cellular accumulation through the EPR effect and prolonged blood circulation.[85] The advantages of DPCs have led to several formulations which are under clinical investigation (**Table 1.8**).

Table 1.8: Drug-polymer conjugates at different stages of clinical development.

Drug	Polymer	Phase	Disease	Reference
Camptothecin	Polyglutamate	Phase I/II	Ovarian cancer	[86]
Doxorubicin	*N*-(2-Hydroxyprol) methacrylamide (HPMA)	Phase II	Lung and breast cancer	[87,88]
Doxorubicin	Dextran	Phase I	Various cancers	[86]
Camptothecin	PEG	Phase I	Various cancers	[89]
Paclitaxel	HPMA	Phase I	Solid tumour	[90]
Carboplantin	HPMA	Phase I/II	Various cancers	[91]

Dendrimers: Dendrimers are polymers with a hyperbranched core structure. [92] The structural features of dendrimers allow encapsulation or conjugation of therapeutics in the core and attachment of targeting moieties on the surface making them attractive carriers for therapeutics.[92] Dendrimers have several unique properties including monodispersity, the consistent and high degree of branching, multi-valency, nano-size, globular architecture and well-defined molecular weights.[93] These properties provide numerous advantageous for drug delivery: (i) the high density of functional groups on the periphery, provide synthetic handles for conjugation to targeting moieties;[94] (ii) The pharmacokinetics of dendrimers is definitive due to their defined structure, molecular weight and dispersity;[95] (iii) dendrimers can penetrate cell membranes which leads to increased intracellular concentrations of drugs;[96] (iv) dendrimers have inhibited immunogenic identification in the blood leading to longer systemic activity;[97] (iv) the nano-size of dendrimers enable accumulation in cancer tissue by exploiting the EPR effect;[98] (vi) site-specific drug release from dendrimers causes lower systemic toxicity.[98] Numerous studies have demonstrated the effectiveness of dendrimers as anticancer drug carriers (**Table 1.9**).

Table 1.9: Examples of dendrimers used as DDSs.

Drug	Material	Effects	Reference
Adriamycin	Poly(amidoamine) (PAMAM)	Effective cellular penetration with lower systemic toxicity and high cancer cell mortality rate	[99]
Docetaxel	Poly(propylene imine)	Higher accumulation of drug molecules in a tumour located in the brain	[100]
Doxorubicin	Poly-L-lysine	Increased cellular accumulation and cytotoxicity	[101]
Camptothecins	Poly(glycerol succinic acid)	Increased solubility of the drug and higher cytotoxicity to MCF-7 human breast cancer cells	[102]

1.1.4 Overview of amphiphilic polymer self-assembly

1.1.2.1 Amphiphilic polymers and their self-assembly in the aqueous systems

In aqueous solutions, amphiphilic block copolymers have a tendency to accumulate at the interfacial boundary to maintain a lower state of free energy, and at the CMC the amphiphiles self-assemble into micelles.[59,60] If the concentration of the amphiphilic block copolymers remains over the CMC the micelles will be thermodynamically stable.[61] This concentration based stability provides a major advantage in the delivery of drugs in biological systems as a dilution in the vascular system does not affect stability as the concentration rarely falls below the CMC. Polymeric micellar-based DDSs are widely used for the encapsulation of different drugs for the treatment of a wide range of diseases.

In micelle systems, the hydrophobic core can encapsulate hydrophobic components.[103,104] The hydrophilic corona provides protection against biological invasion and non-specific protein absorption, ensuring longer blood circulation times and increased bioavailability.[105] The nanoscale size and ability to encapsulate hydrophobic drugs make micelles an ideal candidate for drug delivery.[106] In addition, the versatility of micelles with respect to surface modification enables the conjugation of targeting ligands for site-specific drug delivery. Several polymeric micelle formulations are in different stages of clinical development (**Table 1.7**). For instance, Genexol®-PM,[65] NK105[107] and SP1049C[39] are under evaluation in clinical trials as anticancer DDSs. Genexol-PM is a polymeric micelle which has been approved for breast cancer and lung cancer treatment. Genexol-PM encapsulates paclitaxel and is synthesised from a PEG-*b*-poly(D,L-lactide) (PEG-*b*-PDLLA) block copolymer.

The major advantage of Genexol-PM is its lower toxicity than paclitaxel with the maximum tolerated dose two to three times greater than that of free paclitaxel.[108]

1.1.2.2 Factors affecting micelle formation from block copolymers

Micelle formation is a complex thermodynamic process, and despite extensive research on the aqueous behaviour of amphiphilic polymers, the mechanisms of micelle formation are still disputed.[109] Self-assembly of amphiphilic molecules is governed by the hydrophobic attraction at the water-hydrophobic polymer block interface and hydrophilic-hydrophobic repulsion, which is termed as the hydrophobic effect.[110] The currently accepted models that explain the micellisation process are the mass action model (MAM) and the pseudo-phase transition model (PTM).[111] In the MAM, micellisation is a multistep process dependant on the Gibbs free energy of the system. The first step involves the creation of a cavity (displacement of solvent) in the aqueous system. This is an energy-dependent process where the energy of cavity formation is dependant on the surface area of the cavity and water-vapour surface tension. In the second step, the cavity is filled with the hydrophobic component of the amphiphile. The energy contribution (transfer of free energy) involves the transfer of the hydrophobic component into the cavity and is dependant on the number of amphiphile molecules. The final step is solvation of the hydrophilic component in the aqueous phase. The formation of micelles, according to the MAM requires greater than the minimum concentration of amphiphile molecule (i.e. CMC).[109] The PTM portrays micellisation as a single step process where amphiphiles retain a monomeric (unimer) form in the aqueous phase below the CMC. At the CMC a dramatic phase separation occurs resulting in aggregation of amphiphiles into micelles.[112]

Understanding the factors that regulate the micellisation process is central to their use in many applications as the composition, microstructure and architecture of amphiphiles play a vital role in the micellisation process. Riley *et al.* and Heald *et al.* concluded the size and aggregation number of PEG-*b*-PLA micelle was solely dependent on the copolymer microstructure.[113,114] The result showed when the PEG to PLA molecular weight ratio was low; small micelles with narrow dispersity were formed demonstrating there was a clear relationship between the PEG to PLA molecular weight ratio and the hydrodynamic radius (R_h) and aggregation number (N_{agg}). However, as the PEG to PLA molecular weight ratio was increased the micelle density increased (compaction), and there was no clear relationship between R_h and $N_{agg.}$ They suggested that the morphology of the micelle was related with the PEG to PLA molecular weight ratio;

low PEG to PLA molecular weight ratio resulted in star-like micelles, whereas high PEG to PLA molecular weight ratios resulted in solid particle micelles. Milchev *et al.* conducted a simulation study to establish a relationship between chain length, CMC, the free energy of the system and aggregation behaviour.[115] The study revealed as the molecular weight of the polymer increased the interaction energy between the polymer in the hydrophilic corona decreased.[116,113]

Nicholas *et al.* investigated a triblock poly(oxybutylene/oxyethylene) system where the molecular weight of the hydrophilic block changed, but the ratio with the hydrophobic block remained constant (i.e. increasing overall molecular weight).[117] They found the increase in the overall molecular weight led to an increase in the micelles R_h and N_{agg}. Yang *et al.* used three copolymers with a larger middle hydrophobic block and varying length of the hydrophilic part, however, the R_h and N_{agg} remained approximately constant with the change in hydrophilic part.[118] Rager *et al.* studied PAA-*b*-PMMA block copolymers in aqueous media where the PAA to PMMA molecular weight ratio was varied from 1 to 2. They reported that the block copolymer with shorter PMMA (hydrophobic part) blocks did not form micelles.[119] Similarly, Szczubialka *et al.* investigated a sulfonated polystyrene isoprene block copolymer with a short hydrophobic block which presented evidence for the presence of micelles and unimers in the same solution. Hence, they concluded a certain length of the hydrophobic unit is crucial for micelle formation.[120]

These studies, as well as others, demonstrated that the ratio between the hydrophilic and hydrophobic blocks in amphiphilic polymers significantly influenced the size and morphology of their micelles. A copolymer with a large hydrophilic block (relative to the hydrophobic block) preserved an equilibrium between the unimer and aggregated state and usually forms spherical micelles referred to as star-like micelles.[121] Copolymers with a large hydrophobic block (relative to the hydrophilic block) did not appear to display an equilibrium between the unimer and aggregated states and formed micelles with dense, compact cores, referred to as crew-cut micelle-like aggregates.[122] These types of micelles can have different morphologies, including spherical, rods, vesicles, lamellar and compound micelles.[123] Zhang and Eisenberg conducted a series of studies relating the morphology of the self-assembled products to the microstructure of the amphiphile, including the hydrophilic to hydrophobic ratio. They concluded that as the hydrophobic to hydrophilic ratio increased small spherical micelles transformed into large vesicles, whereas a decrease in the hydrophilic block length favoured the formation of cylindrical micelles.[124,123]

The method or technique of micelle preparation can also affect the self-assembly behaviour of amphiphilic polymers. Common techniques used in micelle formation are dialysis, solvent evaporation, precipitation and lyophilisation (**Table 1.5**).[125] Vangeyte *et al.* conducted a systematic study of different preparation techniques and solvents to evaluate their correlation with the self-assembled products.[126] The size of the micelle was found to be relatively large when the polymer solution was dialysed against an aqueous phase (i.e. dialysis method). The increase in the size was attributed to the rapid mixing of the polymer solution with the aqueous phase due to the large porosity of the dialysis membrane. In the precipitation method, it was determined that the solvent and order of precipitation (organic in aqueous or *vice versa*) did not significantly influence the size of the self-assembled product. However, increasing the concentration of the polymer or using additional surfactants was found to increase the size of the aggregates.[31] The temperature has also been shown to affect the micellisation process. Khoshnood *et al.* concluded on the basis of molecular thermodynamic model predictions and experimental data that the temperature has a profound influence on the CMC,[127] but only when the bulk phase is water due to hydrophobic effects.

Theory

1.2. Thermodynamics of micelle formation

The mechanism of micelle formation and factors regulating this process can be explained using thermodynamic models of micelle formation. The micelle is a self-assembled product of an amphiphilic molecule in a media or phase where one part or component of the molecule is not soluble.[128] In a common scenario, the bulk media is represented by an aqueous phase. The driving force behind self-assembly is the length scale dependence of the hydrophobic effect.[129] The free energy required to solvate a small hydrophobic component of a molecule (e.g. surfactant) in water has a linear relationship with the solute volume, whereas for a large hydrophobic component of a molecule (e.g. amphiphilic polymer) there is a linear relationship with the surface area of the solute.[221] The difference between these two types of molecules is defined by the surface area; if the surface area of a molecule exceeds 1 nm^2 it is considered a large hydrophobic molecule. Due to the scaling relationship, the energy required to solvate a cluster of small molecules in water may exceed the energy needed to solvate a large molecule. This difference in the energy requirement is the thermodynamic driving force behind the self-assembly process.[130]

A longstanding question regarding self-assembly behaviour of amphiphilic molecules has been the mechanism of self-assembly; how does the micelle form, how does the micelle grow, what are the physical limitations of growth? Tanford and Israelachvili pioneered two thermodynamic models explaining the self-assembly behaviour of surfactant molecules in aqueous media.[131,11] Tanford proposed a free energy concept for micelle formation which marked energy differences between a free surfactant molecule in the bulk phase and the micelle core as a driving force.[131] This free energy model explains why aggregation occurs, how micelles grow and why they do not keep growing (i.e. micelles have a finite size and shape). Israelachvili *et al.*, proposed a molecular packing concept which can predict the shape and size of the micelles considering the molecular packing and general thermodynamic principles.[11] The self-assembly behaviour of different types of amphiphiles can be understood and explained using these two models.

Tanford considered the energy changes (Δμ) when forming a micelle consisting of a number of surfactant molecules (i.e. N_{agg}) as being composed of three energy contributions (**Equation 1.1**).

$$\left(\frac{\Delta\mu_g^o}{kT}\right) = \left(\frac{\Delta\mu_g^o}{kT}\right)_{transfer} + \left(\frac{\Delta\mu_g^o}{kT}\right)_{interface} + \left(\frac{\Delta\mu_g^o}{kT}\right)_{head} \quad \textbf{(1.1)}$$

Where k is the Boltzmann constant, T the temperature and μ_g the potential of aggregation (energy change due to micellisation). The first term $\left(\frac{\Delta\mu_g^o}{kT}\right)_{transfer}$ represents the energy required to transfer the hydrophobic tail of N_{agg} surfactant molecules from the unfavourable aqueous phase to the micelle core. This transferred energy is dependant on the hydrophobic tail but not the shape and size of the micelle. The second term $\left(\frac{\Delta\mu_g^o}{kT}\right)_{interface}$ considers the interfacial contact energy of the interfacial boundary between the aqueous phase and micelle core. This energy is dependant on the product of the contact-free energy per unit area of the interface (σ) and the surface area per molecule of the aggregate core (a). The third term $\left(\frac{\Delta\mu_g^o}{kT}\right)_{head}$ considers the repulsive force between the hydrophilic heads or chains in the corona. This repulsive force is due to steric repulsion between the chains, or electrostatic repulsion in the case of ionic head groups. Tanford proposed an inverse relationship with a, and thus Equation 1.1 can be rewritten as **Equation 1.2**.

$$\left(\frac{\Delta\mu_g^o}{kT}\right) = \left(\frac{\Delta\mu_g^o}{kT}\right)_{transfer} + \left(\frac{\sigma}{kT}\right)a + \left(\frac{\alpha}{kT}\right)\frac{1}{a} \quad \textbf{(1.2)}$$

Where α is the head group repulsion parameter. The behaviour of the micelle at equilibrium can be expressed by considering the size distribution of micelle or micelle as a pseudo-phase. If the micelle is a pseudo-phase, it can be considered as the minimum state of the energy, which is dependant on N_{agg} or a. Thus the equilibrium condition can be defined by **Equation 1.3**:

$$\frac{\partial}{\partial a}\left(\frac{\Delta\mu_g^o}{kT}\right) = 0 \Rightarrow \left(\frac{\sigma}{kT}\right) - \left(\frac{\alpha}{kT}\right)\frac{1}{a^2} = 0 \; at \; a = a_e \Rightarrow \quad \textbf{(1.3)}$$

$$a_e = \left(\frac{\alpha}{\sigma}\right)^{1/2}$$

where a_e is the equilibrium area per molecule in the aggregate dependant on repulsions between the surfactant head groups (α) and the CMC. Considering those factors, the equation of the pseudo-phase can be rewritten as **Equation 1.4**:

$$lnX_{CMC} = \left(\frac{\Delta\mu_g^o}{kT}\right)_{transfer} + \left(\frac{\sigma}{kT}\right)a_e + \left(\frac{\alpha}{kT}\right)\frac{1}{a_e} \qquad \textbf{(1.4)}$$

According to **Equation 1.2** the free energy to transfer the hydrophobic tail to the core is a negative contribution, which is responsible for the initial aggregation; this is only dependant on the CMC (**Equation 1.4**), not the equilibrium area per molecule (a_e) or the shape/size of the micelle. The second term representing the interaction energy between the core and aqueous phase is dependent on a_e, which has an inverse relationship with a. However, a has a reciprocal relation with N_{agg} (A = N_{agg} a, due to the geometrical relationship). The third contribution, the free energy due to head group repulsions, increases with an increase in a as a consequence N_{agg} will decrease. This contribution confines the growth of the micelle to a finite level.

Tanford's thermodynamic model of micelle formation incorporates formation, growth and the finite nature of the micelle; however, Tanford realised that the state (conformation) of the hydrophobic component in the aggregate (micelle) core is different from its condition in the bulk liquid state. Because in the core one end of the hydrophobic component remains at the core-aqueous interface, and another end assembles itself in the core as per the shape and size of the core. Therefore Tanford corrected the transfer energy contribution to consider this difference although this does not correctly account for the packing constraint due to the shape and size of the core which is independent of the transfer free energy.

Nevertheless, the shape and size of the core does influence the packing free energy constraint, $\left(\frac{\Delta\mu_g^o}{kT}\right)_{packing}$ has been calculated as a function of shape and size of the core and has been accounted for in later derivatives of the Tanford equation.[13]

It is required that the hydrophobic portion be non-uniformly packed to maintain a uniform density in the micelle core. The $\left(\frac{\Delta\mu_g^o}{kT}\right)_{packing}$ is calculated, as shown in **Equation 1.5**. [11]

$$\left(\frac{\Delta\mu_g^o}{kT}\right)_{packing} = \left(\frac{3\pi^2}{80}\right)\frac{R^2}{NL^2}\ (sphere), \left(\frac{5\pi^2}{80}\right)\frac{R^2}{NL^2}\ (cylinder), \left(\frac{10\pi^2}{80}\right)\frac{R^2}{NL^2}\ (bilayer) \qquad \textbf{(1.5)}$$

Where *L* is a characteristic segment length and *N* is the number of segments in a hydrophobic portion such that $NL^3 = v_o$ since $R = 3\ v_o/a$ *(sphere)*, $2\ v_o/a$ *(cylinder)*, and v_o/a *(bilayer)*. **Equation 1.5** can, therefore, be rewritten as **Equation 1.6**.

$$\left(\frac{\Delta\mu_g^o}{kT}\right)_{packing} = \frac{Q}{a^2} \qquad \textbf{(1.6)}$$

$$Q_{sph} = \left(\frac{27}{8}\right)v_o\,L, Q_{cyl} = \left(\frac{20}{8}\right)v_o\,L, Q_{bilayer} = \left(\frac{10}{8}\right)v_o\,L$$

Where Q denotes the free energy coefficient $1/a^2$ which is influenced by the shape of the micelle. By considering the packing free energy, the Tanford equation can be rewritten as **Equation 1.7**.

$$\frac{\partial}{\partial a}\left(\frac{\Delta\mu_g^o}{kT}\right) = 0 \Rightarrow \left(\frac{\sigma}{kT}\right) - \left(\frac{\alpha}{kT}\right)\frac{1}{a^2} - \frac{2Q}{a^3} = 0\ at\ a = a_e \Rightarrow \qquad \textbf{(1.7)}$$

$$a_e = \left(\frac{\alpha}{\sigma} + \frac{2Q/a_e}{\sigma/kT}\right)^{1/2}$$

This final equation states all thermodynamic parameters currently considered important in micelle formation.

1.3 Characterisation of micellar systems

1.3.1 Analysis of micelles by light scattering techniques

1.3.1.1 Fundamental aspects of light scattering techniques

Light scattering is a unique phenomenon due to the wave-particle duality property of light (i.e. photons) and matter. The interaction of light in the form of electromagnetic waves with a particle causes a distribution or shift of charges within the particle that results in a dipole effect. [132] This dipole is also in continuous oscillation due to the electromagnetic nature of light, which acts as an emitter of electromagnetic waves at the same wavelength (λ) of the incident light in every direction (**Figure 1.1**).[132]

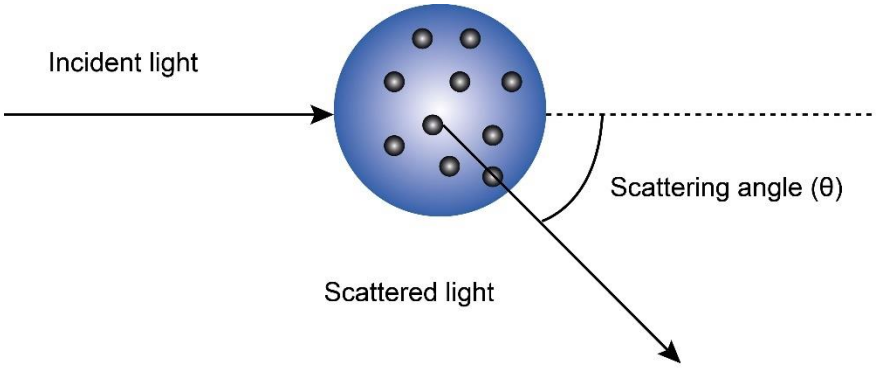


Figure 1.1: Illustration of light scattering by a particle, showing how the incidence light is scattered from a particle at a scattering angle that depends on the dimension of the particle.

The nature of light scattering from a particle depends on the correlation between the dimension of the particle (size and shape) and the wavelength of the incident light. Light interacting with a large particle (> 20 nm) will produce several dipole centres which cause a phase difference in the emitted light. Due to this phase interference, the intensity of the emitted light from the particle will be different at different angles, termed as a '*non-isotropic emission*' (**Figure 1.2**).[133]

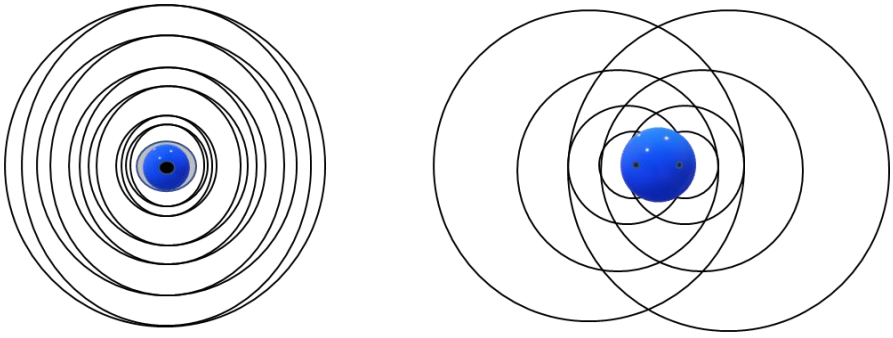


Figure 1.2: Illustration of particle size dependency on light scattering, showing that small particles are responsible for '*non-isotropic emissions*' and large particle demonstrate '*isotropic scattering*'.

This interference pattern is directly correlated with the shape and size of the particle, and as a consequence, it provides the quantitative means for the characterisation of particles by light scattering.[134] In comparison if the particle is smaller than the λ of the incident light (< λ/20), the phase difference between the incident light and the emitted light is negligible, and the intensity of scattered light does not show an angular dependency. This type of scattering is defined as '*isotropic scattering*'.[135]

1.3.1.2 Static light scattering (SLS)

SLS is an optical technique used for measuring the scattering intensity of light from a particle at different angles generating an angular dependency profile of the scattered light (**Figure 1.3**). The primary application of SLS is the determination of molecular weight, radius of gyration (R_g) and structural factors of polymers, proteins and aggregates.[136]

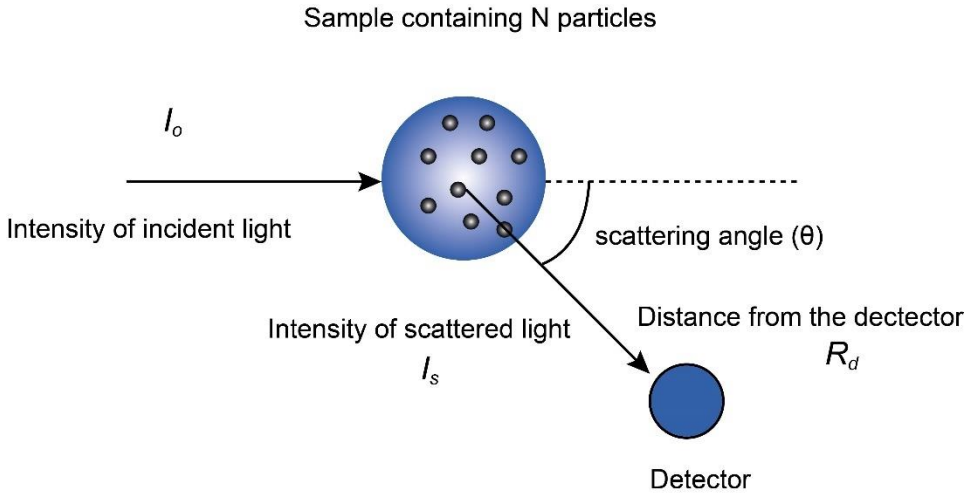


Figure 1.3: Illustration showing the basic components required for a static light scattering experiment; the detector can be moved to different angles to detect scattering intensity at different angles.

As mentioned above, the scattering behaviour of a particle is dependent on shape and size. In a dilute solution, the scattering intensity (*I*) of a small particle (< λ/20) is dependant on the scattering power of the dissolved particle (*b*), the mass concentration of the particle (*c*), and osmotic pressure (π). and are related as stated by **Equation 1.8**;[137]

$$I \sim b^2 kT \frac{c}{\left(\frac{\partial \pi}{\partial c}\right)_{T,N}} \qquad \textbf{(1.8)}$$

From **Equation 1.8** Van't Hoff derived the following equations (**Equations 1.9a** and **1.9b**);[137]

$$\frac{\partial \pi}{\partial c} = \frac{kT}{M} \qquad \text{(for ideal solutions)} \qquad \textbf{(1.9a)}$$

$$\frac{\partial \pi}{\partial c} = kT\left(\frac{1}{M} + 2A_2 c + \cdots \ldots\right) \qquad \text{(for real solutions)} \qquad \textbf{(1.9b)}$$

In the case of a real solution **Equation 1.9b**[138] can be rewritten as **Equation 1.10.**

$$\frac{Kc}{R} = \frac{1}{M} + 2A_2 c + \cdots \qquad \textbf{(1.10)}$$

Where R is the absolute scattering intensity, which is independent of the experimental conditions (i.e. scattering volume and distance from the detector), $2A_2c$ is the second viral coefficient, and M is the molecular weight.

For large particles, there might be several dipole centres, and the scattering intensity is dependant on the scattering angle.[134] For scattering from a large particle, the scattering vector (q) is determined from the scattering angle and wavelength of the incident light (**Equation 1.11**).

$$q = \frac{4\pi n_D \sin(\theta/2)}{\lambda} \quad \textbf{(1.11)}$$

Where n_D is the refractive index of the solvent; θ is the angle of the incident light.

The particle form factor P(q) is defined as the normalised single particle scattering. As large particles have multiple scattering centres P(q) can be considered as mass centres which are described as R_g. P(q) is described by **Equations 1.12** and **1.13**.

$$P(q) = 1 - \frac{1}{3}R_g q^2 + \cdots \quad \textbf{(1.12)}$$

The equation for the absolute scattering intensity R depends on the particle form factor;

$$\frac{Kc}{R} = \frac{1}{MP(q)} + 2A_2c + \cdots \quad \textbf{(1.13)}$$

Equations **1.12** and **1.13** can be combined to give the Zimm equation (**Equation 1.14**).[136]

$$\frac{Kc}{R} = \frac{1}{M}\left(1 + \frac{1}{3}R_g q^2\right) + 2A_2c \quad \textbf{(1.14)}$$

The Zimm equation provides the basis for determination of M and R_g of particles. According to the Zimm equation, when q = 0 the equation represents a straight-line intercepting at the y-axis ($y = mx + c$). Here the y-intercept value is the inverse molecular weight (1/M). However it is not possible to obtain q = 0 experimentally, and therefore a series of Rayleigh ratios ($\frac{Kc}{R}$) are obtained at different angles and interpolated to q = 0 (**Figure 1.4**).

In a Zimm plot $\frac{Kc}{R}$ is the y-axis, $q^2+k'c$ is the x-axis and k' is an arbitrary constant. From the Zimm plot M and R_g can be calculated (**Figure 1.4**).

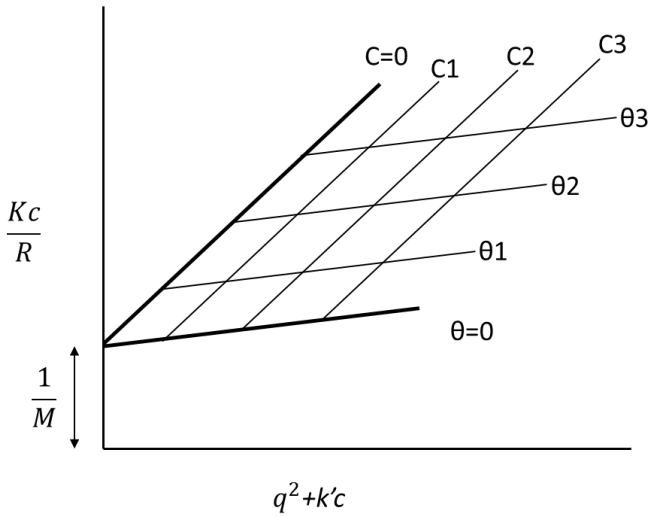


Figure 1.4: Illustration of a Zimm plot for the molecular weight determination of a particle showing the Rayleigh ratio ($\frac{Kc}{R}$) value for solutions with different particle concentrations as determined by multi-angle static light scattering.

Therefore in a Zimm plot the intercept point for c = 0 and θ = 0 can be identified, which transforms **Equation 1.14** to **Equation 1.14a**.

$$\frac{Kc}{R} = \frac{1}{M} \qquad \textbf{(1.14a)}$$

The value of $\frac{Kc}{R}$ is equal to the inverse of the molecular weight.[136]

1.3.1.3 Dynamic light Scattering (DLS)

In DLS instrument, when the laser light passes through a particle system, the incident light scatters in every direction and detector record the intensity of the scattering light. As the particles in the system are in continuous motion (Brownian motion), the scattering light will result in mutually destructive phases and cancel each other out, or in mutually constructive phases to produce a detectable signal. A digital autocorrelator will determine the frequency of intercity fluctuation which related to the diffusion behaviour of the particle. A typical correlation function for a monodisperse sample is shown in **Figure 1.5**.

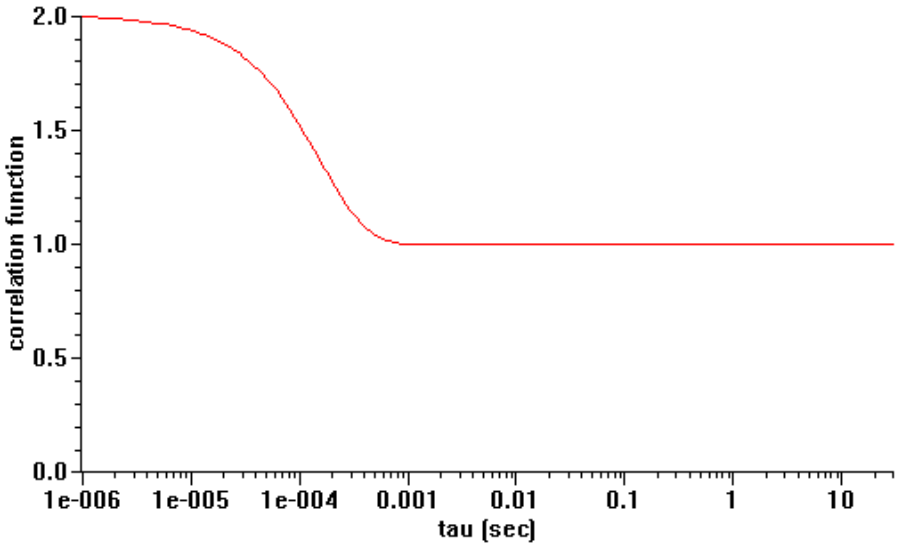


Figure 1.5: Illustrative correlation function measured by DLS for a polystyrene particle dispersion in water, determined to have a R_h of 20 nm. The plot was an output from the Zetasizer (Malvern) software.

The fluctuations are calculated via a second-order correlation function shown by **Equation 1.15**.[139]

$$g^2(\tau) = \frac{\langle I(t)I(t+\tau)\rangle}{\langle I(t)\rangle^2} \quad \textbf{(1.15)}$$

Where *I(t)* is the intensity of the scattered light at any given time *t*, and the brackets designate averaging total time *t*. τ is the amount of duplicate intensity shifted from the original position before performing the average calculation. The following equation (**Equation 1.16**) can be used to analyse the correlation of a monodispersed function;[139]

$$g^2(\tau) = B + \beta \exp(-2\Gamma\tau) \quad \textbf{(1.16)}$$

Where *B* is the baseline of the correlation function at the infinite delay, β is the coherence factor dependant on detector area, optical alignment and scattering properties of macromolecules, Γ is the decay rate, and the self-diffusion constant (*D*) (also known as the diffusion coefficient) is related to the decay function according to **Equation 1.17**:[139]

$$D = \frac{\Gamma}{q^2} \quad \textbf{(1.17)}$$

Where q is the magnitude of the scattering vector and is given by **Equation 1.18**;[139]

$$q = \frac{4\pi n_D \sin(\theta/2)}{\lambda} \quad \textbf{(1.18)}$$

where n_D is the refractive index of the solvent, λ is the vacuum wavelength of the incident light, and θ is the scattering angle.

The hydrodynamic radius (R_h) can be calculated from Stokes-Einstein equation (**Equation 1.19**):[140]

$$D = \frac{kT}{6\pi\eta R_{\mathrm{h}}} \quad \textbf{(1.19)}$$

Where k is Boltzmann's constant, T is the temperature in K, and η is the solvent viscosity. However, the accuracy of R_{h} calculated from the Stokes-Einstein equation is dependant on several key assumptions; the particle is spherical in nature, the viscosity of the system is known, and measurements are recorded at infinite dilution. It should be noted that the dispersity of the (nano) particle solution is a significant consideration when measuring the D value using DLS. A polydisperse solution significantly affects the interference pattern and Γ, with the presence of a small volume of large particles skewing the scattered light intensity. In this instance, DLS can provide erroneous results and incorrect diffusion coefficients and particle sizes. The typical instrument (DLS particle sizer) used to analyse particle size utilises a scattering angle of 90° or 173° to avoid the influence of contaminants (e.g. large aggregates or particles). However, the disadvantages of using such large scattering angle DLS is often overlooked; Fischer *et al.* clearly discussed the drawback in their review article.[141]

1.3.1.4 Application of light scattering techniques

The light scattering profile of polymer solutions has been extensively used to determine the shape and size of self-assembled polymeric aggregates (e.g. micelles). **Table 1.10** gives a brief overview of some examples where light scattering techniques have been used to determine the properties of the polymers and the aqueous self-assemblies.

Table 1.10: Application of light scattering techniques for the characterisation of polymer systems.

Technique	System	Purpose	Reference
SLS/DLS	Liposome	Determination of size and size distribution	[142]
DLS	Micelle-gel system	Transition of micelle to gel system	[143]
SLS	Polymer solution	Molecular weight determination of poly(vinyl acetate)	[144]
DLS/SLS	Polymer solution	Molecular weight determination of polystyrene	[145]
DLS	Micelle solution	Size analysis of micelles synthesised from nona-ethyleneglycol-monododecyl ether	[146]
DLS	Protein-micelle	Study the interaction between micelles and proteins	[147]
DLS	Micelle solution	Determination of polymer CMC	[148]
DLS/SLS	Micelle solution	Determination of R_h, N_{agg} and R_g	[149,150]
DLS/SLS	Micelle solution	Determination of micelle morphologies	[151,152]

1.3.2 Analysis of micelles by nuclear magnetic resonance (NMR) spectroscopy

1.3.2.1 Fundamental aspects of diffusion NMR spectroscopy

A range of physical molecular properties (e.g. molecular size, shape, aggregation, encapsulation, complexation and hydrogen bonding) can be characterised by studying molecular diffusion in solution. Developments in high-resolution NMR spectrometers have provided opportunities to research diffusion behaviour via NMR spectroscopy. High-resolution NMR spectrometers may be equipped with gradient probes capable of measuring diffusion along the direction of the field gradient (typically z-axis).[153] Self-diffusion of the molecule is the result of random translational (Brownian) motion in solution, characterised by the self-diffusion coefficient (D), which can be determined by diffusion NMR experiments.

D can be translated to size using the Stokes-Einstein equation (**Equation 1.19**);[153] however, the complexity and nature of the system need to be considered when using the Stokes-Einstein equation to determine R_h of the molecule. The fundamental aspects of measuring diffusion behaviour (in particular, *D*) using a pulsed field gradient spin-echo (PGSE) experiment is illustrated in **Figure 1.6**. [154]

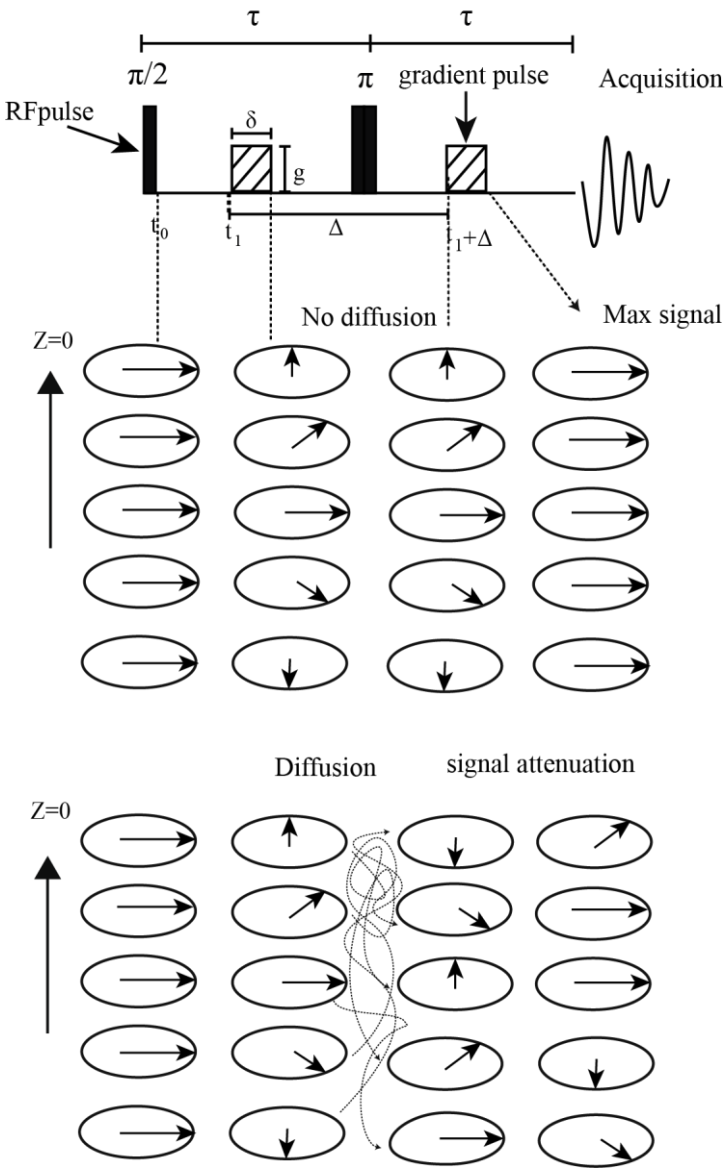


Figure 1.6: A schematic representation of a PGSE pulse sequence measuring diffusion in solution. Two gradient pulses of the same magnitude (*g*) are applied at Δ time interval to determine the signal attenuation due to translational motion of the particle.

For a normal equilibrium state, the net magnetisation is oriented along the z-axis. A π/2 radio frequency (RF) pulse at the beginning of the experiment rotates the macroscopic magnetisation from the z-axis into the x-y plane. A gradient pulse of δ duration and g magnitude is applied after τ period at the t_1 time interval which imposes a spatially dependent phase on the magnetic vector that is refocused by a second gradient applied at time $t_1+\Delta$ (here Δ is the time over which the diffusion is measured) of the same duration and magnitude.

Between the gradient pulses, a second π RF pulse is applied, causing the two gradient pulses to effectively cancel one another (i.e. the sine of phase angle) (**Figure 1.6**). The complete refocussing of the signal only happens when spins have not undergone any **t**ranslational motion along the z-axis. During the diffusion period Δ, molecules that diffuse from their initial physical position will only be partially refocused, resulting in a detected signal that will be attenuated depending upon the distance the molecule has travelled during the Δ period.[153]

Diffusion can be characterised by monitoring the alteration in NMR signal intensity due to the gradual increase in diffusion period Δ, the duration of gradient pulse δ and the magnitude or strength of the gradient pulse g. Experimentally, it is a commonplace to vary g while keeping all other parameters constant; however, the limitation of PSGE experiments, when applied to polymers, is the loss of NMR signal intensity due to transverse relaxation (T_2), which increases with molecular size. This problem can be avoided using a stimulated-echo sequence (STE), termed pulsed-field gradient stimulated-echo (PGSTE). In the PGSTE sequence, the transverse magnetisation is confined in a short τ_1 period by a second π/2 RF pulse; thus magnetisation is dominated by longitudinal relaxation (T_1) during the diffusion period τ_2 (**Figure 1.7**). After that period a third π/2 RF pulse is applied to return the magnetisation into the transverse plane which enables refocusing and detection of the signal.[154]

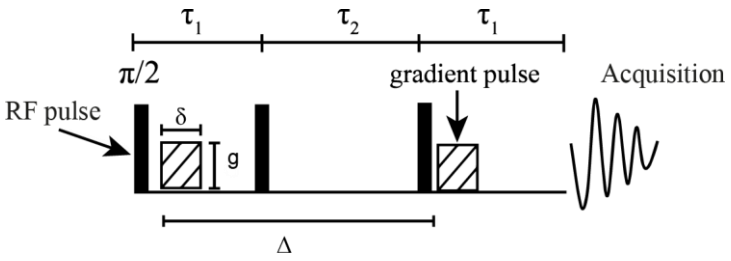


Figure 1.7: A schematic representation of a PGSTE sequence. The PGSTE sequence consists of a second π/2 RF pulse which prevents the loss of NMR signal due to transverse relaxation.

The attenuation of the signal can be described by the Stejskal-Tanner formula in **Equation 1.20** and **1.21a**:[154]

$$I = I_0 e^{-bD} \quad \textbf{(1.20)}$$

$$b = \gamma^2 g^2 \delta^2 (\Delta - \tfrac{1}{3}\delta) \quad \textbf{(1.21a)}$$

In **Equation 1.20** I is the signal intensity in the diffusion pulse sequence after a pair of gradient pulses of strength g, with a duration δ and a delay of Δ between them. I_0 is the initial signal intensity without the diffusion gradient pair. If it can be assumed that $\delta \ll \Delta$, **Equation 1.21a** simplifies to **Equation 1.21b**. [154]

$$b = \gamma^2 g^2 \delta^2 \Delta \quad \textbf{(1.21b)}$$

As a result, **Equation 1.20** can be rewritten as **Equation 1.22**.

$$\frac{I}{I_o} = e^{-bD} \quad \textbf{(1.22)}$$

Therefore a plot of the echo signal attenuation versus b will provide D by fitting the data with a single exponential function; however, the fitting parameter might be more complicated due to the polydisperse nature of the polymer solution. For a polydisperse sample, the initial attenuation can be analysed by **Equation 1.20**; however, as the attenuation increases, it becomes invalid as the attenuation deviates from single exponential behaviour.[155] A polydisperse solution can be modelled using a stretched exponential model (**Equation 1.23**).

$$I = I_o \, e^{(-(bD_o)^{\beta})} \quad \textbf{(1.23)}$$

The Stejskal-Tanner equation can, therefore, be modified to model the signal attenuation from a probability distribution of self-diffusion coefficients (**Equation 1.24**) where a model for the diffusion coefficient distribution, $P(D)$ must be defined.

$$I(b) = I_0 \int_0^{\infty} P(D) \exp(-bD) \, dD, \quad \textbf{(1.24)}$$

The lognormal distribution model $P(D) = 1/\left(D\sigma\sqrt{2\pi}\right)\exp\left[-(\log D - \mu)^2/(2\sigma^2)\right]$, was used in this study as polymers often exhibit heterogeneity resulting in lognormally distributed sizes[154] and the diffusion coefficient distributions in solution.[156] Additionally in the case that the system displays a multimodal distribution of sizes, the lognormal distribution captures the mean $\langle D\rangle = \exp\left(\mu + \sigma^2/2\right)$, and the spread (coefficient of variation, standard deviation/mean) $= \exp(\sigma^2) - 1$ of the distribution.[157] A least-squares fit of the model to signal attenuation data yields the estimated parameters of the diffusion coefficient distribution, μ and σ, and Monte Carlo error analysis provides confidence intervals associated with these estimates.[157] In this research the least-squares fitting routine was implemented in MATLAB R2017b and is publicly available through GitHub.[156]

Finally the D can be interpreted as the R_h of a diffusing sphere via the Stokes-Einstein equation (**Equation 1.19**).[158] However, the Stokes-Einstein equation presumes that the particle is spherical in structure. The Flory equation relates D to M (**Equation 1.25a**):[159]

$$D = KM^{-\upsilon} \qquad \textbf{(1.25a)}$$

where K is a solvent dependent constant and υ (Flory exponent) is a scaling parameter that depends on the particle (i.e. polymer) structure. A logarithmic transformation of **Equation 1.25a** gives **Equation 1.25b**.

$$\log(D) = log\ k\text{-}\upsilon \log \mathrm{M} \qquad \textbf{(1.25b)}$$

A plot of log(D) versus log(M) should give a straight line whereby the slope gives υ. This can provide additional information about the polymer conformation in the solvent.[158]

1.3.2.2 Application of diffusion NMR studies

In diffusion NMR experiments, D is the main point of interest. In principle, any phenomena related to D can be investigated with this technique. Williamson *et al*. successfully determined the molecular weight distribution of a homopolymer (polystyrene) using an PGSTE NMR technique.[157,158]

However, the determination of molecular weight for block copolymer is more complicated than for homopolymers. [160–165] For example, Barrère *et al*. determined the molecular weight of poly(ethylene-*b*-styrene) using PGSTE NMR experiments following the same method as used for homopolymers, which was found to deviate significantly compared to the molecular weight determined by matrix assisted laser desorption ionisation time of flight mass spectrometry (MALDI-ToF MS).[166] Barrère *et al*. concluded that this deviation in molecular weight is caused by the conformational difference of block copolymer in a given solvent.[166] More complex polymers (i.e. stars, and branched polymers) have also been investigated using PGSTE NMR experiments which has enabled researchers to establish a correlation between signal attenuation behaviour, D and R_h.[167,168]

PGSTE NMR experiments have additionally been used to characterise more complex systems, including micelles and emulsions.[169] Law *et al.* investigated micelle formation in hexane using cetyltrimethylammonium bromide (CTAB).[170] They examined the micelle size and distribution using the relation between D and R_h described by the Stokes-Einstein equation (**Equation 1.19**). They found discrepancies between the R_h values obtained from PGSTE NMR experiments and DLS, which were attributed to the fundamental differences in the principles of the analytical techniques.[170] PGSTE NMR experiments have also been extensively used to determine the transition and topology of aggregates and emulsions.[171–173] Whilst these studies highlight the potential of PGSTE NMR experiments for the analysis of polymer aggregate systems there remains significant scope to expand the application of PGSTE NMR experiments to analyse micellar systems in conjunction with other techniques (e.g. X-ray diffraction) to provide complementary information.

1.4 Synthesis and characterisation of amphiphilic polymers

1.4.1 Controlled polymer synthesis

Polymerisation reactions can be classified into different categories on the basis of the mechanism of polymerisation, nature of the propagating species, and method of initiation.[94] Controlled or living polymerisations follow a chain-growth polymerisation mechanism whereby chain transfer and chain termination are eliminated, and the rate of initiation (k_i) is fast compared to the rate of chain propagation (k_p), and therefore the number of kinetic-chain carriers is essentially constant throughout the polymerisation.[174,175]

An ideal controlled or living polymerisation will meet the following conditions:

1. Propagation of every growing polymer chain starts at the same time.
2. The propagation rate for every growing polymer chain is identical.
3. The polymerisation will stop when there is no monomer left or upon a change in the reaction conditions.
4. The polymerisation reaction can restart at any moment given monomer and suitable conditions allowing block polymers to be synthesised.

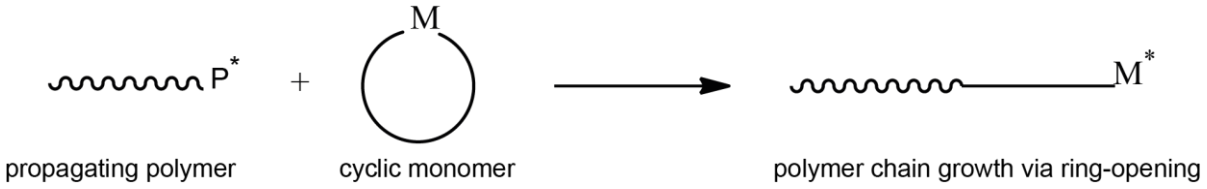
The most successful living polymerisations to date are anionic, cationic or controlled radical polymerisation.[176] Whilst these approaches receive significant attention in academic circles, their industrial application has been hampered by several disadvantages. For example, sensitivity to impurities, poor performance in the presence of water and oxygen, and demanding reaction temperatures.[177] Very few approaches can truly be considered as completely living, but nevertheless, many approaches can be considered as controlled, providing well-defined polymers with narrow dispersity ($Đ$) and defined end-groups. For example, ring-opening metathesis polymerisation (ROMP), ring-opening polymerisation (ROP), coordination-insertion polymerisation and controlled radical polymerisation (CRP) provide well-defined polymers but are susceptible to defects. The dispersity ($Đ$) represents the distribution in polymer chain lengths, which is defined as the ratio between the weight-average molecular weight (M_w) and number-average molecular weight (M_n) (i.e. M_w/M_n).

CRP is perhaps one of the most widely used controlled polymerisation approaches due to the commercial availability of a large monomer family and initiators and tolerance of aqueous solutions. Some of the most common forms of CRP include atom-transfer radical polymerisation (ATRP) and reversible addition-fragmentation transfer (RAFT) polymerisation.

Living polymerisations allow for the preparation of polymers with unique sequence structures and architectures, and defined molecular weight characteristics. By mediating the polymerisation rate and minimising or eliminating side reactions, controlled polymerisation can provide polymers with well-defined molecular weights and end-group functionalities. This characteristic allows the preparation of block copolymers as a second monomer can be polymerised with the original polymer acting as a macroinitiator. In theory, the polymerisation can be stopped and started again with different monomers forming multiblock copolymers. Furthermore, controlled polymerisation allows for the synthesis of different architectures through the use of multifunctional initiators or combinations of different controlled polymerisation techniques.[178]

1.4.2 Ring-opening polymerisation (ROP)

ROP uses an initiator that ring-opens a strained monomer to generate a propagating polymer chain, which can in turn, ring-open more monomer units (**Scheme 1.1**).[179]

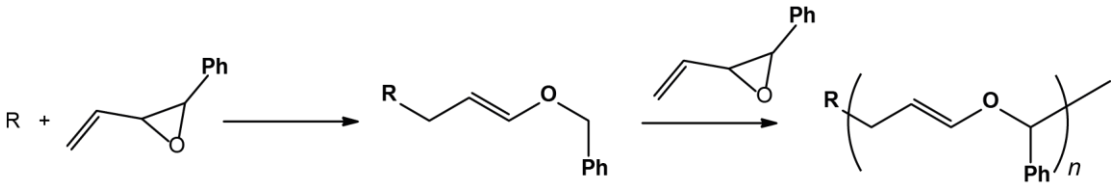


Scheme 1.1: ROP of strained cyclic monomers from a propagating polymer chain or macroinitiator.

ROP is used industrially to synthesise many commercially important polymers including polynorbornene, poly(ethylene oxide) (also known as PEG), polysiloxane, PCL and polyphosphazene. ROPs are classified on the basis of the mechanism of the reaction.[180] Due to the controlled nature of the polymers generated via ROP, it is possible to synthesise block copolymers.

1.4.2.1 Radical ROP

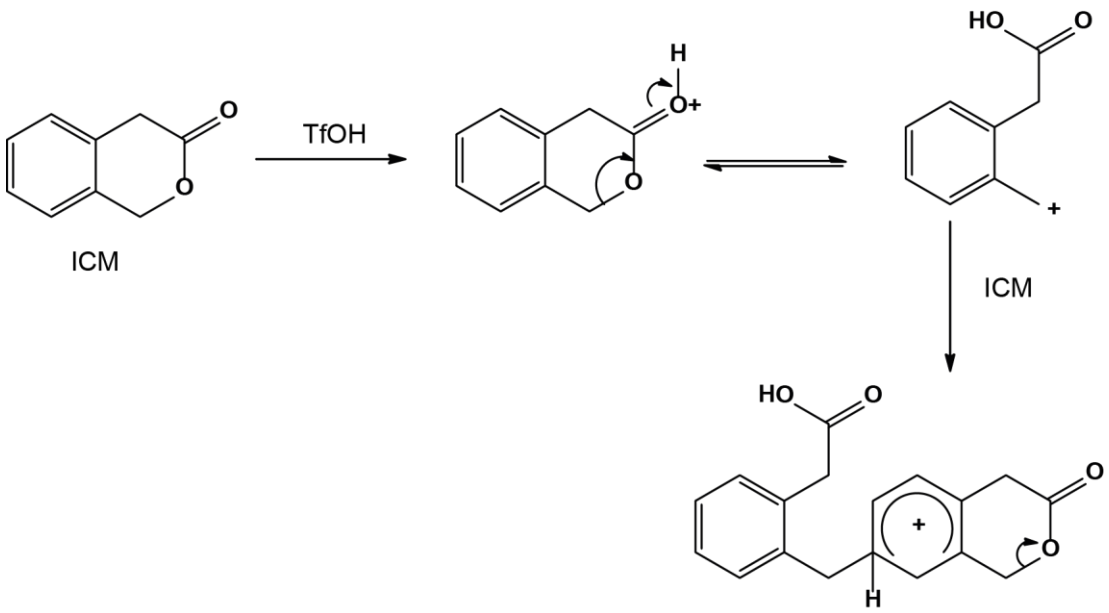
Radical ROP involves the use of a radical initiator and unsaturated cyclic monomers. Initially, the radical adds to the vinyl group of the monomer, which subsequently results in ring-opening and the generation of a terminal propagating radical at the end of the polymer chain (e.g. **Scheme 1.2**).[181] Radical ROP provides access to the polymer that have the same or lower density than their respective monomers making them suitable for applications where a constant volume needs to be maintained.



Scheme 1.2: ROP of a vinyl epoxide monomer via radical addition, ring-opening and the regeneration of a terminal propagating radical.

1.4.2.2 Cationic ROP

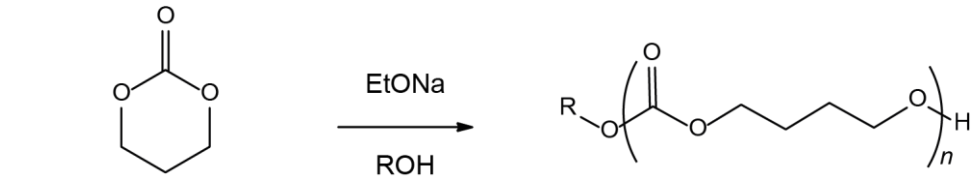
Cationic ROP involves the use of a cationic initiator which can activate a portion of the monomer making it susceptible to nucleophilic attack from another monomer. For example, the addition of an acid to isochromanone (ICM) results in protonation of the monomer and the formation of a cationic initiator to which another monomer unit can add (**Scheme 1.3**).[182] Several important industrial polymers are synthesised utilising cationic ROP including polyacetals, copolymers of 1,3,5-trioxane and oxirane or 1,3,5-trioxane and 1,3-dioxolane, polytetrahydrofurans, copolymers of tetrahydrofuran and oxirane, poly(3,3-bis(chloro-methyl)oxetanes), polysiloxanes, poly(ethylene imine) and polyphosphazenes.[182]



Scheme 1.3: Synthesis of poly(3-isochromanone) via cationic ROP using triflic acid (TfOH) act as a cationic initiator.

1.4.2.3 Anionic ROP

In anionic ROP, a nucleophilic or anionic initiator is used and directly attacks a cyclic monomer to initiate the polymerisation and generates a nucleophilic or anionic group at the end of the propagating polymer chain. Electrophilic or highly strained cyclic monomers are highly susceptible to anionic ROP, including epoxides, episulfides, lactones, cyclic carbonates (**Scheme 1.4**) and lactams.[183]



Scheme 1.4: Synthesis of poly(trimethylene carbonate) via anionic ROP. Alkali metal carboxylates, including sodium acetate, sodium benzoate, and sodium sorbate promote the ROP of trimethylene carbonate in the presence of an alcohol initiator.

1.4.2.4 Kinetics of ROP

The kinetics of ROP consists of four potential reactions including initiation, propagation, segmental exchange and temporary termination (**Equation 1.26a,b,c,d**).[184]

$$I + M \xrightarrow{k_i} P_1^* \qquad \textbf{(1.26a)}$$

$$P_n^* + M \underset{k_d}{\overset{k_p}{\rightleftharpoons}} P_i^* \qquad \textbf{(1.26b)}$$

$$P_x^* + P_y^* \underset{k_{tr2}}{\overset{k_{tr2}}{\rightleftharpoons}} P_{x\text{-}z}^* + P_{y\text{-}z}^* \qquad \textbf{(1.26c)}$$

$$P_n^* + T \underset{k_a}{\overset{k_{da}}{\rightleftharpoons}} P_i^* \qquad \textbf{(1.26d)}$$

Where I is the initiator, M is the monomer, P is the propagating polymer chain; generally, side reactions (**Equations 1.26c** and **d**) can be minimised and neglected, providing a controlled polymerisation where the rate of initiation (k_i) ≥ the rate of propagation (k_p). Thus the kinetics of ROP are dominated by the initiation and propagation rates. The overall rate of polymerisation (R_p) can be expressed by **Equation 1.27**:

$$R_p = -\frac{d[M]}{dt} = k_p \Sigma \left[P_n^* \right][M] - k_d \Sigma \left[P_n^* \right] \qquad \textbf{(1.27)}$$

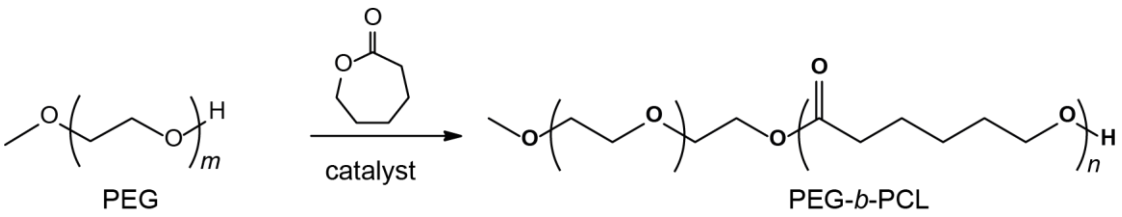
Integration of **Equation 1.27** provides a semilogarithmic relationship between the monomer concentration and reaction time (**Equation 1.28**).

$$\ln \frac{[M]_0 - [M]_{eq}}{[M] - [M]_{eq}} = k_p \sum \left[P_n^* \right] t = k_p [I]_0 \; t = k_{app} \; t \qquad \textbf{(1.28)}$$

As monomer concentration in equilibrium (M_{eq}) is negligible for many ROPs **Equation 1.28** can be simplified and a linear first-order plot of ln ($[M]_0$ / [M]) *vs t* allows the apparent rate of polymer propagation (k_{app}) to be determined. This approach can be used to describe the kinetics of ROP for caprolactone to afford PCL, however, consideration should be given to possible interfering side reactions. In particular, the synthesis of PEG-*b*-PCL block copolymers via ROP can suffer from the initiation of the ROP of caprolactone by impurities (e.g. water) and transesterification reactions, which in many cases is responsible for producing broad *Đ* polymers.[185]

1.4.3 Synthesis of PEG-*b*-PCL copolymers

The common approach presented for synthesis of PEG-*b*-PCL in literature involves ROP of caprolactone initiated by a PEG macroinitiator in the presence of a catalyst, whereby the terminal hydroxyl end-group of the PEG acts as the initiating nucleophilic centre (**Scheme 1.5**). However, the complete synthesis of the copolymer involves two steps, PEG first being prepared via ROP of ethylene oxide followed by ROP of caprolactone.



Scheme 1.5: General scheme showing the synthesis of PEG-*b*-PCL copolymers via ROP of caprolactone, starting from a PEG macroinitiator.

Given the wide commercial availability of well-defined PEG derivatives, they are generally used as starting macroinitiators as the preparation of PEG can be challenging and dangerous without specialist equipment.

1.4.3.1 Synthesis of PEG

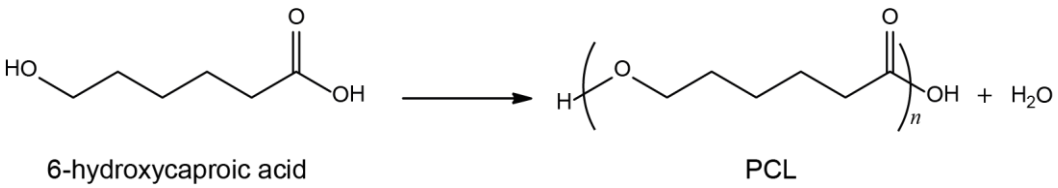
Wurtz first reported the polymerisation of ethylene oxide (EO) in the presence of alkali metal hydroxides in 1859[186] before Staudinger and Schweitzer synthesised and separated a series of PEGs with different molecular weights.[187] In the 1930s PEG became commercially available and was widely used in lubricants, cosmetics and detergents. In 1940 Flory developed a base-initiated polymerisation of EO that represented the first controlled chain-growth process for the production of PEG.[188,189] Nowadays PEG is generally synthesised via oxyanionic or coordination polymerisation.

Oxyanionic polymerisation is the classical approach for the synthesis of PEG from EO using metal alkoxides as initiators. Alkoxides with sodium, potassium or caesium counterions in the presence of polar aprotic solvents (e.g. tetrahydrofuran (THF), dioxane, dimethyl sulfoxide (DMSO), and hexamethylphosphoramide (HMPA)[190]) are the most common initiator systems.[191] Although the mechanism of oxyanionic polymerisation has been well studied,[192-195] this approach only provides access to low molecular weight polymers, and higher molecular weight PEG is synthesised via coordination polymerisation.[196] Coordination polymerisation involves the use of a metal complex to catalyse the polymerisation. Initially, the monomer forms a coordinate complex with the catalyst that activates the monomer resulting in nucleophilic attach from the initiator, ring-opening and formation of a propagating chain that can attack more activated monomer units.[190,196] Dimitrov and Tsvetanov wrote an excellent overview on how to prepare high molecular weight PEG using coordination polymerisation, which covers different aspects of the polymerisation.[197]

1.4.3.2 Synthesis of PCL

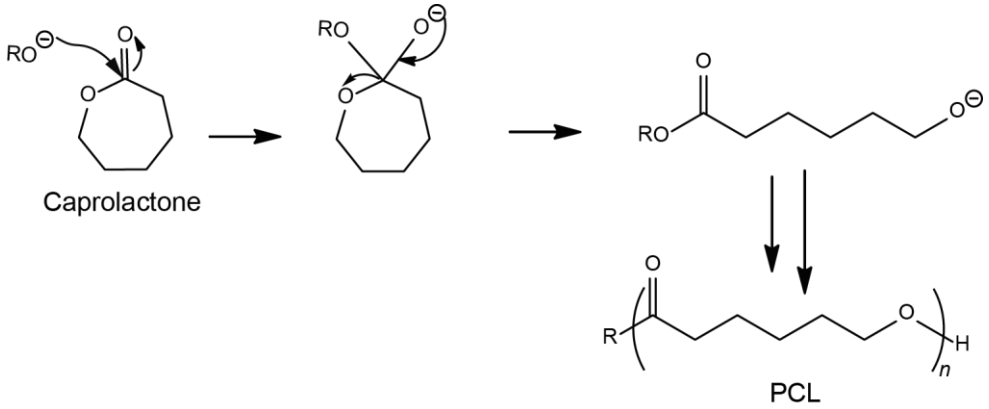
PCL is an aliphatic polyester consisting of hexanoate repeat units and has been extensively used in tissue engineering and drug delivery due to its biodegradability and biocompatibility.[198–200] Whilst the PCL homopolymer is hydrophobic it can easily be incorporated into block copolymers to afford amphiphilic copolymers.[201] PCL can be synthesised via condensation (i.e. step-growth) polymerisation and ROP, although the latter approach is the most popular for producing well-defined narrow $Đ$.

The synthesis of PCL via condensation polymerisation starts from 6-hydroxycaproic acid (6-hydroxyhexanoic acid) as an AB-type monomer (**Scheme 1.6**) using an acid catalyst. However, the major drawback of this approach is the equilibrium that exists between the monomer and polymer. To improve the yield of polymer Braud *et al.* synthesised PCL under vacuum to remove water spontaneously and shift the equilibrium in favour of the polymer.[202] In addition the polycondensation reaction can be conducted using enzyme catalysts, although this results in low monomer conversations and highly polydisperse polymers.[203]



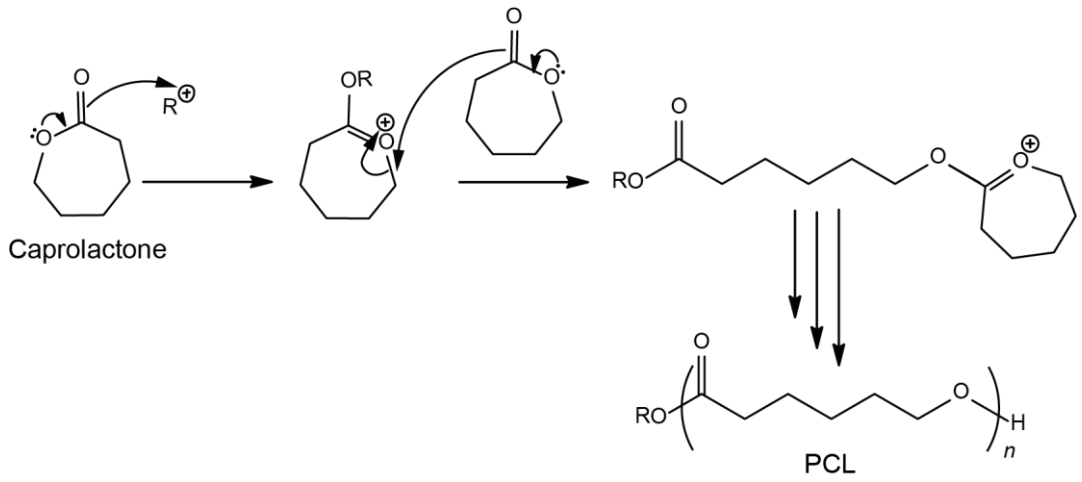
Scheme 1.6: Synthesis of PCL via step-growth condensation polymerisation of the AB-type monomer, 6-hydroxycaproic acid.

The synthesis of PCL via ROP uses caprolactone as the monomer and generally involves an initiator. In some cases, a catalyst can also be used. Anionic ROP involves the use of an anionic initiator (e.g. alkoxide) that attacks the electrophilic carbonyl carbon of the monomer resulting in ring-opening and the generation of a propagating chain with an alkoxide end-group (**Scheme 1.7**). The main problem with synthesising PCL via anionic ROP is that intramolecular back-biting results in the formation of low molecular weight polymers.[204]



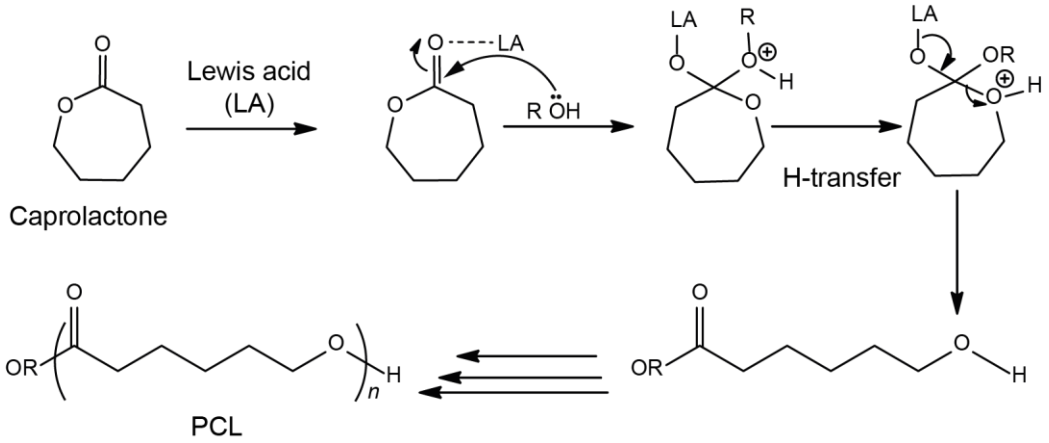
Scheme 1.7: Synthesis of PCL via anionic ROP of caprolactone using an alkoxide initiator. Caprolactone ring opens when an anionic initiator (e.g. alkoxide) attacks the electrophilic carbonyl carbon of the monomer.

In cationic ROP an electrophilic activating agent is used to activate the carbonyl group of the monomer towards nucleophilic attack from another monomer, resulting in ring-opening and the generation of another activated monomer unit at the propagating end of the polymer (**Scheme 1.8**).[204]



Scheme 1.8: Synthesis of PCL via cationic ROP**.** Cationic ROP proceeds via the formation of an activated monomer which is attacked by another monomer through a bimolecular nucleophilic substitution (S_N2) reaction.

In the presence of a lewis acid catalyst and an initiator ROP proceeds via activating the monomer. In that process, the catalyst coordinates to the carbonyl of a monomer resulting in activation towards nucleophilic attack from the initiator and ring-opening resulting in the generation of a hydroxyl end-group at the propagating end of the polymer chain (**Scheme 1.9**).



Scheme 1.9: Synthesis of PCL via monomer activated ROP. Monomer activated ROP involves the activation of the monomer by a lewis acid catalyst, followed by an attack on the activated monomer by the initiator or a propagating polymer chain.

Various catalysts have been used for the ROP of caprolactone and can be classified as metal-based, enzymatic or organic (**Table 1.11**). In **Table 1.12,** polymerisation of PCL initiated by PEG under different conditions is presented.

Table 1.11: Catalysts used in ROP of caprolactone.

Catalyst	Technique	Solvent	[M]:[C]:[I]	M_w (kDa)	T (°C)	Conv (%)	Reaction time	Reference
Lithium diisopropylamide	Anionic	Dioxane	5:1	5.7	25	100	5 min	[205]
Phenyl lithium		None	100:1	77	170	85	120 min	[206]
Cyclopentadienyl sodium		Toluene	250:1	11.6	20	98	60 min	[207]
Magnesium complex	Anionic	Toluene	500:1	47	20		15 min	[208]
Magnesium aryloxide		Toluene	200:0.5:1	19	56	99	180 min	[209]
Calcium complex		Toluene	100:1	22.8	18	10	10 min	[210]
Aluminum Triflate	coordination	none	120:0.3:1	18.4	60		6 h	[211]
Triethyl aluminiumamine		toluene	43:1:3	3.8	40	100	23 h	[212]
Stannous(II) ethylhexanoate		toluene	50:1:1	2.4	110	40	42 h	[212]
Transition metal complexes		toluene	100:1	2.1	20		24 h	[213]

Table 1.12: Conditions used for the synthesis of PEG-*b*-PCL block copolymers and their molecular weight characteristics.

Catalyst	Solvent	M_n of PCL (kDa)	$Đ$	T (ºC)	Conv. (%)	Reaction time	Purification method	Reference
1 M HCl solution	DCM	6.7	1.29	25	92	24 h	Precipitation in hexane	[214]
Stannous(II) ethylhexanoate	Toluene	9.7	-	140	-	-	Precipitation in hexane	[215]
Novozym 435 (lipase)	Toluene	20	1.4	70	95	-	Precipitation in cold methanol	[216]
Stannous(II) ethylhexanoate	Bulk	5	1.08	120	-	24 h	-	[217]
Stannous(II) ethylhexanoate	Bulk	6	-	120	-	12 h	Precipitation in diethyl ether	[218]
Stannous(II) ethylhexanoate	Toluene	19.8	1.59	140	-	24 h	Precipitation in cold methanol	[219]
Stannous(II) ethylhexanoate	Toluene	11.8	1.30	110	-	18 h	Precipitation in diethyl ether	[220]
Stannous(II) ethylhexanoate	Bulk	3.1	1.7	150	-	-	precipitation in diethyl ether	[220]
Calcium ammoniate	Bulk	19.8	-	25		-	precipitation in diethyl ether	[221]

1.4.4 PEG-*b*-PCL copolymer characterisations

The characterisation of block copolymers such as PEG-*b*-PCL may involve the determination of physicochemical properties (i.e., solubility, thermal behaviour and crystallinity), or structural analysis using NMR spectroscopy, size exclusion chromatography (SEC) (also known as GPC) and mass spectrometry (MS).

1.4.4.1 Thermal analysis of polymers

For thermoplastic polymers, the thermal analysis of the polymer is very important and provides information about the melting, crystallisation and phase transitions (e.g. liquid to crystal and glass transitions).[222] The thermal properties of a polymer are related to their tendency to crystallise. The thermal analysis of polymers is usually conducted using differential scanning calorimetry (DSC), thermal gravimetric analysis (TGA), and thermal optical analysis.

The basic principle of DSC involves the determination of the difference in heat flow between the polymer sample and blank reference. Usually, the sample will consume or release thermal energy during the phase transition (solid to liquid, or liquid to solid) and as a result, the heat flow will vary relative to the reference. DSC analysis provides information about the melting temperature (T_m), crystallisation temperature (T_c) and glass transition temperature (T_g), as well as the associated enthalpy changes.[223]

The TGA of polymers is performed to determine the thermal degradation of a polymer. Polymers thermally degrade upon heating which is quantified on the basis of weight loss during a heating cycle. TGA measures the loss of mass during heating of the polymer which provides important information about thermal stability.[224]

The crystalline structure of a polymer is important because it regulates physical and chemical characteristics.[225] The polymer crystallinity is mainly analysed by microscopic techniques, for example, polarised optical microscope (POM) and transmission electron microscopy (TEM).[225] In addition, X-ray diffraction techniques, including wide-angle X-ray diffraction (WXRD) and small-angle X-ray diffraction (SAXS) have also been used.[226]

The crystallinity of PEG-*b*-PCL has been studied to establish a relationship between the architecture of the polymer and its crystalline behaviour. An *et al.* investigated the relationship between polymer microstructure and thermal characteristics for different PCL-*b*-PEG-*b*-PCL triblock copolymers with various PEG and PCL molecular weights.[227] They concluded that when a single block is much larger in length compared to the other blocks, it dominates the crystallisation behaviour. However, the total molecular weight of the polymers studied, and the individual blocks were all quite short (< 5 kilodalton (kDa)).[227] Bogdanov *et al.* investigated PEG/PCL diblock, triblock and star polymers.[228] Using PEG-*b*-PCL block copolymers with PEG and PCL blocks $M_n \geq 4$ kDa, they established that in all cases the PCL block crystallised first, which led to imperfect crystallisation of the PEG block.[228] DSC of the polymers showed multiple melting and crystallisation temperatures which were attributed to the microphase separation of the PEG and PCL blocks. While both of these studies investigated the effect of large PCL blocks on the thermal properties of the copolymers, they did not consider the effect a larger PEG block.

Chen e*t al.* investigated the effect of different lengths of PCL on the thermal behaviour of PEG-*b*-PCL copolymers which included small PCL blocks compared to the PEG block. This study revealed that the crystallisation and melting temperature of the PEG block decreased with increasing PCL length, while PCL showed the opposite thermal behaviour. They concluded that the ratio between the PEG and PCL length influenced the thermal behaviour of the copolymers.[229] It can be concluded from these studies that the thermal behaviour of PEG/PCL block copolymers is regulated by the architecture of the polymer, the ratio between the blocks, and the molecular weight of the blocks.

1.4.4.2 Structural analysis of polymers

The polymer microstructure refers to the composition, sequence of monomers, tacticity, molecular weight and architecture of the polymer. The microstructure of the polymer controls the physicochemical properties.[230] The most widely used techniques for structural characterisation of polymers include NMR spectroscopy and GPC. NMR analysis, especially ^{1}H NMR spectroscopy is widely used to analyse the microstructure of polymers,[231] in addition to ^{13}C NMR[232] and ^{19}F NMR.[233] ^{1}H NMR spectroscopy can also be used to determine the M_n of polymers via end-group analysis. In a ^{1}H NMR spectrum protons from the repeat unit and polymer end-groups show characteristic resonances (proton signals) at specific chemical shifts. By comparison of the integral values of these signals, the number of repeating units in the polymer can be calculated and converted into the M_n by consideration of the repeat unit molecular weight.[234] However, the M_w cannot be determined by NMR spectroscopy, and generally, GPC characterisation is used to determine the M_w and $Đ$.[235]

GPC separates polymers and analytes on the basis of their hydrated size as they pass through columns that contain porous beads. Small analytes travel through more pores and therefore have longer retention times (also referred to as retention volumes), whereas larger analytes only travel through some pores so will have shorter retention times. On this basis, it is possible to a certain degree to separate polymers and obtain a distribution of polymer molecular weights. The polymers can be detected using different detectors or combinations of detectors, including differential refractive index (DRI), viscosity and light scattering detectors. Depending on what detectors are used in combination affects the accuracy of the molecular weight determination. The use of light scattering (multi-angle light scattering technique[145]) in combination with differential refractive index detectors can provide the absolute molecular weight.

A conventional calibration that only uses a DRI detector provides the molecular weight relative to a set of polymer standards. The latter approach can only provide a relative molecular weight as the change in the hydrated size of a polymer in a particular solvent may be different from that of the standards.

1.4.5 Applications of PEG-*b*-PCL copolymers

PEG-*b*-PCL is widely used for developing DDSs for various drugs due to its ease and adaptable synthesis, prolonged systemic circulation and biocompatibility.[236] A key advantage of PEG-*b*-PCL is its ability to form self-assembled aggregates (e.g. micelles) in aqueous media due to its amphiphilic nature.[237] As the micelle core is hydrophobic it is possible to encapsulate hydrophobic drugs. Several PEG-*b*-PCL-based delivery systems are in different stages of clinical trials in different countries. [238,239] **Table 1.13** summarises the application of PEG-*b*-PCL block copolymers for DDSs.

In addition, PEG-*b*-PCL copolymers have also been used in tissue engineering and wound healing.[240] PEG-*b*-PCL hydrogels along with bone repairing medication, have been used to increase the bone healing rates in the rat model.[241] PEG-*b*-PCL scaffolds have also been used to repair cartilage, with chondrocyte-loaded PEG-PCL hydrogels supporting the formation of collagen.[242] PEG-*b*-PCL scaffolds loaded with human epidermal growth factor (EGF) have been used in skin healing[243] and to repair peripheral nerve regeneration in rat models.[244]

Table 1.13: Examples of PEG-*b*-PCL block copolymers as drug delivery systems.

Drug	Log P of drug	MW of drug (Da)	MW of polymer (kDa)	Drug loading efficacy (%)	Application	Reference
Ovalbumin	−9.9		18.2	12.5	Increased the cellular uptake and activity of the drug due to micelle encapsulation	[245]
Goserelin	− 1.5		-	44.2	Demonstrated site-specific and sustained release of drug	[246]
NAPVSIPQ	− 5.6		18	54.2	Increased the drug efficacy	[247]
Doxorubicin	1.3	543.5	-	95.5	Increased the anti- tumor activity of drug	[248]
Sulforaphane	1.4	177.3	-	86.02	Increased drug activity *in vivo*	[249]
Luteolin	1.4	286.2	-	98.3	Increased drug activity	[250]
SN38	1.4	392.4	10	83.8	Increases drug activity and cellular uptake	[251]
Honokiol	5	266.3	4.7	95-41	Drug loaded micelle shows increased efficacy	[252]
Rapamycin	6	914.2	11.2	50	Prevent bust release of drug and increased drug efficacy	[253]
Rapamycin	6	914.2	11.2	50	Prevent bust release of drug and increased drug efficacy	[253]
Docetaxel	1.6	807.9	6.1	90	Increased drug activity *in vivo* with reduced toxicity in the test animal	[254]

MW= Molecular weight

1.5 Aims and objective of the thesis

1.5.1 Aims of the study

The primary aim of this thesis was to investigate the fundamental aspects of micelle drug delivery systems synthesised from amphiphilic PEG-*b*-PCL block copolymers. The specific aims of the thesis were as follows:

1. Prepare well-defined, high purity PEG-*b*-PCL block copolymers with controlled molecular weights and narrow molecular weight distributions to allow a comprehensive investigation of PEG-*b*-PCL self-assembly in aqueous solutions.
2. Study the self-assembly of the PEG-*b*-PCL block copolymers in water and determine how various microstructural parameters (e.g., PCL:PEG molecular weight ratio and PEG molecular weight) influence the formation of self-assembled aggregates.
3. Study and compare the thermal behaviour of PEG-*b*-PCL block copolymers and their self-assembled aggregates, including T_m, T_c and the order of block crystallisation.
4. Study and compare the self-assembly behaviour of drug-loaded micelle systems using PEG-*b*-PCL block copolymers, and interrogate the effect of different drugs, polymer microstructure and drug loading capacities on micelle formation.

1.5.2 Research objectives

To fulfil the aims, the project was divided into four stages: (i) Synthesis of PEG-*b*-PCL block copolymers; (ii) Synthesis and characterisation of micelles prepared from PEG-*b*-PCL block copolymers; (iii) thermal analysis of PEG-*b*-PCL copolymers and their corresponding micelles, and; (iv) investigation of the self-assembly behaviour of PEG-*b*-PCL copolymers in the presence of drugs.

Stage 1: Synthesis of PEG-b-PCL copolymers

Stage 1 involved the synthesis and characterisation of well-defined PEG-*b*-PCL block copolymers. The copolymers were synthesised via ROP of caprolactone using hydroxyl-terminated PEG as a macroinitiator and $Sn(Oct)_2$ as the catalyst.

Initially, conventional synthetic procedures were trailed, and the polymers were characterised using ^{1}H NMR spectroscopy and GPC. The synthetic protocol was then optimised to afford narrow *Đ* polymers with high purity. The molecular weight ratio of the PCL and PEG blocks were varied to produce a library of copolymers that allowed the effect of copolymer microstructure of their self-assembly to be studied.

Stage 2: Synthesis and characterisation of PEG-b-PCL copolymer aggregates

Self-assembled aggregates (e.g. micelles) were prepared from the previously synthesised PEG-*b*-PCL block copolymers using a solvent evaporation technique. Briefly, this method involved the dissolution of the copolymer in a compatible and volatile, water-miscible organic solvent, acetone. Water was then added, and the organic solvent is allowed to evaporate, resulting in a controlled assembly process. The aggregates were characterised using a range of complementary techniques (PGSTE NMR spectroscopy, DLS and SAXS) to determine how the copolymer microstructure relates to the formation of different aggregates.

Stage 3: Thermal analysis of copolymers and their corresponding aggregates

The thermal behaviour of the PEG-*b*-PCL copolymers was analysed using a combination of DSC and WXRD; the melting and crystallisation behaviour was analysed to establish a correlation between the thermal behaviour, polymer microstructure and self-assembly. This investigation allowed the effect of covalent tethering between the blocks on the thermal behaviour to be interpreted in the bulk and self-assembled states.

Stage 4: Investigation of self-assembly behaviour of copolymers in the presence of drugs

Micelles were synthesised using the PEG-*b*-PCL block copolymers in the presence of drugs — gossypol (high hydrophobicity) and phloretin (low hydrophobicity) — at different loadings to investigate the effect of the drug on the self-assembly process. The self-assembled micelles were characterised using PGSTE NMR spectroscopy and DLS and correlated to the results from unloaded micelles (Stage 2). This enabled us to determine the mechanism of drug-loaded micelle formation and interactions between the different parameters of this process, including polymer microstructure, and the characteristics and loading of the drugs.

1.6 References

1. Bhushan, B., Nature's nanotechnology. *Mech. Eng.* **2012**, *134* (12), 28-32.

2. Autumn, K.; Gravish, N., Gecko adhesion: evolutionary nanotechnology. *Philos. Trans. A. Math. Phys. Eng. Sci.* **2008**, *366* (1870), 1575-90.

3. Yarkoni, O.; Frankel, D. J., 3 - Solving the bio-machine interface–a synthetic biology approach. In *Biomimetic. Technologies.*, Ngo, T. D., Ed. Woodhead Publishing: 2015; pp 53-66.

4. Hwang, J.; Jeong, Y.; Park, J. M.; Lee, K. H.; Hong, J. W.; Choi, J., Biomimetics: forecasting the future of science, engineering, and medicine. *Int. J. Nanomedicine.* **2015**, *10*, 5701-5713.

5. Nassif, M.; El Askary, F., Chapter 7−Nanotechnology and nanoparticles in contemporary dental adhesives. In *Nanobiomaterials in Clinical Dentistry*, Subramani, K.; Ahmed, W.; Hartsfield, J. K., Eds. William Andrew Publishing: 2013; pp 131-164.

6. Mendes, A. C.; Baran, E. T.; Reis, R. L.; Azevedo, H. S., Self-assembly in nature: using the principles of nature to create complex nanobiomaterials.*Wiley Interdiscip. Rev. Nanomed. Nanobiotechnol.***2013**, *5* (6), 582-612.

7. Whitesides, G. M.; Grzybowski, B., Self-assembly at all scales. *Science* **2002**, *295* (5564), 2418.

8. Ariga, K.; Hill, J. P.; Lee, M. V.; Vinu, A.; Charvet, R.; Acharya, S., Challenges and breakthroughs in recent research on self-assembly. *Sci. Technol. Adv. Mater.* **2008**, *9* (1), 014109-014109.

9. Bolu, S. B.; Sanyal, R.; Sanyal, A., Drug delivery systems from self-assembly of dendron-polymer conjugates. *Molecules* **2018**, *23* (7).

10. Grzybowski, B. A.; Wilmer, C. E.; Kim, J.; Browne, K. P.; Bishop, K. J. M., Self-assembly: from crystals to cells. *Soft Matter* **2009**, *5* (6), 1110-1128.

11. Israelachvili, J. N.; Mitchell, D. J.; Ninham, B. W., Theory of self-assembly of hydrocarbon amphiphiles into micelles and bilayers. *J. Chem. Soc. Faraday Trans.***1976**, *72* (0), 1525-1568.

12. Karaborni, S.; Esselink, K.; Hilbers, P. A.; Smit, B.; Karthauser, J.; Van, O. N. M.; Zana, R., Simulating the self-assembly of gemini (dimeric) surfactants. *Science* **1994**, *266* (5183), 254-6.

13. Nagarajan, R.; Ruckenstein, E., Theory of surfactant self-assembly: a predictive molecular thermodynamic approach. *Langmuir* **1991**, *7* (12), 2934-2969.

14. Philp, D.; Stoddart, J. F., Self-Assembly in natural and unnatural Systems. *Angew. Chem. Int. Ed.***1996**, *35* (11), 1154-1196.

15. Rizis, G.; Van de Ven, T. G.M; Eisenberg, A., Crystallinity-driven morphological ripening processes for poly(ethylene oxide)-block-polycaprolactone micelles in water. *Soft Matter* **2014**, *10* (16), 2825-35.

16. Benham, C. J.; Harvey, S.; Olson, W. K.; Sumners, D. W.; Swigon, D., Mathematics of DNA structure, function and interactions. Springer New York: 2010.

17. Sina, A. A. I.; Carrascosa, L. G.; Liang, Z.; Grewal, Y. S.; Wardiana, A.; Shiddiky, M. J. A.; Gardiner, R. A.; Samaratunga, H.; Gandhi, M. K.; Scott, R. J.; Korbie, D.; Trau, M., Epigenetically reprogrammed methylation landscape drives the DNA self-assembly and serves as a universal cancer biomarker. *Nat. Commun.***2018**, *9* (1), 4915.

18. Subramani, K.; Ahmed, W., Chapter 13 - Self-Assembly of proteins and peptides and their applications in bionanotechnology and dentistry. In *Emerging Nanotechnologies in Dentistry*, Subramani, K.; Ahmed, W., Eds. William Andrew Publishing: Boston, 2012; pp 209-224.

19. Pippa, N.; Pispas, S.; Demetzos, C., Polymer self-assembled nanostructures as innovative drug nanocarrier platforms. *Curr. Pharm. Des.* **2016**, *22* (19), 2788-95.

20. Bhure, R.; Mahapatro, A., Surface patterning using self assembled monolayers (SAMs). In *Biomaterials*, American Chemical Society: 2010; Vol. 1054, pp 65-107.

21. Copeland, M. F.; Weibel, D. B., Bacterial swarming: a model system for studying dynamic self-assembly. *Soft matter* **2009**, *5* (6), 1174-1187.

22. Guo, Y. M.; Oike, H.; Aida, T., Chiroptical transcription of helical information through supramolecular harmonization with dynamic helices. *J. Am. Chem. Soc.* **2004**, *126* (3), 716-7.

23. Tominaga, M.; Tashiro, S.; Aoyagi, M.; Fujita, M., Dynamic aspects in host-guest complexation by coordination nanotubes. *Chem. Commun. (Camb)* **2002**, (18), 2038-9.

24. Matsuda, R.; Kitaura, R.; Kitagawa, S.; Kubota, Y.; Belosludov, R. V.; Kobayashi, T. C.; Sakamoto, H.; Chiba, T.; Takata, M.; Kawazoe, Y.; Mita, Y., Highly controlled acetylene accommodation in a metal-organic microporous material. *Nature* **2005**, *436* (7048), 238-41.

25. Allen, T. M., Liposomes. opportunities in drug delivery. *Drugs* **1997**, *54 Suppl 4*, 8-14.

26. Ichimura, K., Photoalignment of liquid-crystal systems. *Chem. Rev.* **2000**, *100* (5), 1847-1874.

27. Menon, G.; Okeke, C.; Krishnan, J., Modelling compartmentalization towards elucidation and engineering of spatial organization in biochemical pathways. *Sci. Rep.* **2017**, *7* (1), 12057.

28. Peetla, C.; Stine, A.; Labhasetwar, V., Biophysical interactions with model lipid membranes: applications in drug discovery and drug delivery. *Mol. Pharm.* **2009**, *6* (5), 1264-1276.

29. Kim, S. C.; Kim, D. W.; Shim, Y. H.; Bang, J. S.; Oh, H. S.; Wan Kim, S.; Seo, M. H., In vivo evaluation of polymeric micellar paclitaxel formulation: toxicity and efficacy. *J. Control. Release.* **2001**, *72* (1-3), 191-202.

30. Ameller, T.; Marsaud, V.; Legrand, P.; Gref, R.; Barratt, G.; Renoir, J. M., Polyester-poly(ethylene glycol) nanoparticles loaded with the pure antiestrogen RU58668: Physicochemical and opsonization properties. *Pharm. Res.* **2003**, *20* (7), 1063-1070.

31. De Faria, T. J.; De Campos, A. M.; Senna, E. L., Preparation and characterisation of poly(D,L-Lactide) (PLA) and poly(D,L-Lactide)-poly(Ethylene Glycol) (PLA-PEG) nanocapsules containing antitumoral agent methotrexate. *Macromol. Symp.* **2005**, *229*, 228-233.

32. Meng, F.; Hiemstra, C.; Engbers, G. H. M.; Feijen, J., Biodegradable polymersomes. *Macromolecules* **2003**, *36* (9), 3004-3006.

33. Kim, S. Y.; Lee, Y. M.; Shin, H. J.; Kang, J. S., Indomethacin-loaded methoxy poly(ethylene glycol)/poly(ε-caprolactone) diblock copolymeric nanosphere: Pharmacokinetic characteristics of indomethacin in the normal Sprague-Dawley rats. *Biomaterials* **2001**, *22* (14), 2049-2056.

34. Ahmed, F.; Discher, D. E., Self-porating polymersomes of PEG-PLA and PEG-PCL: Hydrolysis-triggered controlled release vesicles. *J. Control. Release.* **2004**, *96* (1), 37-53.

35. Allen, C.; Han, J.; Yu, Y.; Maysinger, D.; Eisenberg, A., Polycaprolactone-*b*-poly(ethylene oxide) copolymer micelles as a delivery vehicle for dihydrotestosterone. *J. Control. Release.* **2000**, *63* (3), 275-286.

36. Suh, H.; Jeong, B.; Rathi, R.; Kim, S. W., Regulation of smooth muscle cell proliferation using paclitaxel-loaded poly(ethylene oxide)-poly(lactide/glycolide) nanospheres. *J. Biomed. Mater. Res.* **1998**, *42* (2), 331-338.

37. Yoo, H. S.; Park, T. G., Biodegradable polymeric micelles composed of doxorubicin conjugated PLGA-PEG block copolymer. *J. Control. Release.* **2001**, *70* (1-2), 63-70.

38. Alexandridis, P.; Holzwarth, J. F.; Hatton, T. A., Micellization of poly(ethylene oxide)-poly(propylene oxide)-poly(ethylene oxide) triblock copolymers in aqueous solutions: Thermodynamics of copolymer Association. *Macromolecules* **1994**, *27* (9), 2414-2425.

39. Valle, J. W.; Armstrong, A.; Newman, C.; Alakhov, V.; Pietrzynski, G.; Brewer, J.; Campbell, S.; Corrie, P.; Rowinsky, E. K.; Ranson, M., A phase 2 study of SP1049C, doxorubicin in P-glycoprotein-targeting pluronics, in patients with advanced adenocarcinoma of the esophagus and gastroesophageal junction. *Invest. New. Drug.***2011**, *29* (5), 1029-1037.

40. Lian, T.; Ho, R. J., Trends and developments in liposome drug delivery systems. *J. Pharm. Sci.* **2001**, *90* (6), 667-80.

41. Immordino, M. L.; Dosio, F.; Cattel, L., Stealth liposomes: review of the basic science, rationale, and clinical applications, existing and potential. *Int. J. Nanomedicine.* **2006**, *1* (3), 297-315.

42. Portney, N. G.; Ozkan, M., Nano-oncology: drug delivery, imaging, and sensing. *Anal. Bioanal. Chem.* **2006**, *384* (3), 620-30.

43. Koo, O. M.; Rubinstein, I.; Onyuksel, H., Role of nanotechnology in targeted drug delivery and imaging: a concise review. *Nanomed. Nanotechnol. Biol. Med.* **2005**, *1* (3), 193-212.

44. Fassas, A.; Anagnostopoulos, A., The use of liposomal daunorubicin (DaunoXome) in acute myeloid leukemia. *Leuk. Lymphoma.* **2005**, *46* (6), 795-802.

45. Seetharamu, N.; Kim, E.; Hochster, H.; Martin, F.; Muggia, F., Phase II study of liposomal cisplatin (SPI-77) in platinum-sensitive recurrences of ovarian cancer. *Anticancer Res.* **2010**, *30* (2), 541-545.

46. Wittgen, B. P. H.; Kunst, P. W. A.; Perkins, W. R.; Lee, J. K.; Postmus, P. E., Assessing a system to capture stray aerosol during inhalation of nebulized liposomal cisplatin. *J Aerosol Med* **2006**, *19* (3), 385-391.

47. Sarris, A. H.; Hagemeister, F.; Romaguera, J.; Rodriguez, M. A.; McLaughlin, P.; Tsimberidou, A. M.; Medeiros, L. J.; Samuels, B.; Pate, O.; Oholendt, M.; Kantarjian, H.; Burge, C.; Cabanillas, F., Liposomal vincristine in relapsed non-Hodgkin's lymphomas: early results of an ongoing phase II trial. *Ann. Oncol.* **2000**, *11* (1), 69-72.

48. Offner, F.; Krcmery, V.; Boogaerts, M.; Doyen, C.; Engelhard, D.; Ribaud, P.; Cordonnier, C.; De Pauw, B.; Durrant, S.; Marie, J.-P.; Moreau, P.; Guiot, H.; Samonis, G.; Sylvester, R.; Herbrecht, R.; Liposomal Nystatin in patients with Invasive Aspergillosis Refractory to or intolerant of Amphotericin B. *Antimicrob. Agents Chemother* .**2004**, *48* (12), 4808-4812.

49. Dragovich, T.; Mendelson, D.; Kurtin, S.; Richardson, K.; Von Hoff, D.; Hoos, A., A Phase 2 trial of the liposomal DACH platinum L-NDz in patients with therapy-refractory advanced colorectal cancer. *Cancer Chemother. Pharmacol* **2006**, *58* (6), 759-764.

50. Booser, D. J.; Esteva, F. J.; Rivera, E.; Valero, V.; Esparza-Guerra, L.; Priebe, W.; Hortobagyi, G. N., Phase II study of liposomal annamycin in the treatment of doxorubicin-resistant breast cancer. *Cancer Chemother. Pharmacol* **2002,** *50* (1), 6-8.

51. Koshkaryev, A.; Sawant, R.; Deshpande, M.; Torchilin, V., Immunoconjugates and long circulating systems: Origins, current state of the art and future directions. *Adv. Drug. Del. Rev.* **2013**, *65* (1), 24-35.

52. Torchilin, V. P., Recent advances with liposomes as pharmaceutical carriers. *Nat. Rev. Drug Discov.* **2005**, *4* (2), 145-160.

53. Kedar, U.; Phutane, P.; Shidhaye, S.; Kadam, V., Advances in polymeric micelles for drug delivery and tumor targeting. *Nanomed. Nanotechnol. Biol. Med.* **2010**, *6* (6), 714-729.

54. Kwon, G. S., Polymeric micelles for delivery of poorly water-soluble compounds. *Crit. Rev. Ther. Drug. Carrier. Syst.* **2003**, *20* (5), 357-403.

55. Tong, R.; Cheng, J., Anticancer polymeric nanomedicines. *Polym. Rev.***2007**, *47* (3), 345-381.

56. Zhang, Z.; Grijpma, D. W.; Feijen, J., Thermo-sensitive transition of monomethoxy poly(ethylene glycol)-block-poly(trimethylene carbonate) films to micellar-like nanoparticles. *J. Control. Release.* **2006**, *112* (1), 57-63.

57. Lavasanifar, A.; Samuel, J.; Kwon, G. S., Poly(ethylene oxide)-block-poly(L-amino acid) micelles for drug delivery. *Adv. Drug. Deliv. Rev.* **2002**, *54* (2), 169-90.

58. Yu, M. K.; Park, J.; Jon, S., Targeting strategies for multifunctional nanoparticles in cancer imaging and therapy. *Theranostics* **2012**, *2* (1), 3-44.

59. Lukyanov, A. N.; Torchilin, V. P., Micelles from lipid derivatives of water-soluble polymers as delivery systems for poorly soluble drugs. *Adv. Drug. Del. Rev.* **2004**, *56* (9), 1273-1289.

60. Park, E. K.; Lee, S. B.; Lee, Y. M., Preparation and characterisation of methoxy poly(ethylene glycol)/poly(epsilon-caprolactone) amphiphilic block copolymeric nanospheres for tumor-specific folate-mediated targeting of anticancer drugs. *Biomaterials* **2005**, *26* (9), 1053-61.

61. Letchford, K.; Burt, H., A review of the formation and classification of amphiphilic block copolymer nanoparticulate structures: micelles, nanospheres, nanocapsules and polymersomes. *Eur. J. Pharm. Biopharm.* **2007**, *65* (3), 259-69.

62. Zhang, J.; Wu, M.; Yang, J.; Wu, Q.; Jin, Z., Anionic poly (lactic acid)-polyurethane micelles as potential biodegradable drug delivery carriers. *Colloids Surf. A Physicochem. Eng. Asp.* **2009**, *337* (1–3), 200-204.

63. Gaucher, G.; Dufresne, M.-H.; Sant, V. P.; Kang, N.; Maysinger, D.; Leroux, J.-C., Block copolymer micelles: preparation, characterisation and application in drug delivery. *J. Control. Release.* **2005**, *109* (1–3), 169-188.

64. Torchilin, V. P., Micellar nanocarriers: Pharmaceutical perspectives. *Pharm. Res.* **2007**, *24* (1), 1-16.

65. Ahn, H. K.; Jung, M.; Sym, S. J.; Shin, D. B.; Kang, S. M.; Kyung, S. Y.; Park, J.-W.; Jeong, S. H.; Cho, E. K., A phase II trial of Cremorphor EL-free paclitaxel (Genexol-PM) and gemcitabine in patients with advanced non-small cell lung cancer. *Cancer. Chemother. Pharmacol.* **2014**, *74* (2), 277-282.

66. Nishiyama, N.; Okazaki, S.; Cabral, H.; Miyamoto, M.; Kato, Y.; Sugiyama, Y.; Nishio, K.; Matsumura, Y.; Kataoka, K., Novel cisplatin-incorporated polymeric micelles can eradicate solid tumors in mice. *Cancer. Res.* **2003**, *63* (24), 8977-83.

67. Vega, J.; Ke, S.; Fan, Z.; Wallace, S.; Charsangavej, C.; Li, C., Targeting doxorubicin to epidermal growth factor receptors by site-specific conjugation of C225 to poly(L-glutamic acid) through a polyethylene glycol spacer. *Pharm. Res.* **2003**, *20* (5), 826-32.

68. Yoo, H. S.; Park, T. G., Folate receptor targeted biodegradable polymeric doxorubicin micelles. *J. Control. Release.* **2004**, *96* (2), 273-83.

69. Anton, N.; Benoit, J. P.; Saulnier, P., Design and production of nanoparticles formulated from nano-emulsion templates-a review. *J. Control. Release.* **2008**, *128* (3), 185-99.

70. Prabhu, R. H.; Patravale, V. B.; Joshi, M. D., Polymeric nanoparticles for targeted treatment in oncology: current insights. *Int. J. Nanomedicine.* **2015**, *10*, 1001-1018.

71. Mora-Huertas, C. E.; Fessi, H.; Elaissari, A., Polymer-based nanocapsules for drug delivery. *Int. J. Pharm.* **2010,** *385* (1–2), 113-142.

72. Lu, Y.; Park, K., Polymeric micelles and alternative nanonized delivery vehicles for poorly soluble drugs. *Int. J. Pharm.* **2013**, *453* (1), 198-214.

73. Lee, K. S.; Chung, H. C.; Im, S. A.; Park, Y. H.; Kim, C. S.; Kim, S. B.; Rha, S. Y.; Lee, M. Y.; Ro, J., Multicenter phase II trial of Genexol-PM, a Cremophor-free, polymeric micelle formulation of paclitaxel, in patients with metastatic breast cancer. *Breast Cancer Res. Treat.* **2008**, *108* (2), 241-250.

74. Kim, D. W.; Kim, S. Y.; Kim, H. K.; Kim, S. W.; Shin, S. W.; Kim, J. S.; Park, K.; Lee, M. Y.; Heo, D. S., Multicenter phase II trial of Genexol-PM, a novel Cremophor-free, polymeric micelle formulation of paclitaxel, with cisplatin in patients with advanced non-small-cell lung cancer. *Ann. Oncol.* **2007**, *18* (12), 2009-2014.

75. Pérez-Herrero, E.; Fernández-Medarde, A., Advanced targeted therapies in cancer: Drug nanocarriers, the future of chemotherapy. *Eur. J. Pharm. Biopharm.* **2015**, *93*, 52-79.

76. Lee, S. W.; Yun, M. H.; Jeong, S. W.; In, C. H.; Kim, J. Y.; Seo, M. H.; Pai, C. M.; Kim, S. O., Development of docetaxel-loaded intravenous formulation, Nanoxel-PM™ using polymer-based delivery system. *J. Control. Release.* **2011**, *155* (2), 262-271.

77. Plummer, R.; Wilson, R. H.; Calvert, H.; Boddy, A. V.; Griffin, M.; Sludden, J.; Tilby, M. J.; Eatock, M.; Pearson, D. G.; Ottley, C. J.; Matsumura, Y.; Kataoka, K.; Nishiya, T., A Phase I clinical study of cisplatin-incorporated polymeric micelles (NC-6004) in patients with solid tumours. *Br. J. Cancer* **2011**, *104* (4), 593-598.

78. Schütz, C. A.; Juillerat-Jeanneret, L.; Mueller, H.; Lynch, I.; Riediker, M., Therapeutic nanoparticles in clinics and under clinical evaluation. *Nanomedicine* **2013**, *8* (3), 449-467.

79. Hamaguchi, T.; Kato, K.; Yasui, H.; Morizane, C.; Ikeda, M.; Ueno, H.; Muro, K.; Yamada, Y.; Okusaka, T.; Shirao, K.; Shimada, Y.; Nakahama, H.; Matsumura, Y., A phase I and pharmacokinetic study of NK105, a paclitaxel-incorporating micellar nanoparticle formulation. *Br. J. Cancer* **2007**, *97* (2), 170-176.

80. Hamaguchi, T.; Doi, T.; Eguchi-Nakajima, T.; Kato, K.; Yamada, Y.; Shimada, Y.; Fuse, N.; Ohtsu, A.; Matsumoto, S. I.; Takanashi, M.; Matsumura, Y., Phase I study of NK012, a novel SN-38-incorporating micellar nanoparticle, in adult patients with solid tumors. *Clin. Cancer Res.* **2010**, *16* (20), 5058-5066.

81. Gref, R.; Minamitake, Y.; Peracchia, M. T.; Trubetskoy, V.; Torchilin, V.; Langer, R., Biodegradable long-circulating polymeric nanospheres. *Science* **1994**, *263* (5153), 1600-1603.

82. Soppimath, K. S.; Aminabhavi, T. M.; Kulkarni, A. R.;Rudzinski, W. E., Biodegradable polymeric nanoparticles as drug delivery devices. *J. Control. Release.* **2001**, *70* (1-2), 1-20.

83. Galindo-Rodriguez, S.; Allémann, E.; Fessi, H.; Doelker, E., Physicochemical parameters associated with nanoparticle formation in the salting-out, emulsification-diffusion, and nanoprecipitation methods. *Pharm. Res.* **2004**, *21* (8), 1428-1439.

84. Ringsdorf, H. (1975)., Structure and properties of pharmacologically active polymers. *J. polym. sci. C Polym. Symp.* **1975**, 51: 135-153

85. Larson, N.; Ghandehari, H., Polymeric conjugates for drug delivery. *Chem. Mater.* **2012**, *24* (5), 840-853.

86. Li, C.; Wallace, S., Polymer-Drug Conjugates: Recent development in clinical oncology. *Adv. Drug. Del. Rev.* **2008**, *60* (8), 886-898.

87. Bilim, V., Technology evaluation: PK1, Pfizer/Cancer Research UK *Curr. Opin. Mol. Ther.* **2003**, *5* (3), 326-30.

88. Vasey, P. A.; Kaye, S. B.; Morrison, R.; Twelves, C.; Wilson, P.; Duncan, R.; Thomson, A. H.; Murray, L. S.; Hilditch, T. E.; Murray, T.; Burtles, S.; Fraier, D.; Frigerio, E.; Cassidy, J., Phase I clinical and pharmacokinetic study of PK1 [N-(2-hydroxypropyl)methacrylamide copolymer doxorubicin]: first member of a new class of chemotherapeutic agents-drug-polymer conjugates. Cancer Research Campaign Phase I/II Committee. *Clin Cancer. Res.* **1999**, *5* (1), 83-94.

89. Posey, J. A.; Saif, M. W.; Carlisle, R.; Goetz, A.; Rizzo, J.; Stevenson, S.; Rudoltz, M. S.; Kwiatek, J.; Simmons, P.; Rowinsky, E. K.; Takimoto, C. H.; Tolcher, A. W., Phase 1 study of weekly polyethylene glycol-camptothecin in patients with advanced solid tumors and lymphomas. *Clin Cancer. Res.* **2005**, *11* (21), 7866-71.

90. Meerum Terwogt, J. M.; ten Bokkel Huinink, W. W.; Schellens, J. H.; Schot, M.; Mandjes, I. A.; Zurlo, M. G.; Rocchetti, M.; Rosing, H.; Koopman, F. J.; Beijnen, J. H., Phase I clinical and pharmacokinetic study of PNU166945, a novel water-soluble polymer-conjugated prodrug of paclitaxel. *Anticancer Drugs* **2001**, *12* (4), 315-23.

91. Campone, M.; Rademaker-Lakhai, J. M.; Bennouna, J.; Howell, S. B.; Nowotnik, D. P.; Beijnen, J. H.; Schellens, J. H., Phase I and pharmacokinetic trial of AP5346, a DACH-platinum-polymer conjugate, administered weekly for three out of every 4 weeks to advanced solid tumor patients. *Cancer Chemother. Pharmacol.* **2007**, *60* (4), 523-33.

92. Svenson, S.; Tomalia, D. A., Dendrimers in biomedical applications-reflections on the field. *Adv. Drug. Del. Rev.* **2005**, *57* (15), 2106-2129.

93. Cheng, Y.; Xu, T., The effect of dendrimers on the pharmacodynamic and pharmacokinetic behaviors of non-covalently or covalently attached drugs. *European J. Med. Chem.* **2008**, *43* (11), 2291-2297.

94. D'Emanuele, A.; Attwood, D., Dendrimer-drug interactions. *Adv. Drug. Del. Rev.* **2005**, *57* (15), 2147-2162.

95. Aulenta, F.; Hayes, W.; Rannard, S., Dendrimers: A new class of nanoscopic containers and delivery devices. *Eur. Polym. J.* **2003**, *39* (9), 1741-1771.

96. Lee, C. C.; MacKay, J. A.; Fréchet, J. M. J.; Szoka, F. C., Designing dendrimers for biological applications. *Nat. Biotechnol.***2005**, *23* (12), 1517-1526.

97. Duncan, R.; Izzo, L., Dendrimer biocompatibility and toxicity. *Adv. Drug. Del. Rev.* **2005**, *57* (15), 2215-2237.

98. Malik, N.; Evagorou, E. G.; Duncan, R., Dendrimer-platinate: A novel approach to cancer chemotherapy. *Anti-Cancer Drugs* **1999**, *10* (8), 767-776.

99. Jia, L.; Xu, J. P.; Wang, H.; Ji, J., Polyamidoamine dendrimers surface-engineered with biomimetic phosphorylcholine as potential drug delivery carriers. *Colloids Surf. B* **2011**, *84* (1), 49-54.

100. Gajbhiye, V.; Jain, N. K., The treatment of Glioblastoma Xenografts by surfactant conjugated dendritic nanoconjugates. *Biomaterials* **2011**, *32* (26), 6213-6225.

101. Al-Jamal, K. T.; Al-Jamal, W. T.; Wang, J. T. W.; Rubio, N.; Buddle, J.; Gathercole, D.; Zloh, M.; Kostarelos, K., Cationic poly-L-Lysine dendrimer complexes doxorubicin and delays tumor growth in vitro and in vivo. *ACS Nano* **2013**, *7* (3), 1905-1917.

102. Wolinsky, J. B.; Grinstaff, M. W., Therapeutic and diagnostic applications of dendrimers for cancer treatment. *Adv. Drug. Del. Rev.* **2008**, *60* (9), 1037-1055.

103. Pérez-Herrero, E.; Fernández-Medarde, A., Advanced targeted therapies in cancer: Drug nanocarriers, the future of chemotherapy. *Eur. J. Pharm. Biopharm.* **2015**, *93*, 52-79.

104. Zhang Y, Huang Y, Li S. Polymeric micelles: nanocarriers for cancer-targeted drug delivery. *AAPS Pharm,SciTech.* **2014**;15(4):862–871.

105. Gong, J.; Chen, M.; Zheng, Y.; Wang, S.;Wang, Y., Polymeric micelles drug delivery system in oncology. *J. Control. Release.* **2012**, *159* (3), 312-323.

106. Banik, B. L.; Fattahi, P.; Brown, J. L., Polymeric nanoparticles: the future of nanomedicine. *Wiley Interdiscip.Rev.Nanomed.Nanobiotechnol* .**2016**, *8* (2), 271-299.

107. Negishi, T.; Koizumi, F.; Uchino, H.; Kuroda, J.; Kawaguchi, T.; Naito, S.; Matsumura, Y., NK105, a paclitaxel-incorporating micellar nanoparticle, is a more potent radiosensitising agent compared to free paclitaxel. *Br. J. Cancer* **2006**, *95* (5), 601-606.

108. Lee, K. S.; Chung, H. C.; Im, S. A.; Park, Y. H.; Kim, C. S.; Kim, S.-B.; Rha, S. Y.; Lee, M. Y.; Ro, J., Multicenter phase II trial of Genexol-PM, a Cremophor-free, polymeric micelle formulation of paclitaxel, in patients with metastatic breast cancer. *Breast Cancer Res. Treat.* **2008**, *108* (2), 241-250.

109. Cui, X.; Mao, S.; Liu, M.; Yuan, H.; Du, Y., Mechanism of surfactant micelle formation. *Langmuir* **2008**, *24* (19), 10771-10775.

110. Tanford, C., The Hydrophobic Effect: Formation of micelles and biological membranes. Krieger: 1991.

111. Fujiwara, S.; Itoh, T.; Hashimoto, M.; Tamura, Y., Molecular dynamics simulation of micelle formation in amphiphilic solution. *Mol. Simul.* **2007**, *33* (1-2), 115-119.

112. Blandamer, M. J.; Cullis, P. M.; Soldi, L. G.; Engberts, J. B. F. N.; Kacperska, A.; Van Os, N. M.; Subha, M. C. S., Thermodynamics of micellar systems: Comparison of mass action and phase equilibrium models for the calculation of standard Gibbs energies of micelle formation. *Adv. Colloid Interface Sci.* **1995**, *58* (2), 171-209.

113. Heald, C. R.; Stolnik, S.; Kujawinski, K. S.; De Matteis, C.; Garnett, M. C.; Illum, L.; Davis, S. S.; Purkiss, S. C.; Barlow, R. J.; Gellert, P. R., Poly(lactic acid)-poly(ethylene oxide) (PLA-PEG) nanoparticles: NMR studies of the central solidlike PLA core and the liquid PEG corona. *Langmuir* **2002**, *18* (9), 3669-3675.

114. Riley, T.; Stolnik, S.; Heald, C. R.; Xiong, C. D.; Garnett, M. C.; Illum, L.; Davis, S. S.; Purkiss, S. C.; Barlow, R. J.; Gellert, P. R., Physicochemical evaluation of nanoparticles assembled from poly(lactic acid)-poly(ethylene glycol) (PLA-PEG) block copolymers as drug delivery vehicles. *Langmuir* **2001**, *17* (11), 3168-3174.

115. Milchev, A.; Bhattacharya, A.; Binder, K., Formation of block copolymer micelles in solution: A Monte Carlo Study of chain length dependence. *Macromolecules* **2001**, *34* (6), 1881-1893.

116. Hadgiivanova, R.; Diamant, H., Premicellar aggregation of amphiphilic molecules. *J. Phys. Chem. B* **2007**, *111* (30), 8854-8859.

117. Nicholas, C. V.; Luo, Y.-Z.; Deng, N.-J.; Attwood, D.; Collett, J. H.; Price, C.; Booth, C., Effect of chain length on the micellization and gelation of block copoly(oxyethylene/oxybutylene/oxyethylene) $E_mB_nE_m$. *Polymer* **1993**, *34* (1), 138-144.

118. Yang, Y.-W.; Yang, Z.; Zhou, Z.-K.; Attwood, D.; Booth, C., Association of triblock copolymers of ethylene oxide and butylene oxide in aqueous Solution: A study of $B_nE_mB_n$ copolymers. *Macromolecules* **1996**, *29* (2), 670-680.

119. Rager, T.; Meyer, W. H.; Wegner, G.; Winnik, M. A., Influence of chain length and salt concentration on block copolymer micellization. *Macromolecules* **1997**, *30* (17), 4911-4919.

120. Szczubialka, K.; Ishikawa, K.; Morishima, Y., Micelle formation of diblock copolymers of styrene and sulfonated isoprene in aqueous solution. *Langmuir* **1999**, *15* (2), 454-462.

121. Halperin, A., Polymeric micelles: A star model. *Macromolecules* **1987**, *20* (11), 2943-2946.

122. Zhang, L.; Eisenberg, A., Multiple morphologies of "Crew-Cut" aggregates of Polystyrene-b-poly(acrylic acid) block copolymers. *Science* **1995**, *268* (5218), 1728.

123. Zhang, L.; Eisenberg, A., Multiple morphologies and characteristics of "Crew-Cut" micelle-like aggregates of Polystyrene-b-poly(acrylic acid) diblock copolymers in aqueous Solutions. *J. Am. Chem. Soc.* **1996**, *118* (13), 3168-3181.

124. Zhang, L.; Eisenberg, A., Formation of crew-cut aggregates of various morphologies from amphiphilic block copolymers in solution. *Polym. Adv. Technol.* **1998**, *9* (10-11), 677-699.

125. Gaucher, G.; Dufresne, M. H.; Sant, V. P.; Kang, N.; Maysinger, D.; Leroux, J. C., Block copolymer micelles: Preparation, characterisation and application in drug delivery. *J. Control. Release.* **2005**, *109* (1-3), 169-188.

126. Vangeyte, P.; Gautier, S.; Jérôme, R., About the methods of preparation of poly(ethylene oxide)-b-poly(ε-caprolactone) nanoparticles in water: Analysis by dynamic light scattering. *Colloids Surf. A Physicochem. Eng. Asp.* **2004**, *242* (1), 203-211.

127. Khoshnood, A.; Lukanov, B.; Firoozabadi, A., Temperature effect on micelle formation: Molecular Thermodynamic model revisited. *Langmuir* **2016**, *32* (9), 2175-2183.

128. Chandler, D., Hydrophobicity: two faces of water. *Nature* **2002**, *417* (6888), 491.

129. Lum, K.; Chandler, D.; Weeks, J. D., Hydrophobicity at small and large length scales. *J. Phys. Chem. B* **1999**, *103* (22), 4570-4577.

130. Maibaum, L.; Dinner, A. R.; Chandler, D., Micelle formation and the hydrophobic effect. *J. Phys. Chem. B* **2004**, *108* (21), 6778-6781.

131. Tanford, C., Thermodynamics of micelle formation: Prediction of micelle size and size distribution. *Proceedings of the National Academy of Sciences of the United States of America* **1974**, *71* (5), 1811-1815.

132. Hulst, H. C.; Van de Hulst, H. C., Light scattering by small particles. Dover Publications: 1981.

133. Chýlekt, P., Light scattering by small particles in an absorbing medium. *J. Opt. Soc. Am.***1977**, *67* (4), 561-563.

134. Bottlinger, M.; Umhauer, H., Single particle light scattering size analysis: Quantification and elimination of the effect of particle shape and structure. *Part. Part Syst. Charact.***1989**, *6* (1-4), 100-109.

135. Rayleigh, J. W. S., In *The collected optics papers of Lord Rayleigh.* Optical Society of America: 1994

136. Misono, T., Static Light Scattering (SLS). In *Measurement Techniques and Practices of Colloid and Interface Phenomena*, Abe, M., Ed. Springer Singapore: Singapore, 2019; pp 59-64.

137. Kerker, M., CHAPTER 3 - Scattering by a Sphere. In *The Scattering of Light and Other Electromagnetic Radiation*, Kerker, M., Ed. Academic Press: 1969; Vol. 16, pp 27-96.

138. Debye, P., Zerstreuung von Röntgenstrahlen. *Annalen. Der. Physik.* **1915**, *351* (6), 809-823.

139. Chu, B., IV - photon correlation spectroscopy. In *Laser Light Scattering (Second Edition)*, Chu, B., Ed. Academic Press: 1991; pp 93-136.

140. Miller, C. C.; Walker, J., The Stokes-Einstein law for diffusion in solution. *Proceedings of the Royal Society of London. Series A, Containing Papers of a Mathematical and Physical Character* **1924**, *106* (740), 724-749.

141. Fischer, K.; Schmidt, M., Pitfalls and novel applications of particle sizing by dynamic light scattering. *Biomaterials* **2016**, *98*, 79-91.

142. Hupfeld, S.; Holsæter, A. M.; Skar, M.; Frantzen, C. B.; Brandl, M., Liposome size analysis by dynamic/static light scattering upon size exclusion-/field flow-fractionation. *J. Nanosci. Nanotechnol.* **2006**, *6* (9-10), 3025-3031.

143. Brown, W.; Schillen, K.; Almgren, M.; Hvidt, S.; Bahadur, P., Micelle and gel formation in a poly(ethylene oxide)/poly(propylene oxide)/poly(ethylene oxide) triblock copolymer in water solution: dynamic and static light scattering and oscillatory shear measurements. *J. Chem. Phys.* **1991**, *95* (4), 1850-1858.

144. Chinai, S. N.; Scherer, P. C.; Levi, D. W., Molecular weight of polyvinyl acetate by light scattering and viscosity techniques. *J. Polym. Sci.* **1955**, *17* (83), 117-124.

145. Hérail, M.; Le Guennec, M.; Le Goff, D.; Proutière, A., Molecular weight determination from light scattering and refraction in solutions. A new and coherent theoretical equation. *J. Mol. Struc-Theochem* **1996**, *380* (3), 171-193.

146. da Silva, G. C.; Rossi, C. G. F. T.; Dantas Neto, A. A.; Dantas, T. N. C.; Fonseca, J. L. C., Characterisation of wormlike micellar systems using DLS, rheometry and tensiometry. *Colloids Surf. A Physicochem. Eng. Asp.* **2011**, *377* (1), 35-43.

147. Dahani, M.; Barret, L. A.; Raynal, S.; Jungas, C.; Pernot, P.; Polidori, A.; Bonneté, F., Use of dynamic light scattering and small-angle X-ray scattering to characterize new surfactants in solution conditions for membrane-protein crystallization. *Acta Cryst. F* **2015**, *71* (Pt 7), 838-846.

148. Topel, Ö.; Çakır, B. A.; Budama, L.; Hoda, N., Determination of critical micelle concentration of polybutadiene-block-poly(ethyleneoxide) diblock copolymer by fluorescence spectroscopy and dynamic light scattering. *J. Mol. Liq.* **2013**, *177*, 40-43.

149. Gracia, C. A.; Gomez-Barreiro, S.; Gonzalez-Perez, A.; Nimo, J.; Rodriguez, J. R., Static and dynamic light-scattering studies on micellar solutions of alkyldimethylbenzylammonium chlorides. *J. Colloid Interface Sci.* **2004**, *276* (2), 408-13.

150. Molina-BolÍVar, J. A.; Aguiar, J.; Peula-GarcÍA, J. M.; Ruiz, C. C., Photophysical and light scattering studies on the aggregation behaviour of Triton X-100 in formamide-water mixed solvents. *Mol. Phys.* **2002**, *100* (20), 3259-3269.

151. Yoshimura, S.; Shirai, S.; Einaga, Y., Light-Scattering characterisation of the wormlike micelles of hexaoxyethylene dodecyl C12E6 and hexaoxyethylene tetradecyl C14E6 ethers in dilute aqueous Solution. *J. Phys. Chem. B* **2004**, *108* (40), 15477-15487.

152. Hua, Z.; Pitto-Barry, A.; Kang, Y.; Kirby, N.; Wilks, T. R.; O'Reilly, R. K., Micellar nanoparticles with tuneable morphologies through interactions between nucleobase-containing synthetic polymers in aqueous solution. *Polym. Chem.* **2016**, *7* (25), 4254-4262.

153. Zubkov, M.; Dennis, G. R.; Stait-Gardner, T.; Torres, A. M.; Willis, S. A.; Zheng, G.; Price, W. S., Physical characterisation using diffusion NMR spectroscopy. *Magn. Reson. Chem.* **2017**, *55* (5), 414-424.

154. Stejskal, E. O.; Tanner, J. E., Spin diffusion measurements: spin echoes in the Presence of a time-dependent field gradient. *J Chem Phys* **1965**, *42* (1), 288-292.

155. Callaghan, P. T.; Stepišnik, J., Generalized Analysis of motion using magnetic field gradients. In *Advances in Magnetic and Optical Resonance*, Warren, W. S., Ed. Academic Press: 1996; Vol. 19, pp 325-388.

156. Williamson, N. H. Parametric distribution model fitting routines for analysing relaxation and diffusion data. https://github.com/nathanwilliamson/NMR_decay_analysis (accessed 22-05-2017).

157. Williamson, N. H.; Nyden, M.; Roding, M., The lognormal and gamma distribution models for estimating molecular weight distributions of polymers using PGSE NMR. *J. Magn. Reson.* **2016**, *267*, 54-62.

158. Williamson, N. H.; Röding, M.; Miklavcic, S. J.; Nydén, M., Scaling exponent and dispersity of polymers in solution by diffusion NMR. *J. Colloid Interface Sci.* **2017**, *493*, 393-397.

159. de Gennes, P. G.; Press, C. U., Scaling Concepts in Polymer PhysicsScience and technology of advanced materials. Cornell University Press: 1979.

160. Augé, S.; Schmit, P.-O.; Crutchfield, C. A.; Islam, M. T.; Harris, D. J.; Durand, E.; Clemancey, M.; Quoineaud, A.-A.; Lancelin, J.-M.; Prigent, Y.; Taulelle, F.; Delsuc, M.-A., NMR measure of translational diffusion and fractal Dimension. application to molecular mass measurement. *J. Phys. Chem. B* **2009**, *113* (7), 1914-1918.

161. Gu, K.; Onorato, J.; Xiao, S. S.; Luscombe, C. K.; Loo, Y.-L., Determination of the molecular weight of conjugated polymers with diffusion-ordered NMR Spectroscopy. *Chem. Mater.* **2018**, *30* (3), 570-576.

162. Guo, X.; Laryea, E.; Wilhelm, M.; Luy, B.; Nirschl, H.; Guthausen, G., Diffusion in polymer solutions: Molecular weight Distribution by PFG-NMR and relation to SEC. *Macromol. Chem. Phys.* **2017**, *218* (1), 1600440.

163. Håkansson, B.; Nydén, M.; Söderman, O., The influence of polymer molecular weight distributions on pulsed field gradient nuclear magnetic resonance self-diffusion experiments. *Colloid Polym. Sci.* **2000**, *278* (5), 399-405.

164. Kuz'mina, N. E.; Moiseev, S. V.; Krylov, V. I.; Yashkir, V. A.; Merkulov, V. A., Determination of the average molecular weight of hydroxyethyl starches by diffusion ordered NMR spectroscopy. *J. Anal. Chem.* **2015**, *70* (1), 32-38.

165. Macchioni, A.; Ciancaleoni, G.; Zuccaccia, C.; Zuccaccia, D., Determining accurate molecular sizes in solution through NMR diffusion spectroscopy. *Chem. Soc. Rev.* **2008**, *37* (3), 479-489.

166. Barrère, C.; Mazarin, M.; Giordanengo, R.; Phan, T. N. T.; Thévand, A.; Viel, S.; Charles, L., Molecular weight determination of block copolymers by pulsed gradient apin echo NMR. *Anal. Chem.* **2009**, *81* (19), 8054-8060.

167. Willis, S. A.; Dennis, G. R.; Zheng, G.; Price, W. S., Hydrodynamic size and scaling relations for linear and 4 arm star PVAC studied using PGSE NMR. *J. Mol. Liq.* **2010**, *156* (1), 45-51.

168. Willis, S. A.; Price, W. S.; Eriksson-Scott, I. K.; Zheng, G.; Dennis, G. R., Influence of polymer architecture on the averaging effects in PGSE NMR attenuations for bimodal solutions of linear and star poly(vinyl acetates). *J. Mol. Liq.* **2012**, *167*, 110-114.

169. Furó, I., NMR spectroscopy of micelles and related systems. *J. Mol. Liq.* **2005**, *117* (1), 117-137.

170. Law, S. J.; Britton, M. M., Sizing of reverse micelles in microemulsions using NMR measurements of diffusion. *Langmuir* **2012**, *28* (32), 11699-11706.

171. Balinov, B.; Olsson, U.; Soederman, O., Structural similarities between the L3 and bicontinuous cubic phases in the AOT-brine system. *J. Chem. Phys.* **1991**, *95* (15), 5931-5936.

172. Guéring, P.; Lindman, B., Droplet and bicontinuous structures in microemulsions from multicomponent self-diffusion measurements. *Langmuir* **1985**, *1* (4), 464-468.

173. Jonströmer, M.; Jönsson, B.; Lindman, B., Self-diffusion in nonionic surfactant-water systems. *J. Phys. Chem.* **1991**, *95* (8), 3293-3300.

174. Halasa, A. F., Recent Advances in anionic polymerization. *Rubber Chem. Technol.***1981**, *54* (3), 627-640.

175. Jenkins, A. D.; Kratochvíl, P.; Stepto, R. F. T.; Suter, U. W., Glossary of basic terms in polymer science (IUPAC Recommendations 1996). *Pure Appl Chem*, 1996; Vol. 68, p 2287.

176. Rudin, A., Chapter 6 - Free-Radical Polymerization. In *Elements of Polymer Science and Engineering (Second Edition)*, Rudin, A., Ed. Academic Press: San Diego, 1999; pp 189-239.

177. Webster, O. W., Living Polymerization Methods. *Science* **1991**, *251* (4996), 887.

178. Jennings, J.; He, G.; M. Howdle, S.; Zetterlund, P., Block copolymer synthesis by controlled/living radical polymerization in heterogeneous systems. 2016; Vol. 45.

179. Nuyken, O.; Pask, D. S., Ring-opening p[olymerization—An introductory review. *Polymers* **2013**, *5* (2).

180. McGrath, J. E., Ring-opening polymerization: Introduction in ring-opening polymerization, American Chemical Society: 1985; Vol. 286, pp 1-22.

181. Cho, I.; Kim, J.-B., Exploratory ring-opening polymerization. VIII. Radical ring-opening polymerization of 2-phenyl-3-vinyloxirane: A C−C bond scission polymerization of the epoxide ring. *J. Polym. Sci., Polym. Lett. Ed.* **1983**, *21* (6), 433-436

182. Penczek, S., Cationic ring-opening polymerization (CROP) major mechanistic phenomena. *J. Polym. Sc., Part A: Polym. Chem.* **2000**, *38* (11), 1919-1933.

183. Sudo, A., Anionic ring-opening polymerization. In *Encyclopedia of Polymeric Nanomaterials*, Kobayashi, S.; Müllen, K., Eds. Springer Berlin Heidelberg: Berlin, Heidelberg, 2021; pp 1-11.

184. Dubois, P.; Coulembier, O.; Raquez, J. M., Handbook of Ring-Opening Polymerization. Wiley: 2009.

185. Labet, M.; Thielemans, W., Synthesis of polycaprolactone: a review. *Chem. Soc. Rev.* **2009**, *38* (12), 3484-3504.

186. Herzberger, J.; Niederer, K.; Pohlit, H.; Seiwert, J.; Worm, M.; Wurm, F. R.; Frey, H., Polymerization of ethylene oxide, propylene oxide, and Other alkylene oxides: Synthesis, novel polymer architectures, and bioconjugation. *Chem. Rev.* **2016**, *116* (4), 2170-2243.

187. Staudinger, H.; Schweitzer, O., Über Hochpolymere Verbindungen, 20. Mitteil.: Über Die Poly-Äthylenoxyde. *Ber. Dtsch. Chem. Ges.* **1929**, *62* (8), 2395-2405.

188. Flory, P. J., Molecular size distribution in ethylene oxide polymers. *J. Am. Chem. Soc.* **1940,** *62* (6), 1561-1565.

189. Ehrfeld, W.; Hessel, V.; Haverkamp, V., *Ullmann's Encyclopedia of Industrial Chemistry* **1999**.

190. Deffieux, A.; Carlotti, S.; Barrère, A., Anionic ring-opening polymerization of epoxides and related nucleophilic polymerization processes. In *Polymer Science: A Comprehensive Reference, 10 Volume Set*, 2012; Vol. 4, pp 117-140.

191. Deffieux, A.; Boileau, S., Anionic polymerization of ethylene oxide with cryptates as counterions: 1. *Polymer* **1977**, *18* (10), 1047-1050.

192. Tsvetanov, C. B.; Petrova, E. B.; Panayotov, I. M., Polymerization of 1,P-epoxides initiated by tetraalkyl aluminates. I. Polymerization of ethylene oxide in the presence of sodium tetrabutyl aluminate. *J. Macromol. Sci. A.* **1985**, *22* (9), 1309-1324.

193. Arkhipovich, G. N.; Dubrovskii, S. A.; Kazanskii, K. S.; Shupik, A. N., Complexing of Na^+ ion with polyethylene glycol. *Polym. Sci. USSR* **1981**, *23* (7), 1827-1841.

194. Ptitsyna, N. V.; Ovsyannikova, S. V.; Gel'fer, T. M.; Kazanskii, K. S., Synthesis of polyethylene glycols of molecular weight above 10,000 by anionic polymerization. *Polym. Sci. USSR* **1980**, *22* (11), 2779-2786.

195. Kazanskii, K. S., Donor-acceptor and solvation interactions in anionic polymerization of some heterocycles. *Pure Appl. Chem.* **1981**, *53*.

196. Helfferich, F. G., Chapter 10 - Polymerization. In *Comprehensive Chemical Kinetics*, Helfferich, F. G., Ed. Elsevier: 2001; Vol. 38, pp 299-354.

197. Dimitrov, I.; Tsvetanov, C. B., 4.21 - High-Molecular-Weight Poly(ethylene oxide). In *Polymer Science: A Comprehensive Reference*, Matyjaszewski, K.; Möller, M., Eds. Elsevier: Amsterdam, 2012; pp 551-569.

198. Peña, J.; Corrales, T.; Izquierdo-Barba, I.; Doadrio, A. L.; Vallet-Regí, M., Long term degradation of poly(ε-caprolactone) films in biologically related fluids. *Polym. Degrad. Stab.* **2006**, *91* (7), 1424-1432.

199. Jenkins, M. J.; Harrison, K. L.; Silva, M. M. C. G.; Whitaker, M. J.; Shakesheff, K. M.; Howdle, S. M., Characterisation of microcellular foams produced from semi-crystalline PCL using supercritical carbon dioxide. *Eur. Polym. J.* **2006**, *42* (11), 3145-3151.

200. Hutmacher, D. W.; Schantz, T.; Zein, I.; Ng, K. W.; Teoh, S. H.; Tan, K. C., Mechanical properties and cell cultural response of polycaprolactone scaffolds designed and fabricated via fused deposition modeling. *J. Biomed. Mater. Res.* **2001**, *55* (2), 203-216.

201. Cuong, N.-V.; Li, Y.-L.; Hsieh, M.-F., Targeted delivery of doxorubicin to human breast cancers by folate-decorated star-shaped PEG–PCL micelle. *J. Mater. Chem.* **2012**, *22* (3), 1006-1020.

202. Braud, C.; Devarieux, R.; Atlan, A.; Ducos, C.; Michel, V., Capillary zone electrophoresis in normal or reverse polarity separation modes for the analysis of hydroxy acid oligomers in neutral phosphate buffer. *Journal of Chromatography B: Biomedical Sciences and Applications* **1998**, *706* (1), 73-82.

203. Mahapatro, A.; Kumar, A.; Gross, R. A., Mild, Solvent-free ω-hydroxy acid polycondensations catalyzed by *Candida antarctica* Lipase B. *Biomacromolecules* **2004**, *5* (1), 62-68.

204. Khanna, A.; Sudha, Y. S.; Pillai, S.; Rath, S. S., Molecular modeling studies of poly lactic acid initiation mechanisms. *J Mol. Model.* **2008**, *14* (5), 367-374.

205. Bhaw-Luximon, A.; Jhurry, D.; Motala-Timol, S.; Lochee, Y., Polymerization of ε-caprolactone and its copolymerization with γ-butyrolactone using metal complexes. *Macromol. Symp.* **2005**, *231* (1), 60-68.

206. Deng, X.; Yuan, M.; Xiong, C.; Li, X., Polymerization of lactides and lactones. IV. Ring-opening polymerization of ε-caprolactone by rare earth phenyl compounds. *J. Appl. Polym. Sci.***1999**, *73* (8), 1401-1408.

207. Yuan, M.; Xiong, C.; Deng, X., Ring-opening polymerization of ε-caprolactone initiated by cyclopentadienyl sodium. *J. Appl. Polym. Sci.***1998**, *67* (7), 1273-1276.

208. Sánchez-Barba, L. F.; Garcés, A.; Fajardo, M.; Alonso-Moreno, C.; Fernández-Baeza, J.; Otero, A.; Antiñolo, A.; Tejeda, J.; Lara-Sánchez, A.; López-Solera, M. I., Well-defined alkyl heteroscorpionate magnesium complexes as excellent initiators for the ROP of cyclic esters. *Organometallics* **2007**, *26* (25), 6403-6411.

209. Shueh, M.-L.; Wang, Y.-S.; Huang, B.-H.; Kuo, C.-Y.; Lin, C.-C., Reactions of 2,2‘-methylenebis(4-chloro-6-isopropyl-3-methylphenol) and 2,2‘-ethylidenebis(4,6-di-tert-butylphenol) with Mg^nBu_2: Efficient catalysts for ring-opening polymerization of ε-caprolactone and l-lactide. *Macromolecules* **2004**, *37* (14), 5155-5162.

210. Zhong, Z.; Dijkstra, P. J.; Birg, C.; Westerhausen, M.; Feijen, J., A novel and versatile calcium-based initiator system for the ring-opening polymerization of cyclic esters. *Macromolecules* **2001**, *34* (12), 3863-3868.

211. Wang, Y.; Kunioka, M., Ring-opening polymerization of cyclic monomers with aluminum triflate. *Macromol. Symp.* **2005**, *224* (1), 193-206.

212. Dubois, P.; Degee, P.; Jerome, R.; Teyssie, P., Macromolecular engineering of polylactones and polylactides. 8. Ring-opening polymerization of ε-caprolactone initiated by primary amines and trialkylaluminum. *Macromolecules* **1992**, *25* (10), 2614-2618.

213. Davidson, M. G.; Jones, M. D.; Lunn, M. D.; Mahon, M. F., Synthesis and X-ray structures of new Titanium(IV) aryloxides and their exploitation for the ring opening polymerization of ε-caprolactone. *Inorg. Chem.* **2006**, *45* (5), 2282-2287.

214. Kim, M. S.; Hyun, H.; Cho, Y. H.; Seo, K. S.; Jang, W. Y.; Kim, S. K.; Khang, G.; Lee, H. B., Preparation of methoxy poly(ethyleneglycol)-block-poly(caprolactone) via activated monomer mechanism and examination of micellar characterisation. *Polym. Bull.* **2005**, *55* (3), 149-156.

215. Eawsakul, K.; Chinavinijkul, P.; Saeeng, R.; Chairoungdua, A.; Tuchinda, P.; Nasongkla, N., Preparation and Characterisations of RSPP050-loaded polymeric micelles using poly(ethylene glycol)-b-poly(epsilon-caprolactone) and poly(ethylene glycol)-b-poly(D,L-lactide). *Chem. Pharm. Bull. (Tokyo)* **2017**, *65* (6), 530-537.

216. Zhang, Y.; Hou, J.; Qian, C.; Song, L.; Guo, S., Taxol-loaded nanoparticles with methoxy poly(ethylene glycol)-b-poly(ε-caprolactone) as a novel additive in the outer aqueous phase. *J. Appl. Polym. Sci.* **2011**, *121* (4), 2386-2393.

217. Irfan, M.; Bhayo, A. M.; Musharraf, S. G.; Malik, M. I., Chromatographic characterisation of amphiphilic di- and tri-block copolymers of poly(ethylene oxide) and poly(ε-caprolactone). *J. Sep. Sci.* **2018**, *41* (17), 3352-3359.

218. Zhao, L.; Zhang, X.; Liu, X.; Li, J.; Luan, Y., pH-responsive poly(ethylene glycol)-poly(ϵ-caprolactone)-poly(glutamic acid) polymersome as an efficient doxorubicin carrier for cancer therapy. *Polym. Int.* **2017**, *66* (11), 1579-1586.

219. Xu, B.; Yuan, J.; Ding, T.; Gao, Q., Amphiphilic biodegradable poly(ε-caprolactone)-poly(ethylene glycol)-poly(ε-caprolactone) triblock copolymers: synthesis, characterisation and their use as drug carriers for folic acid. *Polym. Bull.* **2010**, *64* (6), 537-551.

220. Koutroumanis, K. P.; Holdich, R. G.; Georgiadou, S., Synthesis and micellization of a pH-sensitive diblock copolymer for drug delivery. *Int. J. Pharm.* **2013**, *455* (1), 5-13.

221. Han, M.; Diao, Y.-Y.; Jiang, H.-L.; Ying, X.-Y.; Chen, D.-W.; Liang, W.-Q.; Gao, J.-Q., Molecular mechanism study of chemosensitization of doxorubicin-resistant human myelogenous leukemia cells induced by a composite polymer micelle. *Int. J. Pharm.* **2011**, *420* (2), 404-411.

222. Gedde, U. W., Thermal analysis of polymers. *Drug Dev. Ind .Pharm.* **1990**, *16* (17), 2465-2486.

223. Michell, A. J. M. R. M., Differential scanning calorimetry of polymers. In *Polymer Morphology*. 2016; p 72-99

224. Ng, H. M.; Mohamad saidi, N.; Saiha Omar, F.; Kasi, R.; T subramaniam, R.; Baig, S., In *Thermogravimetric Analysis of Polymers*. 2018; p 1-29.

225. Lotz, B., Analysis of the structure and morphology of crystalline polymers by electron microscopy imaging and diffraction: a personal journey. *Microscopy* **2014**, *63* (2), 95-109.

226. Lee, T. H.; Boey, F. Y. C.; Khor, K. A., X-ray diffraction analysis technique for determining the polymer crystallinity in a polyphenylene sulfide composite. *Polym. Compos.* **1995**, *16* (6), 481-488.

227. An, J. H.; Kim, H. S.; Chung, D. J.; Lee, D. S.; Kim, S., Thermal behaviour of poly(ε-caprolactone)-poly(ethylene glycol)-poly(ε-caprolactone) tri-block copolymers. *J. Mater. Sci.* **2001**, *36* (3), 715-722.

228. Bogdanov, B.; Vidts, A.; Van Den Buicke, A.; Verbeeck, R.; Schacht, E., Synthesis and thermal properties of poly(ethylene glycol)-poly(ε-caprolactone) copolymers. *Polymer* **1998**, *39* (8), 1631-1636.

229. He, C.; Sun, J.; Deng, C.; Zhao, T.; Deng, M.; Chen, X.; Jing, X., Study of the synthesis, crystallization, and morphology of poly(ethylene glycol)−poly(ε-caprolactone) diblock copolymers. *Biomacromolecules* **2004**, *5* (5), 2042-2047.

230. Pethrick, R. A.; Chemistry, R. S. o., Polymer structure characterisation: from nano to macro organization. RSC Pub.: 2007.

231. Nguyen, T. B. T.; Nguyen, T. T. C.; Tran, H. C.; Nguyen, C. K.; Tran, N. Q., ^{1}H NMR spectroscopy as an effective method for predicting molecular Weight of polyaminoamine dendrimers and their derivatives. *Int. J. Polym. Anal. Charact.* **2015**, *20* (1), 57-68.

232. Cunliffe, A. V., ^{13}C NMR spectroscopy of polymers. In *Developments in polymer characterisation—1*, Dawkins, J. V., Ed. Springer Netherlands: Dordrecht, 1978; pp 1-39.

233. Tonelli, A. E.; Schilling, F. C.; Cais, R. E., Fluorine-19 NMR chemical shifts and the microstructure of fluoro polymers. *Macromolecules* **1982**, *15* (3), 849-853.

234. Shit, S. C.; Maiti, S., Application of NMR spectroscopy in molecular weight determination of polymers. *Eur. Polym. J.* **1986**, *22* (12), 1001-1008.

235. Kidera, A.; Higashira, T.; Ikeda, Y.; Urayama, K.; Kohjiya, S., GPC analysis of polymer network formation. *Polym. Bull.* **1997**, *38* (4), 461-468.

236. He, X.; Li, L.; Su, H.; Zhou, D.; Song, H.; Wang, L.; Jiang, X., Poly(ethylene glycol)-block-poly(ε-caprolactone)–and phospholipid-based stealth nanoparticles with enhanced therapeutic efficacy on murine breast cancer by improved intracellular drug delivery. *Int. J. Nanomedicine.* **2015**, *10*, 1791-1804.

237. Alexandridis, P., Amphiphilic copolymers and their applications. *Curr. Opin. Colloid Interface Sci.* **1996**, *1* (4), 490-501.

238. Kim, D. W.; Kim, S. Y.; Kim, H. K.; Kim, S. W.; Shin, S. W.; Kim, J. S.; Park, K.; Lee, M. Y.; Heo, D. S., Multicenter phase II trial of Genexol-PM, a novel Cremophor-free, polymeric micelle formulation of paclitaxel, with cisplatin in patients with advanced non-small-cell lung cancer. *Ann. Oncol.* **2007**, *18* (12), 2009-14.

239. Lee, K. S.; Chung, H. C.; Im, S. A.; Park, Y. H.; Kim, C. S.; Kim, S. B.; Rha, S. Y.; Lee, M. Y.; Ro, J., Multicenter phase II trial of Genexol-PM, a Cremophor-free, polymeric micelle formulation of paclitaxel, in patients with metastatic breast cancer. *Breast Cancer. Res. Treat.* **2008**, *108* (2), 241-50.

240. Woodruff, M. A.; Hutmacher, D. W., The return of a forgotten polymer—Polycaprolactone in the 21st century. *Prog. Polym. Sci.* **2010**, *35* (10), 1217-1256.

241. Kim, M. S.; Kim, S. K.; Kim, S. H.; Hyun, H.; Khang, G.; Lee, H. B., In vivo osteogenic differentiation of rat bone marrow stromal cells in thermosensitive MPEG-PCL diblock copolymer gels. *Tissue Eng.* **2006**, *12* (10), 2863-73.

242. Park, J. S.; Woo, D. G.; Sun, B. K.; Chung, H. M.; Im, S. J.; Choi, Y. M.; Park, K.; Huh, K. M.; Park, K. H., In vitro and in vivo test of PEG/PCL-based hydrogel scaffold for cell delivery application. *J. Control. Release.* **2007**, *124* (1-2), 51-9.

243. Choi, J. S.; Leong, K. W.; Yoo, H. S., In vivo wound healing of diabetic ulcers using electrospun nanofibers immobilized with human epidermal growth factor (EGF). *Biomaterials* **2008**, *29* (5), 587-96.

244. Niu, Y.; Chen, K. C.; He, T.; Yu, W.; Huang, S.; Xu, K., Scaffolds from block polyurethanes based on poly(varepsilon-caprolactone) (PCL) and poly(ethylene glycol) (PEG) for peripheral nerve regeneration. *Biomaterials* **2014**, *35* (14), 4266-77.

245. Fievez, V.; Plapied, L.; des Rieux, A.; Pourcelle, V.; Freichels, H.; Wascotte, V.; Vanderhaeghen, M.-L.; Jerôme, C.; Vanderplasschen, A.; Marchand-Brynaert, J.; Schneider, Y.-J.; Préat, V., Targeting nanoparticles to M cells with non-peptidic ligands for oral vaccination. *Eur. J. Pharm. Biopharm.* **2009**, *73* (1), 16-24.

246. Tomar, P.; Jain, N.; Dixit, V. K., Nanoparticulate delivery of LHRH analogue for the treatment of prostate cancer. *Pharm. Dev. Technol.***2013**, *18* (3), 645-652.

247. Liu, Z.; Jiang, M.; Kang, T.; Miao, D.; Gu, G.; Song, Q.; Yao, L.; Hu, Q.; Tu, Y.; Pang, Z.; Chen, H.; Jiang, X.; Gao, X.; Chen, J., Lactoferrin-modified PEG-co-PCL nanoparticles for enhanced brain delivery of NAP peptide following intranasal administration. *Biomaterials* **2013**, *34* (15), 3870-3881.

248. Yadav, A. K.; Mishra, P.; Jain, S.; Mishra, P.; Mishra, A. K.; Agrawal, G. P., Preparation and characterisation of HA–PEG–PCL intelligent core–corona nanoparticles for delivery of doxorubicin. *J. Drug. Target.* **2008**, *16* (6), 464-478.

249. Danafar, H.; Schumacher, U., MPEG–PCL copolymeric nanoparticles in drug delivery systems. *Cogent Medicine.* **2016**, *3*, 1.

250. Grossen, P.; Witzigmann, D.; Sieber, S.; Huwyler, J., PEG-PCL-based nanomedicines: A biodegradable drug delivery system and its application. *J. Control. Release.* **2017**, *260*, 46-60.

251. Gu, Q.; Xing, J. Z.; Huang, M.; He, C.; Chen, J., SN-38 loaded polymeric micelles to enhance cancer therapy. *Nanotechnology* **2012**, *23* (20), 205101.

252. Gou, M.; Zheng, X.; Men, K.; Zhang, J.; Wang, B.; Lv, L.; Wang, X.; Zhao, Y.; Luo, F.; Chen, L.; Zhao, X.; Wei, Y.; Qian, Z., Self-assembled hydrophobic Honokiol loaded MPEG-PCL diblock copolymer micelles. *Pharm. Res.* **2009**, *26* (9), 2164-2173.

253. Forrest, M. L.; Won, C.-Y.; Malick, A. W.; Kwon, G. S., In vitro release of the mTOR inhibitor rapamycin from poly(ethylene glycol)-b-poly(ε-caprolactone) micelles. *J. Control. Release.* **2006**, *110* (2), 370-377.

254. Ungaro, F.; Conte, C.; Ostacolo, L.; Maglio, G.; Barbieri, A.; Arra, C.; Misso, G.; Abbruzzese, A.; Caraglia, M.; Quaglia, F., Core-shell biodegradable nano-assemblies for the passive targeting of docetaxel: features, antiproliferative activity and in vivo toxicity. *Nanomed. Nanotechnol. Biol. Med.* **2012**, *8* (5), 637-646.

255. Peng, W.; Jiang, X.-y.; Zhu, Y.; Omari-Siaw, E.; Deng, W.-w.; Yu, J.-n.; Xu, X.-m.; Zhang, W.-m., Oral delivery of capsaicin using MPEG-PCL nanoparticles. *Acta Pharmacol. Sin.* **2014**, *36*, 139.

Chapter 2

Synthesis and characterisation of poly(ethylene glycol-*b*-caprolactone) block copolymers

Chapter overview

The synthesis and purification of well-defined and pure PEG-*b*-PCL copolymers are fundamental to the study of their physicochemical properties, and interpretation of structure-related trends. Therefore, a comprehensive study was conducted to synthesise a large family of well-defined PEG-*b*-PCL diblock copolymers with different PEG and PCL molecular weights. The main goal of this section of work was to synthesise PEG-*b*-PCL copolymers with narrow $Đ$ and free from impurities (e.g., homopolymers). The copolymers were synthesised via ROP of ε-caprolactone using commercially available α-methoxy-ω-hydroxy PEG (PEG) as a macroinitiator and stannous octanoate ($Sn(Oct)_2$) as the catalyst.

In this study, copolymers of narrow $Đ$ were obtained by optimising the reaction conditions and minimising side reactions (e.g., transesterification) through the use of bulk or highly concentrated polymerisation mixtures, high monomer to initiator ratios and targeting low monomer conversions.

In addition, a novel purification approach was developed that may be more widely applicable for the purification of PEG-*b*-PCL copolymers, particularly for the removal of PCL homopolymer contaminants, whereas traditional precipitation approaches do not effectively remove PCL impurities and are mainly designed to remove unreacted monomer and catalyst.

2.1 Results and Discussion

2.1.1 Synthesis of PEG-*b*-PCL copolymers

In this chapter, the successful synthesis of 13 high-purity PEG-*b*-PCL block copolymers with narrow *Đ* is presented (**Table 2.1**). The polymers were synthesised via ROP of ε-caprolactone in the presence of $Sn(Oct)_2$ and initiated by different molecular weight PEG macroinitiators (M_n = 2, 5, 10 kDa). The macroinitiators and purified copolymers were characterised using a combination of ^{1}H NMR spectroscopy and GPC, and the molecular weight characteristics of the polymers are summarised in **Table 2.1**. However, to prepare these copolymers, it was necessary to modify and optimise the available synthetic procedures reported in the literature to obtain high purity, narrow *Đ* copolymers. Optimisation of the synthetic protocols and the development of purification strategies are discussed in the following sections.

2.1.1.1 Synthesis of PEG-b-PCL copolymers using solvents

The ROP of caprolactone was initially conducted using an [initator]:[monomer]:[catalyst] ([I]:[M]:[cat.]) ratio of 1:70:2 with a monomer concentration of 0.6 M, PEG macroinitiator with an M_n = 2 kDa (PEG_2) and toluene as the solvent as previously reported.[1,2] The ROP was conducted over 72 h at 120 °C and aliquots were removed every 24 h for GPC analysis. After 24 h GPC differential refractive index (DRI) chromatograms revealed a peak with a slight shoulder to lower retention volume (i.e., high molecular weight polymer), which continued to increase in intensity at 48 and 72 h, resulting in a polymer with a broad *Đ* and possibly consisting of two compositionally distinct polymer species (**Figure 2.1**).

Table 2.1: Composition and molecular weight characteristics of PEG macroinitiators and PEG-*b*-PCL block copolymers.

Polymer Code	M_n of PEG[a]	M_n of PEG[b]	[I]:[M]:[cat]	PCL : PEG	Targeted M_n of PCL (Da)	M_n of PCL[a] (Da)	M_n of PEG-PCL[a] (Da)	M_n of PEG-PCL[b] (Da)	M_w of PEG-PCL[b] (Da)	Đ (M_w/M_n)[b]
PEG_2	1991	1979	1:105:0.5	–	–	–	–	1979	2039	1.03
$PEG_2PCL_{0.4}$				0.25:1	500	416	2407	2210	2281	1.03
$PEG_2PCL_{1.1}$				0.5:1	1000	1140	3131	2897	2967	1.02
$PEG_2PCL_{1.8}$				1:1	2000	1824	3815	3010	3085	1.02
$PEG_2PCL_{3.9}$				2:1	4000	3990	5981	3374	3466	1.03
PEG_5	5368	4656	1:105:0.5	–	–	–	–	4656	4708	1.02
$PEG_5PCL_{0.6}$				0.10:1	500	648	6016	4878	4977	1.01
$PEG_5PCL_{1.3}$				0.25:1	1250	1331	6699	5565	5633	1.02
$PEG_5PCL_{2.3}$				0.5:1	2500	2394	7762	5962	6086	1.02
$PEG_5PCL_{4.2}$				1:1	5000	4218	9586	7272	7492	1.03
$PEG_5PCL_{9.4}$				2:1	10000	9462	14830	9958	10857	1.09
PEG_{10}	7821	9166	1:395:2	–	–	–	–	9024	9166	1.02
$PEG_{10}PCL_{3.1}$				0.30:1	2500	3192	12358	11835	12016	1.02
$PEG_{10}PCL_{7.8}$				0.75:1	7500	7866	17032	13093	13642	1.04
$PEG_{10}PCL_{10.7}$				1:1	10000	10773	19939	14518	15137	1.04
$PEG_{10}PCL_{14.7}$				1.5:1	15000	14877	24043	16718	18779	1.12

[a] number average molecular weight (M_n) was determined from ^{1}H NMR spectroscopy.
[b] number average molecular weight (M_n) and weight average molecular weight (M_w) were determined from GPC, unsing a conventional calibration

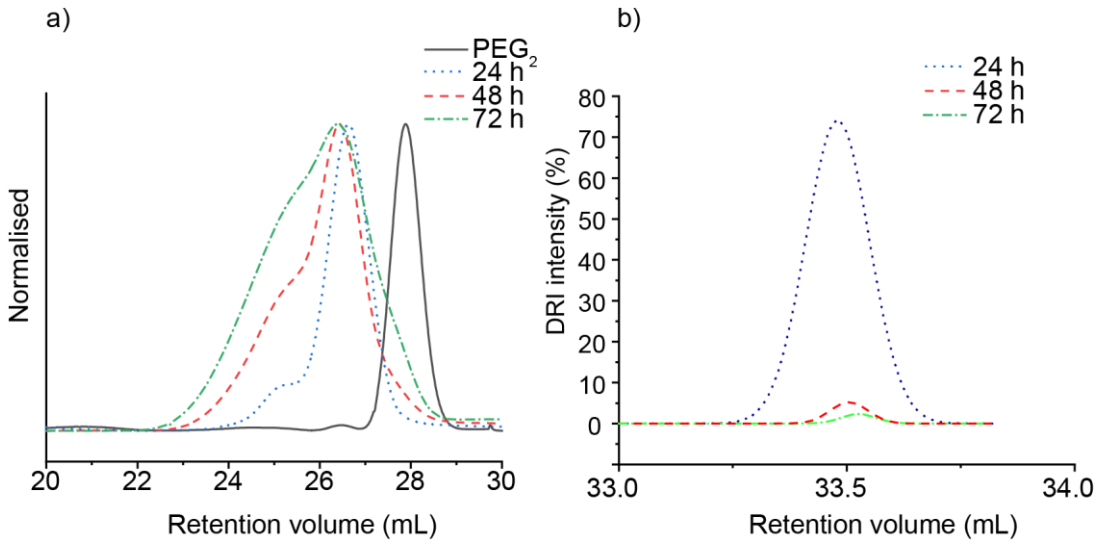


Figure 2.1: GPC DRI chromatograms following the a) formation of PEG-*b*-PCL copolymers over time from the polymerisation of caprolactone from a PEG_2 macroinitiator, and b) the relative decrease in the caprolactone monomer peak at 24, 48 and 72 h. The shift in the copolymer peak to lower retention volumes with increasing polymerisation time is an indication of an increase in the copolymer molecular weight, while the decrease in intensity of the caprolactone peak is consistent with a decrease in concentration as it is consumed in the polymerisation. Normalisation was conducted relative to the copolymer peak height for each sample**.**

The broad and asymmetric distribution of the polymer peak is believed to be caused by a combination of intermolecular chain-transfer between separate growing polymer chains and intramolecular back-biting within the same polymer chain, which both occur through a transesterification mechanism (**Figure 2.2**). Intermolecular chain-transfer and intramolecular back-biting cause an uneven distribution of polymer chain lengths (a mixture of higher and lower molecular weight polymer chains). For example, intermolecular chain-transfer leads to the formation of shorter and longer copolymers relative to the average molecular weight. In contrast, intramolecular back-biting leads to a shorter copolymer and the formation of a cyclic PCL homopolymer. These side reactions are likely to be caused by the decrease in monomer concentration and depletion at longer polymerisation times, which was confirmed by GPC DRI chromatograms that revealed almost complete consumption of caprolactone at 48 h (**Figure 2.1**). This transesterification behaviour is commonly reported for PCL synthesis, particularly when the monomer conversion is high.[3]

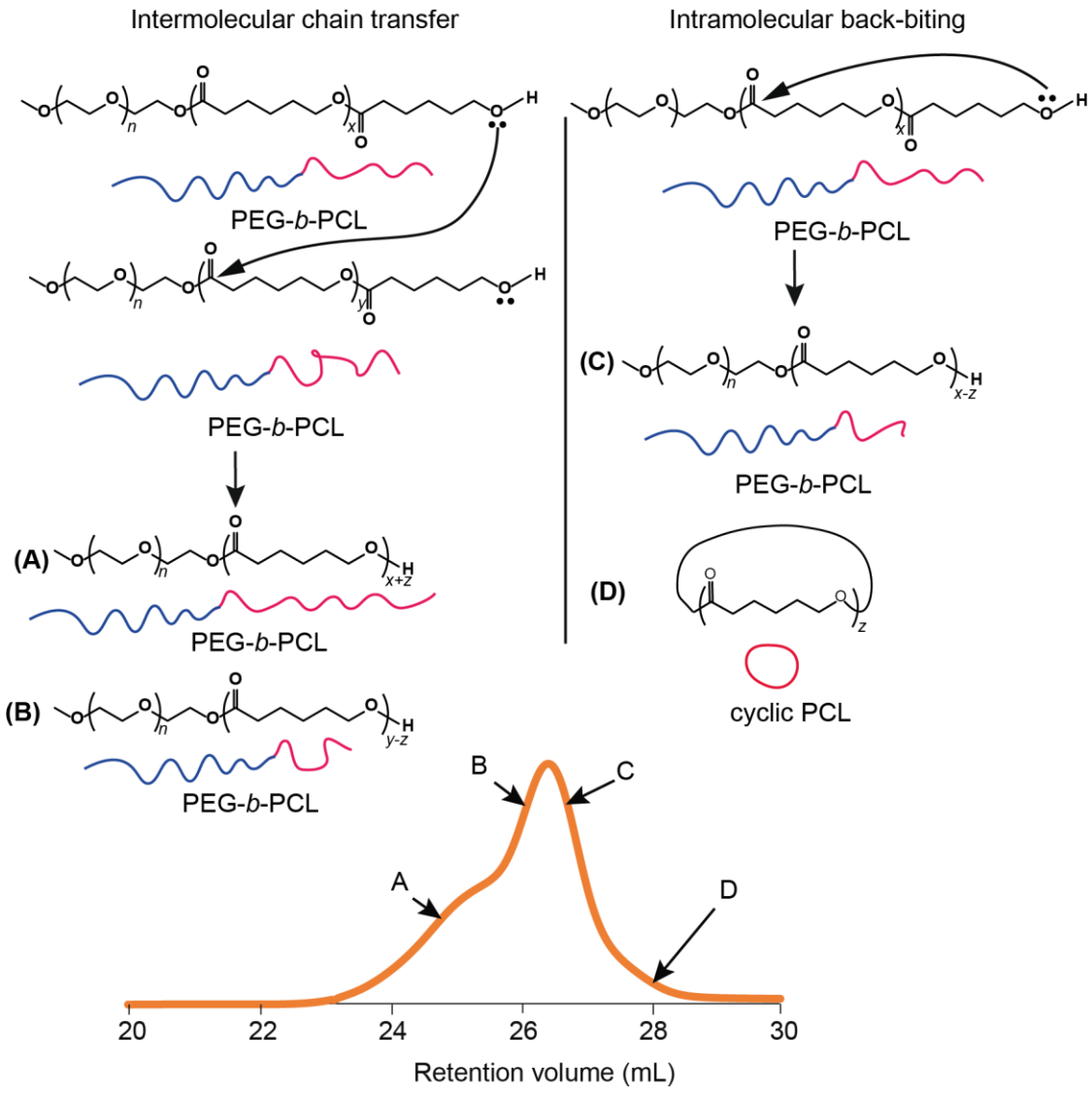


Figure 2.2: Illustration showing the mechanistic detail of intermolecular chain-transfer and intramolecular back-biting and their influence on a typical GPC DRI chromatogram. Chain-transfer leads to the formation of lower and higher molecular weight copolymer chains and intramolecular back-biting forms a lower molecular weight copolymer chain and a cyclic homopolymer, resulting in an increase in dispersity, observed as a broadening of the polymer peak in the GPC chromatogram.

Side reactions are mainly due to an increase in the transesterification rate relative to the propagation rate (refer to Chapter 1). One of the major causes of slow propagation is the insufficient reaction between the propagating chains and monomer due to the depletion of monomer (low monomer concentration) when the polymerisation proceeds to high monomer conversions (e.g., monomer conversion > 90%).[4]

In this situation, there is less monomer to react with the propagating species; as a result, the propagating chain-end is more prone to undergo transesterification with the same polymer chain (i.e., intramolecular back-biting) or another polymer chain (i.e., intermolecular chain transfer).[5] This situation can be avoided by polymerising caprolactone in bulk (without solvent) and operating at low monomer conversions, which ensures a high monomer concentration and high propagation rate due to the increased probability of reactions between the propagating chain and monomer.[5]

2.1.1.2 Synthesis of PEG_2PCL_y copolymers series

To avoid the side reactions discussed above and obtain low *Đ* copolymers, the ROP was carried out in bulk (without any solvent) and only allowed to proceed to a low monomer conversion, as previous literature had shown that this provided copolymers with narrow *Đ*.[3] Therefore, a series of copolymers were prepared using the PEG macroinitiator with an M_n of 2 kDa and an [I]:[M]:[cat.] ratio of 1:105:0.5. Initially, the ROP was monitored to establish a kinetic profile for the polymerisation by removing samples periodically for NMR spectroscopy and GPC (**Figure 2.3**). Whilst the GPC DRI chromatograms revealed a clear shift in the main peak to lower retention volume s with increasing time; a second peak was also observed at higher retention volume from the beginning of the polymerisation (retention volume ~ 30 mL). This peak was found to grow larger with time (decreasing in retention volume) indicating that it was most probably PCL homopolymer, probably initialised by water present in the PEG macroinitiator (**Figure 2.3**). The peak shift towards lower retention volume indicates that the PCL homopolymer increases in molecular weight with time, similar to the copolymer. In addition, the reaction kinetics for the polymerisation were found to deviate from pseudo-first-order kinetics, which was hypothesised to be caused by the increased monomer consumption caused by PCL homopolymerisation (**Figure 2.3**).

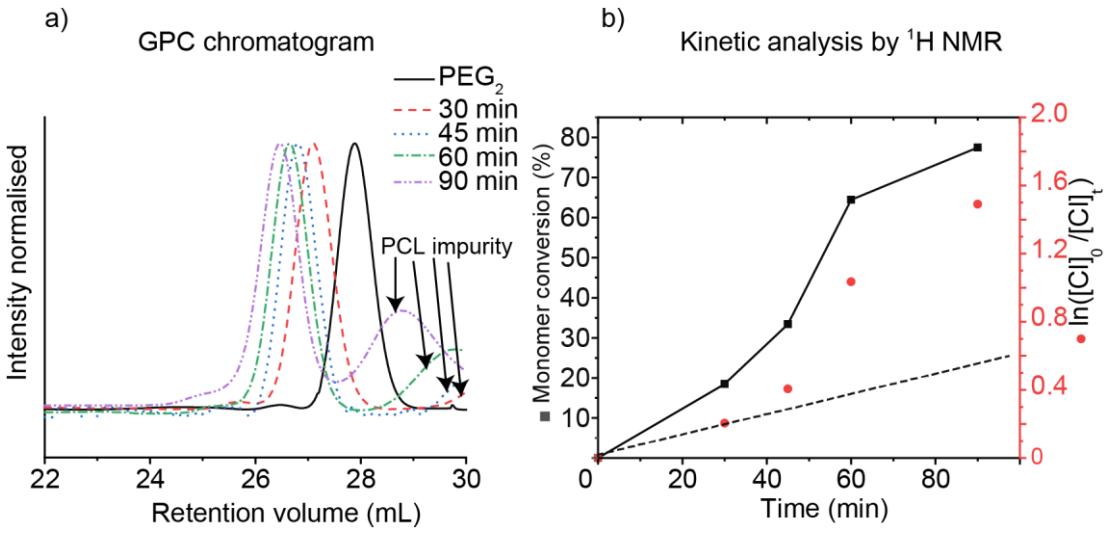


Figure 2.3: a) Normalised GPC DRI chromatograms following the ROP of caprolactone from the PEG_2 macroinitiator at different timepoints and; b) monomer conversion and pseudo-first-order kinetics plot for the polymerisation and the dotted line represents the first-order kinetics. Normalisation was conducted relative to the copolymer peak height for each sample.

The PEG macroinitiator was heated at 120 °C under vacuum (0.1 mbar) for 1 h to remove residual water which might be responsible for initiating PCL homopolymerisation. Then the ROP was repeated using the same conditions as above. GPC analysis of the polymerisation at various timepoints revealed that polymerisation proceeded without any side reactions, as indicated by the absence of homopolymer peaks (**Figure 2.4**). In addition, a narrow $Đ$ was observed throughout the polymerisation, very similar to that of the initial PEG macroinitiator $Đ$, which indicated a well-controlled polymerisation (**Figure 2.4**).

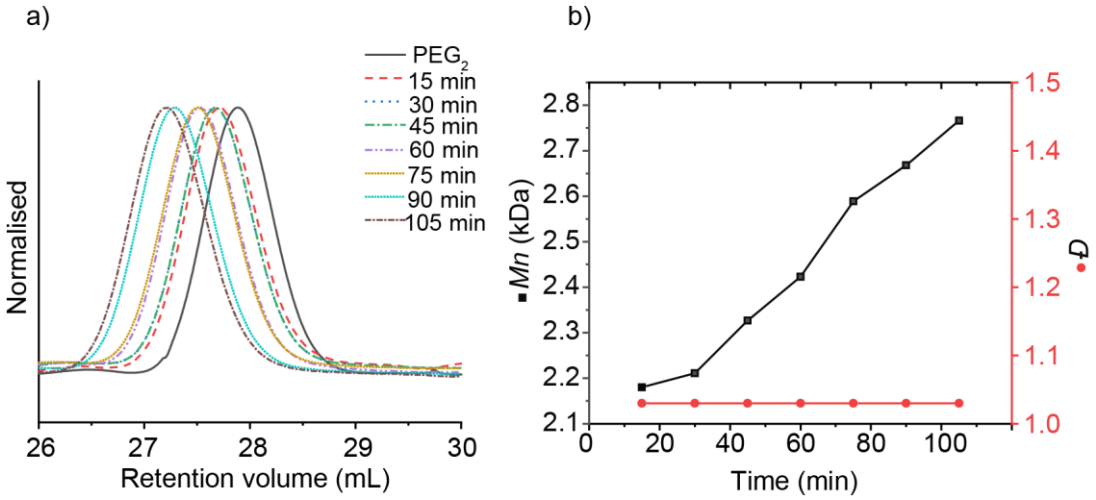


Figure 2.4: a) Normalised GPC DRI chromatograms for ROP of caprolactone from the PEG_2 macroinitiator at various timepoints and b) M_n and $Đ$ of the copolymers over time for the polymerisation (M_n determined from ^{1}H NMR spectroscopy and $Đ$ from GPC analysis). Normalisation was conducted relative to the copolymer peak height for each sample.

^{1}H NMR spectroscopy of the polymerisation mixture over time revealed successful ROP of caprolactone with a decrease in the intensity of the signal at δ_H = 4.20 ppm corresponding to the methylene protons adjacent to the ester group of the monomer (**Figure 2.5**, a), and the appearance of a signal at δ_H = 4.06 ppm corresponding to the methylene protons adjacent to the ester of the PCL backbone (**Figure 2.5**, a*).

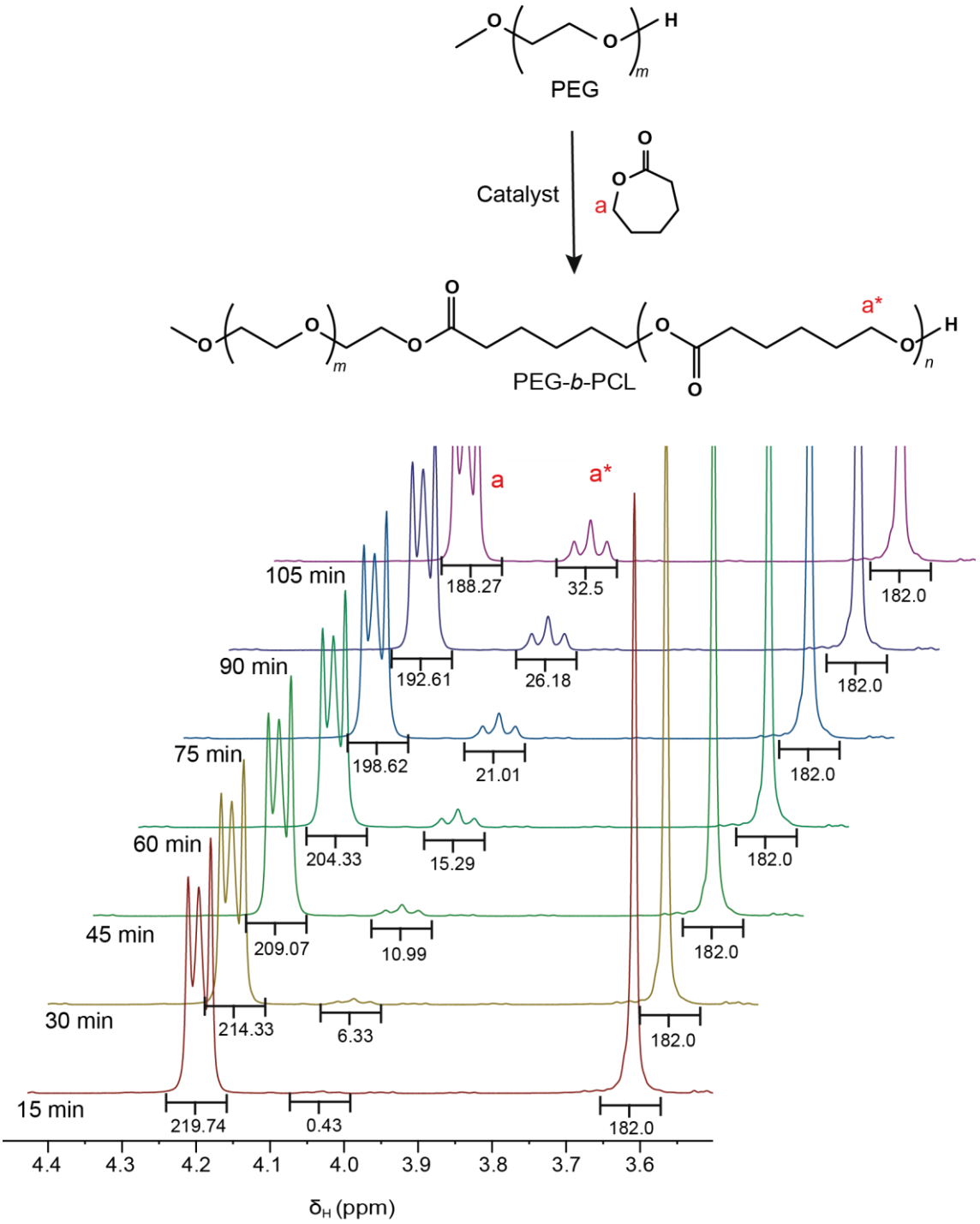


Figure 2.5: ^{1}H NMR spectra ($CDCl_3$, 298 K) following the ROP of caprolactone from the PEG_2 macroinitiator at various timepoints. Labels a and a* indicate the methylene proton signals from the monomer and polymer, respectively. Integral values are shown under each signal and are relative to the PEG signal integral value.

By comparing the change in the integration of the signals from the monomer and polymer over time, it was possible to calculate the conversion of monomer and reaction kinetics (**Figure 2.6**). Presuming that the polymerisation follows first-order kinetics in the propagation stage, the apparent rate of propagation (k_{app}) for the conversion of caprolactone was determined to be 0.00015 min^{-1}, which was later used to target block copolymers with specific PCL molecular weights. Interestingly, the rate of reaction was much slower compared to the polymerisation carried out using undried PEG (k_{app} = 0.0017 min^{-1}), which may indicate that the presence of water acts to accelerate the rate of the polymerisation and consume more caprolactone monomer. In this study k_{app} is reported using simplified pseudo-first-order kinetics as the absolute rate of propagation (k_p) requires the initial concentration of propagating species to be known (although it is reasonable to assume that it remains constant).

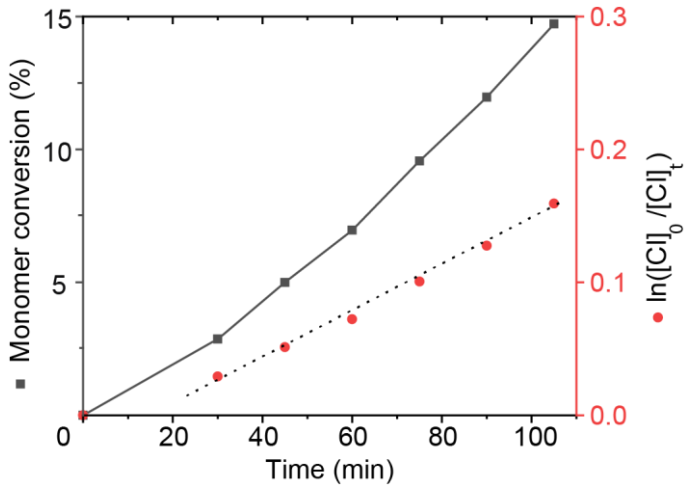


Figure 2.6: Monomer conversion and pseudo-first-order kinetic plot for the ROP of caprolactone from the PEG_2 macroinitiator. Monomer conversion was calculated from NMR spectroscopy by comparing the relative integration of signals corresponding to the monomer and polymer (**Figure 2.5**).

Subsequently, the rate constant was used to calculate the exact time required to prepare PEG_2PCL_y copolymers with specific molecular weight PCL blocks. To prepare copolymers with PCL M_n values of 0.25, 1, 2 and 4 kDa – providing block copolymers with PCL:PEG molecular weight ratios of 0.25:1, 0.5:1, 1:1 and 2:1 – the ROP was conducted under identical conditions for 40, 60, 120 and 230 min, respectively. After the designated time, the polymers were isolated via precipitation into diethyl ether and analysed via GPC (**Figure 2.7**) and ^{1}H NMR spectroscopy (**Figure 2.8**).

GPC analysis revealed that the copolymers were free from polymeric impurities and possessed monomodal distributions with narrow *Đ* ranging from 1.02 to 1.03 (**Table 2.1**). Whilst the GPC can provide a good indication of the *Đ* and molecular weight trends, the use of PEG standards to calibrate the system means that the molecular weight values provided by the GPC may not be absolute and are only relative to the standards used. Given the compositional differences between PEG homopolymers and PEG-*b*-PCL copolymers, it is likely that they have different hydrated sizes in the solvent used. Thus, it is common to assume that molecular weight values provided by the GPC with a conventional calibration will not be accurate, and therefore, NMR spectroscopy was used to provide a more accurate determination of the M_n of the copolymers.

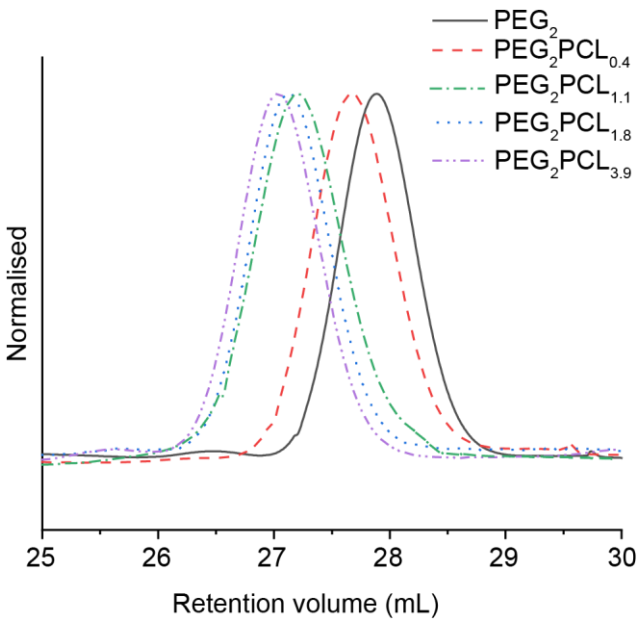


Figure 2.7: Normalised GPC DRI chromatograms of the isolated PEG_2PCL_y copolymer series. A clear shift towards lower retention volumes is observed, indicative of the formation of larger PCL blocks and higher molecular weight copolymers. Normalisation was conducted relative to the copolymer peak height for each sample.

The ^{1}H NMR spectra of the copolymers revealed characteristic resonances consistent with both PEG and PCL, and confirmed the successful removal of unreacted monomer (**Figure 2.8**).

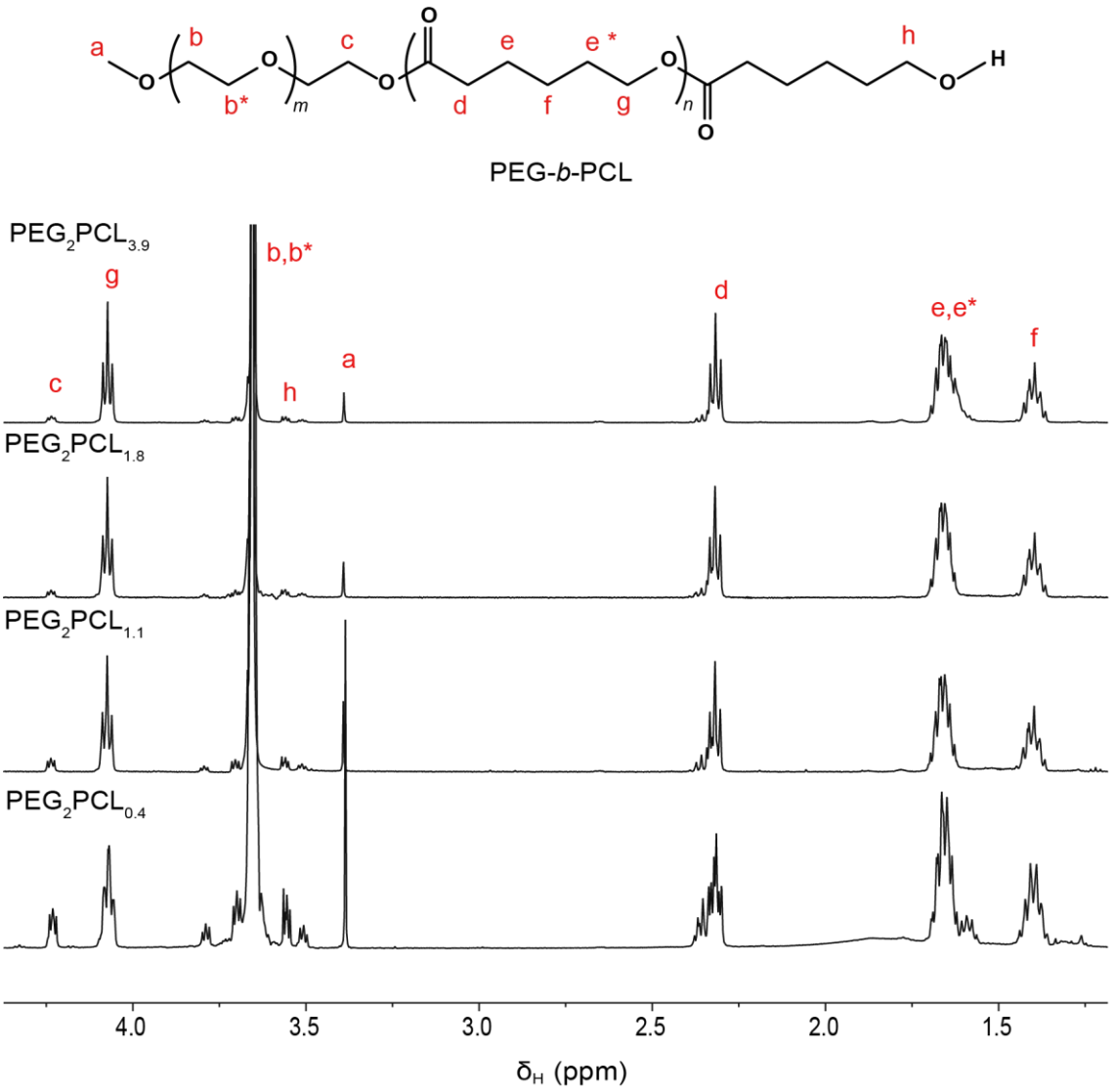


Figure 2.8: ^{1}H NMR spectra ($CDCl_3$, 298 K) of the purified PEG_2PCL_y block copolymer series. The M_n values of PCL block was calculated from the ratio of the integral values of the methylene protons for PEG (δ_H = 3.64 ppm) and the methylene protons adjacent to the ester group in PCL (δ_H = 4.06 ppm).

^{1}H NMR spectra of all copolymers revealed characteristic resonances corresponding to the methylene protons of the PEG repeat unit (RU) at δ_H = 3.60 ppm and PCL RU at δ_H = 1.43 (– $CH_2C\mathbf{H}_2CH_2$–), 1.65 (–$C\mathbf{H}_2CH_2C\mathbf{H}_2$–), 2.37 (–$COC\mathbf{H}_2CH_2$–) and 4.06 (–$CH_2C\mathbf{H}_2O$–) ppm. For lower molecular weight polymers, resonances corresponding to the methoxy protons from the PEG end-group (δ_H = 3.40 ppm), the methylene protons adjacent to the hydroxyl end-group of the PCL block (δ_H = 3.56 ppm) and the methylene protons from the PEG RU adjacent to the ester group joining the PEG and PCL blocks (δ_H = 4.23 ppm) were also clearly visible (e.g., **Figure 2.8**). The relative integration of the PEG backbone methylene signal and PCL backbone

methylene signal (**Figure 2.8**, b,b* and g) were compared to determine the M_n of the PCL block (**Table 2.1**). The narrow $Đ$ of the copolymers indicates that the polymers have a very narrow molecular weight distribution, which indicates that the M_n values calculated from ^{1}H NMR spectroscopic analysis should be accurate (**Figure 2.8**).

2.1.1.3 Synthesis of PEG_5PCL_y copolymers series

The synthesis of the PEG_5PCL_y copolymers was initially attempted in the same way as described previously for the PEG_2PCL_y copolymers but using a PEG_5 macroinitiator. A [I]:[M]:[cat.] ratio of 1:105:0.5 was used, and the ROP was monitored using NMR spectroscopy (**Figures 2.9** and **2.10**) and GPC (**Figure 2.11**).

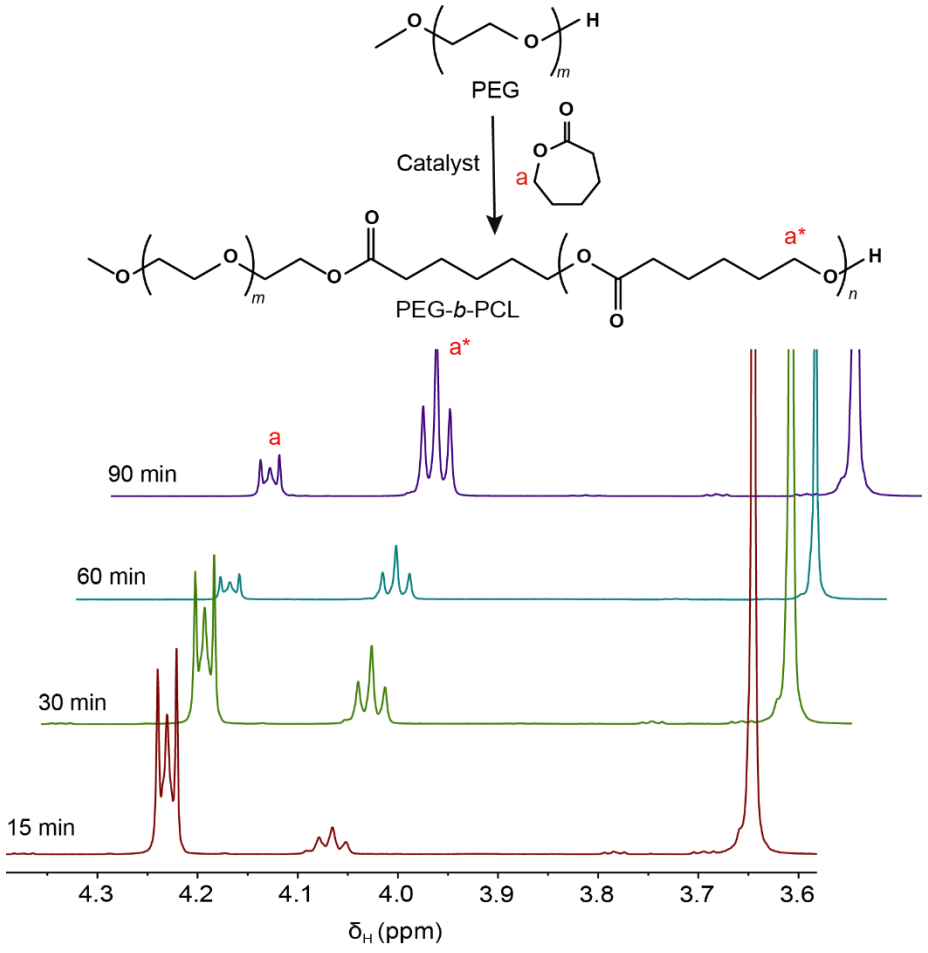


Figure 2.9: ^{1}H NMR spectra ($CDCl_3$, 298 K) following the ROP of caprolactone from the PEG_5 macroinitiator at various timepoints. Labels a and a* indicate the methylene proton signals from the monomer and polymer, respectively.

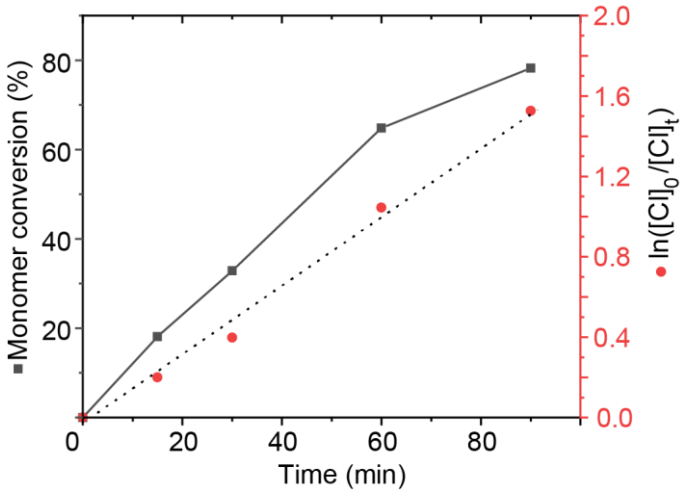


Figure 2.10: Monomer conversion and pseudo-first-order kinetic plot for the ROP of caprolactone from the PEG_5 macroinitiator. Monomer conversion was calculated from ^{1}H NMR spectroscopy by comparing the relative integration of signals corresponding to the monomer and polymer (**Figure 2.9**).

Firstly, it should be noted that the PEG homopolymer obtained from the commercial supplier displayed a bimodal peak (**Figure 2.11**).

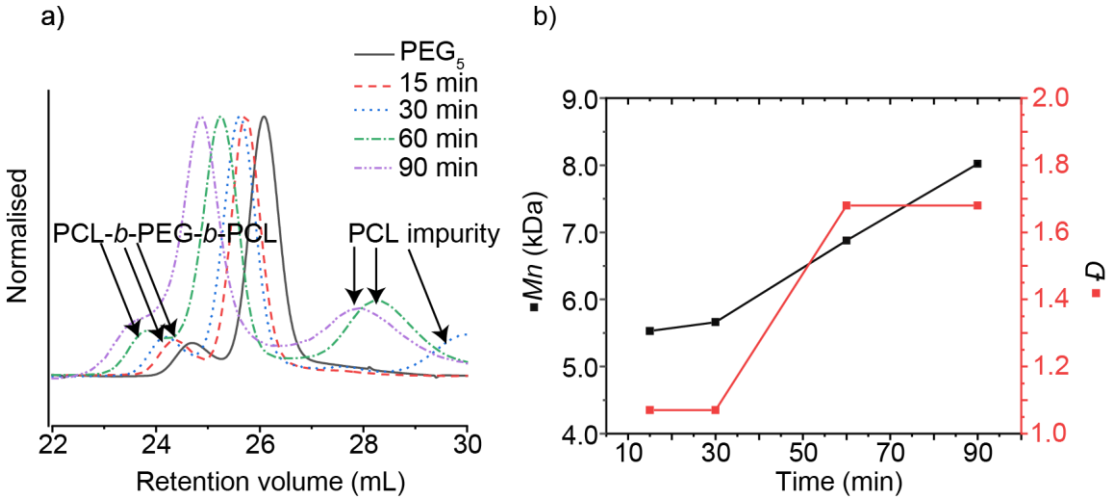


Figure 2.11: a) Normalised GPC DRI chromatograms for ROP of caprolactone from the PEG_5 macroinitiator at various timepoints and b) M_n and $Đ$ values over time for the polymerisation (M_n was determined from ^{1}H NMR spectroscopy and $Đ$ from GPC analysis). Normalisation was conducted relative to the copolymer peak height for each sample.

The smaller peak at higher retention volume is believed to be α,ω-dihydroxy PEG, a common impurity in PEG. PEG is synthesised commercially via ROP of ethylene oxide using methanol or a metal methoxide.[6] If water or hydroxide contaminants are present in the reactants or become introduced during the polymerisation, they can cause ROP of ethylene oxide to produce a diol that acts as a difunctional macroinitiator.[7] The molecular weight of the small peak was determined from GPC to be ~9.6 kDa, which is almost double the main peak corresponding to PEG, which is consistent with it being a dihydroxy PEG. Whilst it is impossible to differentiate between these two different species in the NMR spectra, the areas under the peaks in the GPC chromatogram were compared to calculate the relative amount of dihydroxy PEG, which was determined to be 11% w/w.

As can be seen from the GPC chromatograms, polymerisation of caprolactone leads to a high molecular weight (low retention volume) shoulder that most likely corresponds to a triblock PCL-*b*-PEG-*b*-PCL copolymer formed as a result of the dihydroxy PEG contaminant (**Figure 2.11**). Since this triblock would complicate and interfere with any structure-property trends investigated for the diblock copolymer, attempts were made to remove and eliminate the impurity. Initially, fractional precipitation of PEG_5 macroinitiator was investigated to try and remove the higher molecular weight dihydroxy PEG; however, this proved unsuccessful. Another important feature in the GPC chromatograms is the appearance of a peak at higher retention volume (**Figure 2.11**), which was believed to be PCL homopolymer caused by water initiating caprolactone polymerisation, as observed when conducting ROP with the undried PEG_2 macroinitiator.

Therefore, the PEG_5 macroinitiator was dried (120 °C for 1 h at 0.1 mbar), and the synthesis was repeated; however, this did not eliminate the formation of PCL homopolymer. Possible explanations for this include a high water content in the PEG and higher molecular weight of the PEG, leading to a stronger interaction with water. Thus, drying was not sufficient to remove all of the water. Secondly, there may be other sources of moisture, including the monomer, the inert gas used for the reaction (nitrogen) and residual moisture from glassware. Therefore, the monomer was distilled, PEG dried more thoroughly (120 ^{o}C for 12 h at 0.1 mbar), and all the glassware was flame dried.

Nevertheless, the formation of PCL homopolymer was still observed. Given that everything was dried and the high-purity nitrogen gas was passed through a calcium chloride drying tube prior to use, it was not water that is responsible for the initiation of PCL homopolymerisation; however, there may be other, unidentified impurities (other than water) in the monomer and PEG that could be responsible. Since the impurities responsible for the formation of PCL homopolymer was not removed successfully and the triblock copolymer from the desired diblock copolymer, the next logical step was to attempt to purify the crude polymerisation mixture.

The solubility profile of PEG and PCL homopolymers is significantly different,[8] and theoretically, a solvent mixture which is capable of solubilising the PCL homopolymer but is a non-solvent for PEG, might allow separation of the PCL homopolymer from PEG-*b*-PCL copolymers. Furthermore, since a PCL-*b*-PEG-*b*-PCL triblock contains more PCL than a PEG-*b*-PCL diblock with the same block lengths, it was hypothesised that it might also be possible to separate the triblock using this approach. PCL is insoluble in diethyl ether (DEE) and hexane, and partially soluble in ethyl acetate (EtOAC). However, the solubility of PCL is also dependent on molecular weight.[8] Therefore, the precipitation of the crude polymer in different solvent systems was investigated as an approach to remove unwanted polymeric species. The crude polymer isolated at the end of the kinetic study was dissolved in chloroform and precipitated into hexane, methanol (MeOH) or DEE. The resulting precipitate was collected and analysed via GPC (**Figure 2.12**). The precipitation into hexane and DEE did not result in a significant difference in the crude polymer composition, precipitation into methanol lead to a decrease in the PEG-*b*-PCL diblock copolymer. This usual as PEG homopolymers are readily soluble in methanol, and therefore, copolymers containing PEG may also have some solubility in methanol even if the other block is not. Subsequently, a binary solvent mixture for the precipitation, consisting of DEE (a non-solvent for both blocks) and EtOAc(a solvent for PCL) experimented. Once again, the crude polymer was dissolved in chloroform, precipitated into the binary solvent mixture, and the precipitate was isolated and analysed via GPC.

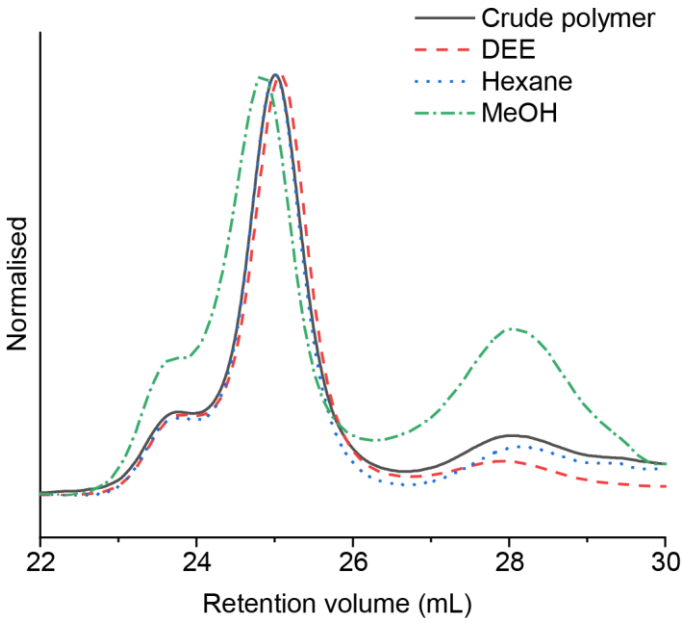


Figure 2.12: Normalised GPC DRI chromatograms of the insoluble component obtained from precipitation of the crude PEG_5PCL_5 copolymer in different solvents. A slight reduction in the intensity of the peak at 28 mL corresponding to the PCL homopolymer was observed for hexane and DEE, indicating the partial fraction of the PCL homopolymer impurities. Normalisation was conducted relative to the copolymer peak height for each sample.

From the GPC chromatograms, the peak areas for the copolymers and the PCL homopolymer were measured and used to calculate the relative amount of the PCL homopolymer in the copolymer on a % w/w basis, assuming that the change in refractive index with concentration is similar for both (**Table 2.2**).

Table 2.2: PCL homopolymer in copolymer after precipitation in different binary mixtures of EtOAc and DEE, as determined from GPC.

Solvent	PCL homopolymer % w/w
DEE	28.7
10% v/v EtOAC in DEE	18.3
30% v/v EtOAC in DEE	5.9
50% v/v EtOAC in DEE	23.5
70% v/v EtOAC in DEE	26.3

The results indicated that 30% v/v of EtOAc in DEE could remove the majority of the PCL homopolymer impurities. However, as the EtOAc content in the binary mixture increased further, PEG-*b*-PCL copolymer becomes more soluble in the solvent. As a result, when the crude mixture precipitate in that mixture it precipitate less amount of PEG-*b*-PCL copolymer.

Therefore, 30% v/v EtOAc in DEE was used as the precipitation solvent, which resulted in the complete removal of the PCL homopolymer (**Figure 2.13**). Once again, this behaviour is consistent with the solubility of the respective blocks. PEG is not soluble in EtOAc, whereas PCL has limited solubility in EtOAc, and therefore, polymers with a higher proportion of PCL (i.e., the triblock) are likely to display some solubility.

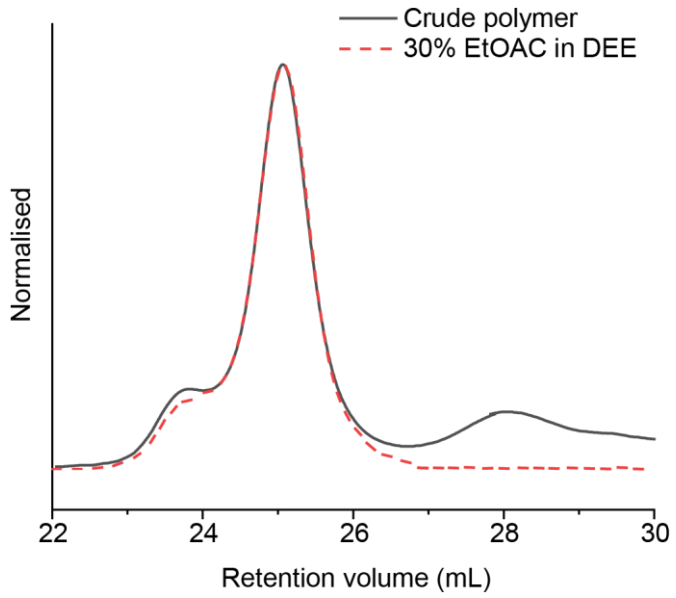


Figure 2.13: Normalised GPC DRI chromatograms of crude PEG_5PCL_5 polymer before and after precipitation in 30% v/v EtOAc in DEE. A reduction in the peak at a retention volume of 28 mL indicates the removal of the PCL homopolymer. Normalisation was conducted relative to the copolymer peak height for each sample.

As the PCL-*b*-PEG-*b*-PCL triblock copolymer could not be fully separated from the desired block copolymer and it might influence the properties of the diblock copolymer during self-assembly and aggregate formation, the block copolymer was synthesised using a different PEG macroinitiator obtained from a different commercial batch that was free of dihydroxy PEG impurities.

Using the kinetic data collected previously, a series of PEG_5PCL_y copolymers were prepared to target PCL block lengths of M_n = 0.5, 1.25, 2.5, 5 and 10 kDa by reacting the new macroinitiator and monomer for 2, 6, 10, 24 and 50 min, respectively. The crude polymers were then precipitated three times in 30% v/v EtOAc in DEE to remove PCL homopolymer and unreacted monomer. The polymers were then analysed by ^{1}H NMR spectroscopy (**Figure 2.14**) and GPC (**Figure 2.15**).

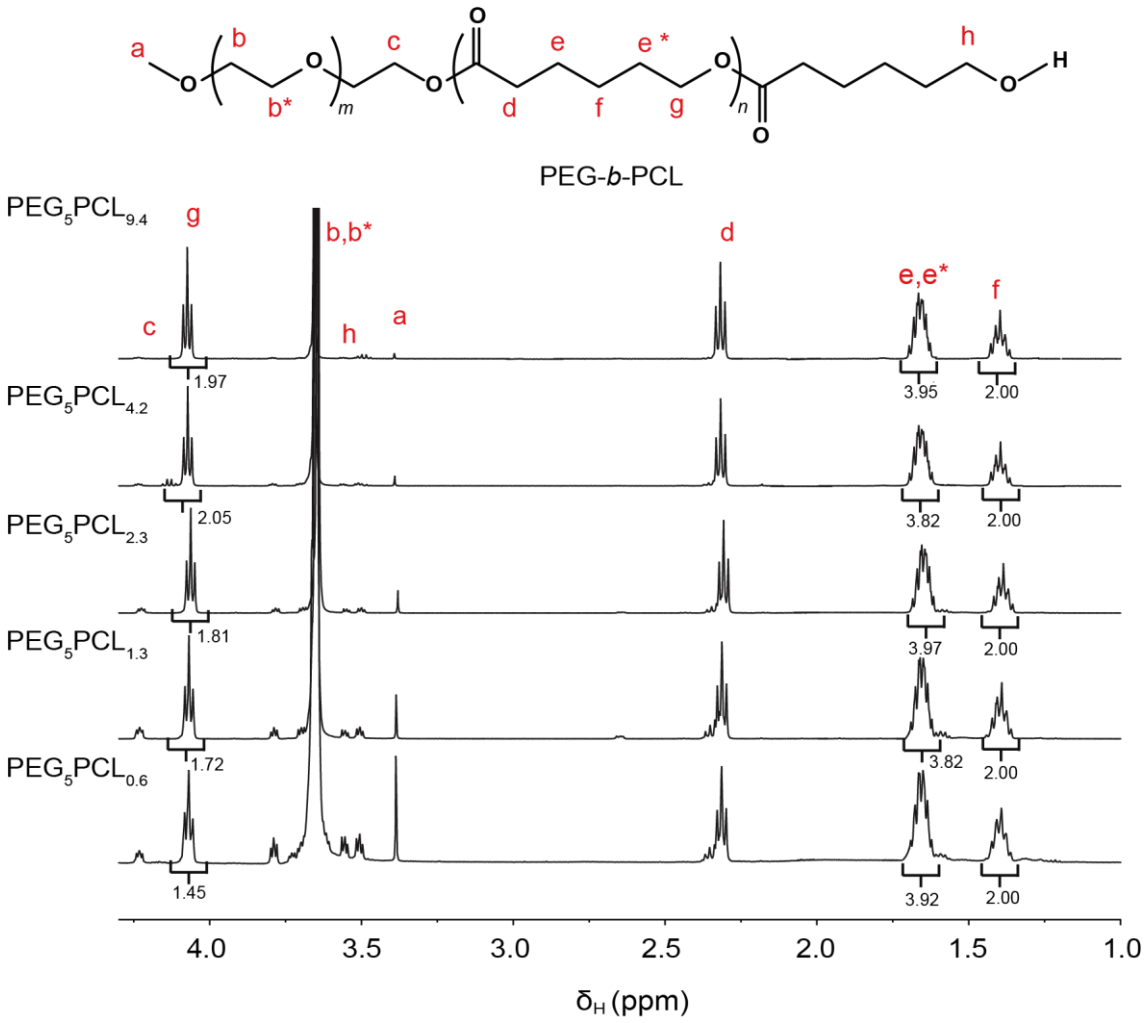


Figure 2.14: ^{1}H NMR spectra ($CDCl_3$, 298 K) of the purified PEG_5PCL_y block copolymer series. The M_n values of PCL block was calculated from the ratio of the integral values of the methylene protons for PEG (δ_H = 3.64 ppm) and the methylene protons adjacent to the ester group in PCL (δ_H = 4.06 ppm).

The ^{1}H NMR spectra and GPC analysis confirmed the purity of the PEG_5PCL_y copolymers. GPC analysis confirmed the absence of PCL homopolymer and NMR spectroscopic analysis revealed characteristic peaks as described previously for the PEG_2PCL_y series.

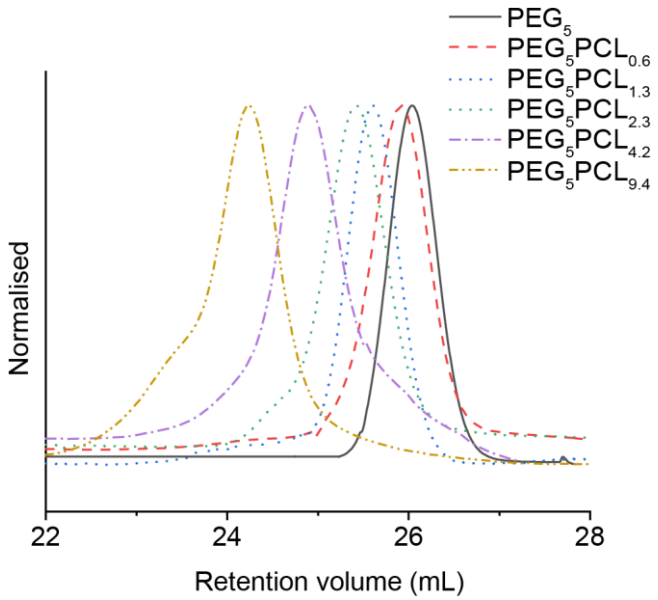


Figure 2.15: Normalised GPC DRI chromatograms of the purified PEG_5PCL_y copolymer series. A clear shift of the peaks with time to higher retention volumes confirmed the successful synthesis of the block copolymers. Normalisation was conducted relative to the copolymer peak height for each sample.

2.1.1.4 Synthesis of $PEG_{10}PCL_y$ copolymers series

The synthesis of the $PEG_{10}PCL_y$ series was initially investigated in bulk using an [I]:[M]:[cat.] ratio of 1:395:2 and a PEG_{10} macroinitiator. However, the polymerisation mixture became very viscous during the polymerisation, which significantly impacted the rate of polymerisation.[5] In highly viscous reaction systems, the monomer diffusion rate is limited. As a result, chain propagation becomes slower, leading to side reactions.[5] To avoid this problem, the polymerisation was conducted using a 20% v/v toluene mixture with the monomer. Aliquots were taken from the reaction after 1, 4, and 7 h and analysed by ^{1}H NMR spectroscopy and GPC to create a kinetic profile for the reaction.

The monomer conversion and kinetic plot determined from analysis of ^{1}H NMR spectroscopy results revealed that at lower monomer conversion (< 60%) the ROP followed pseudo-first-order kinetics, however, deviation from this is observed at higher monomer conversions. This deviation is attributed to the high viscosity of the reaction mixture, which slows the rate of monomer conversion (**Figure 2.16**).

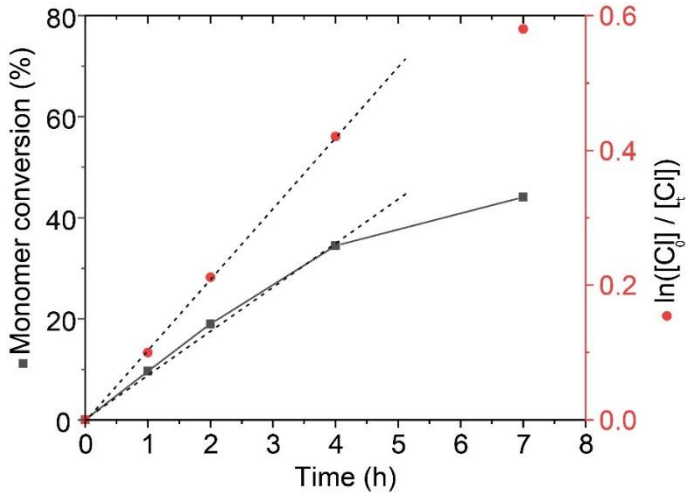


Figure 2.16: Monomer conversion and pseudo-first-order kinetics plot for the polymerisation of caprolactone from the PEG_{10} macroinitiator. Monomer conversion was calculated from NMR spectroscopy by comparing the relative integration of signals corresponding to the monomer and polymer.

GPC analysis revealed a definite shift in the copolymer peak to lower retention volumes (higher molecular weight) with time and confirmed that the block copolymer was free of PCL homopolymer impurities (**Figure 2.17**). Given that the same monomer, catalyst and gas lines were used when conducting ROP with the PEG_5 and PEG_{10} macroinitiators, it can be concluded that the original PEG_5 macroinitiator must have included other impurities that initiate polymerisation. In addition, the $Đ$ did not change significantly over the course of the polymerisation for the PEG_{10} macroinitiator, which also indicates that the polymerisation was free from side reactions.

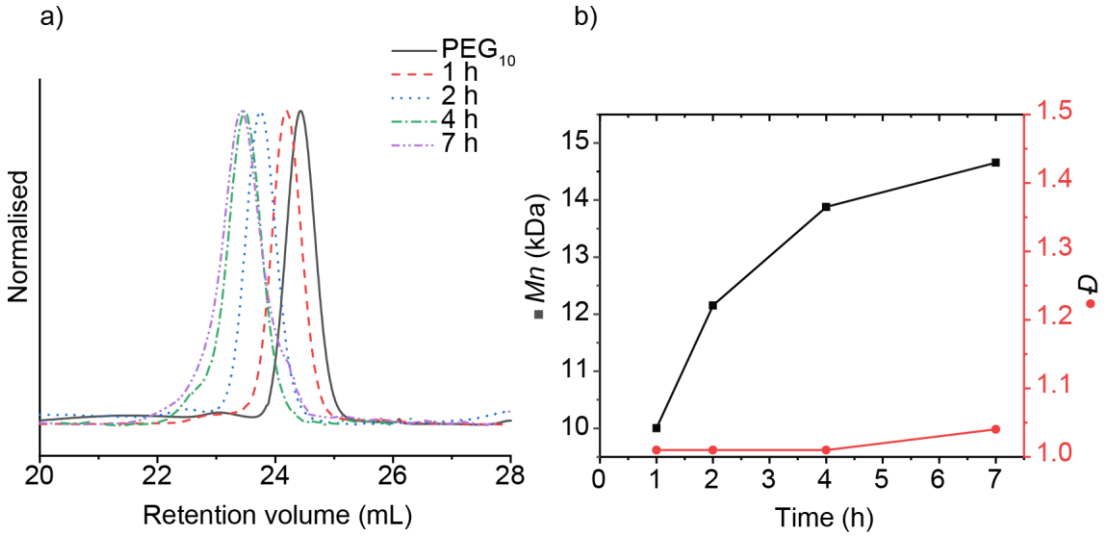


Figure 2.17: a) Normalised GPC DRI chromatograms for ROP of caprolactone from the PEG_{10} macroinitiator at various timepoints and b) M_n and $Đ$ values over time for the polymerisation (M_n determined from ^{1}H NMR spectroscopy and $Đ$ from GPC analysis). Normalisation was conducted relative to the copolymer peak height for each sample.

After establishing the kinetic profile, a series of $PEG_{10}PCL_y$ copolymers were prepared with targeted PCL molecular weights of M_n = 2.5, 7.50, 10 and 15 kDa, by conducting the ROP for 0.5, 2.15, 3.5 and 5 h. Given the absence of PCL homopolymer contamination, the polymers were isolated via precipitation into DEE and analysed via ^{1}H NMR spectroscopy (**Figure 2.18**) and GPC (**Figure 2.19**), which both confirmed successful formation of the desired block copolymers.

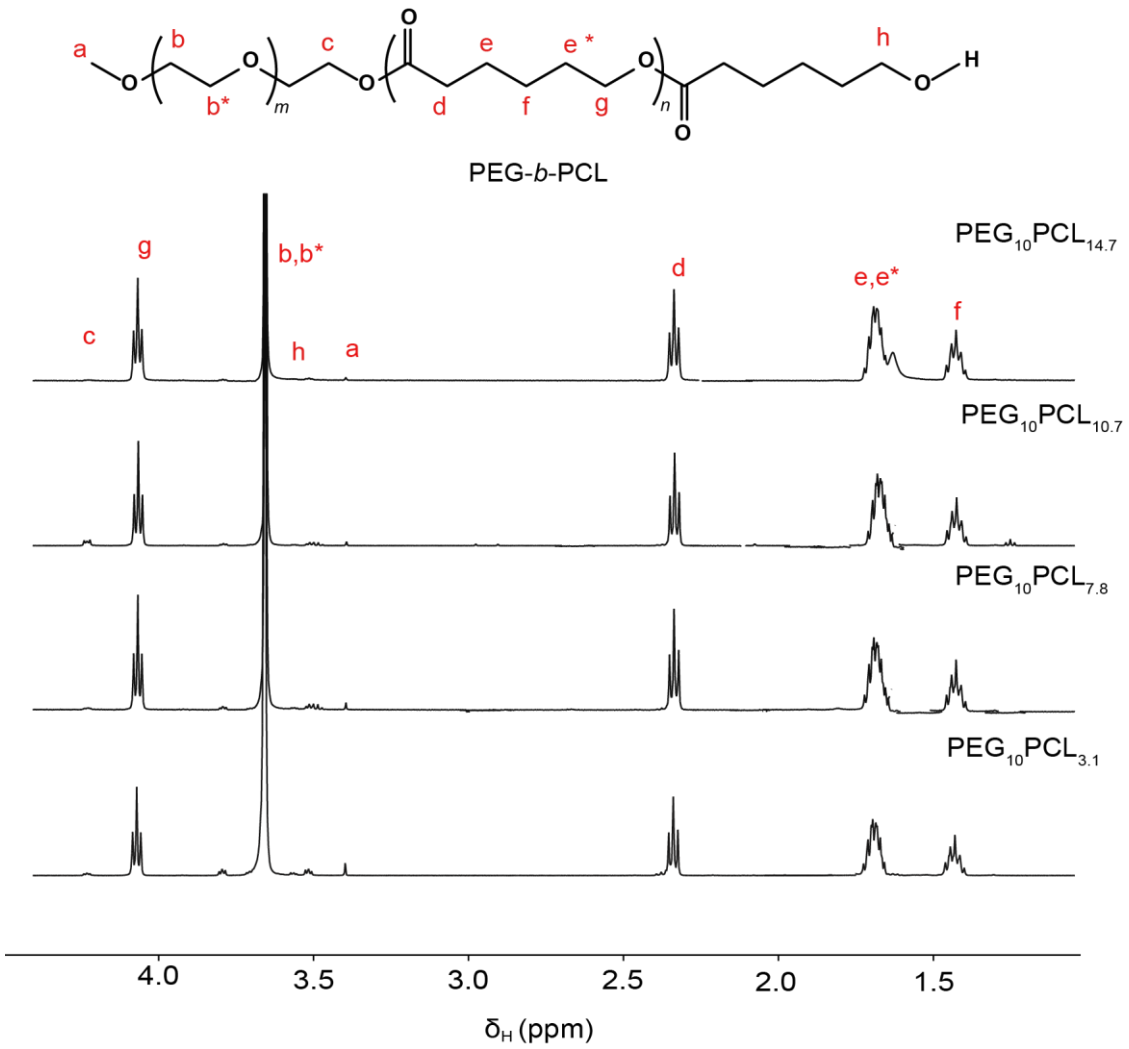


Figure 2.18: ^{1}H NMR spectra ($CDCl_3$, 298 K) of the purified $PEG_{10}PCL_y$ block copolymer series. The M_n values of PCL block was calculated from the ratio of the integral values of the methylene protons for PEG (δ_H = 3.64 ppm) and the methylene protons adjacent to the ester group in PCL (δ_H = 4.06 ppm).

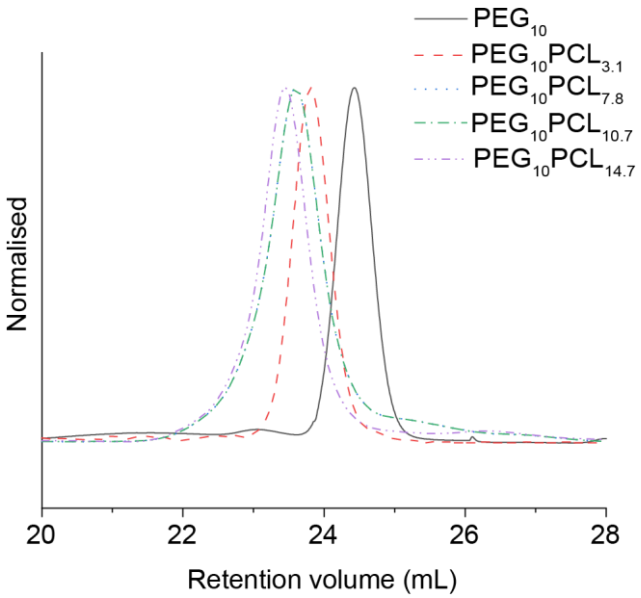


Figure 2.19: Normalised GPC DRI chromatograms of the purified $PEG_{10}PCL_y$ copolymer series. A clear shift of the peaks with time to higher retention volumes confirmed the successful synthesis of the block copolymers. Normalisation was conducted relative to the copolymer peak height for each sample.

2.2 Conclusion

The synthesis of PEG-*b*-PCL block copolymer with narrow *Đ* and free from impurity was successfully achieved through optimisation of the polymerisation conditions. Initially, conventional ROP polymerisation in dilute solution was studied, which resulted in polymers with broad *Đ* due to side reactions (intermolecular chain-transfer and intramolecular back-biting) at higher monomer conversation and long reaction time. In comparison, bulk polymerisation at low monomer conversions was found to provide satisfactory results with narrow *Đ* and high purity copolymers. Three different copolymer series were prepared using PEG macroinitiators with molecular weights of 2 kDa (PEG_2), 5 kDa (PEG_5) and 10 kDa (PEG_{10}) to afford copolymers with a range of different PCL:PEG molecular weight ratios ranging from 0.1:1 to 2:1. Detailed kinetic experiments revealed that the PCL polymerisation generally follows first-order reaction kinetics in the absence of side reactions and at lower monomer conversions. For the synthesis of the PEG_2PCL_y copolymer series, polymerisations were conducted at low monomer conversions (< 50%) to provide copolymers with targeted PCL M_n and proved to be acceptable to avoid side reaction. In contrast, this technique inhibits the extent of side reactions in polymerisations with the PEG_5 and PEG_{10} macroinitiators; however, they are not completely unavoidable. Therefore, pure copolymers were obtained by using a binary solvent mixture of 30% v/v EtOAc in DEE to purify the crude polymers of PCL homopolymer impurities which displayed good solubility in this solvent mixture. The use of binary solvent mixtures provides a novel approach for the purification of these polymers which has not been reported previously and may be applicable to other copolymer systems. This study has also highlighted the need to ensure that the macroinitiators are free of impurities that could interfere with the desired polymerisation. Whereas PEG-*b*-PCL copolymers of narrow *Đ* (< 1.12) were prepared in this work, it is evident that more studies are required to develop efficient synthetic methods that are translatable to commercial production, particularly considering the broader applications of PEG-*b*-PCL copolymers in the biomedical sector.

2.3 Experimental

2.3.1 Materials

ε-Caprolactone (ε-CL, Aldrich) was dried under vacuum (0.1 mbar) for 1 h prior to use. α-methoxy-ω-hydroxy poly(ethylene glycol) (PEG): M_n = 2 kDa and 5 kDa (two batches) were purchased from Aldrich, and M_n = 10 kDa was purchased from Creative PEG works. PEG_2 and PEG_5 were dried at 120 °C under vacuum (0.1 mbar) for 1 h to remove residual water. Stannous octoate ($Sn(Oct)_2$, Aldrich) was used without further purification. DEE, chloroform ($CDCl_3$), MeOH, toluene, EtOAC, dimethylformamide (DMF) and hexane were purchased from Chem-Supply and used as received. All the solvents used are analytical grade. Anhydrous toluene, $CDCl_3$, deuterated chloroform ($CDCl_3$; 99.8%), and lithium chloride (LiCl) were purchased from Sigma-Aldrich.

2.3.2 Characterisation of PEG-*b*-PCL copolymers

^1H NMR spectroscopy was conducted on an Agilent 500 MHz spectrometer operating at 500 MHz (A500a Agilent, Santa Clara, California, United States). A sample concentration of 5 mg/mL in $CDCl_3$ was used. The ratio of the integral values of the methylene protons from PEG (δ_H = 3.64 ppm) and the methylene protons adjacent to the ester bond in PCL (δ_H = 4.06 ppm) was used to calculate the number of repeating units, and subsequently the M_n values by multiplying by the molecular weight of a single repeating unit.

GPC was performed on a Prominence Liquid Chromatography system (Shimadzu, Japan) equipped with a RID-10A refractive index detector and three Shim-pack columns in series (GPC-8025D, GPC-805D and GPC-80MD) at 60 °C. 0.05 M LiCl in DMF was used as the mobile phase at a flow rate of 1.0 mL/min. The injection volume was 50 µL. Molecular weight characteristics were determined with reference to a conventional calibration with PEG standards (Sigma-Aldrich).

2.3.3 Synthesis of PEG-*b*-PCL copolymers

PEG-*b*-PCL block copolymers were synthesised via ROP of ε-caprolactone from PEG macroinitiators (M_n = 2, 5 and 10 kDa) using $Sn(Oct)_2$ as the catalyst. Slightly different methods were used for each of the macroinitiators as described in more detail below. The block copolymers were referred to as PEG_xPCL_y copolymers where the subscript x and y refer to the M_n (kDa) of the respective blocks.

Synthesis of PEG_2PCL_y copolymers in solution

PEG_2 macroinitiator (0.500 g, 0.250 mmol) was weighed into a round bottom flask and attached to a nitrogen line. The whole system was purged with nitrogen. Anhydrous toluene (25 mL) was added, and the flask was heated at 120 °C using a preheated oil bath. ε-Caprolactone (1.95 mL, 17.5 mmol) was then added, followed by $Sn(Oct)_2$ (0.162 mL, 0.500 mmol). The [I]:[M]:[cat.] ratio was 1:70:2. Every 24 h a 0.1 mL aliquot was taken from the reaction mixture and diluted in 0.9 mL of 0.05 M LiCl in DMF and analysed by GPC.

Synthesis of PEG$_2$PCLy copolymers in bulk

For the PEG_2PCL_y block copolymer series, PEG_2 macroinitiator (1.5 g, 0.750 mmol) was weighed into a Schlenk flask and dried *in vacuo* (0.1 mbar) at 120 °C for 1 h before back-purging with nitrogen. The flask was placed in a preheated oil bath at 115 °C, and ε-caprolactone (8.8 mL, 790 mmol) and $Sn(Oct)_2$ (0.122 mL, 0.378 mmol) were added to provide a [M]:[I]:[cat] mole ratio of 105:1:0.5. $PEG_2PCL_{0.4}$, $PEG_2PCL_{1.1}$, $PEG_2PCL_{1.8}$ and $PEG_2PCL_{3.9}$ were prepared using polymerisation times of 40, 60, 120 and 230 min, respectively. The crude polymerisation mixture was cooled to room temperature, diluted in chloroform (4 mL) and precipitated in diethyl ether (40 mL). The polymer was isolated via centrifugation (6000 rpm, 15 min). This precipitation procedure was repeated three times to remove all unreacted monomer and catalyst. Finally, the polymer was then dried *in vacuo* (0.01 mbar) for 72 h and stored at room temperature in the dark.

Synthesis of PEG_5PCLy copolymers in bulk

For the PEG_5PCL_y block copolymer series, PEG_5 macroinitiator (1.5 g, 0.300 mmol) was weighed into a Schlenk flask and dried *in vacuo* at 120 °C for 1 h before back-purging with nitrogen. The flask was placed in a preheated oil bath at 120 °C, and ε-caprolactone (3.5 mL, 32 mmol) and Sn(Oct)2 (0.049 mL, 0.15 mmol) were added to provide a [M]:[I]:[cat] mole ratio of 105:1:0.5. $PEG_5PCL_{0.6}$, $PEG_5PCL_{1.3}$, $PEG_5PCL_{2.3}$, $PEG_5PCL_{4.2}$ and $PEG_5PCL_{9.4}$ were prepared using polymerisation times of 2, 6, 10, 24 and 50 min, respectively. The crude polymerisation mixture was cooled to room temperature, diluted in chloroform (4 mL) and precipitated into 30% v/v ethyl acetate in diethyl ether (40 mL). The polymer was isolated via centrifugation (6000 rpm, 15 min). This precipitation procedure was repeated three times and the polymers were then dried *in vacuo* (0.01 mbar) for 72 h and stored at room temperature in the dark.

Synthesis of $PEG_{10}PCLy$ copolymers in bulk

For the $PEG_{10}PCL_y$ block copolymer series, PEG_{10} macroinitiator (1.0 g, 0.10 mmol) was weighed into a Schlenk flask and purged with nitrogen. The Schlenk flask was then placed in an oil bath at 120 °C. Anhydrous toluene (5 mL), ε-caprolactone (4.3 mL, 39 mmol) and $Sn(Oct)_2$ (0.064 mL, 0.2 mmol) were added to provide a [M]:[I]:[cat] mole ratio of 395:1:2. $PEG_{10}PCL_{3.1}$, $PEG_{10}PCL_{7.8}$, $PEG_{10}PCL_{10.7}$, and $PEG_{10}PCL_{14.7}$ were prepared using polymerisation times of 30, 135, 210 and 300 min. The crude polymerisation mixture was cooled to room temperature, diluted in chloroform (4 mL) and precipitated into diethyl ether (40 mL). The polymer was isolated via centrifugation (6000 rpm, 15 min). This precipitation procedure was repeated three times, and the polymers were then dried *in vacuo* (0.01 mbar) for 72 h and stored at room temperature in the dark.

2.4 References

1. Hwang, M. J.; Suh, J. M.; Bae, Y. H.; Kim, S. W.; Jeong, B., Caprolactonic poloxamer analog: PEG-PCL-PEG. *Biomacromolecules* **2005**, *6* (2), 885-890.

2. Koutroumanis, K. P.; Holdich, R. G.; Georgiadou, S., Synthesis and micellization of a pH-sensitive diblock copolymer for drug delivery. *Int. J. Pharm.* **2013**, *455* (1), 5-13.

3. Labet, M.; Thielemans, W., Synthesis of polycaprolactone: a review. *Chem. Soc. Rev.* **2009**, *38* (12), 3484-3504.

4. Penczek, S., Cationic ring-opening polymerisation (CROP) major mechanistic phenomena. *J. Polym. Sci., Part A: Polym. Chem.* **2000**, *38* (11), 1919-1933.

5. Wu, D.; Lv, Y.; Guo, R.; Li, J.; Habadati, A.; Lu, B.; Wang, H.; Wei, Z., Kinetics of Sn(Oct)2-catalyzed ring opening polymerisation of caprolactone. *Macromol. Res.* **2017**, *25* (11), 1070-1075.

6. Herzberger, J.; Niederer, K.; Pohlit, H.; Seiwert, J.; Worm, M.; Wurm, F. R.; Frey, H., Polymerisation of ethylene oxide, propylene oxide, and other alkylene oxides: Synthesis, novel polymer architectures, and bioconjugation. *Chem. Rev.* **2016**, *116* (4), 2170-2243.

7. Zhang, J.; Zhao, Y.-J.; Su, Z.-G.; Ma, G.-H., Synthesis of monomethoxy poly(ethylene glycol) without diol poly(ethylene glycol). *J. Appl. Polym. Sci.* **2007**, *105* (6), 3782-3786.

8. Bordes, C.; Fréville, V.; Ruffin, E.; Marote, P.; Gauvrit, J. Y.; Briançon, S.; Lantéri, P., Determination of poly(ε-caprolactone) solubility parameters: Application to solvent substitution in a microencapsulation process. *Int. J. Pharm.* **2010,** *383* (1), 236-243.

Chapter 3

Relationship between molecular structure and self-assembly of poly(ethylene glycol-*b*-caprolactone) copolymers in aqueous solution

Chapter overview

The self-assembly of amphiphilic block copolymers in aqueous solution is an inherent characteristic that is fundamental to the formation of hierarchically structured aggregate systems (e.g., aggregates and polymersomes) with importance to nanomedicine drug delivery, cosmetics and food technologies. Understanding the microstructural parameters that control aggregate formation and structure are paramount for the rational design and application of such systems. Nevertheless, the self-assembly process of block copolymers in aqueous solution remains an area of conjecture.

An integrated approach has been employed in this study to investigate the correlation between self-assembly behaviour of PEG-*b*-PCL with the microstructural properties of the copolymer; specifically, the PCL:PEG ratio and PEG molecular weight of PEG-*b*-PCL block copolymers. PEG-*b*-PCL, block copolymer systems have received significant attention due to their ability to encapsulate a wide range of insoluble drugs into their aggregate cores, as well as for their biocompatibility which ensures their safe post-application clearance from the body. A large family of well-defined blocks copolymers were synthesised with variable PEG and PCL block lengths and the narrow $Đ$ (< 1.12) to guarantee that reliable and comprehensive trends in the self-assembly behaviour of PEG-*b*-PCL aggregate systems. The M_n of PEG and PCL is between 2 to 10 and 0.5 to 15 kDa, respectively.

A combination of PGSTE NMR spectroscopy, DLS and SAXS techniques have been used to characterise the polymer aggregate system. The PGSTE NMR spectroscopy of the block copolymer solutions allowed the diffusivity of both the PEG and PCL blocks to be determined, from which their aggregation characteristics could be inferred; this has proved to be a valuable tool for the identification of heterogeneity within the aggregate structures. DLS analysis provided further evidence for the dispersity of the aggregate structures, whereas SAXS analysis was used to determine the morphology and size of the aggregates.

For all of the copolymers, a clear transition in the aggregate structure was observed when the PCL:PEG ratio was increased at a constant PEG block length. However, the nature of this transition is also dependent on the PEG block length. Copolymers with low PEG molecular weight (2 kDa) were observed to transition from unimers and loosely associated unimers to metastable aggregates and finally defined cylindrical aggregates as the PCL molecular weight was increased. In comparison, copolymers with PEG molecular weight of 5 and 10 kDa transitioned from heterogenous gel-like aggregates to cylindrical aggregates and finally well-defined ellipsoid aggregates as the PCL:PEG ratio was increased. In all cases the PGSTE NMR spectroscopy, DLS and SAXS results provided complementary information and the grounds for a phase diagram relating the copolymer microstructure to their aggregation behaviour. Importantly, the absence of commonly depicted spherical aggregates has implications for applications where properties may be governed by shape, for example, cellular uptake for nanomedicine formulations.

3.1 Results and Discussion

3.1.1 Synthesis and characterisation of PEG-*b*-PCL copolymers

PEG-*b*-PCL copolymers with different molecular weights and compositions were prepared via ROP as outlined in detail in Chapter 2. As discussed at Chapter 2 and **Table 2.1**, the copolymers were categorised into three groups based on the M_n of the PEG block, and are referred to as PEG_xPCL_y, whereby x and y refer to the approximate M_n of each block.

3.1.2 Correlating PEG-*b*-PCL microstructure to self-assembly behaviours

In this study, thirteen well-defined PEG-*b*-PCL copolymers prepared and used to provide a comprehensive scenario of their self-assembly behaviour in water and the resulting morphology of the self-assembled aggregates. The extensive investigation of PEG-*b*-PCL copolymers self-assembly using DLS, PGSTE NMR spectroscopy and SAXS has not been reported before. The self-assembled aggregates were initially studied by PGSTE NMR spectroscopy and DLS analysis to provide complementary information about the effect of the copolymer microstructure on the dispersity of the aggregates. Subsequently, SAXS analysis was employed to provide details about the structure and size of the aggregates.

3.1.2.1 PGSTE NMR spectroscopy of self-assembled PEG-b-PCL copolymer aggregates

The dispersity of the aggregates in D_2O was analysed by interpreting the *D* distribution obtained from PGSTE NMR experiments (refer to Experimental section for further details and definitions). The *D* distribution also reflects the distribution of aggregate sizes as described by the Stokes-Einstein–Sutherland.[1,2] Analysis of the PEG_2, PEG_5, and PEG_{10} homopolymers (1 mg/mL) in water (D_2O) was initially conducted to establish a baseline from which to compare with the copolymer aggregates (**Figure 3.1**). The attenuation of the methylene proton resonance from the PEG backbone (δ_H = 3.6 ppm) has been used to calculate *D* value. The value of *D* for PEG_2, PEG_5, and PEG_{10} is 14.2×10^{-11}, 8.61×10^{-11} and 5.8×10^{-11} m^2/s respectively, which is similar to the values reported previously.[3]

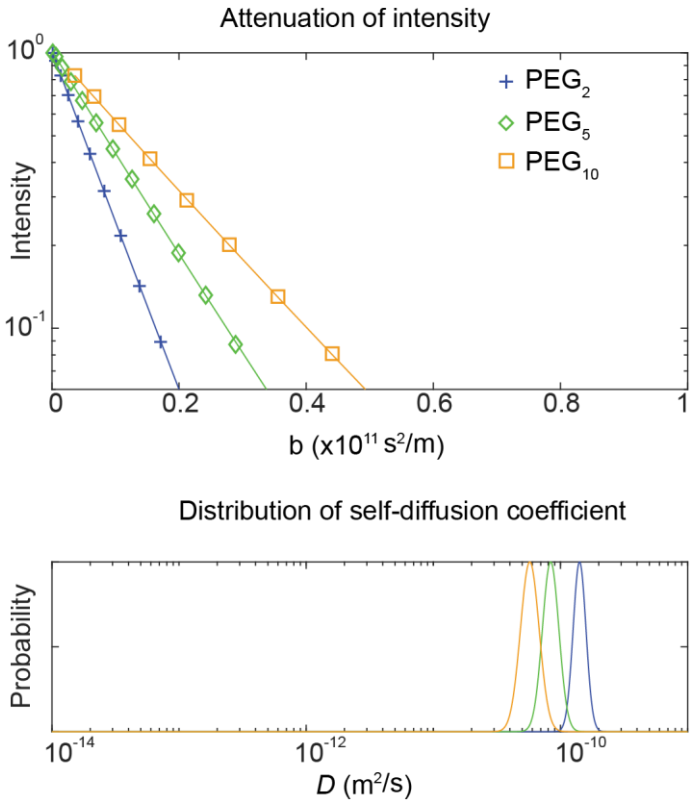


Figure 3.1: a) PGSTE NMR signal intensity decay profile and b) *D* distributions for the methylene protons of the PEG backbone (δ_H = 3.6 ppm) of the PEG_2 (blue), PEG_5 (green) and PEG_{10} (yellow) homopolymers in D_2O.

As expected, the *D* value decreased with increasing molecular weight due to an increase in the hydrodynamic size of the randomly coiled polymers in solution, and the *D* distributions were narrow due to the homopolymers narrow *Đ*.

Analysis of the ^{1}H NMR spectra of PEG-*b*-PCL copolymer in $CDCl_3$ revealed characteristic methylene proton resonances of the PEG repeating unit (RU) at δ_H = 3.6 ppm and resonances corresponding to those of the PCL RU at δ_H = 1.4 (–$CH_2C\mathbf{H}_2CH_2$–), 1.6 (–$C\mathbf{H}_2CH_2C\mathbf{H}_2$), 2.3 (– $COC\mathbf{H}_2CH_2$–) and 4.1 (–$CH_2C\mathbf{H}_2O$–) ppm, respectively (**Figure 3.2b**). The ^{1}H NMR spectra of the copolymers in D_2O shows the characteristic methylene proton resonances from the PEG and PCL blocks (**Figure 3.2c**). The proton spectra relate to the core-forming block of the polymer generally do not appear in the ^{1}H NMR due to the integration of the hydrophobic component within the solid dehydrated aggregate core.[4,5]

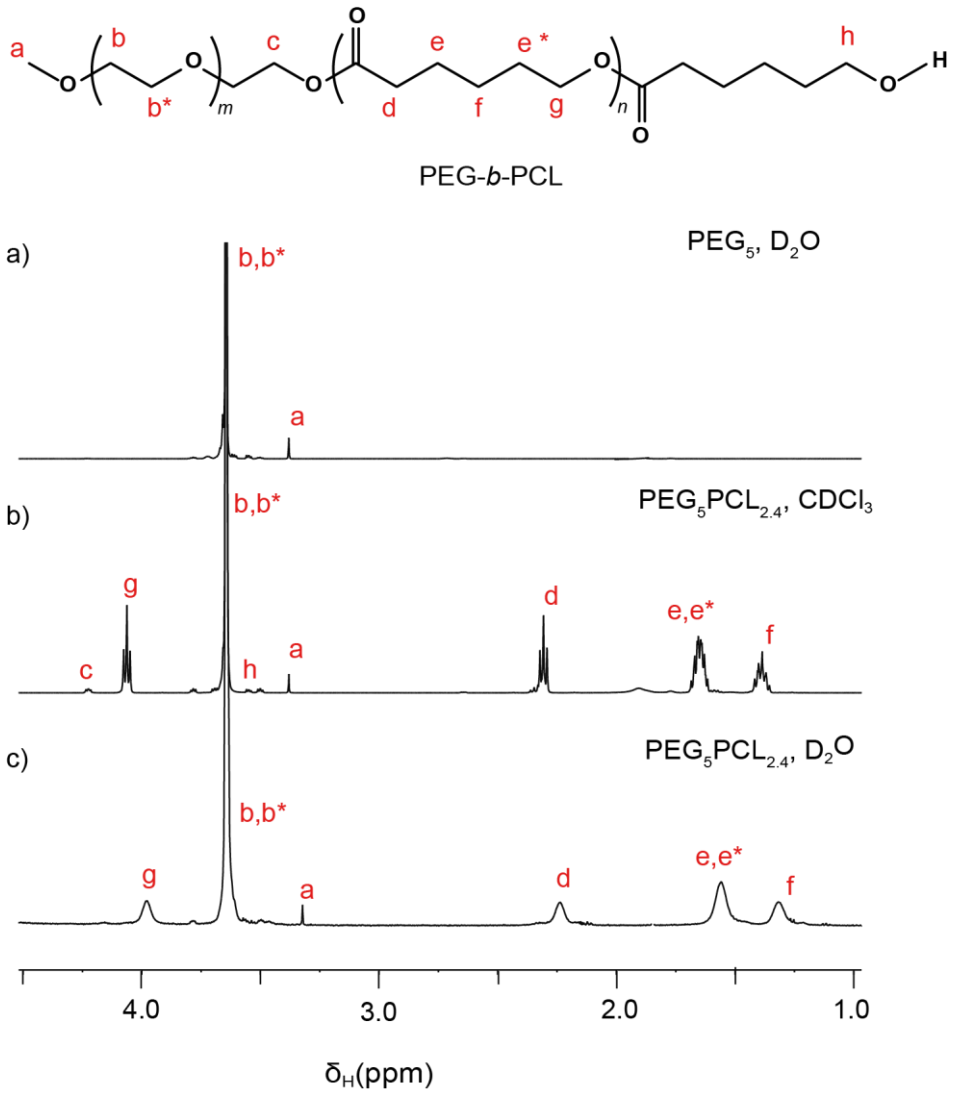


Figure 3.2: ^{1}H NMR spectra of a) PEG_5 homopolymer in D_2O solution; b) $PEG_5PCL_{2.4}$ copolymer in chloroform ($CDCl_3$, 298 K) solution; c) $PEG_5PCL_{2.4}$ copolymer in D_2O solution. PEG and PCL characteristic peaks from PEG-*b*-PCL copolymer in D_2O solution are broad comparing to $CDCl_3$ solution indicates polymer individual polymer units are experiencing slightly different environment from each other.

It is possible there is a hydrated boundary area exists between core and corona (shell) of the polymer aggregate; as penetration of water in polymer, the aggregate core is previously reported in the literature.[6,7] PCL characteristic signal might be originated from that hydrated layer (**Figure 3.3**).

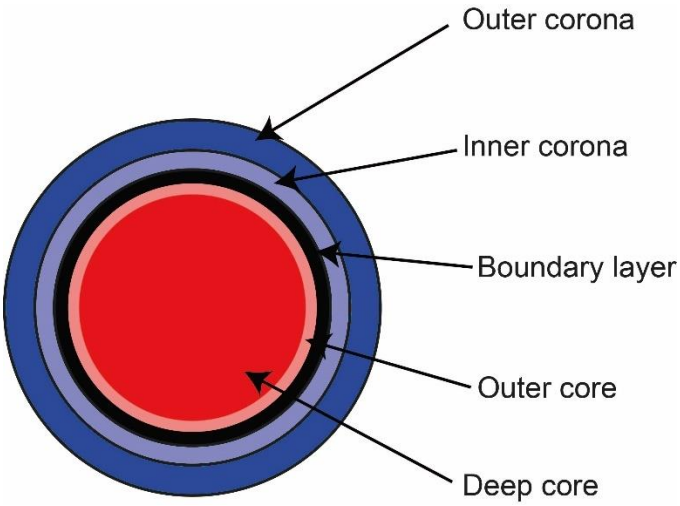


Figure 3.3: An illustration of the hypothetical layered aggregate structure. An aggregate structure was hypothesised that consisted of five distinct regions (i) the outer corona which is completely hydrated by the solvent; (ii) the inner corona which is well hydrated and adjacent to the boundary layer; (iii) the boundary layer, where the core and corona meet and is partially hydrated (the movement of polymer here is restricted); (iv) outer core which is adjacent to the boundary layer, and; (v) the deep core which is totally segregated from the solvent and the aqueous surroundings.

PCL characteristic peaks appear as a broad apparent singlet in D_2O, whereas a distinct triplet and multiplet signals appear in $CDCl_3$ (**Figure 3.2b and c**). The shape of the PCL peak represents superpositioned peaks attributed to a collection of species which are chemically equivalent yet experiencing the different magnetic environment.

Liu *et al.* investigated the assembly of a PEG-*b*-PCL and poly(caprolactone)-*b*-poly(4-vinylpyridine) (PCL-*b*-P4VP) in different pH observing the characteristic aromatic proton signal from P4VP.[8] The work of Liu *et al*. showed that at lower pH 2.0, the aromatic proton signal appears as P4VP become protonated and water soluble; the signal disappears at pH 7.0 as P4VP become hydrophobic and moves to aggregate core. It can be concluded appearance of PCL signal in ^{1}H NMR spectra relates to hydration level of PCL; the part of the core which is close to the boundary layer PCL might be in a hydrated state. It can be hypothesised if PCL in that boundary layer anchored with the core, the mobility of the PCL will significantly be reduced. Analysis of *D* of the PCL using PGSTE experiment will provide more evidence to support that.

In this study, both PEG and PCL characteristic proton resonance (PEG (δ_H = 3.6 ppm) and PCL (δ_H = 1.6 ppm)) were separately analysed to produce two *D* distributions. As the PEG and PCL blocks are covalently tethered to one another in the copolymers one may expect that the distributions should be similar for the self-assembled aggregates. However, certain weighting effects can cause deviations of the two measured distributions, which can be indicative of underlying heterogeneity.[9] In particular, differences in NMR relaxation times between blocks, a dependence of relaxation time on aggregate structure, and a broad distribution of structures can cause the measured *D* distributions of the two blocks to deviate from one another, an effect broadly known as relaxation weighting. In all polymer (expect $PEG_2PCL_{0.4}$) series *D* distribution shifted to a lower value for both PCL and PEG, which confirms self-assembly of the polymer. As *D* distribution of PCL also shifted to a lower value, it confirms PCL signal is originated from the boundary layer in the polymer aggregate (**Figure 3.4**).

The *D* distributions for the PEG_2PCL_y copolymers series revealed that there was a significant change in aggregate assembly as the PCL block length was varied (**Figure 3.4a**). The PEG and PCL *D* distributions for the $PEG_2PCL_{0.4}$ copolymer revealed a similar pattern to the PEG_2 homopolymer distribution, although slightly broadened. The lack of a shift in the *D* value is indicative of the block copolymers existing as individually solvated molecules (unimers) or loosely associated unimers in solution, whereas the overlapping and narrow *D* distributions for the two blocks suggest that the sample is homogenous. These results imply that the low PCL:PEG ratio (0.25:1) fails to stabilise aggregation or a hydrophobic core structure. As the main driving force behind aggregate formation is the hydrophobic interactions between the PCL blocks within the core resulting from energetically unfavourable PCL–water interactions.[10,11] Hence, it is evident that for the $PEG_2PCL_{0.4}$ copolymer, with the short PCL block (degree of polymerisation (DP) ~ 4), is insufficient to induce self-assembly.

Furthermore, at very low DPs the interaction of the hydroxyl end-group of the PCL block with water may still be significant when compared to PCL blocks with much higher DPs, which might increase the solvation of the PCL and reduce hydrophobic interactions between the short PCL blocks resulting in unfavourable conditions for aggregate formation.[12]

This behaviour has not been described for PEG-*b*-PCL; however, this behaviour has observed for poly(acrylic acid-*b*-methyl methacrylate) (PAA-*b*-MMA) block copolymers with short MMA blocks, which were reported to be mainly present in aqueous solution as unassociated unimer.[13]

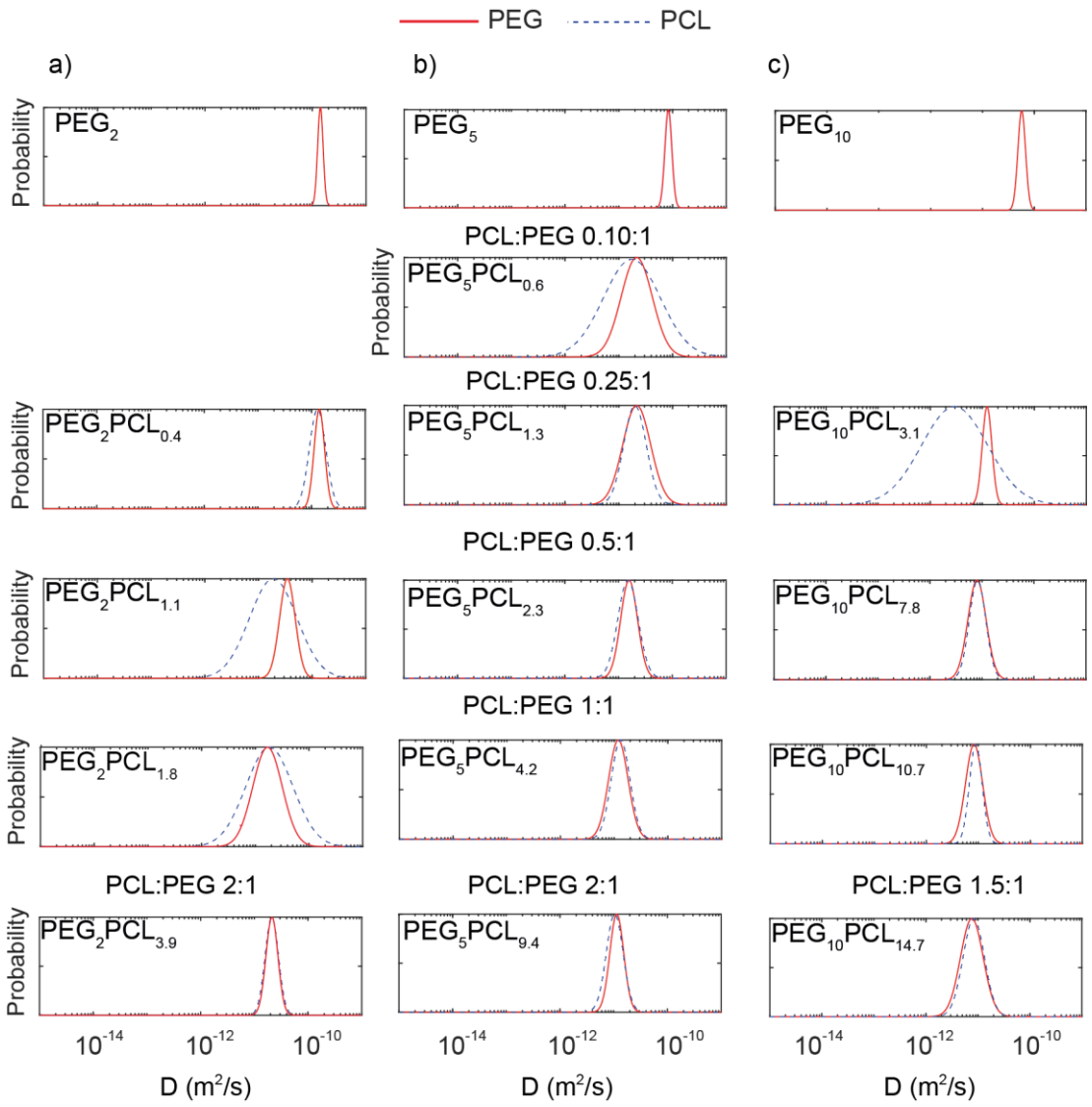


Figure 3.4: *D* distribution for the PEG (red) and PCL (blue) blocks of a) PEG_2 homopolymer and PEG_2PCL_y copolymers series; b) PEG_5 homopolymer and PEG_5PCL_y copolymers series; c) PEG_{10} homopolymer and $PEG_{10}PCL_y$ copolymers series in D_2O.

In comparison, the *D* distributions for the $PEG_2PCL_{1.1}$ and $PEG_2PCL_{1.8}$ copolymers were shifted toward significantly lower values, consistent with the formation of larger aggregates. Furthermore, the PEG and PCL *D* distributions were broader and diverged from one another, indicating some underlying heterogeneity in the size of the aggregates. These results are consistent with TEM studies conducted by Rizis *et al.* on PEG_2PCL_2 copolymer, which was found to adopt heterogeneous aggregates characterised by spherical and rod-like structures.[14] For the $PEG_2PCL_{3.9}$ copolymer the narrow *D* distributions for the PEG and PCL blocks coincided and were shifted to lower *D* values compared to the PEG_2 homopolymer, indicative of well-defined aggregates such as aggregates with low dispersity.

For the PEG_5PCL_y copolymers series, the *D* distributions were very similar to one another with the exception of the $PEG_5PCL_{0.6}$ copolymer (**Figure 3.4b**). For the $PEG_5PCL_{0.6}$ copolymer the shift in *D* values relative to the PEG_5 homopolymer indicates aggregate formation, but the *D* distribution for the PCL block was significantly broader than that of the PEG block, implying some underlying heterogeneity in the aggerate structure, possibly due to the formation of loose or unstable aggregates. $PEG_5PCL_{0.6}$ copolymer forms aggregate when the $PEG_2PCL_{0.4}$ copolymer does not, suggests that either the PCL block length (DP ~ 5) is sufficient to induce hydrophobic interactions in the former or that the PEG block length plays a role in stabilising hydrophobic interactions. In general, the *D* distributions for the PEG and PCL blocks overlapped and shifted to lower *D* values when compared to the PEG_5 homopolymer, indicating that they all form defined aggregates of similar size. As the PCL block length was increased from $PEG_5PCL_{1.3}$ (DP ~ 11) to $PEG_5PCL_{9.4}$ (DP ~ 83) the *D* distributions were found to narrow, indicating the formation of lower dispersity aggregates coinciding with an increase in hydrophobic interactions.

The trends observed for the *D* distributions for the $PEG_{10}PCL_y$ copolymers series (**Figure 3.4c**) somewhat resemble those for the PEG_5PCL_y copolymers series, with larger PCL block lengths leading to the formation of well-defined aggregates. However, The PEG and PCL *D* distributions for the $PEG_{10}PCL_{3.1}$ copolymer are distinctly different, with the former being narrow and the latter very broad. This would indicate that the aggregates are very heterogeneous, although the reason for this is not obvious given that the PCL DP (~ 28) is reasonably large and PEG_5PCL_y copolymers with similar PCL block lengths formed well-defined aggregates.

The mean self-diffusivities ($\langle D \rangle$) and their standard deviations for the copolymers were calculated from triplicate experiments and plotted against the PCL:PEG ratios to allow trends across the three copolymers series to be examined (**Figure 3.5**). The significant standard deviation of $\langle D \rangle$ represents instability of polymer aggregate in the aqueous system. Interestingly, the standard deviations of $\langle D \rangle$ were significant for the $PEG_2PCL_{0.4}$, $PEG_2PCL_{1.1}$ and $PEG_{10}PCL_{3.1}$ copolymers revealing the presence of dispersed aggregates for which the fractions of molecules filling those states can vary from sample-to-sample, and indicating the possible formation of metastable aggregates. In general, once the PCL:PEG ratio was > 0.5:1 the standard deviations of $\langle D \rangle$ were insignificant, indicating that there is either a single aggregation state (e.g., $PEG_2PCL_{3.9}$).

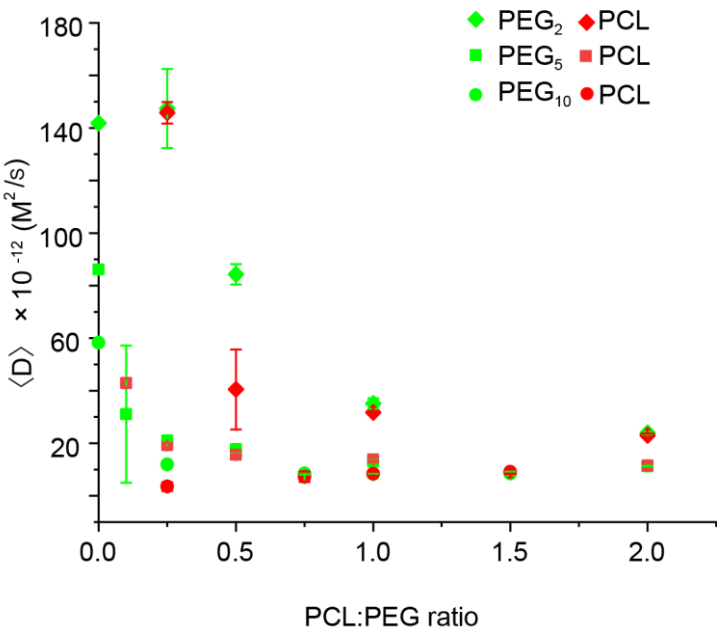


Figure 3.5: Mean (marker) and standard deviation (error bars) of $\langle D \rangle$ measured on three separate self-assembled samples for each PEG_xPCL_y copolymer, plotted against PCL:PEG ratio. The green and red symbols represent the $\langle D \rangle$ of PEG and PCL blocks, respectively, whereas the diamond, square and circle symbols correspond to the PEG_2PCL_y, PEG_5PCL_y and $PEG_{10}PCL_y$ copolymers series, respectively.

3.1.2.2 DLS analysis of self-assembled PEG-b-PCL copolymer aggregates

DLS is commonly used to measure the size (R_h) and particle size distribution (PSD) of nanoparticles in solution. The intensity PSD provides a distribution of particle sizes based on scattering intensity. As large particles scatter light more, this analysis is weighted towards larger particle. Thus, it is also essential to consider the volume PSD that calculates PSD based on the volume percentage, which gives a more unambiguous interpretation of a particle's contribution to scattering. At a PCL:PEG 0.1:1 ($PEG_5PCL_{0.6}$), the DLS measurements revealed a bimodal distribution (both intensity and number PSD), suggesting the presence of large aggregates (R_h ~1 to 10 µm) and small aggregates (R_h ~ 150 nm) (**Figure 3.6**).

These results support the NMR experiments that at a low PCL to PEG ratio, the block copolymers are forming a very disperse system containing loose polymer aggregate which responsible for a broad *D* distribution. As the PCL to PEG ratio increases, the DLS results indicate that the distribution of particle sizes becomes narrower. Intensity PSD suggests the presence of large particles, although volume PSD proves that large particles are negligible in amount. This is consistent with the monodisperse *D* distributions shown in PGSTE NMR diffusion study. In the case of PEG_2PCL_y series, at lower PCL: PEG ratio ($PEG_2PCL_{0.4}$), DLS suggests that the polymer solution is very polydisperse and contains large aggregates. However, NMR analysis revealed that there are only unimers present in solution. In a polydisperse and concentrated sample, DLS might consider a small cluster of unimers as a single large aggregate due to their proximity.[15]

DLS analysis of $PEG_2PCL_{0.4}$ was conducted in chloroform (to ensure solubility of both blocks) which again showed the presence of large particles, which would not be expected as the polymer is completely solvated, indicating that DLS is not suitable for analysis of unimers in solution (**Figure 3.7**). The decrease in width and the shift to lower R_h with increasing PCL:PEG ratio indicates the formation of more stable polymer aggregate. The $PEG_2PCL_{3.9}$ composition shows the narrowest distribution width, and $R_h \approx 10$ nm, consistent with aggregation.

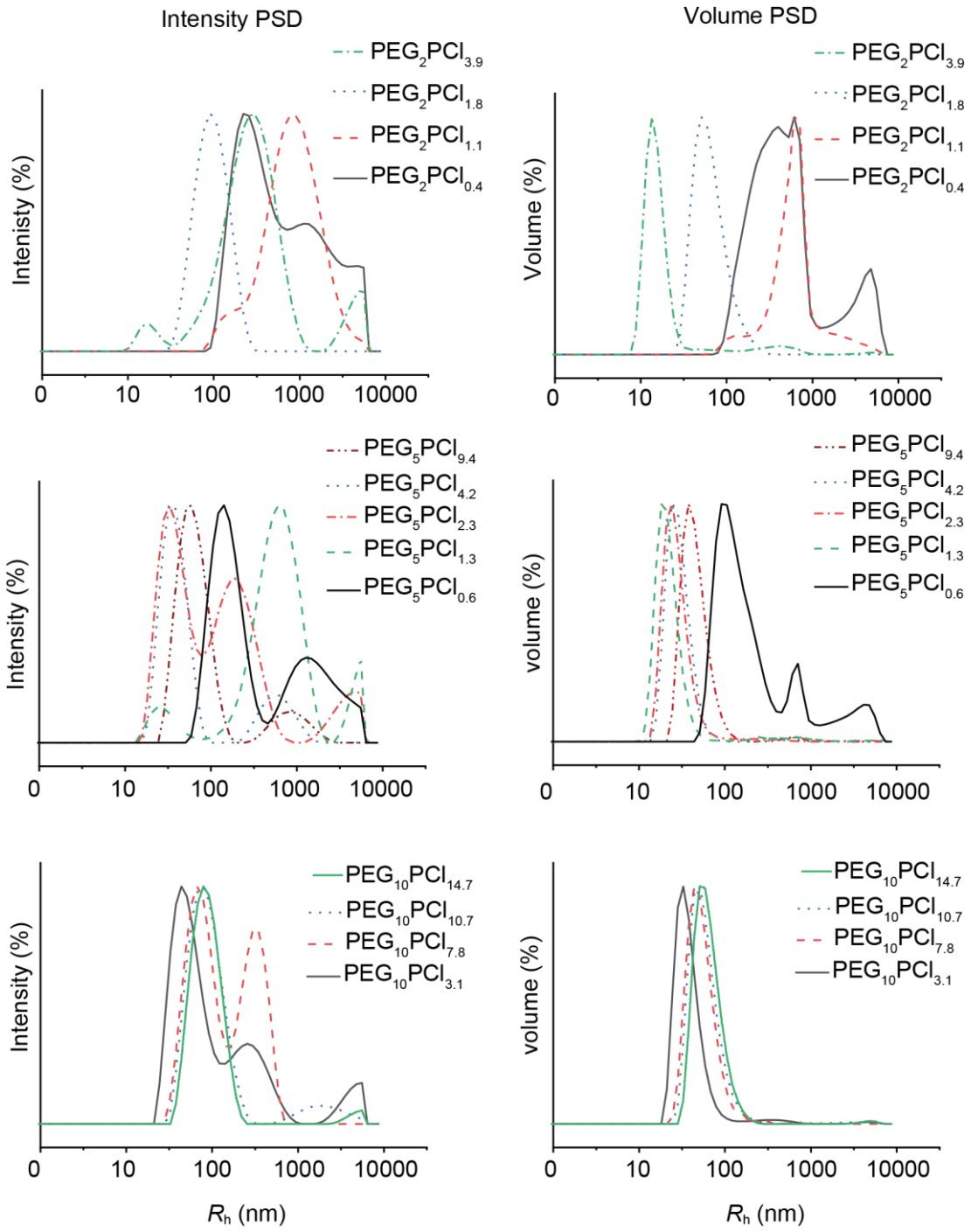


Figure 3.6: DLS analysis of particle size distribution of aggregates synthesised from PEG_xPCL_y copolymers series. The bimodal characteristic at lower PCL:PEG ratio indicates a polydisperse system.

The DLS analysis corroborates the NMR results and indicates that polymer aggregates synthesised from the PEG_5PCL_y and $PEG_{10}PCL_y$ copolymers series are more stable and symmetrical as both *D* distribution from NMR and volume PSD from DLS shows narrow distributions (**Figure 3.4** and **3.6**). However, the PSD by volume shows a bimodal distribution for polymers with a lower PCL:PEG ratio $PEG_{10}PCL_{3.1}$, similar to $PEG_2PCL_{0.4}$ and $PEG_5PCL_{0.6}$.

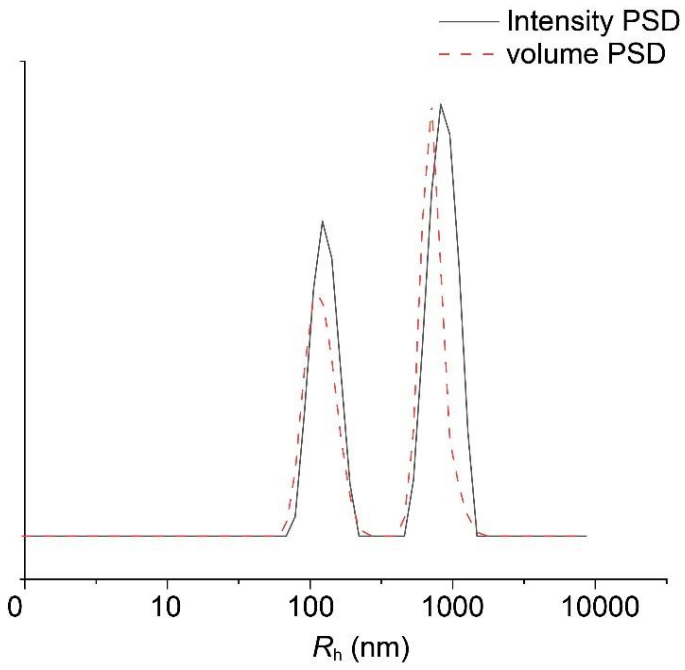


Figure 3.7: DLS analysis of the particle size distribution of $PEG_2PCL_{0.4}$ polymer solution in chloroform. The bimodal characteristic indicates DLS analysis of unimer is not providing the correct information about the system, as it should be monomodal.

The analysis of PSD by intensity and volume indicates at lower PCL:PEG ratios, polymer fails to form well-defined aggregates, evident by their broad distribution. The polydispersity index (PDI) of the polymer solutions also pointed towards the same conclusion. Similarly to the NMR experiments, the PDI acts as a measure of the aggregate dispersity, with values approaching zero representative of a monodisperse system. Therefore, DLS experiments were performed in triplicate on all copolymer solutions to determine the PDI of the aggregates with respect to the PCL:PEG ratio (**Figure 3.8**). As the PCL:PEG ratio was increased, the PDI was found to decrease, indicating the formation of well-defined aggregates, consistent with NMR spectroscopy results.

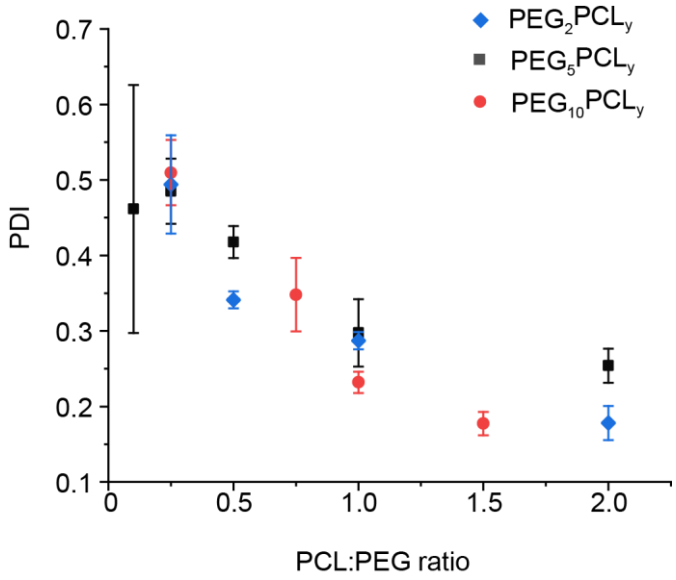


Figure 3.8: Mean (marker) and standard deviation (error bars) of PDI measured on three separate samples made for each PEG_xPCL_y composition, plotted against PCL:PEG ratios.

Nevertheless, the PDI of aggregates formed from copolymers with PCL:PEG ratios of ≤ 1:1 exhibit higher polydispersity compared to those with ratios > 1:1 indicating a transition towards the formation of more well-defined aggregate structures. For the $PEG_2PCL_{0.4}$ copolymer, the PDI (0.46) and deviation of the PDI across multiple samples was very high, which may be consistent with the presence of metastable, loosely associated unimers. Similar trends in PDI values were also observed in PEG_5PCL_y and $PEG_{10}PCL_y$ series with smaller PCL:PEG ratios, which could be indicated the inability to form well-defined aggregate at lower PCL:PEG ratios. As PCL:PEG ratio increases PDI value decreases, however, PCL:PEG ratios below 1:1 PDI values are significantly larger compared to ratios above 1:1 which indicates a transition in the self-assembly system to more well-defined aggregate.

3.1.2.3 SAXS analysis of self-assembled PEG-b-PCL copolymer aggregates

SAXS experiments were performed on the copolymer solutions in water (1 mg/mL) and the scattering intensity was fitted to various models to determine the shape and size of the resulting aggregates (**Figure 3.9**). Interestingly, the model fitting revealed that there is a transition in the aggregate structure across each copolymer series as the PCL:PEG ratio is increased, trending towards well-defined cylindrical and ellipsoidal aggregates (**Figure 3.9**).

The scattering profile of the $PEG_2PCL_{0.4}$ copolymer solution reveals a monotonic increase in scattering with a decrease in low Q (scattering vector) values which indicates the presence of large particles; however, the high Q region fit with mono gaussian polymer model (**Figure 3.9**). A combination of power-law and mono gaussian polymer model was used to interpret the scattering data and indicates the solution consists of unimers, which further support the NMR spectroscopy results. The scattering profiles of the $PEG_2PCL_{1.1}$ and $PEG_2PCL_{4.0}$ copolymer solutions were fitted best with a combination of a low Q power-law, with a cylinder form factor evident at high Q (**Figure 3.9**). The presence of the power-law at low Q was attributed to the presence of large aggregates in the solution, which could be due to the further aggregation of the primary aggregates. Unfortunately, the cylindrical length of the aggregates could not be determined as the low Q Guinier plateau was obscured by the power-law scattering from the larger aggregates. In comparison, fitting of the scattering profile for the $PEG_2PCL_{1.8}$ copolymer solution to a flexible cylinder or worm-like aggregate model worked best when a polydispersity parameter (radius scale 0.2) was added. These results are consistent with previous studies by Rizis *et al.* on PEG-*b*-PCL copolymers with short PEG (2 kDa) block lengths whereby long thread-like or cylindrical aggregates were observed via TEM,[14] and support the predictions of Nagarajan based upon thermodynamic considerations between the core and corona that small hydrophilic blocks will result in the formation of cylindrical aggregates.[16]

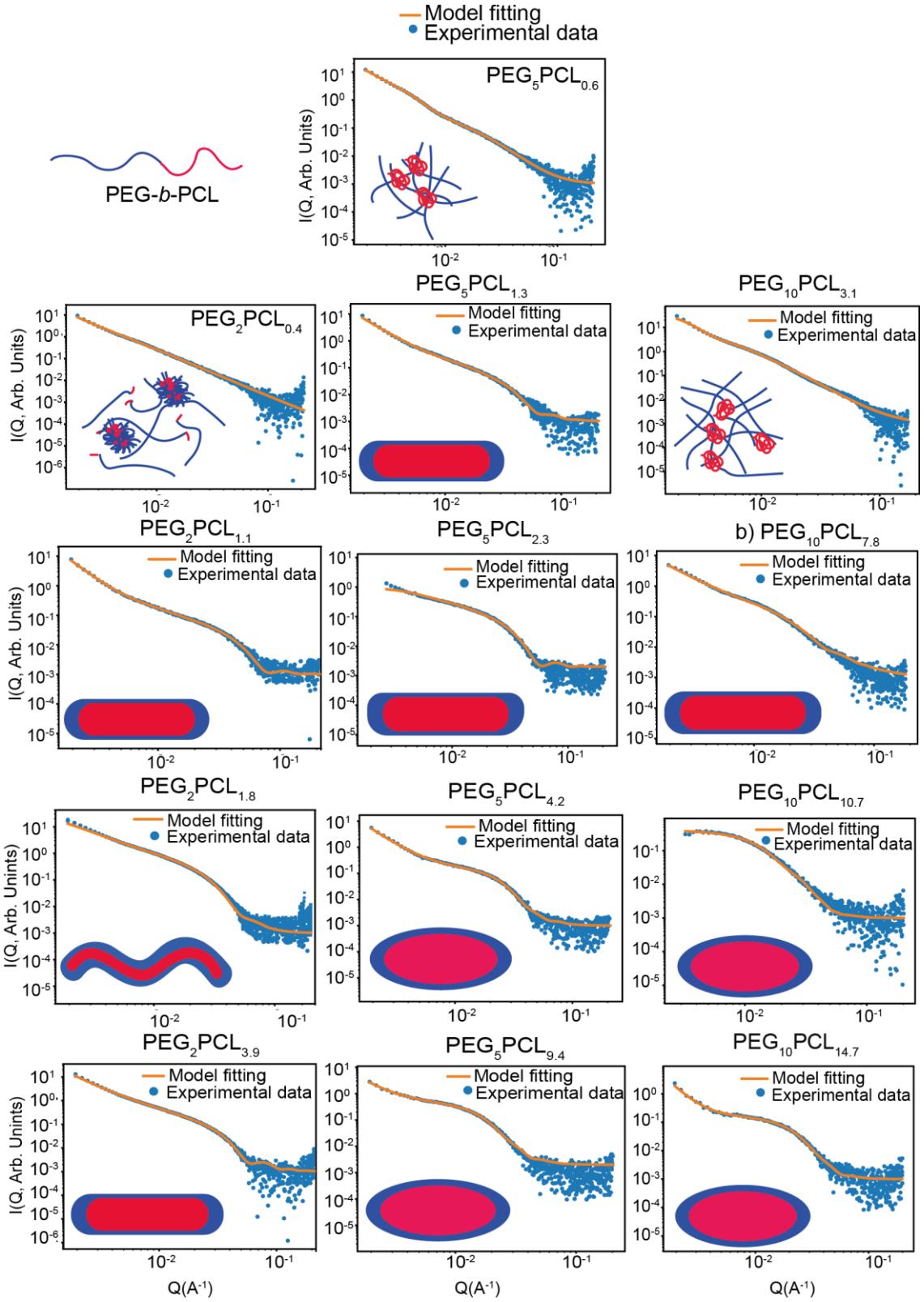


Figure 3.9: SAXS scattering profile of aggregates synthesised from PEG_xPCL_y polymer series. Illustrations at the bottom left of each scattering profile show proposed morphology of each aggregate.

Interestingly, the scattering profile for the $PEG_5PCL_{0.6}$ copolymer solution was fitted best by a combination of a gelfit (SASview) model at high Q and a power law at low Q consistent with unimers and aggregates, respectively (**Figure 3.9**). This may represent a weak polymer network or gel formed from the loose aggregation of the copolymers. In this polymer network, polymers self-assembled into small aggregate and some polymers act as a bridge between the small polymer aggregates and forms a larger aggregate.[17] The shorter correlation length (3.6 nm) represents the link between the aggregates and the larger R_g value (43.33 nm) represents the large polymer aggregates. Papadakis and Tsitsilianis investigated pH-responsive hydrogel, and they found block copolymers can self-assembled into this gel-like state consist of the weak polymer network, which is very similar to the behaviour of $PEG_5PCL_{0.6}$ copolymer solution in water.[18] In this gel-like network, the interaction between PEG and PCL would be irregular, and the system will be very dispersed in nature. This polydisperse system would explain the broad *D* distribution observed in the NMR spectroscopy experiments and high PDI in the DLS results.

A slight increase in the PCL block length for the $PEG_5PCL_{1.3}$ copolymer resulted in a transition of this gel-like network to cylindrical aggregates as indicated by model fitting to the scattering profile, which was also accompanied by larger secondary aggregates (**Figure 3.9**). Further increases in the PCL block length for the PEG_5PCL_y copolymers series resulted in a transition from cylindrical to ellipsoidal aggregates (the aspect ratio between the equatorial and polar radii was ~2), which is consistent with thermodynamic model of polymer aggregation.[19] Thermodynamically, the increase in the molecular weight of the hydrophobic PCL block results in an increase in the water-PCL interfacial tension, which is counteracted by a decrease in the surface area of the aggregates and results in more ellipsoidal or spherical structures.[19]

In general, for all of the PEG_5PCL_y copolymers model fitting of the SAXS profiles revealed a power-law at low Q consistent with larger secondary aggregates, which were not observed in the NMR spectroscopy experiments that displayed the narrow *D* distribution (with the exception of $PEG_5PCL_{0.6}$) (**Figure 3.9**). This discrepancy may result from the relative proportion of secondary aggregates being very small and below the threshold detection limit of the NMR spectroscopy experiments.[20] This is also supported by the narrow PDI values obtained from DLS for the $PEG_5PCL_{4.2}$ and $PEG_5PCL_{9.4}$ copolymers, which imply that the proportion or larger secondary aggregates are negligible.

The scattering profile of the $PEG_{10}PCL_{3.2}$ copolymer solution was similar to that of the $PEG_5PCL_{0.6}$ copolymer and indicated the presence of polydisperse gel-like aggregates (**Figure 3.9**). These results suggest that at lower PCL:PEG ratios the copolymers are observed in a transitional state between unimers and defined aggregates, supporting the NMR spectroscopy experiments and DLS results. As for the PEG_5PCL_y copolymers series, the $PEG_{10}PCL_y$ copolymers series is observed to undergo a transition from gel-like aggregates to cylindrical and finally ellipsoidal aggregates as the molecular weight of the PCL block is increased. Overall, the SAXS analysis reveals the emergence of defined aggregate shapes, including cylinders and ellipsoids with increasing PCL block molecular weight, regardless of the PEG block molecular weight (**Figure 3.10**).

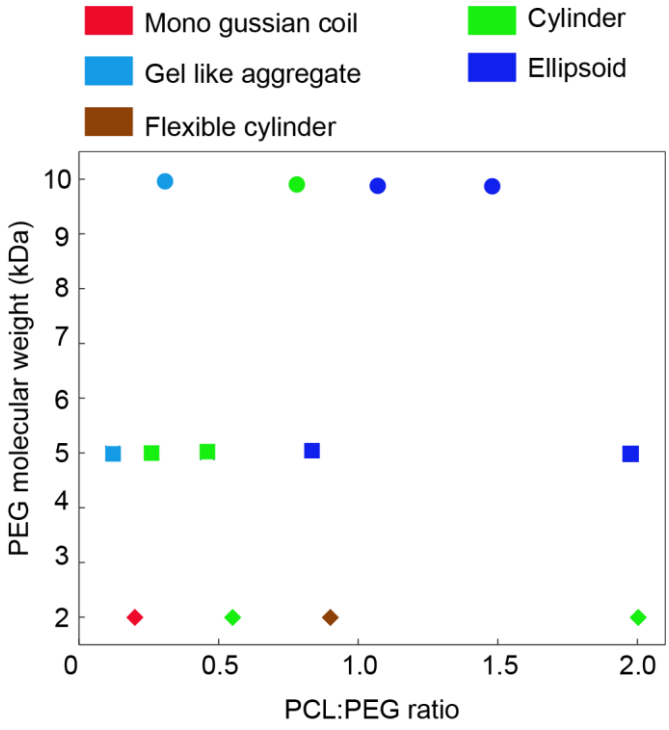


Figure 3.10: Aggregate structure determined for the PEG_xPCL_y block copolymers in water via SAXS analysis. A clear transition of a cylinder to ellipsoid shape is observed in PEG_5PCL_y and $PEG_{10}PCL_y$ copolymers series.

SAXS analysis was also used to calculate the dimensions of the aggregates, which provided the R_g for unimers and gel-like aggregates, the radius of cylindrical aggregates, and the polar radii of ellipsoidal aggregates (**Figure 3.11**). Unfortunately, the cylindrical length can not be determined as the power-law at low Q obscured the Guinier. The R_g of the $PEG_2PCL_{0.4}$ copolymer (27 nm) was consistent with the formation of loosely associated unimers , analysis

of the scattering profiles for the gel-like aggregates of $PEG_5PCL_{0.6}$ and $PEG_{10}PCL_{3.2}$ provided two characteristic lengths; a shorter correlation length (3.6 and 19 nm, respectively) that describes the fluctuation of the polymer in the aggregate (i.e., the polymer motion) and a larger length that describe the R_g of the aggregate (43 and 90 nm, respectively). At lower PCL:PEG ratio aggregate size also indicates the presence of a disperse system.

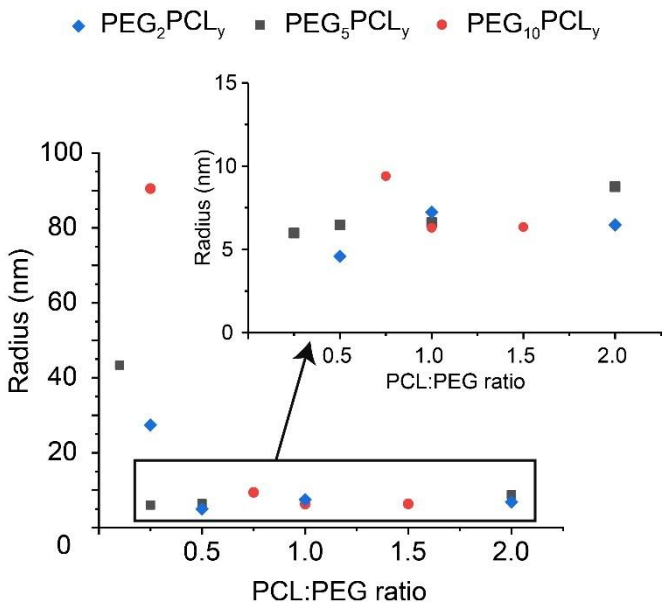


Figure 3.11: Radius of aggregates as determined by SAXS analysis versus the PCL:PEG ratios for the copolymers. For cylindrical and ellipsoidal aggregates the diameter and polar radii, respectively, are presented.

As PCL:PEG ratio increases from 0.25 to 0.5 aggregates radius decreases significantly across all polymer series, this indicates self-assembly of the polymers, as it forms a compact core; although the pattern in aggregate size change across the series is irregular. In PEG_2PCL_y series there is a slight increase when PCL:PEG ratio increases from 0.5 to 1; however, it decreases at 2:1 ratio. In PEG_5PCL_y series a see a gradual increase although the increase is not significant. In $PEG_{10}PCL_y$ series size decreases a slight when PCL:PEG ratio increases a from 0.75 to 1, but there is no change in a further increase in ratio. Overall, the aggregate size did not change regardless of the change in PCL:PEG ratio or PEG block molecular weight; similar trends observed in $\langle D \rangle$ values in **Figure 3.5**.

The aggregate size increase due to an increase in the aggregation number; according to thermodynamic modelling; the increase in the length of polymer (increase in PCL length and PCL:PEG ratio) will increase the area per polymer occupied in the aggregate core as well as aggregation number. An increase in aggregation number will also increase repulsion between the polymer chain in the corona, and it will prevent further increase in aggregation number. The fine balance between these two thermodynamic parameter controls the aggregate size.[16] According to that, as PCL:PEG ratio increase, there should be an increase in the aggregate size; however, the SAXS data didn't show any significant change in size in a given polymer series (**Figure 3.11**). It should be considered the change in PCL in a series might not be significant to affect the aggregation significantly. Aggregate size did not change significantly either in between polymer series; the increase in PEG molecular weight might increase the polymer chain repulsion, which prevents an increase in the aggregation number.

3.1.2.4 Correlation of NMR spectroscopy, DLS and SAXS data, and interpretation of trends in copolymers self-assembly

Taken together, the PGSTE NMR spectroscopy, DLS and SAXS results present a coherent and comprehensive picture of aggregate formation for the copolymers investigated in this study. The PGSTE NMR spectroscopy experiments have shown that the mean $\langle D \rangle$ and spread of the D distributions can be utilised as a measure of the transition in dispersity of the copolymer aggregates in solution with respect to changes in the PEG molecular weight and the PCL:PEG ratio; along with PDI value measured from DLS experiments. Under the conditions studied, these results indicate that there are three different aggregate states, namely loosely associated aggregates (unimer+aggregate), metastable aggregates (a very disperse system containing aggregates of differing sizes) and stable aggregates (aggregates with a well-defined core and corona of narrow size dispersity) (**Figure 3.12**).

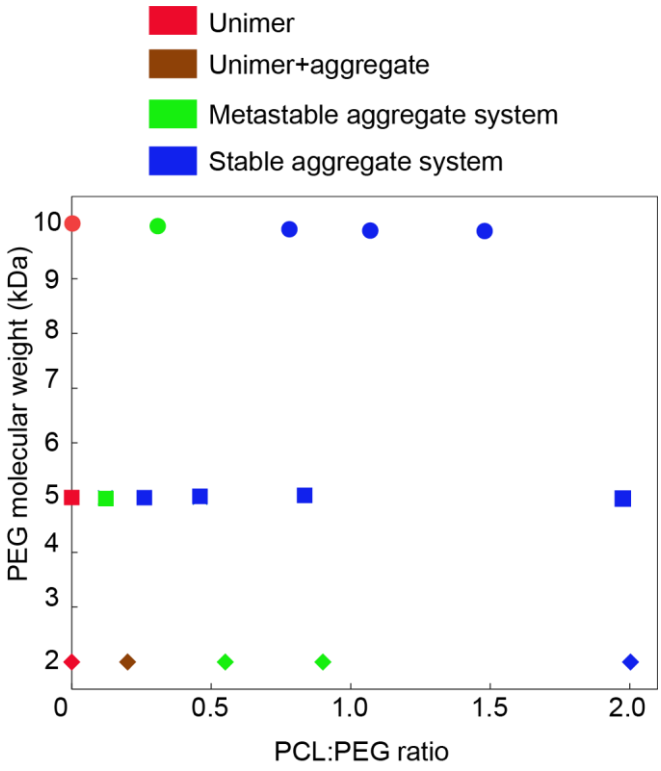


Figure 3.12: Phase diagram of the aggregate system for the PEG_xPCL_y block copolymers systems at different PCL:PEG ratios. A clear transition between unimer to stable aggregate system as PCL:PEG ratio increased.

For low PEG molecular weights and PEG:PCL ratios (e.g., $PEG_2PCL_{0.4}$) analysis by PGSTE NMR spectroscopy has indicated the presence of unimers (**Figure 3.4**) and analysis by DLS has indicated the presence of very disperse aggregates (**Figure 3.8**), which implies that the system consists of loosely associated aggregates which retain the mobility and diffusivity of the unimers. This is further supported by the SAXS analysis for which the scattering profile is consistent with unimers, although the calculated R_g of 27 nm implies that they are present in a loosely associated state (unimer + aggregate).

For the $PEG_5PCL_{0.6}$ and $PEG_{10}PCL_{3.1}$ copolymers with a low PCL:PEG ratio analysis by PGSTE NMR spectroscopy revealed a significant decrease in the diffusivity indicative of aggregate formation. The large differences in the *D* distribution for the two blocks indicate that they behave very differently. Interpretation of DLS data also indicated the presence of very disperse aggregates, further supported by SAXS analysis. This gel-like or metastable aggregates consists of short correlation lengths (3.6 and 19 nm) and large R_g values (43 and 90 nm, respectively) that support the differences seen in the *D* distributions of in the NMR

spectroscopy experiments. The differences in *D* distributions and broad dispersity are also observed for the $PEG_2PCL_{1.1}$ and $PEG_2PCL_{1.8}$ copolymers suggesting the formation of metastable aggregates. The power-law at low Q region of SAXS scattering data indicates the presence of large particle along with cylindrical aggregate with a radius of 4.72 and 7.15 nm (high Q region); which explains the disperse system indicted in NMR data (**Figure 3.9**).

With increasing PCL molecular weight, the SAXS analysis reveals that the $PEG_5PCL_{1.3}$, $PEG_5PCL_{2.4}$ and $PEG_{10}PCL_{7.8}$ copolymers series also form cylindrical aggregates, however, the good agreement between the *D* distribution for the PEG and PCL blocks in the NMR spectroscopy experiments and lower dispersity in DLS analysis implies that these are stable and relatively defined aggregates. At high PCL:PEG ratios the results from all three complementary analytical techniques indicate well-defined and stable aggregates that trend towards ellipsoidal aggregates with lower aspect ratios with increasing PCL molecular weight.

Overall, several trends in the aggregation behaviour with respect to the copolymer microstructure have been identified within this study. Whilst an increase in the PCL:PEG ratio results in more stable and well-defined aggregates; the PEG molecular weight is also important, with lower molecular weight PEG (e.g., 2 kDa) failing to stabilise aggregate formation until the PCL block molecular weight is almost double that of the PEG block. This is further supported by the fact that copolymers with the same PCL:PEG block ratio (e.g., $PEG_2PCL_{1.8}$ versus $PEG_5PCL_{4.8}$) behave very differently, implying that the molecular weight of the individual blocks, as well as their respective ratio, is critical in controlling the self-assembly process. Whilst the increase in PCL block molecular weight between the $PEG_2PCL_{1.8}$ and $PEG_5PCL_{4.8}$ copolymers might be attributed to the formation of stable aggregates. However, it does not explain why the $PEG_5PCL_{1.3}$ copolymer forms stable aggregates, whereas $PEG_2PCL_{1.8}$ failed to do so. Thus, it can be concluded that there is a threshold ratio between the PCL:PEG ratio and PEG molecular weight that is responsible for controlling the formation of stable and well-defined aggregates.

From a thermodynamic perspective, the self-assembly of block copolymers is governed by the interfacial energy between core and solvent, the elastic energy of the chains in the core, and the free energy associated with the chains in the corona. However, the current thermodynamic model for aggregate formation relies on two key assumptions: (i) the aggregate core is fully segregated with no solvent, and (ii) the core and corona has a sharp interface.[21]

As has been shown previously by Long *et al.* water penetration into the hydrophobic core of aggregates is significant, which clearly indicates that there is a region of the core or boundary layer between the core and corona that is more hydrated.[7] Furthermore, in this study, the presence of characteristic PCL signal in NMR spectra of aggregates also implies the presence of hydrated boundary layer. The presence of a boundary layer will change the interfacial tension and deformation of the blocks, which is not currently accounted for in the existing thermodynamic model of block copolymers self-assembly.

3.2 Conclusion

The self-assembly of PEG-*b*-PCL block copolymers in water was investigated using PGSTE NMR spectroscopy, DLS and SAXS to understand the relationships between the polymer microstructure and aggregate formation. The width of *D* distribution in PGSTE NMR spectroscopy and PDI values in DLS provided a marker for the heterogeneity in aggregate structure. These two techniques provided complimentary views of the heterogeneity of the aggregates, with NMR spectroscopy providing detailed information on structures in the range of unimers to aggregates, and DLS providing sensitivity to primary aggregates and larger secondary aggregates. Furthermore, estimates of the mean diffusivities of the aggregates from PGSTE NMR spectroscopy revealed that separate samples made from the same composition block copolymers were inconsistent in some for low PCL:PEG ratios, suggesting the formation of metastable aggregates. Thus, the PCL:PEG ratio was found to have a dominating effect on aggregate formation and stability, whereas the PEG molecular weight was found to have a larger effect on the size of the aggregates. SAXS provided complementary information about the aggregate morphology and revealed that at low PCL:PEG ratios the copolymers existed as loose metastable aggregates and transitioned to cylindrical and ellipsoidal aggregates with increasing PCL:PEG ratio.

This study provides evidence that there exists a critical PCL:PEG ratio and molecular weight for stable aggregate formation from PEG-*b*-PCL block copolymers in water, and that the aggregate size and shape can be tuned by careful section of the polymer microstructure. Significantly, the formation of perfectly spherical micelle-like aggregates was not observed for the family of PEG-*b*-PCL block copolymers investigated in this study. This is particularly important for drug delivery applications where the self-assembled aggregate shape is closely correlated with their biological fate, and therefore, this study to provide a fundamental understanding of aggregate formation from PEG-*b*-PCL block copolymers which may prove valuable for the rational design of drug delivery systems. However, further studies are required to fully understand the contribution of small hydrophobic molecules (e.g., drugs) on the block copolymer self-assembly process and aggregate structure, and to determine if the trends observed for the PEG-*b*-PCL block copolymer system are more broadly applicable to other types of amphiphilic copolymers.

3.3 Experimental

3.3.1 Materials

Deuterated chloroform ($CDCl_3$; 99.8% D), and deuterium oxide (D_2O; 99.9% D) were purchased from Sigma-Aldrich. All reagents were used as received unless otherwise stated. Ultrapure water with a resistivity of >18 MΩ.cm was obtained from an arium® ultra water purifier system (Sartorius, Germany).

3.3.2 Methods

3.3.2.1 Synthesis of PEG-b-PCL copolymers

The PEG-*b*-PCL copolymer synthesis was described in details in **Chapter 2**.

3.3.2.2 Self-assembly of PEG-b-PCL copolymers in water

Self-assembly of PEG-*b*-PCL copolymers in water was conducted using the solvent evaporation technique.[28] Polymer solutions were prepared in acetone (1 mL, 1 mg/mL) in graduated vials (4 mL). To the prepared solutions was added D_2O (1 mL) (for NMR experiments,) or H_2O (for DLS and SAXS experiments from a milliQ ultrafiltration system) in a dropwise fashion. The vials were placed in a pre-heated block heater at 60 °C and the solvent level was checked periodically until the volume was ~ 1 mL. The vials were then placed in a vacuum desiccator (0.1 mbar) for 1 h to remove residual acetone, and the solvent volume was readjusted with D_2O or H_2O to give a polymer concentration of 1 mg/mL. All solutions were prepared fresh prior to analysis. In this study, the polymer concentration was 1 mg/mL to avoid microscopic averaging effects; but still, sufficient to generate detectable NMR signal.[24] It should be noted that this concentration is in excess of the reported CMC (0.3 to 1.8 µg/mL) for PEG-*b*-PCL copolymers.[29,30]

3.3.3 Characterisation of PEG-*b*-PCL copolymer aggregate solutions

3.3.2.1 PGSTE NMR measurements of PEG-b-PCL copolymer aggregate solutions

PGSTE NMR spectroscopy experiments were performed on a 600 MHz Bruker Avance III HD spectrometer with PEG and PEG-*b*-PCL copolymer solutions (1 mg/mL, 500 µL) in D_2O, using standard 5 mm NMR tubes. The *D* of the polymers were measured using PGSTE NMR experiments at 600 MHz with a 14.09 T superconducting vertical bore magnet, a Micro5 Imaging Probe, a 5 mm radiofrequency coil, and a Diff30 (11.7 T/m maximum) gradient set.[18] PGSTE experiments were performed in the Diff module of TopSpin 3.2 (Bruker BioSpin) and used sinusoidal gradient pulse shapes with pulse duration of δ = 1.58 ms. The time between leading edges of the pulses was Δ = 100 ms unless otherwise specified and the repetition time was 10 s. 16 scans and 32 gradient points with gradient amplitude, g, varied linearly to 11.67 T/m. Experiments were performed at a core of temperature 25 °C.

Echo signals were Fourier transformed to frequency spectra and baseline offsets, calculated far from the spectral peaks, and were subtracted from the spectra using TopSpin 3.2. PEG and PCL signals were defined by integrating under the methylene proton signal for PEG (δ_H = 3.6 ppm) and PCL (δ_H = 1.6 ppm). Attenuation of the intensity of the PEG and PCL signals was then used to estimate the *D* distributions.

Self-diffusion coefficients of individual species can be calculated by fitting the Stejskal-Tanner equation,[19] $I(b) = I_0 \exp(-bD)$, to the attenuation of the signal intensity. Here, the variable parameter is $b = (\gamma g \delta)^2 \frac{4}{\pi^2}\left(\Delta - \frac{\delta}{4}\right)$ for sinusoidal gradient pulse shapes. This single exponential form is often valid for molecules of a defined molecular weight, that are well-solvated in a homogeneous medium. In comparison, polymers are described by a *D* distribution due to the molecular mass dispersity of the molecules, as well as the distribution of sizes of the aggregates upon self-assembly. The Stejskal-Tanner equation can be modified to model the signal attenuation from a probability distribution of *D* as $I(b) = I_0 \int_0^\infty P(D) \exp(-bD)\, dD$, where a model for the diffusion coefficient distribution, $P(D)$ must be defined. $P(D)$ is the probability of finding a component with a self- diffusion coefficient of *D*. The lognormal distribution model, $P(D) = 1/\left(D\sigma\sqrt{2\pi}\right) \exp[-(\log D - \mu)^2/(2\sigma^2)]$, was used in this study as polymers often exhibit heterogeneity which results in lognormally distributed sizes[22,3] and thus, *D* distributions in solution.[23] Additionally, in the case that the system displays a

multimodal distribution of sizes, the lognormal distribution captures the mean, $\langle D \rangle = \exp(\mu + \sigma^2/2)$, and the spread (coefficient of variation, standard deviation/mean) $= \exp(\sigma^2) - 1$ of the distribution.[24] A least-squares fit of the model to the signal attenuation data yielded the estimated parameters of the *D* distribution, μ and σ, and Monte Carlo error analysis provided confidence intervals associated with the estimates.[24] The least-squares fitting routine was implemented in MATLAB R2017b and is publicly available through GitHub.[23]

3.3.2.2 DLS analysis of PEG-b-PCL copolymer aggregate solutions

DLS was conducted on a Malvern Zetasizer NANO ZS (Malvern Instruments Limited, UK) equipped with a 4 mW He–Ne laser operating at a wavelength of 633 nm. Samples were prepared in ultrapure water and analysed at an angle of 173º using a quartz cuvette. The PDI values were determined from the correlograms using the Zetasizer 7.11 software (Malvern Instruments Limited, UK). All measurements were repeated three times in order to check their reproducibility, and all DLS experiments were conducted in triplicate to calculate the average values and standard deviation of the R_h and PDI.

3.3.2.3 SAXS analysis of PEG-b-PCL copolymer aggregate solutions

SAXS measurements were performed on the SAXS/WAXS beamline of the Australian Synchrotron (ANSTO, Victoria, Australia).[25] Samples were loaded into 1.5 mm external diameter glass capillaries (Charles Supper, MA USA) that were placed into a capillary holder. The temperature of the capillary holder was equilibrated to 37 °C by flowing water from a water heater/circulator bath through the capillary holder and the temperature was monitored using a thermocouple at the sample position throughout the measurements. Two detector configurations were used: (i) photon energy = 15.1 keV (wavelength λ = 0.821 Å) with a sample-to detector distance of 1350 mm, and (ii) photon energy = 11.0 keV (λ = 1.127 Å) with a sample-detector distance of 7398 mm. 2D scattering patterns were recorded for each sample using a Dectris Pilatus 2M detector and the data were reduced to profiles of scattered X-ray intensity [(*I(Q)*] *versus* the scattering vector *Q* [= $(4\pi/\lambda)\sin\theta$, 2θ = scattering angle] using the in-house developed software scatterbrain. Data from the two detector configurations were stitched together into a single continuous scattering profile with a *Q* range from 1.94×10^{-3} to 2.04×10^{-1} Å^{-1} using the *IRENA* small-angle scattering macros (release 2.68) within the

IgorPro graphing and modelling software package (version 7.0.8.1).[26] These scattering profiles were subsequently analysed using the SASView small angle scattering data analysis package (version 5.0).[27] Given the slightly varying size of the sample capillaries the scattered X-ray intensity was not placed on an absolute scale as the absolute scattering volume was not known precisely and only the shape of the particles in solution was analysed, not their scattering power.

3.4 References

1. Edward, J. T., Molecular volumes and the Stokes-Einstein equation. *J. Chem. Educ.* **1970**, *47* (4), 261.

2. Einstein, A., Zur Elektrodynamik bewegter Körper. *Ann. Phy.* **1905**, *322* (10), 891-921.

3. Håkansson, B.; Nydén, M.; Söderman, O., The influence of polymer molecular-weight distributions on pulsed field gradient nuclear magnetic resonance self-diffusion experiments. *Colloid Polym. Sci.* **2000**, *278* (5), 399-405.

4. Glavas, L.; Olsén, P.; Odelius, K.; Albertsson, A.-C., Achieving micelle control through core crystallinity. *Biomacromolecules* **2013**, *14* (11), 4150-4156.

5. Hrkach, J. S.; Peracchia, M. T.; Bomb, A.; Lotan, n.; Langer, R., Nanotechnology for biomaterials engineering: structural characterisation of amphiphilic polymeric nanoparticles by 1H NMR spectroscopy. *Biomaterials* **1997**, *18* (1), 27-30.

6. Zachariasse, K. A.; Kozankiewicz, B.; Kühnle, W., Micellar structure and water penetration studied by NMR and Optical Spectroscopy. In *Surfactants in Solution*, Mittal, K. L.; Lindman, B., Eds. Springer US: Boston, MA, 1984; pp 565-584.

7. Long, J. A.; Rankin, B. M.; Ben-Amotz, D., Micelle structure and hydrophobic hydration. *J. Am. Chem. Soc.* **2015**, *137* (33), 10809-10815.

8. Liu, X.; Hou, Y.; Tang, X.; Wu, Q.; Wu, C.; Yi, J.; Zhang, G., Multicompartment micelles based on hierarchical co-assembly of PCL-*b*-PEG and PCL-*b*-P4VP diblock copolymers. *RSC Advances.* **2016**, *6* (7), 5312-5319.

9. Fleischer, G., The effect of polydispersity on measuring polymer self-diffusion with the n.m.r. pulsed field gradient technique. *Polymer* **1985**, *26* (11), 1677-1682.

10. Kidd, B. E.; Li, X.; Piemonte, R. C.; Cooksey, T. J.; Singh, A.; Robertson, M. L.; Madsen, L. A., Tuning biocompatible block copolymer micelles by varying solvent composition: Dynamics and populations of micelles and unimers. *Macromolecules* **2017**, *50* (11), 4335-4343.

11. Blandamer, M. J.; Cullis, P. M.; Soldi, L. G.; Engberts, J. B. F. N.; Kacperska, A.; Van Os, N. M.; Subha, M. C. S., Thermodynamics of micellar systems: Comparison of mass action and phase equilibrium models for the calculation of standard Gibbs energies of micelle formation. *Adv. Colloid Interface Sci.* **1995**, *58* (2), 171-209.

12. Fujiwara, S.; Itoh, T.; Hashimoto, M.; Tamura, Y., Molecular dynamics simulation of micelle formation in amphiphilic solution. *Mol Simul.* **2007**, *33* (1-2), 115-119.

13. Rager, T.; Meyer, W. H.; Wegner, G.; Winnik, M. A., Influence of chain length and salt concentration on block copolymer micellization. *Macromolecules* **1997**, *30* (17), 4911-4919.

14. Rizis, G.; Van de Ven, T. G.M; Eisenberg, A., Crystallinity-driven morphological ripening processes for poly(ethylene oxide)-block-polycaprolactone micelles in water. *Soft Matter* **2014**, *10* (16), 2825-35.

15. Sitar, S.; Vezocnik, V.; Macek, P.; Kogej, K.; Pahovnik, D.; Zagar, E., Pitfalls in size characterisation of soft particles by dynamic light scattering online coupled to asymmetrical flow field-flow fractionation. *Anal. Chem.* **2017**, *89* (21), 11744-11752.

16. Nagarajan, R., Amphiphilic Surfactants and Amphiphilic Polymers: Principles of molecular assembly. In *Amphiphiles: Molecular Assembly and Applications*, American Chemical Society: 2011; Vol. 1070, pp 1-22.

17. Winnik, M. A.; Yekta, A., Associative polymers in aqueous solution. *Curr. Opin. Colloid Interface Sci.* **1997**, *2* (4), 424-436.

18. Papadakis, M. C.; Tsitsilianis, C., Responsive hydrogels from associative block copolymers: Physical gelling through polyion complexation. *Gels* **2017**, *3* (1).

19. Israelachvili, J. N.; Mitchell, D. J.; Ninham, B. W., Theory of self-assembly of hydrocarbon amphiphiles into micelles and bilayers. *J. Chem. Soc. Faraday Trans* **1976**, *72* (0), 1525-1568.

20. Röding, M.; Williamson, N. H.; Nydén, M., Gamma convolution models for self-diffusion coefficient distributions in PGSE NMR. *J. Magn. Reson.* **2015**, *261*, 6-10.

21. Nagarajan, R.; Ganesh, K., Solubilization in spherical block copolymer micelles: Scaling analysis based on star model. *J. Chem. Phys.* **1993**, *98* (9), 7440-7450.

22. Stejskal, E. O.; Tanner, J. E., Spin Diffusion Measurements: Spin Echoes in the presence of a time-dependent field gradient. *J. Chem. Phys.* **1965**, *42* (1), 288-292.

23. Williamson, N. H. Parametric distribution model fitting for analysing relaxation and diffusion data. https://github.com/nathanwilliamson/NMR_decay_analysis (accessed 22-05-2017).

24. Williamson, N. H.; Nyden, M.; Roding, M., The lognormal and gamma distribution models for estimating molecular weight distributions of polymers using PGSE NMR. *J. Magn. Reson.* **2016**, *267*, 54-62.

25. Kirby, N. M.; Mudie, S. T.; Hawley, A. M.; Cookson, D. J.; Mertens, H. D. T.; Cowieson, N.; Samardzic-Boban, V., A low-background-intensity focusing small-angle X-ray scattering undulator beamline. *J. Appl. Crystallogr.* **2013**, *46* (6), 1670-1680.

26. Ilavsky, J.; Jemian, P. R., Irena: tool suite for modeling and analysis of small-angle scattering. *J. Appl. Crystallogr.* **2009**, *42* (2), 347-353.

27. GIT_COMMIT SasView 5.0. http://www.sasview.org/ (accessed 7/07/2019).

28. Letchford, K.; Burt, H., A review of the formation and classification of amphiphilic block copolymer nanoparticulate structures: micelles, nanospheres, nanocapsules and polymersomes. *Eur J Pharm Biopharm* **2007**, *65* (3), 259-69.

29. Mohanty, A. K.; Jana, U.; Manna, P. K.; Mohanta, G. P., Synthesis and evaluation of MePEG-PCL diblock copolymers: surface properties and controlled release behavior. *Progress in biomaterials* **2015**, *4* (2-4), 89-100.

30. Yoon, K.; Kang, H. C.; Li, L.; Cho, H.; Park, M.-K.; Lee, E.; Bae, Y. H.; Huh, K. M., Amphiphilic poly(ethylene glycol)-poly(ε-caprolactone) AB_2 miktoarm copolymers for self-assembled nanocarrier systems: synthesis, characterisation, and effects of morphology on antitumor activity. *Polymer Chemistry* **2015**, *6* (4), 531-542.

Chapter 4

Effect of poly(ethylene glycol-*b*-caprolactone) microstructure and self-assembly on polymer morphology and thermal characteristics

Chapter overview

The morphology of a polymer system can be defined by the crystalline or amorphous nature of the polymer chains. The crystallinity of a polymer plays a significant role in controlling the physical characteristics of that polymer, such as softening and melting behaviour, and solubility. This is important for processing polymers and determining their suitability for specific applications. The thermal behaviour and morphology of PEG-*b*-PCL copolymers have been studied previously,[1-6] however, in most cases the morphology is examined for the bulk processed polymer and the effect of aggregation on the polymer's morphology, and thermal characteristics is not considered. Hence, the relationship between the polymer microstructure and the organisation of the polymer chains in PEG-*b*-PCL copolymers has been explored using DSC and WXRD. The effect of polymer aggregation on the thermal characteristic was also investigated, which has implications for drug delivery systems, where crystalline or amorphous characteristics can regulate their stability and solubility. DSC was employed to study the melting and crystallisation behaviour of the PEG and PCL blocks in the copolymer, with reference to their differing microstructure and the individual homopolymers. Temperature-dependent WXRD was conducted to investigate the order of crystallisation of the PEG and PCL blocks in relation to the PCL:PEG ratio. Melting and crystallisation behaviour of polymer aggregate also analysed and compared with bulk polymer (its non-aggregated form) to understand the PEG and PCL crystalline state in aggregate core or corona. However, previous reports have suggested that PEG-*b*-PCL aggregates exhibit an amorphous core; there is no definitive evidence to support these claims.[7]

4.1 Results and Discussion

4.1.1 Synthesis and characterisation of PEG-*b*-PCL copolymers

Refer to Chapter 2, Section 2.4.3 for the discussion of the synthesis of the PEG-*b*-PCL block copolymers.

4.1.2 Thermal characterisation of PEG-*b*-PCL copolymers

The aim was to investigate and understand the correlation between PEG-*b*-PCL microstructure and its thermal behaviour. The PEG and PCL blocks of the copolymer are covalently attached to one another, and therefore it is conceivable that each block could be influenced by the differential behaviour of the other. To fully interpret the effect of this covalent attachment, it was first necessary to understand the behaviour of the individual PEG and PCL homopolymers and homopolymer physical blends. Generally, the second heating cycle results are reported for polymers as they provide more comparative results that are independent of the effects of these processing parameters. However, in the context of this study, the analysis of the first heating cycle is important for several reasons. Firstly, the thermal histories of the copolymers are the same as they are synthesised and purified using the same procedure (i.e., precipitation in a non-solvent), so the observed differences in polymer thermal behaviour between polymers are not due to the processing conditions. Secondly, to understand the effect of the polymer aggregation, it is necessary to compare precipitated copolymers (i.e., that undergo an instant change in solvated to solid states) directly with the aggregated copolymers that undergo a gradual self-assembly process. During the latter process, the polymer is hypothesised to adopt a phase-separated system, wherein the PEG and PCL blocks are segregated in the core and corona, respectively.

4.1.2.1 Thermal characterisation of PEG and PCL homopolymers

The thermal behaviour of PEG (M_n = 2, 5, 10 kDa) and PCL (M_n = 2 kDa) homopolymers were initially analysed via DSC by heating from −20 to 80 °C at a rate of 10 °C/min, then cooling at a rate of 10 °C/min to −65 °C (**Figure 4.1**). The same heating and cooling cycles were then repeated for a second time.

The DSC thermograms of the PEG homopolymer revealed a clear relationship between their molecular weight and thermal properties. As the molecular weight of PEG increased, the melting temperature (T_m) also increased. The T_m increased by 10 °C when the PEG molecular weight increased from 2 to 5 kDa, but only 3 °C when increased further from 5 to 10 kDa. This is a common trend for most homopolymers, where above a certain molecular weight the T_m remains approximately constant, whereas below it the T_m decreases with decreasing molecular weight.[8] Thus, the type of crystallites that are formed and the crystallisation mechanism are dependent upon the molecular weight; lower molecular weight PEG crystallises as an extended chain, whereas at higher molecular weight, PEG crystallites are formed with folded chains.[9]

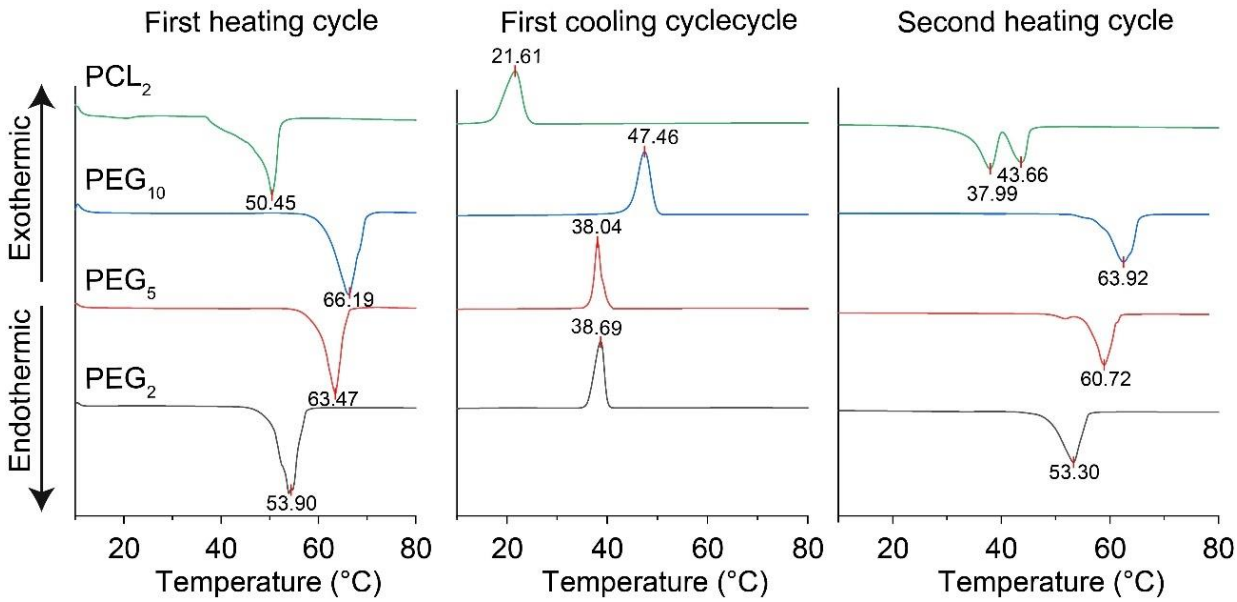


Figure 4.1: DSC thermograms of PEG (M_n = 2, 5 and 10 kDa) and PCL (M_n = 2 kDa) homopolymers showing the first heating, first cooling and second heating profiles (ramp rate 10 °C /min). The melting behaviour of the PCL homopolymer is different between the first and second heating cycles due to the erosion of the polymers thermal history.

For the PEG homopolymers, the T_m was slightly changed on the second heating cycle as compared to the first heating cycle (**Figure 4.1** and **Table 4.1**) as a result of the 'thermal history' of the polymer.[10] The thermal history of a polymer is attributed to the crystalline characteristics of the polymer resulting from synthesis, processing and storage conditions.[11] The DSC thermograms of the PCL homopolymer revealed an interesting monomodal to bimodal transition across the first and second heating cycles (**Figure 4.1**).

The double melting peak of PCL has been reported previously and proposed to result from PCL crystallites with different fold lengths.[12,13] However, the PCL molecular weight is relatively short (M_n = 2 kDa), which may restrict the formation of different fold lengths. Further, the double peak may actually occur due to successive melting, recrystallisation and re-melting processes as has been previously reported.[13,14] This phenomenon is hypothesised to occur when the polymer forms crystallites with imperfections, which result in their lower T_m (in the first crystallisation cycle). Those imperfect crystals melt at a lower temperature and have the mobility to reform more perfect crystals that melt again at an elevated temperature.[15] Compared to PEG, it is apparent that the enthalpy change for the melting (ΔH_m) and crystallisation (ΔH_c) processes for PCL is lower (**Table 4.1**), which is indicative of reduced crystallinity,[16] though this does not account for differences in the strength of the intermolecular interactions responsible for crystallinity.

Table 4.1: Thermal properties of PEG and PCL homopolymers determined via DSC (n = 3) from the first and second heating/cooling cycles. Thermal properties include T_m and T_c, and the associated enthalpy changes (ΔH_m and ΔH_c respectively).

			First cycle			
Homopolyer	T_m	ΔH_m(J/g)	ΔH_m (kJ/mol)	T_c	ΔH_c (J/g)	ΔH_c (kJ/mol)
PEG_2	53.7 ± 0.14	181.8 ± 5.8	363.7 ± 11.5	32.9 ±0.37	134.7 ± 2.57	269.4 ± 2.14
PEG_5	62.0 ± 1.46	188.6 ± 3.28	943.2 ± 16.	37.6 ± 0.4	156.6 ± 3.2	783.4 ± 16.05
PEG_{10}	66.1 ± 0.02	188.9 ± 3.28	1889.1±42.1	45.8 ±0.37	152.3±10.23	1523.1 ± 102.3
PCL_2	50.7 ± 0.32	78.0 ± 4.07	156.1±8.14	21.9 ±0.34	67.52 ± 0.73	135.1 ± 1.46
			second cycle			
Homopolyer	T_m	ΔH_m (J/g)	ΔH_m (kJ/mol)	T_c	ΔH_c (J/g)	ΔH_c (kJ/mol)
PEG_2	52.05 ± 1.25	156.7 ± 11.7	313.4 ± 23.5	35.9 ± 2.7	155.1 ± 15.1	310.2 ± 30.2
PEG_5	58.35 ± 1.10	157.9 ± 5.18	789.8 ± 25.9	36.5 ± 1.7	151.7 ± 8.6	758.7 ± 23.3
PEG_{10}	62.5 ± 0.50	165.3 ± 4.47	1653.1 ± 5.2	45.9 ± 0.4	158.4 ± 6.2	1584.8 ± 6.2
PCL_2	38.1 ± 0.39, 43.6 ± 0.31	64.6 ± 2.0	129.32 ± 4.0	21.9 ± 0.3	66.08 ± 1.09	132.2 ± 2.2

4.1.2.2 Thermal characterisation of PEG and PCL homopolymer blends

Physical blends were prepared by mixing PEG (M_n = 2, 5 and 10 kDa) and PCL (M_n = 2 kDa) homopolymer powders in a 1:1 (%w/w) ratio via mechanical agitation. The physical blends were analysed via DSC using the previously described protocol (for details refer to Section 4.1.2.1). The DSC thermograms of the PEG_2 and PCL_2 homopolymers and their blends are provided in **Figure 4.2**.

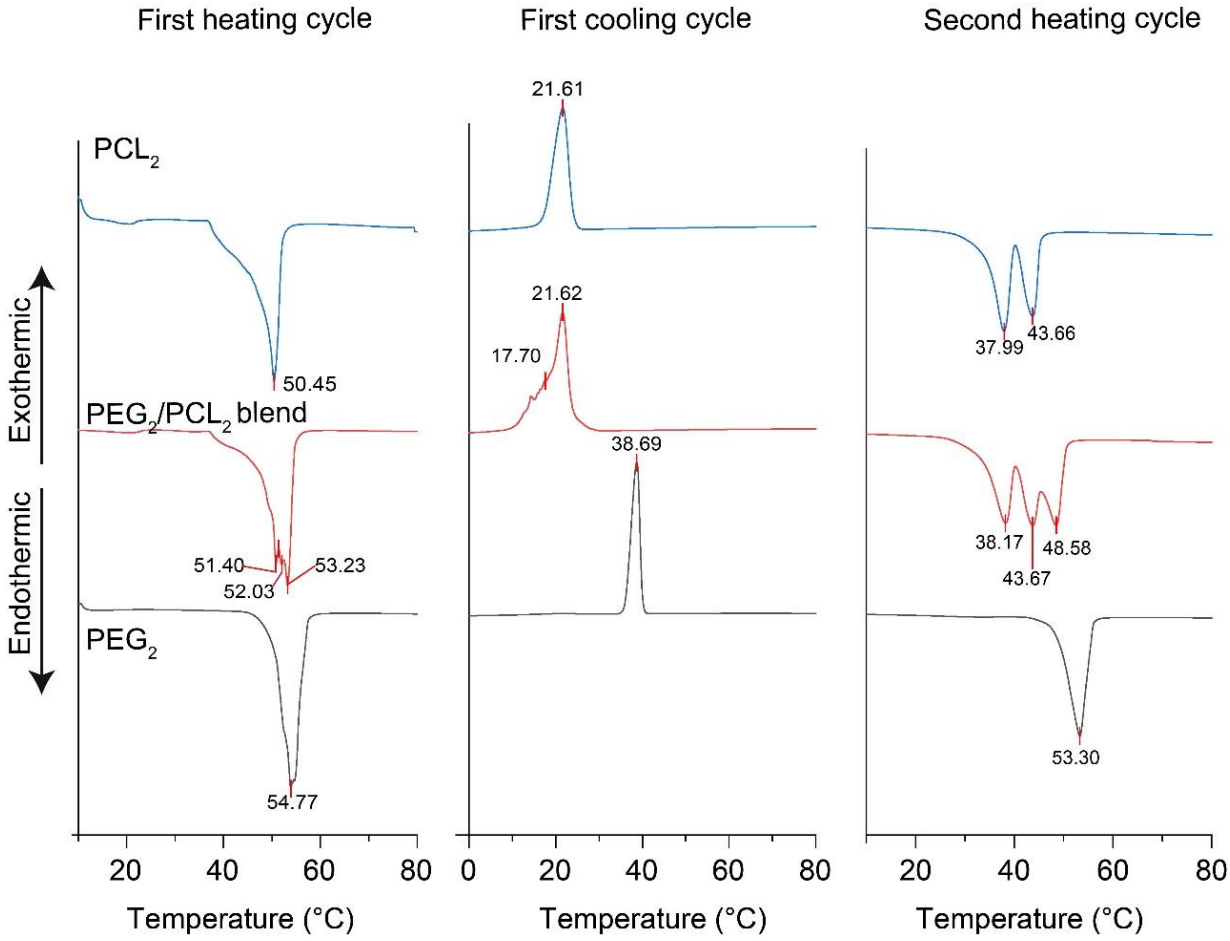


Figure 4.2: DSC thermograms of the PEG_2 and PCL_2 homopolymers and PEG_2/PCL_2 physical blend 1:1 (%w/w) showing the first heating, first cooling and second heating profiles (ramp rate 10 ºC/min). The reduction of the PEG T_c in the first cooling cycle of the blend indicates that PCL influences the crystallisation of PEG, which is supported by the observed decrease in the PEG T_m in the second heating cycle.

In the first heating cycle, PEG and PCL were in a heterogeneous physical mixture, and as a result, the mixture exhibits melting behaviour characteristic of both homopolymers. After the first heating cycle, both polymers were molten and can potentially form microdomains or a homogeneous mixture (if their interactions are favourable), which could affect their crystallisation behaviour. Upon cooling, the PEG and PCL blend showed a broad crystallisation peak, with a peak maximum at 21.62 ºC, which was very similar to the PCL homopolymer crystallisation temperature of 21.61 ºC (**Figure 4.2**).

In addition, there was a shoulder at ~ 17 ºC, which is hypothesised to result from the crystallisation of PEG. Thus, it can be concluded that the physical blending of PEG and PCL with a molecular weight of 2 kDa significantly affects the crystallisation behaviour of the mixture (both PEG and PCL). This reduction in the crystallisation temperature of PEG by almost 20 ºC is believed to be due to the formation of PEG microdomains inside a PCL domain.[17] PEG crystallises under confinement in those microdomains and less crystalline in nature relative to pure PEG homopolymer.[17,18] This behaviour also explains the decrease in T_m of PEG from ~ 53 to ~ 49 ºC in the second heating cycle (**Figure 4.2**). In the second heating cycle, two characteristic PCL melting peaks were observed at ~ 38 and 44 ºC, which was similar to the PCL homopolymer. However, the PEG T_m was 5 ºC lower in the blend compared to the PEG homopolymer.

The thermal characteristics of blends prepared with higher PEG molecular weight were also studied. For the PEG_5/PCL_2 blend, two T_m were observed in the first heating cycle at ~ 51 ºC and ~ 61 ºC, consistent with the T_m of the individual PCL_2 and PEG_5 homopolymers (**Figure 4.3**). Upon cooling, the PEG_5/PCL_2 blend crystallisation peaks appeared at ~ 22 and ~ 38 ºC, which is also similar to that observed for the PCL_2 and PEG_5 homopolymers. In contrast to the PEG_2/PCL_2 blend, only a slight depression in the T_c was observed for the PEG component in the PEG_5/PCL_2 blend, which is due to the fractional crystallisation effect, whereby the polymers crystallise in a phase-separated environment. In this case, the increase in PEG molecular weight prevents PCL from significantly influencing the PEG crystallisation.[17]

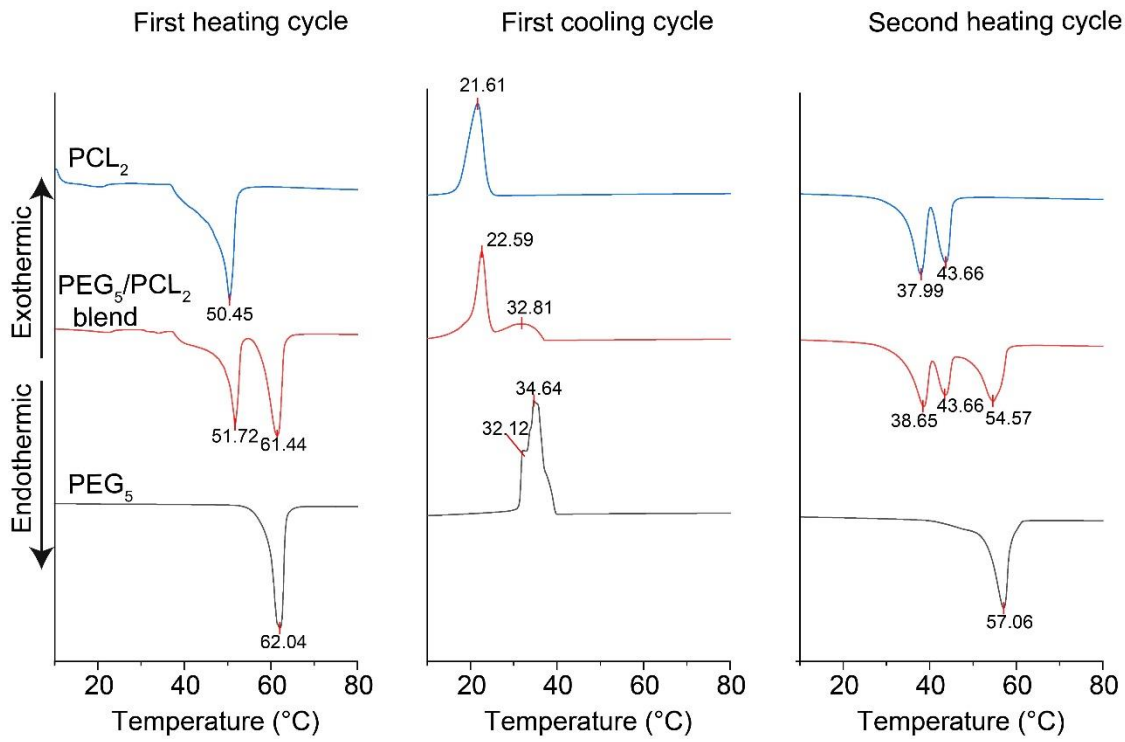


Figure 4.3: DSC thermograms of the PEG_5 and PCL_2 homopolymers and PEG_5/PCL_2 physical blend 1:1 (%w/w) showing the first heating, first cooling and second heating profiles (ramp rate 10 ºC/min). The blend does not appear to have a significant impact on the melting or crystallisation of the PCL component; however, a slight decrease in the PEG melting and crystallisation temperatures is observed, indicating fractional crystallisation has occurred.

The PEG_{10}/PCL_2 blend also showed similar transition temperatures and trends to those observed for the PEG_5/PCL_2 blend (**Figure 4.4**). In the PEG_5/PCL_2 blend, the ΔH_m of PEG (T_m ~ 54 ºC) (**Figure 4.3**) in the second heating cycle was 37.27 J/g, which is significantly lower than the PEG_5 homopolymer (~ 157 J/g), and can be attributed to the imperfect crystallisation of PEG in the presence of PCL in the blend. A similar trend was also observed in the PEG_{10}/PCL_2 and PEG_2/PCL_2 blends (**Table 4.2**).

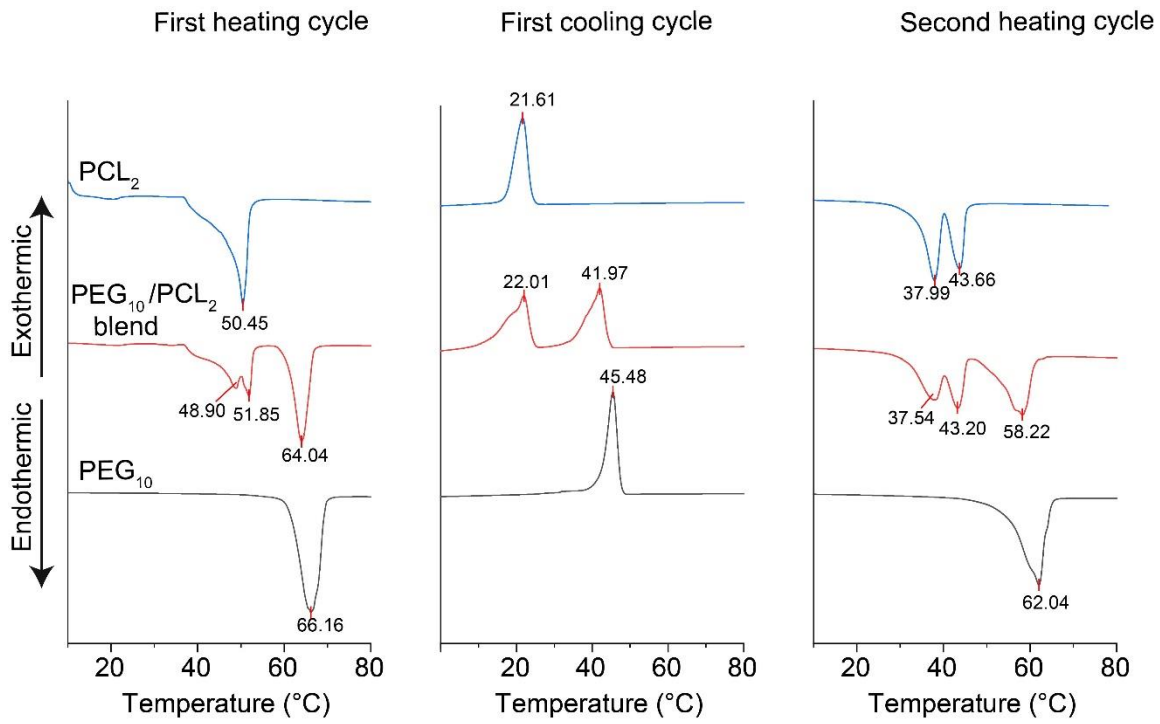


Figure 4.4: DSC thermograms of the PEG_{10} and PCL_2 homopolymers, and PEG_{10}/PCL_2 physical blend 1:1 (%w/w) showing the first heating, first cooling and second heating profiles (ramp rate 10 ºC/min). The blend does not appear to have a significant impact on the melting or crystallisation of the PCL component; however, a slight decrease in the PEG melting and crystallisation temperatures is observed, indicating fractional crystallisation has occurred.

From analysing the PEG/PCL blends, several trends are apparent. Firstly, the thermal behaviour of PEG changes significantly when it is blended with PCL, including depression of the PEG T_m and T_c. Nevertheless, even in the blend, the thermal behaviours of PEG and PCL are distinguishable from each other. Secondly, there is a significant change in the ΔH_m and ΔH_c of the blends compared to the homopolymers; this is indicative of an overall reduction in crystallinity. Taken together, these results suggest the imperfect crystallisation of PEG and PCL occurs when they are blended together, which is consistent with previous observations.[19]

Table 4.2: Thermal properties of PEG and PCL homopolymers, and PEG/PCL physical blend 1:1 (%w/w) determined via DSC (n = 3) from the first and second heating/cooling cycles. Thermal properties include the T_m and T_c and the associated enthalpy changes (ΔH_m and ΔH_c, respectively).

First Cycle				
Polymer	T_m (°C)	ΔH_m (J/g)	T_c (°C)	ΔH_c (J/g)
PEG_2	53.76 ± 0.14	181.86 ± 5.77	32.98 ± 0.37	134.72 ± 2.57
PEG_2/PCL_2 blend	53.23 ± 0.23	108.29 ± 1.30	21.62 ± 0.47	87.5 ± 1.27
PEG_5	62.06 ± 1.46	188.64 ± 3.20	37.63 ± 0.40	156.69 ± 3.21
PEG_5/PCL_2 blend	61.44 ± 0.12, 51.69 ± 0.62	48.27 ± 0.10, 47.14 ± 0.79	38.99 ± 0.53, 22.59 ± 0.93	81.91 ± 4.22
PEG_{10}	66.18 ± 0.02	188.91 ± 3.20	45.83 ± 0.37	152.3 ± 10.23
PEG_{10}/PCL_2 blend	64.04 ± 0.92 51.85±0.65, 49.67 ± 0.80	52.72 ± 0.20 49.35 ± 0.58	41.97 ± 0.23 42.19 ± 0.37, 21.99 ± 0.87	39.19 ± 0.62 45.65 ± 2.23
PCL_2	50.77 ± 0.32	78.04 ± 4.07	21.94 ± 0.34	67.52 ± 0.73
Second Cycle				
Polymer	T_m (°C)	ΔH_m (J/g)	T_c (°C)	ΔH_c (J/g)
PEG_2	52.05 ± 1.25	156.7 ± 11.74	35.88 ± 2.76	155.1 ± 15.07
PEG_2 /PCL_2 blend	49.58 ± 0.25, 43.67 ± 0.60, 38.17 ± 0.10	94.9 ± 2.44	21.6 ± 0.65	87.39 ± 1.22
PEG_5	58.35 ± 1.10	157.97 ± 5.18	36.47 ± 1.72	151.75 ± 8.65
PEG_5/PCL_2 blend	38.65 ± 0.58, 43.72 ± 0.67 55.05 ± 0.17	48.55 ± 1.25 37.21 ± 0.75	38.79 ± 0.23, 22.39 ± 0.23	82.71 ± 3.52
PEG_{10}	62.54 ± 0.39	165.30 ± 4.47	45.91 ± 0.13	158.48 ± 6.22
PEG_{10}/PCL_2 blend	58.22 ± 0.44 45.19 ± 0.12, 43.20 ± 0.32	36.52 ± 1.69, 43.52 ± 3.37	41.76 ± 0.36 41.19 ± 0.17, 21.92 ± 0.12	39.33 ± 2.36 41.99 ± 2.14
PCL_2	38.13 ± 0.39, 43.62 ± 0.31	64.66 ± 2.0	21.99 ± 0.32	66.08 ± 1.09

4.1.2.3 Thermal characterisation of PEG-b-PCL copolymers

In this work, copolymers were synthesised in bulk (without any solvent) and purified via precipitation into diethyl ether. It is possible that interaction between the blocks is limited during precipitation, due to the rapid rate at which it occurs. This may, in turn, limit the effect of these interactions on crystallisation, in a similar manner to that observed when a polymer melt is rapidly cooled.[13]

It can be hypothesised that if the PEG and PCL blocks crystallise separately without influencing each other, then their thermal behaviour will be distinguishable when they are blended together (PEG/PCL blend). Any changes in the thermal behaviour of the PEG or PCL blocks would suggest that for the precipitated copolymers, the covalent tethering of the blocks has a marked effect on their thermal behaviour. The data from the first heating, first cooling, and second heating cycles were analysed to investigate the effect of the covalent tethering between the blocks on the thermal behaviour of the synthesised polymers.

Thermal characterisation of PEG_2PCL_y copolymers series

From previous studies with the homopolymers and their blends, it is evident that the presence of PCL has a significant effect on the thermal characteristics of PEG. Therefore, the thermal properties of PEG_2, PCL_2, PEG_2/PCL_2 blend and the $PEG_2PCL_{1.8}$ were investigated and compared using DSC (**Figure 4.5**).

The T_m and T_c of $PEG_2PCL_{1.8}$ copolymer in the first heating cycle were significantly different to that of the PEG and PCL homopolymers, and the 1:1 binary blend. One key observation from the DSC thermograms of the first heating cycle is that $PEG_2PCL_{1.8}$ copolymer had a single T_m at ~ 47 ºC, which is 7 ºC less than the T_m of the PEG homopolymer, whereas the PEG component of the PEG/PCL blend does not show any significant decrease in T_m. This is clearly inconsistent with the hypothesis that in a block copolymer, precipitation in a non-solvent media (DEE) causes the PEG and PCL blocks to crystalise separately without influencing each other. It can be concluded that the covalent tethering of the blocks influences the thermal behaviour of each block. In $PEG_2PCL_{1.8}$, T_c was significantly lower (~15 ºC) than that observed for the PEG homopolymer and more closely resembles the PCL homopolymer and PEG/PCL blend. This indicates that following the first heating cycle, PEG and PCL influence each other during crystallisation (cooling cycle), which results in imperfect crystal formation. Further, a decrease of T_m (~ 10 ºC) in the second heating cycle support this hypothesis. $PEG_2PCL_{1.8}$ exhibited a single endothermic peak in the second heating cycle, whereas the PEG/PCL blend shows a triple melting peak. This further supports the statement that the covalent tethering between the blocks modifies the thermal behaviour of the $PEG_2PCL_{1.8}$ copolymer, in comparison to the PEG and PCL homopolymer.

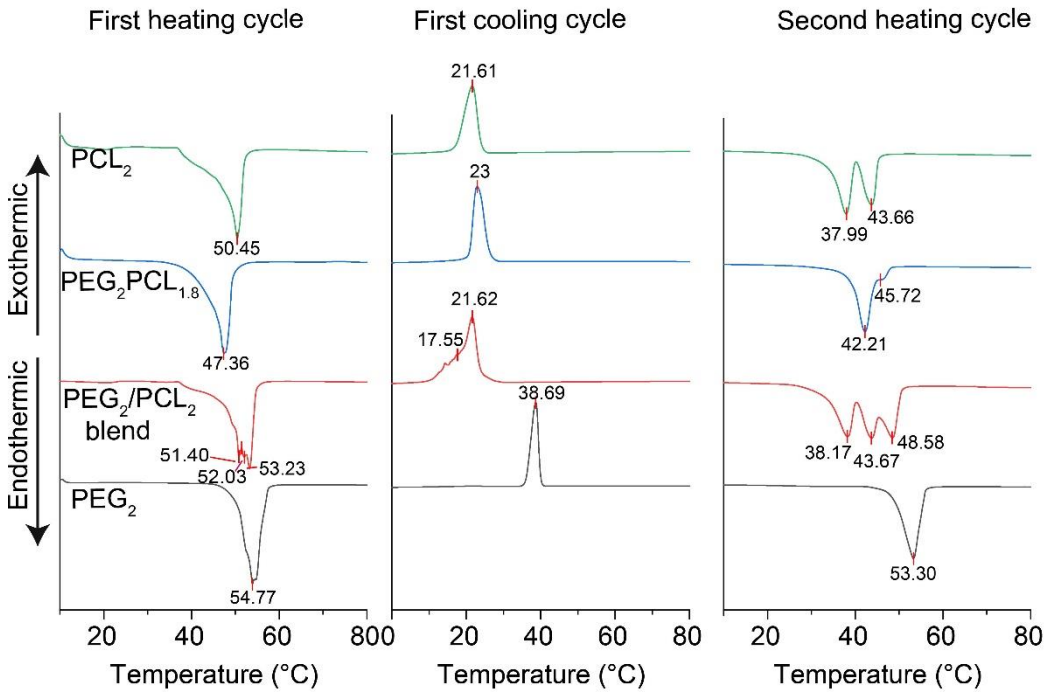


Figure 4.5: DSC thermograms of PEG_2 and PCL_2 homopolymers, PEG_2PCL_2 physical blend 1:1 (%w/w), and $PEG_2PCL_{1.8}$ block copolymer showing the first heating, first cooling and second heating profiles (ramp rate 10 ºC /min). The $PEG_2PCL_{1.8}$ copolymer displays significantly different behaviour to the homopolymers and the blend, with only a sharp T_c on the first cooling cycle and a distinct T_m peak on the second heating.

Subsequently, DSC was conducted on the remaining copolymers in the PEG_2PCL_y series, and the thermal characteristics were determined from the first heating (**Figure 4.6**) and cooling cycle (**Figure 4.7**). In general, as the PCL to PEG ratio was increased, the T_m was found to decrease, with the exception of the PCL:PEG 2:1 ($PEG_2PCL_{3.9}$) copolymer.

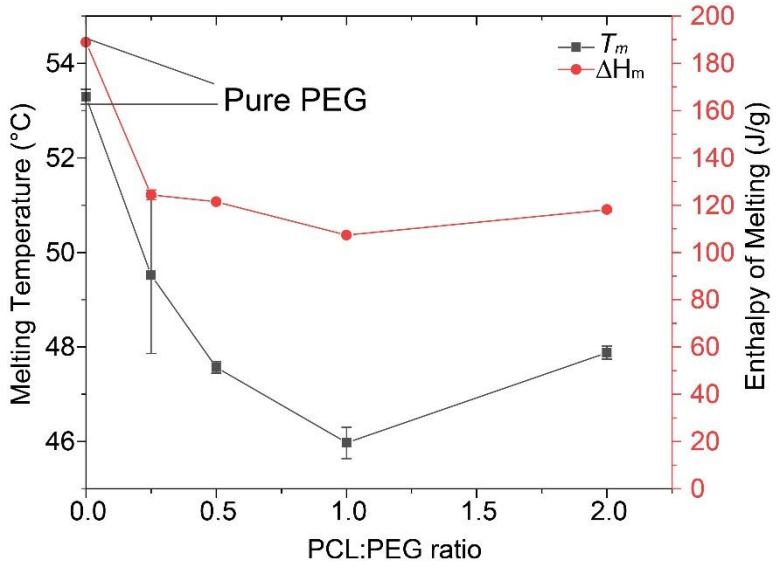


Figure 4.6: T_m and ΔH_m of the PEG_2PCL_y copolymer series recorded during the first heating cycle, with increasing PCL:PEG ratios (n = 3). The T_m and ΔH_m of the copolymers were found to be less than that of the PEG homopolymer.

This depression of T_m has been observed previously by Cerrai *et al.* who synthesised PCL-*b*-PEG-*b*-PCL block copolymers with PEG (M_n = 950 Da) and different PCL molecular weight. They concluded that the crystallisation of PCL occurs first and freezes the polymer morphology leading to imperfections in the PEG crystallites, which causes the depression in T_m.[20] The T_m depression of the block copolymer arises from kinetic and thermodynamic effects, and the relationship between lamellar thickness (L) and T_m can be expressed as follows:[21]

$$T_m = T_m^0 \left(1 - \frac{2v_e}{\Delta H_f L}\right) \quad \textbf{(4.1)}$$

Where v_e is the free energy needed to fold the polymer chain in a lamellar and ΔH_f is the heat of fusion of the lamellar. T_m^0 represents the equilibrium melting temperature, where the polymer forms perfect crystals. However, the T_m^0 is always larger than T_m and increases as the L increases ("Thomson's rule").[22] For a block copolymer having an amorphous block and a crystalline block; the imperfections in the crystal are introduced when an amorphous layer is formed, which results in a decrease in L. It can be predicted that as the PCL molecular weight increases, it would cause thinning of the PEG crystal lamellae as well as a decrease in T_m (**Figure 4.6**). A reduction in the L could also explain the decrease in T_c and ΔH_c in the PEG_2PCL_y copolymer series when compared to the PEG_2 homopolymer (**Figure 4.7**).

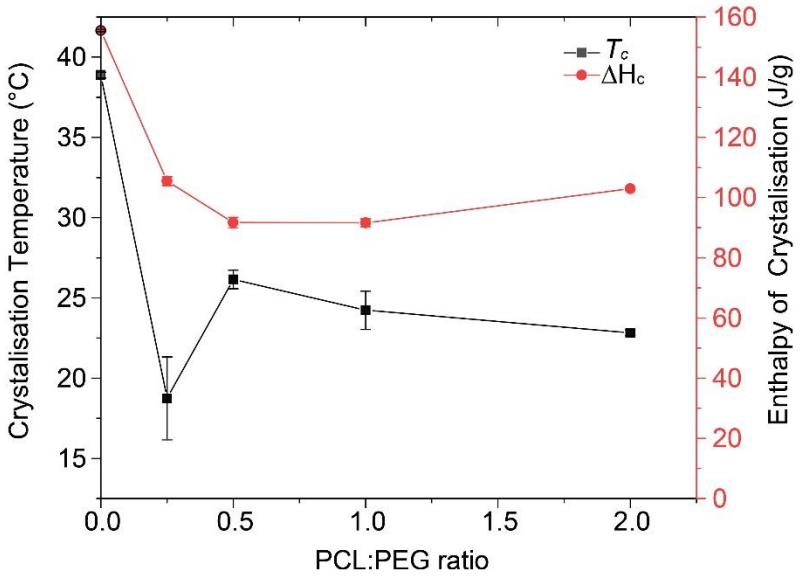


Figure 4.7: T_c and ΔH_c of the PEG_2PCL_y copolymer series obtained from the first cooling cycle, with increasing PCL:PEG ratio (n = 3). The T_c and ΔH_c of the copolymers were found to be less than that of the PEG homopolymer.

In general, the T_c of the copolymers remained approximately 23–26 ºC, regardless of the PCL:PEG molecular weight ratio, which is slightly higher than the T_c of the PCL homopolymer and significantly lower than the T_c of the PEG homopolymer. Nojima *et al.* investigated the crystallisation behaviour of PCL-*b*-PEG-*b*-PCL triblock copolymers and found that increasing the PCL fraction caused depression in the T_m and a reduction of the lamellar thickness.[19] Also, when the PCL component was substantial (PCL:PEG 10:1) XRD revealed the absence of characteristic PEG diffraction peaks. They concluded that during crystallisation, the minor component was rejected from the crystallites and accommodated in the space between the crystal lamellar in an amorphous state.[19,23] He *et al.* conducted a similar study using a PEG-*b*-PCL diblock copolymer with varying the PCL fraction,[9] and they found double crystallisation peaks at higher PCL:PEG ratios, from which they hypothesised that PCL crystallises first, followed by PEG in a confined microdomain. However, there was no direct evidence to support this hypothesis. In this study, the PEG_2PCL_y copolymers series did not show any clear double crystallisation peaks at even higher PCL:PEG ratios (**Figure 4.8**).

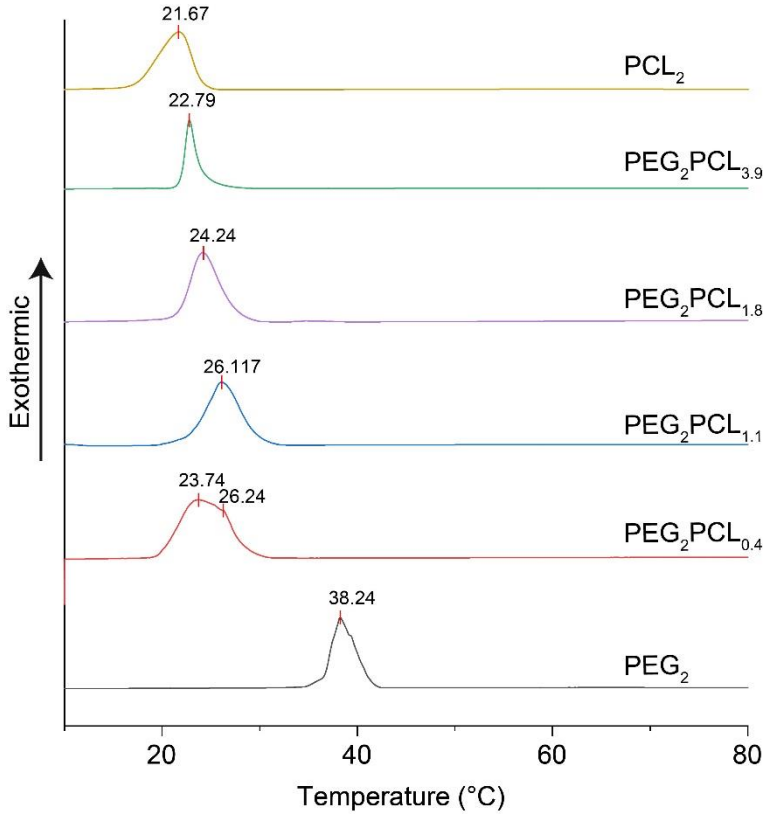


Figure 4.8: DSC thermograms of PEG, PEG_2 and PCL_2 homopolymers, and the PEG_2PCL_y copolymers series obtained during the first cooling cycle (ramp rate 10 ºC /min). Minimal variation in the T_c was observed with different PCL:PEG ratios.

The crystallisation process was further investigated using temperature-dependent WXRD of the copolymers, which can provide information on the extent of crystallisation and order of block crystallisation. WXRD was conducted during the heating and cooling of the block copolymers (**Figure 4.9**). Initially, the X-ray diffraction pattern of the copolymer powder was acquired at 25 ºC prior to heating. The sample was then heated to 80 ºC (temperature above the melting temperature of both blocks), and the molten state diffraction pattern was recorded. Finally, the sample was cooled down to the T_c for each of the copolymers (as determined from DSC (**Figure 4.8**) and the diffraction pattern was recorded again. For example, for the $PEG_2PCL_{0.4}$ copolymer the T_c was determined to be ~ 24 ºC, and the diffraction pattern was recorded at an onset temperature of 25 ºC (**Figure 4.9**).

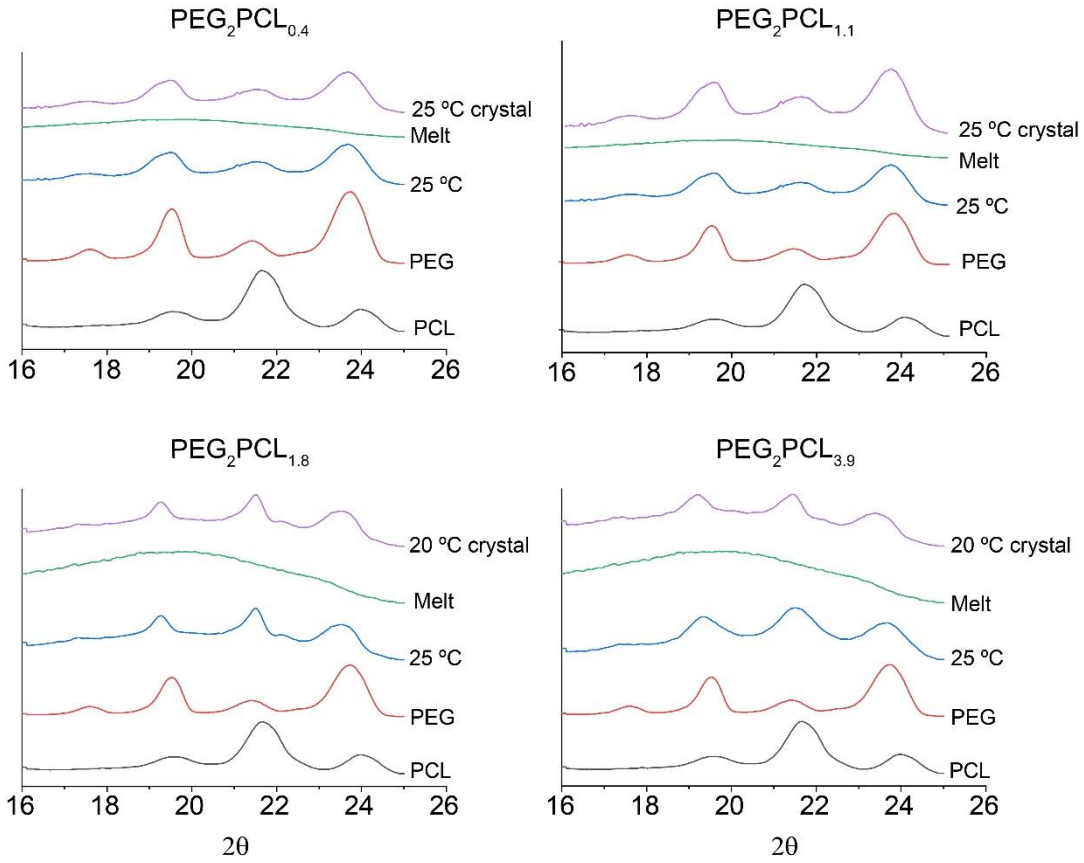


Figure 4.9: Stacked WXRD patterns of the PEG_2 and PCL_2 homopolymers recorded at 25 °C, and the PEG_2PCL_y block copolymers recorded at room temperature (25 °C), in the molten state (80 °C) and near to the T_c upon cooling.

WXRD of the PEG and PCL homopolymers revealed characteristics patterns with major peaks at 19.2° and 23.7° for the former and 21.8° (2θ) for the latter at 25 °C. Analysis of the copolymers before thermal treatment at 25 °C revealed that at the lower PCL:PEG ratios (0.25:1 and 0.5:1) the characteristic PCL peak at 21.8° was absent (**Figure 4.9**), indicating that PCL is amorphous in these copolymers due to its short length and the influence of the larger PEG chains. Additional DSC experiments where the copolymers were cooled to −65 °C (**Appendix A 4.1**) did not show any other crystallisation events, which indicates that PCL remains in an amorphous state, and confirms previous predictions that when PCL is small in length, it remains amorphous.[19] At higher PCL:PEG ratios (1:1 and 2:1) the diffraction patterns recorded at 25 °C revealed characteristic peaks for both PEG and PCL (**Figure 4.9**) and confirmed that both blocks are crystallised in these copolymers.

The thermal history of the polymers[10] was eliminated by heating the copolymers to the molten state (80 °C) and was confirmed by WXRD, which revealed the absence of any specific peaks (**Figure 4.9**). Subsequently, the copolymers were cooled to the T_c (**Figure 4.8**) and the WXRD patterns were recorded again (**Figure 4.9**). At lower PCL:PEG ratios (0.25:1 and 0.5:1) the T_c was approximately 26 °C and presented as a monomodal exothermic peak, which could result from crystallisation of a single block or both blocks (**Figure 4.8**). However, when cooled to 25 °C, the WXRD patterns recorded for $PEG_2PCL_{0.4}$ and $PEG_2PCL_{1.1}$ only revealed PEG crystallisation peaks. Therefore, it can be concluded that in these copolymers the PEG block crystallises and the PCL block remains amorphous as described earlier. As the PCL:PEG ratio was increased (1:1 and 2:1), the PEG and PCL blocks were found to crystallise simultaneously (**Figure 4.9**), and the larger PCL block does not appear to cause the PEG block to form an amorphous domain as predicted by some previous studies.[19] However, it is logical to assume that there might be a threshold limit of PCL length responsible for that effect and that it was not reached in this study, particularly considering that in other studies the length of the PCL was much larger (e.g., PCL:PEG ratio 10:1).[19,23]

Whilst the WXRD patterns of the PEG_2PCL_y copolymers confirmed that at higher PCL:PEG ratios PCL co-crystallises with PEG, DSC thermograms did not show characteristic PCL melting peaks, such as those observed for the PEG/PCL blends (**Figure 4.2**). At PCL:PEG ratios up to 1:1, all copolymers displayed a monomodal endothermic melting peak in the DSC thermograms upon the second heating cycle, but at a ratio of 2:1 ($PEG_2PCL_{3.9}$) a bimodal peak was observed (**Figure 4.10**). The combined results of DSC and WXRD indicate that the crystal morphology of PEG-*b*-PCL copolymers is utterly different from the PEG/PCL polymers blend. In DSC thermogram, the presence of characteristic melting peaks of PEG and PCL in the second heating cycle indicate that PEG and PCL form individual crystal domains during crystallisation (after the first heating cycle).

This is observed in crystalline/crystalline polymer blends, for example, high-density polyethylene/low-density polyethylene systems.[24] In the case of the crystalline-*b*-crystalline block copolymers, complete segregation of the crystal domains is not possible due to the covalent bonding between the blocks. Consequently, during crystallisation, a minor component is rejected from the crystal and accommodated in the amorphous layer between the crystal lamellae; this explains the absence of the characteristic PCL peaks in WXRD at lower PCL:PEG ratios ($PEG_2PCL_{0.4}$ and $PEG_2PCL_{1.1}$).

For block copolymers with a comparable fraction (≥ PCL:PEG 1:1), the PCL and PEG blocks crystallise simultaneously and coexist within the same crystal domain. However, this coexistence results in a significant reduction in L, which explains the decrease in T_m and T_c at higher PCL:PEG ratios.

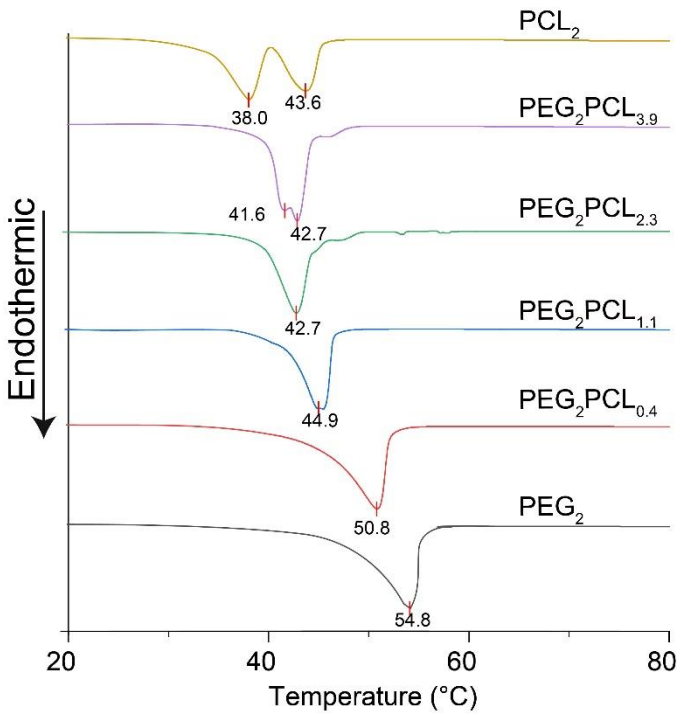


Figure 4.10: DSC thermograms of the PEG_2 and PCL_2 homopolymers, and the PEG_2PCL_y block copolymer series, showing the second heating profiles (ramp rate 10 °C/min). The T_m was found to decrease with increasing PCL:PEG ratio.

Thermal characterisation of the PEG_5PCL_y copolymers series

The thermal behaviour of the PEG_5PCL_y copolymers series (as determined by DSC) displayed different trends when compared to the PEG_2PCL_y series (**Figure 4.11**).

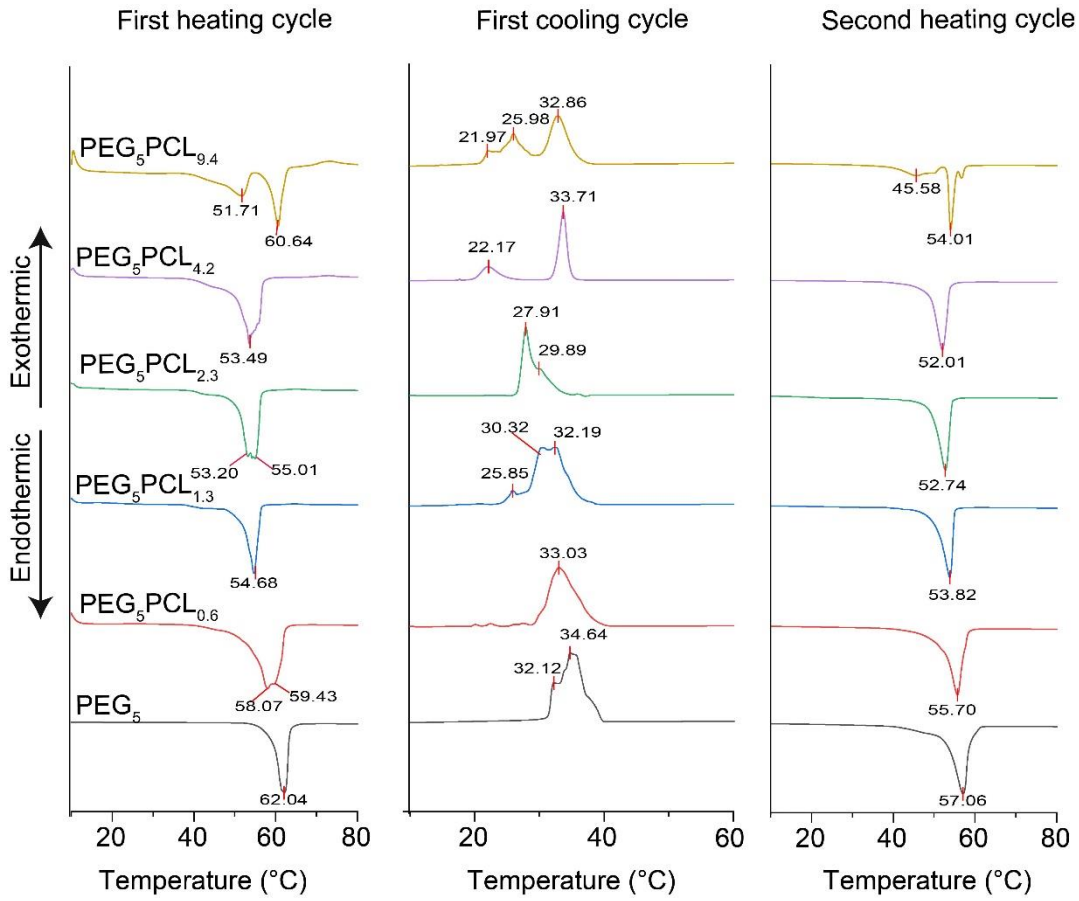


Figure 4.11: DSC thermograms of the PEG_5 homopolymer and the PEG_5PCL_y polymer series, showing the first heating, first cooling and second heating profiles (ramp rate 10 °C/min). The T_m was found to decrease with increasing PCL:PEG ratio. The DSC thermogram of the first cooling cycle shows a bimodal exothermic peak at the highest PCL:PEG ratio.

Compared to the PEG_5 homopolymer that has a relatively sharp T_m (62.04 °C) on the first melting cycle, the T_m for the PEG_5PCL_y copolymer series (except $PEG_5PCL_{9.4}$) decreased and melting peaks broadened, with tailing towards lower temperatures observed. This might indicate that there is some separation between the crystalline microdomains. However, the second heating cycle only showed a single sharp peak, indicating that there is only one crystalline component.

For the $PEG_5PCL_{9.4}$ copolymer, two melting peaks were observed on the first and second heating cycles, which would indicate that the PEG and PCL components are present as discrete crystalline microdomains. The crystallisation of the PEG_5 homopolymer presents as a broad exothermic peak (T_c = 34.6 °C) occurring over a wide temperature range (**Figure 4.11**), which is characteristic of integral folding chain crystals (heterogenous folding) consisting of different chain folding conformations and lamellar thickness.[25]

This phenomenon is generally observed for low molecular weight polymers and diminishes as the molecular weight increases.[25] A similar crystallisation peak (T_c = 33.0 ºC) is also observed for the $PEG_5PCL_{0.6}$ copolymer, although slightly skewed to a lower temperature, indicating that the PEG crystallisation may be affected by the PCL block even though the PCL block remains amorphous, similar to that observed for the PEG_2PCL_y series. For the $PEG_5PCL_{1.3}$ and $PEG_5PCL_{2.3}$ copolymers, broad multimodal crystallisation peaks shifted to lower temperatures were observed, which could result from the increase in PCL length interfering with PEG crystallisation, which is supported by a decrease in ΔH_m (**Figure 4.12**). However, as the PCL:PEG ratio increases further (1:1 and 2:1) two crystallisation peaks were observed, indicating that both blocks are crystallising separately, though the order of crystallisation cannot be determined by DSC (**Figure 4.11**).

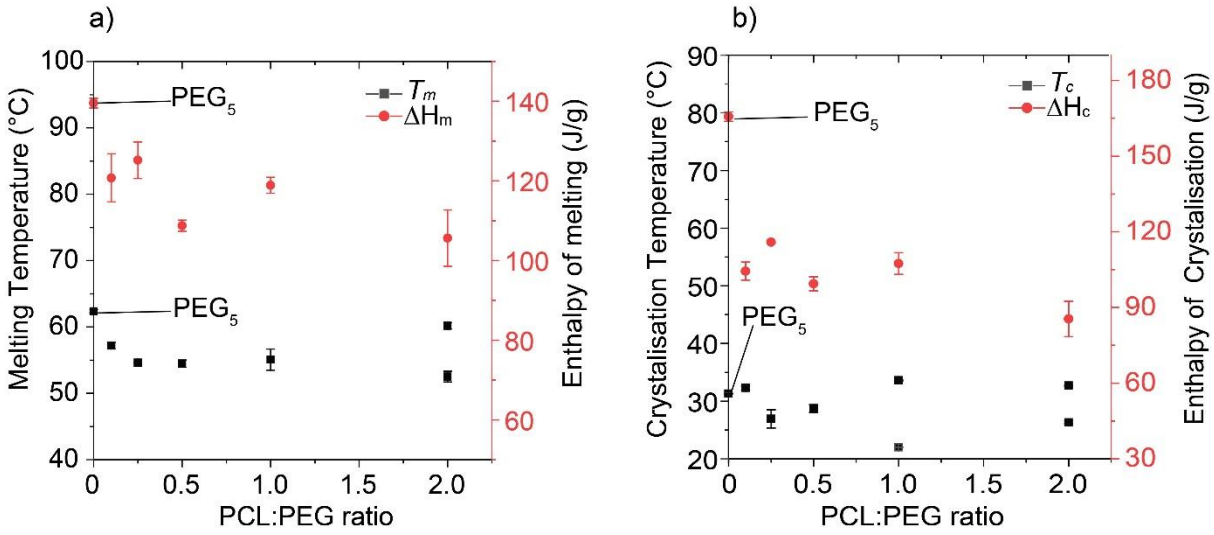


Figure 4.12: a) T_m and ΔH_m (first heating cycle) values of the PEG_5PCL_y copolymer series as a function of the PCL:PEG ratio (n = 3). b) T_c and ΔH_c (first cooling cycle) of the PEG_5PCL_y copolymer series as a function of the PCL:PEG ratio (n = 3).

To determine which block crystallises first for the PEG_5PCL_y copolymers. WXRD was conducted. As described previously, X-ray diffraction patterns were recorded at 25 ºC initially, then polymer in the molten state and then polymer at various temperatures upon cooling to coincide with the T_c peak or between separate T_c peaks.

For the $PEG_5PCL_{0.6}$, $PEG_5PCL_{1.3}$ and $PEG_5PCL_{2.3}$ copolymers (where PCL:PEG ratio is low), the diffraction patterns recorded before heating (at 25 ^oC) and at the onset of the T_c were very similar and absent of characteristic PCL peaks (**Figure 4.13**). The same pattern as observed for the PEG_2PCL_y copolymer series at lower PCL:PEG ratios.

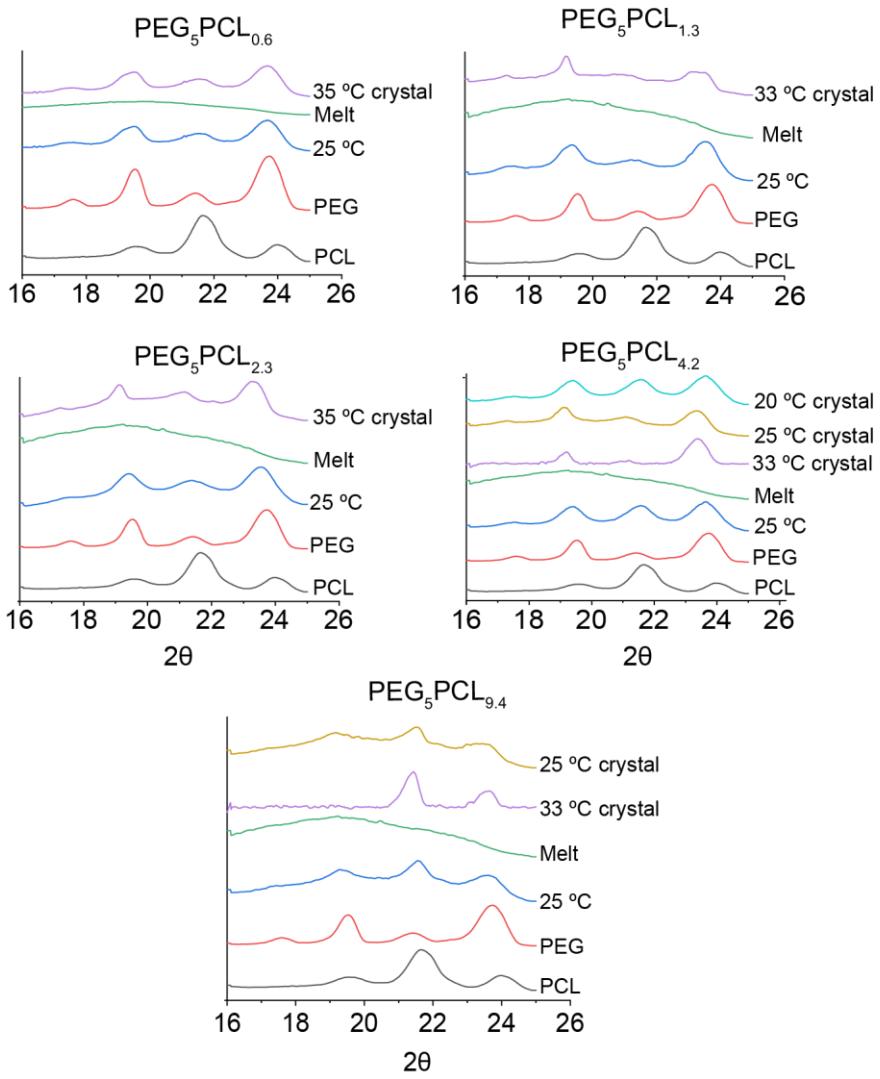


Figure 4.13: Stacked WXRD patterns of the PEG_5 and PCL_2 homopolymers recorded at 25 °C, and the PEG_5PCL_y copolymer series at room temperature (25 °C), in the molten state (80 °C) and near the T_c peak or between separate T_c peaks.

However, as the ratio is increased for the $PEG_5PCL_{4.2}$ and $PEG_5PCL_{9.4}$ copolymers, characteristic peaks for both PEG and PCL were observed in the diffraction patterns. The WXRD results confirm that for the $PEG_5PCL_{0.6}$, $PEG_5PCL_{1.3}$ and $PEG_5PCL_{2.3}$ copolymers PEG is the dominant crystalline component (**Figure 4.13**), which is consistent with the second heating cycle of the DSC that showed a single sharp melting peak (**Figure 4.11**).

$PEG_5PCL_{4.2}$ copolymer also shows the same trends in the DSC heating cycles; however, the DSC cooling cycle and WXRD results indicate that there is a crystalline PCL component present along with PEG, with the PEG component crystallising first followed by the PCL component (**Figure 4.13**). As the PEG component dominates crystallisation, it would 'freeze' the polymer conformation leading to imperfect PCL crystallisation, which would result in a lower intensity melting peak (compared to the PEG component) that may not be observable in the DSC thermogram. Interestingly, this behaviour is reversed for the $PEG_5PCL_{9.4}$ copolymer with crystallisation appearing to be dominated by the PCL component, followed by PEG crystallisation (**Figure 4.11**). Nojima *et al.* concluded from their work on PCL-*b*-PEG-*b*-PCL that at higher PCL:PEG ratios, PEG crystallisation is influenced by PCL, resulting in a significant reduction in L; this causes a reduction in the T_m as observed in $PEG_5PCL_{9.4}$ copolymer.[19] These results indicate that there is a threshold limit of the length at which PCL begins to dominate the crystallisation process as previously hypothesised previously.

Thermal characterisation of the $PEG_{10}PCL_y$ copolymers series

DSC analysis of the $PEG_{10}PCL_y$ copolymer series revealed similar trends to that observed for the PEG_5PCL_y copolymers series (**Figure 4.14**). While the PEG_{10} homopolymer displayed a broad but relatively symmetrical melting peak on the first heating cycle, the T_m for the $PEG_{10}PCL_y$ copolymer series decreased and broadened, with tailing towards lower temperatures. In comparison, the second heating cycle only showed single, narrow melting peaks for the copolymers.

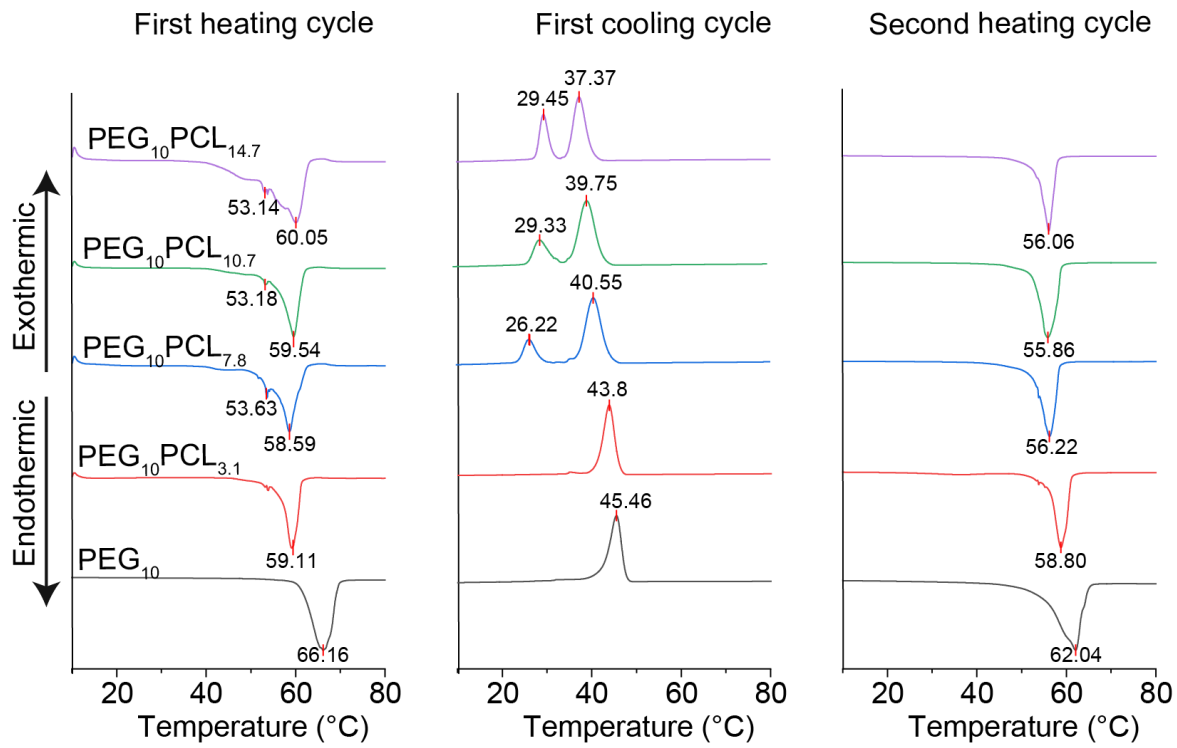


Figure 4.14: DSC thermograms of the PEG_{10} homopolymer and the $PEG_{10}PCL_y$ copolymer series showing the first heating, first cooling and second heating profiles (ramp rate 10 °C/min). A gradual decrease in T_c across the series as the PCL:PEG ratio increases is observed, with bimodal crystallisation peaks.

The crystallisation of the $PEG_{10}PCL_{3.1}$ copolymer presented as a single symmetrical peak similar to that observed for the PEG_{10} homopolymer, however, as the PCL:PEG ratio increased; two separate peaks were observed, indicating that PCL and PEG crystallise independently (**Figure 4.14**). In general, it was observed that the T_m and ΔH_m, as well as T_c and ΔH_c were depressed as the PCL:PEG ratio increased (**Figure 4.15**).

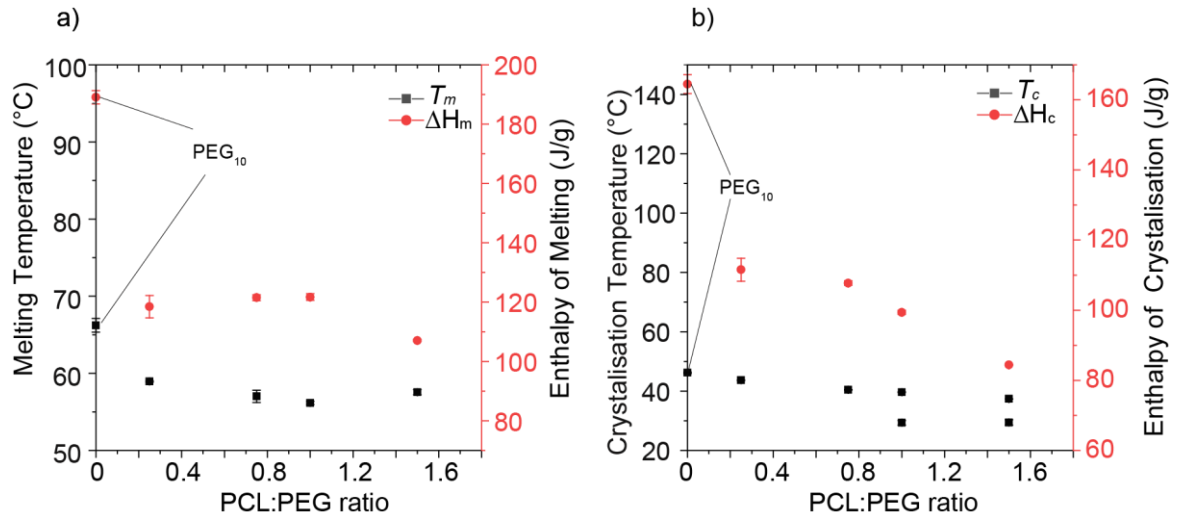


Figure 4.15: a) T_m and ΔH_m of the first heating cycle as a function of the PCL:PEG ratio for the $PEG_{10}PCL_y$ copolymer series (n = 3). b) T_c and ΔH_c of the first cooling cycle as a function of the PCL:PEG ratio for the $PEG_{10}PCL_y$ copolymer series (n = 3).

WAXD of $PEG_{10}PCL_{3.1}$ revealed the absence of characteristic PCL peaks upon crystallization, whereas for all other $PEG_{10}PCL_y$ copolymers the PEG component was found to dominate crystallisation followed by crystallisation the PCL component (**Figure 4.16**). This also indicates that the two components form separate microdomains for these copolymers, however, only one T_m is observed on the second heating cycle; a possible explanation for this is the imperfect crystallisation of PCL and weak melting peak.

It can be concluded from these results that the molecular weight ratio between the PCL and PEG blocks controls the crystallisation behaviour, but there is also a certain critical length of PEG whereby it will dominate the crystallisation. For example, $PEG_5PCL_{9.4}$ and $PEG_{10}PCL_{10.7}$ have almost identical PCL molecular weights, but in the former crystallisation is dominated by the PCL block, whereas in later crystallisation is dominated by the PEG block. Furthermore, for these polymers, the two blocks crystallise at separate temperatures, and it is evident that crystallisation of the first block causes a significant depression in the T_c of the second block (relative to the homopolymer). As the molecular weights of the copolymers get smaller, the distinction between the crystallisation of the two blocks becomes less obvious.

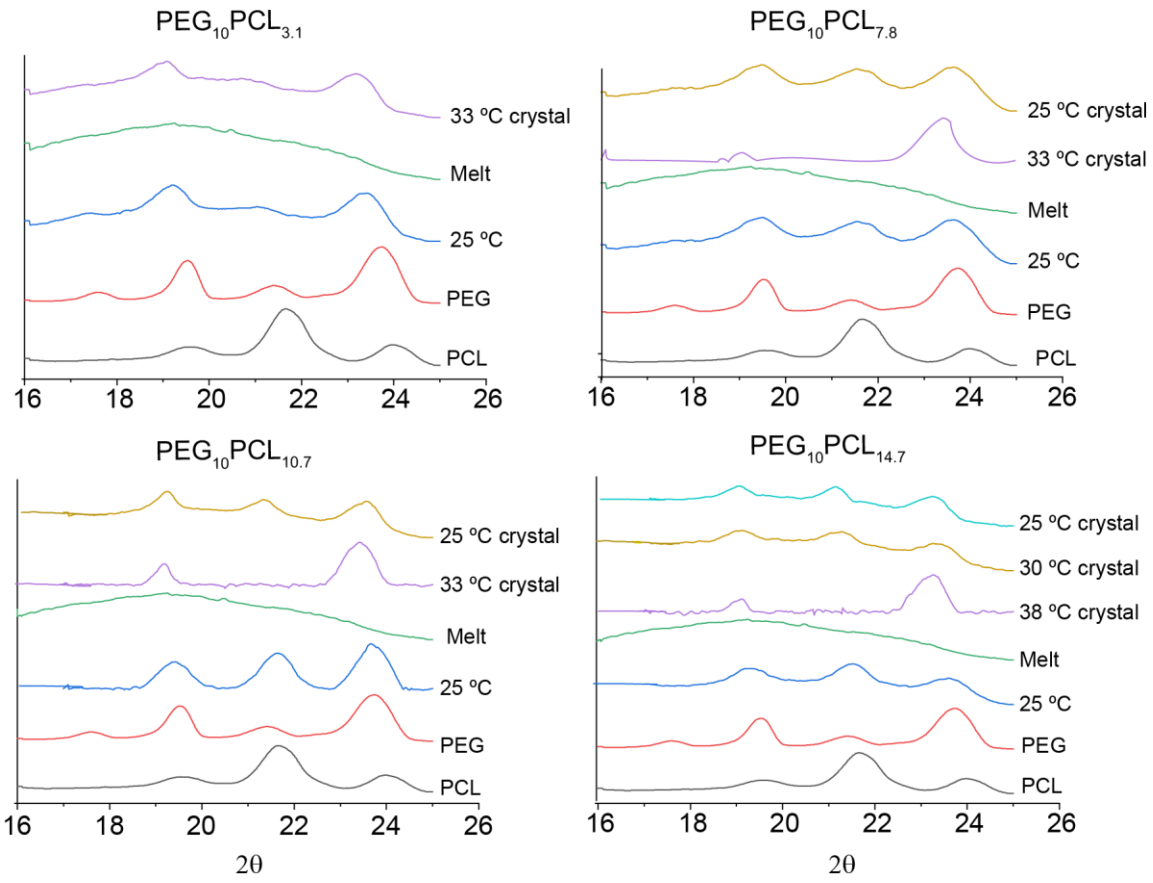


Figure 4.16: Stacked WXRD patterns of the PEG_5 and PCL_2 homopolymers recorded at 25 °C, and the $PEG_{10}PCL_y$ copolymer series at room temperature (25 °C), in the molten state (80 °C) and near the T_c peak or between separate T_c peaks.

4.1.2.4 Thermal characterisation of lyophilised PEG-b-PCL copolymer aggregates

As PEG-*b*-PCL copolymers self-assembled into aggregate in aqueous media, the PEG and PCL blocks are nanophase segregated in the corona and core, respectively. During this self-assembly, the PCL blocks aggregate together, which could result in their crystallisation, whereas the PEG block remains hydrated. Organisation and potentially crystallisation of the polymer chains in the aggregate core could have consequences in controlling the encapsulation and release of therapeutics from these aggregate as drug delivery systems. To date, the relationship between aggregation and the thermal behaviour of copolymers is not well established.

Therefore, the thermal characteristics of the polymer aggregate were analysed to determine the crystalline nature of the polymer in the aggregate. Solid aggregate powders were prepared via the lyophilisation of snap-frozen (−80 °C) polymer aggregate solutions (refer to Section 4.4.3 for more details). Theoretically, the lyophilised aggregate powder is a solid dispersion, wherein PEG forms a continuous amorphous phase with PCL cores dispersed therein (**Figure 4.17**).[26,27]

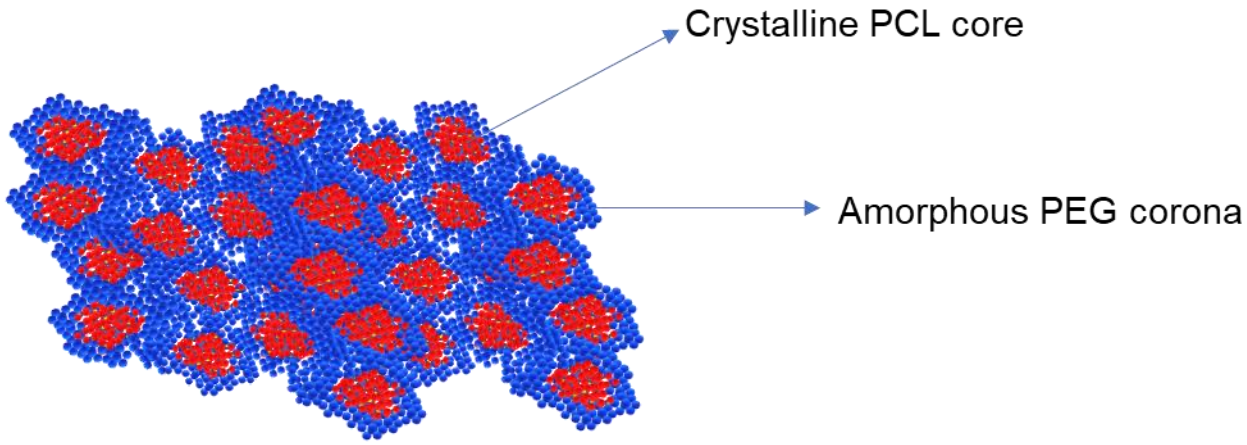


Figure 4.17: Illustration of the solid dispersion formed by lyophilisation of the micelle solution, showing the hypothesised amorphous PEG (blue) continuous phase with PCL(red) cores dispersed therein.

Initially, the $PEG_5PCL_{2.3}$ copolymer was investigated to determine the effect of self-assembly on the polymer morphology, as large differences in the T_m were noted in comparison to the PEG_5 and PCL_2 homopolymers. The thermal characteristics of the lyophilised polymer aggregate were analysed via DSC using a single heating profile from −30 °C to 80 °C at a ramp rate of 10 °C/min, and the thermograms were compared to their respective homopolymers, blends and block copolymers isolated via precipitation. For the $PEG_5PCL_{2.3}$ aggregate powder, the thermogram revealed a bimodal distribution with a broad peak at ~ 41 °C, followed by a major peak at ~53 °C, which was distinctly different from the thermogram of the block copolymer and more closely resembled the thermogram of the PCL homopolymer (**Figure 4.18**).

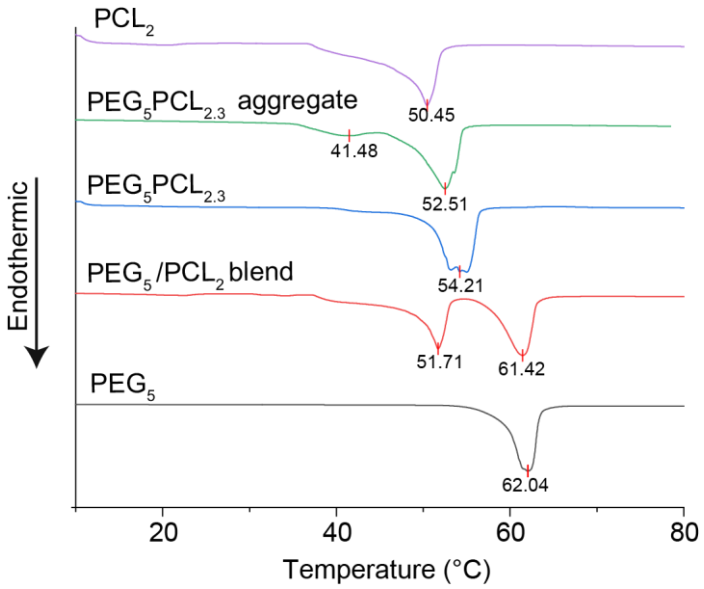


Figure 4.18: DSC thermograms of the PEG_5 and PCL_2 homopolymers, PEG_5/PCL_2 physical blend 1:1 (%w/w), $PEG_5PCL_{2.3}$ block copolymer, and $PEG_2PCL_{2.3}$ block copolymer aggregate (lyophilised powder), showing the first heating profiles (ramp rate 10 °C/min).

The lack of a distinctive PEG T_m peak would suggest that the PEG block remains amorphous. These results are consistent with previous studies and suggest that the melting curve may predominately be from semi-crystalline PCL in the core.[26] The lower melting peak at ~ 41 °C may originate from PCL crystallites in the core with a very thin lamellar, whereas the peak at ~53 °C may correspond to crystallites with thicker lamellar. As discussed earlier, the T_m is controlled by the lamellar thickness of the crystal (**Equation 4.1**). These results support the proposed hypothesis regarding the structure of the aggregate, as discussed in Chapter 3. The thin lamellar PCL crystallites may form at the boundary region of the aggregate where PCL is slightly hydrated, resulting in the formation of imperfect crystals, crystals with different lamellar thicknesses, or heterogeneous folding (**Figure 4.20**).[28,29]

For the PEG_2PCL_y copolymer aggregate series, both $PEG_2PCL_{1.8}$ and $PEG_2PCL_{3.9}$ possess longer PCL blocks and display bimodal peaks in the DSC thermograms (**Figure 4.19**). However, for these polymers, the major T_m peak occurs at ~ 42–44 °C, with a minor peak at ~52 °C. Interestingly, these are very similar to the peak locations observed for the $PEG_5PCL_{2.3}$ copolymer aggregate with almost the same PCL length, with the exception of a change in intensity (**Figure 4.19**). This could be an indication that the PCL cores have different types of crystallites, with different PCL folding conformations (**Figure 4.20**). This is further supported by the fact that $PEG_{10}PCL_{3.1}$ (**Figure 4.21**) also displays the same bimodal melting curve with peak intensities similar to $PEG_5PCL_{2.3}$ (**Figure 4.19**).

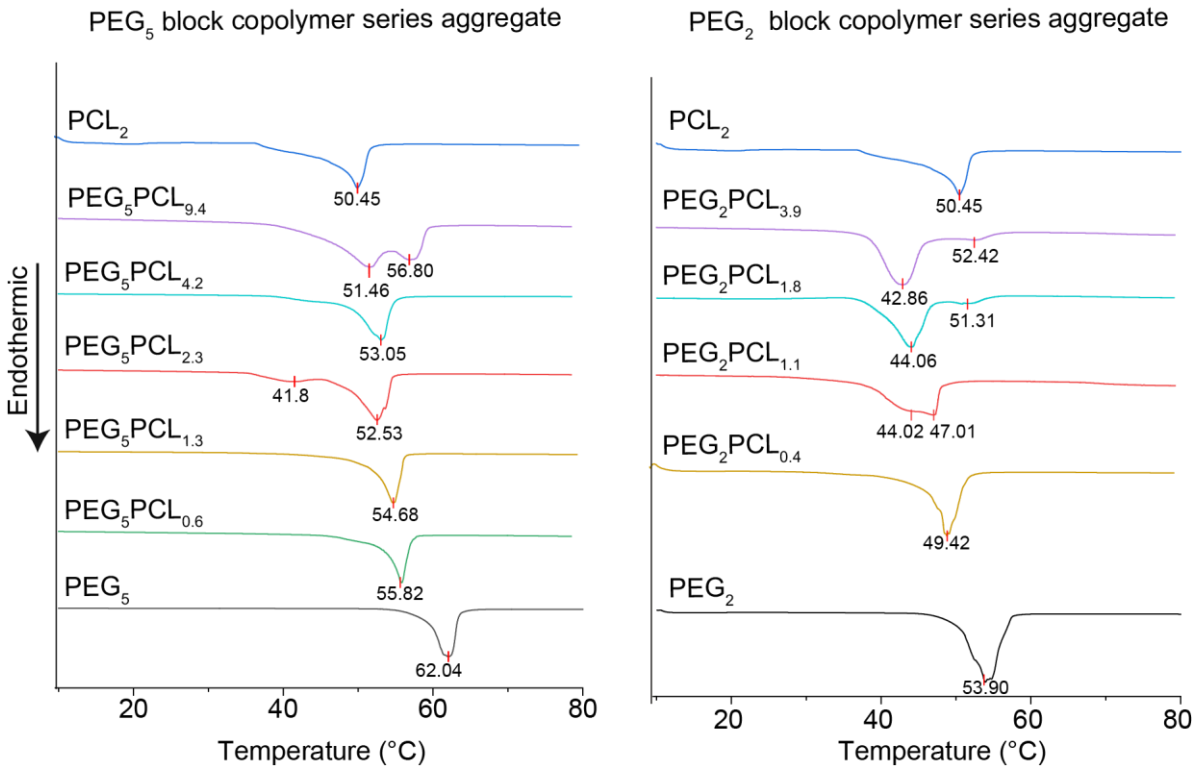


Figure 4.19: DSC thermograms of the PEG_2 and PCL_2 homopolymers, and PEG_5PCL_y and PEG_2PCL_y copolymer aggregate (lyophilised powder), showing the first heating profiles (ramp rate 10 °C/min).

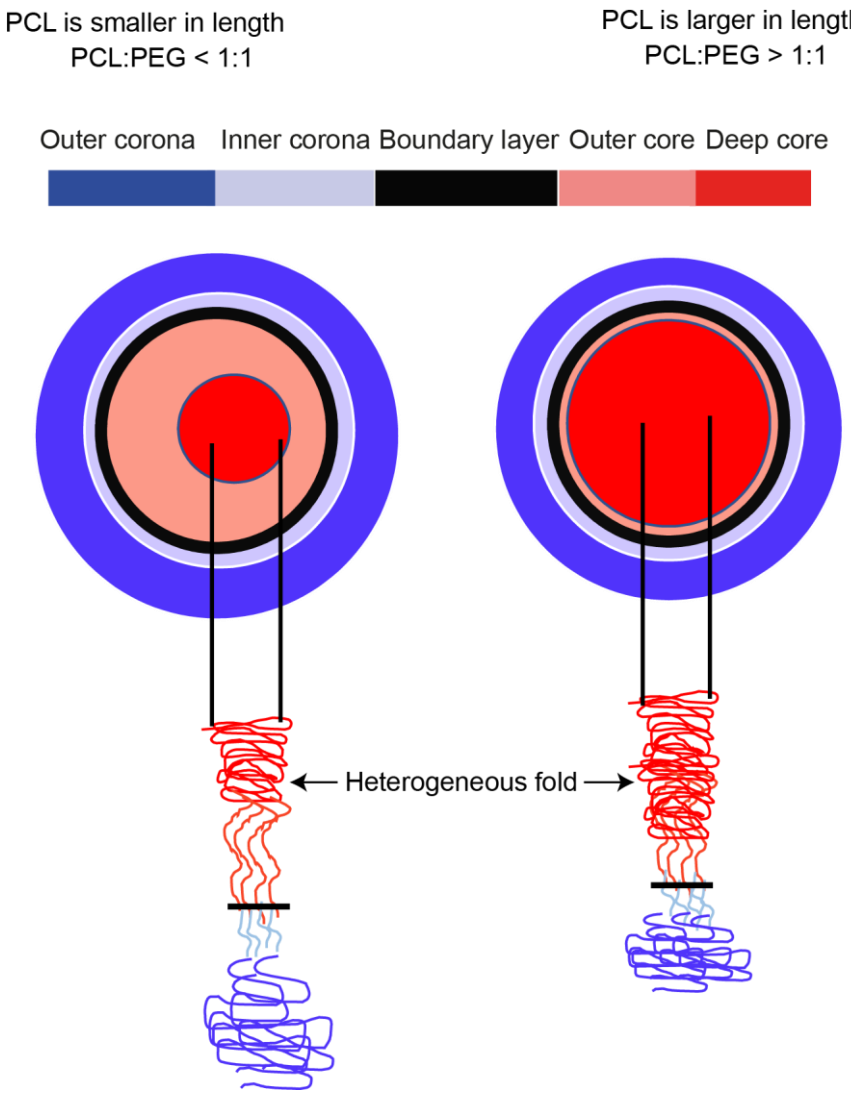


Figure 4.20: Illustration showing the proposed structure of PCL in the aggregate core with different PCL lengths (PCL:PEG ratio).

Glover *et al.* conducted DSC on polymeric aggregate solutions prepared from PEG_2PCL_2 and PEG_2PCL_5 copolymers and observed bimodal melting peaks at ~ 37 and 51 °C, which is very similar to the results observed in this study.[26] Importantly, as the PEG block remains hydrated in the aggregate corona they concluded that the melting peaks must originate from different PCL crystallites in the core.[26] WXRD was also conducted on the lyophilised aggregate powder, but no characteristic peaks for either the PEG or PCL blocks were detected, which may be due to peak broadening effects due to the small crystallite size, or the sensitivity of the instrument.[30]

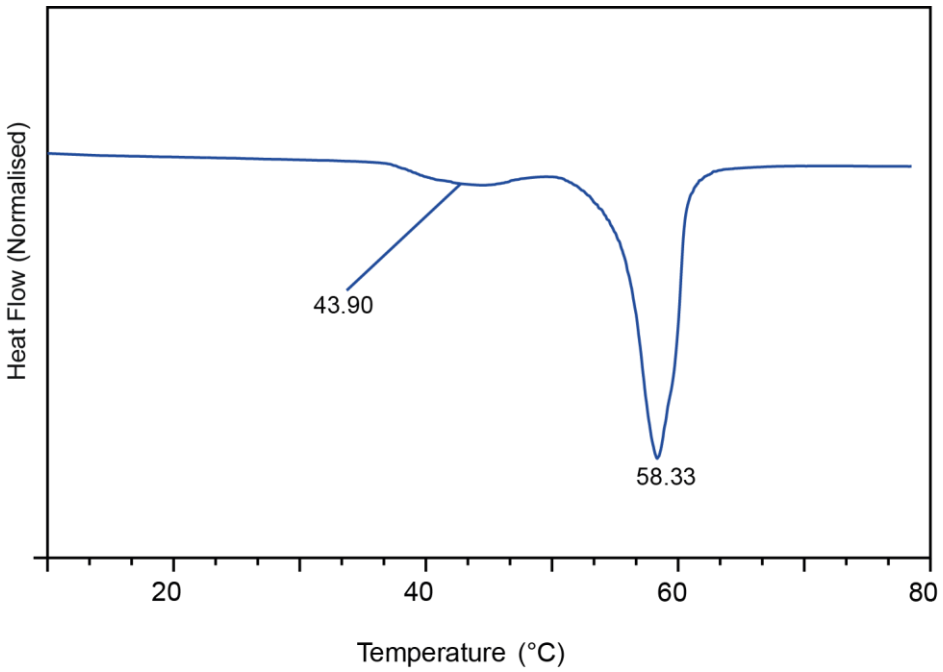


Figure 4.21: DSC thermogram of the $PEG_{10}PCL_{2.5}$ copolymer micelle showing the first heating profile (ramp rate 10 ^{o}C/min).

In both the PEG_2PCL_y and PEG_5PCL_y copolymer aggregates powders, only a single melting peak was observed in the DSC thermograms when the PCL:PEG ratio was < 0.5:1. It can be concluded polymers might not aggregate in a phase-separated system where PEG and PCL are confined in core and corona; therefore, the thermal behaviour is similar to the precipitated polymer before aggregation. The PGSTE NMR studies (refer to Chapter 3), it was concluded that these polymers do not form stable aggregate systems (polydisperse system). At a PCL:PEG ratio of 0.5:1, two melting peaks are observed for the $PEG_5PCL_{2.3}$ micelles at ~ 41 and 52 °C, whereas the $PEG_2PCL_{1.1}$ micelles show a broad bimodal melting peak (**Figure 4.19**). As the ratio increases further to 1:1, the $PEG_5PCL_{2.3}$ micelles also display two melting peaks at ~ 44 and 51 °C. At a PCL:PEG ratio of 2:1, the $PEG_5PCL_{9.4}$ micelle shows two melting peaks at ~ 51 and 56 °C, whereas the $PEG_2PCL_{3.9}$ aggregates show melting peaks at ~ 42 and 52 °C. It is hypothesised that the changes observed in the T_m relate to the different conformations of PCL in the core (nature of folding and lamellar thickness). As the PCL length increases, there is more to accommodate in the core.

In **Chapter 3** SAXS data reveals aggregate size did not changes across the polymer series despite the increase in molecular weight. It can be hypothesised that the PCL in the core of the PEG_2PCL_y aggregate will be more extended (elongated), whereas the PCL in the core of the PEG_5PCL_y aggregate is folded and more compact to occupy the same volume of the core. The folding of the polymer chains produces more stable crystals, which results in increased melting temperatures, and correlates with an increase in molecular weight.[12]This hypothesis fits with the DSC results for copolymers having similar PCL length; $PEG_5PCL_{2.3}$ shows a higher intensity melting peak at 52 °C, and a lower intensity melting peak at 41 °C, whereas $PEG_2PCL_{1.8}$ shows the opposite behaviour (**Figure 4.19**).

Xu *et. al* investigated the microstructure effect of poly(oxyethylene-*b*-oxybutylene) block copolymer aggregate formed in hexane, whereby the poly(oxyethylene) (POE) forms the core and poly(oxybutylene) (POB) forms the corona. SAXS analysis of these micelles revealed that when the POE is short (POE:POB ratio is low), the POE in the core adopts a more stretched conformation. As the POE length increases, it retains a more compact folded structure.[27] These reports support our hypothesis that PCL in the micelle core might have a different folding pattern. However, this hypothesis cannot be confirmed without further experimentation, such as SAXS of the lyophilised aggregate, as the melting points at higher temperature could result from PEG, which has crystallised during processing (i.e., lyophilisation). Nevertheless, the DSC results for the lyophilised aggregate powders indicate that aggregation significantly affects the thermal properties of the copolymers compared to their non-aggregated form.

4.2 Conclusion

In this chapter, the morphology and thermal behaviour of PEG-*b*-PCL block copolymers were analysed, and it was determined that the microstructure of the polymer regulates these properties. The depression in the T_m of the block copolymers (≈10 °C) compared to their PEG homopolymer counterparts, was a familiar pattern observed in all of the polymer series. The crystallisation temperatures of the copolymers, as well as corresponding enthalpy change, when compared to the PEG and PCL homopolymers, indicates that covalent tethering of the blocks leads to imperfect crystallisation of both blocks. The PCL:PEG ratio mainly controls the thermal behaviour as evidenced by the depression of T_m and T_c increasing as the PCL:PEG ratio increases. These changes could be attributed to imperfect crystallisation of both PEG and PCL blocks as a result of competition during the crystallisation process (i.e. the order of crystallisation). In previously published studies it has been concluded that the order of crystallisation is dominated by the PCL block length; however, this study has revealed that the order of crystallisation is not dependent on a particular block. For example, for the $PEG_5PCL_{9.4}$ copolymer, crystallisation is dominated by the PCL block, whereas for the $PEG_{10}PCL_{10.7}$ copolymer, crystallisation is dominated by the PEG block. Thus, as PEG is generally more crystalline in nature relative to PCL, at a critical PEG molecular weight, it begins to dominate crystallisation in the copolymers. Therefore, it can be concluded that the PCL:PEG ratio plays a vital role in controlling the thermal characteristics of the block copolymers. In this chapter, the effect of self-assembly on the thermal behaviour of the block copolymers was also investigated. In the lyophilised polymer aggregate that represents a physically nanophase separated system, the appearance of melting peaks in the DSC thermograms indicates that the polymer aggregate core are in crystalised state, . Furthermore, in some cases double melting peaks were observed (e.g., $PEG_5PCL_{2.3}$), indicating different folding and lamellar thicknesses of the polymer crystallites in the core. Thus, PCL appears to crystallise in the core of the micelles in different patterns (fold number, heterogenous fold). However, this cannot be concluded without further investigation of the aggregate core structure. Nevertheless, the results demonstrate that relative to copolymers isolated via precipitation, aggregation provides a unique approach to manipulate the polymer morphology and thermal behaviour of copolymers.

4.3 Experimental

4.3.1 Synthesis and characterisation of PEG-*b*-PCL copolymers

The PEG-*b*-PCL copolymers synthesis and characterisation was described in details in **Chapter 2**.

4.3.2 Preparation of PEG-*b*-PCL copolymer aggregates and their lyophilisation

Micelles were prepared as described in **Chapter 3.** Lyophilisation of the polymer aggregate aqueous solution was conducted immediately after their synthesis. The solution was frozen at −80 ºC in a refrigerator for 1 h. The solution was then placed in a freeze dryer (Alpha 1-2 LDplus, Martin Christ GmbH Germany) at −20 ºC under vacuum for 72 h for complete removal of water. After 72 h vials were collected and stored in a desiccator for further analysis.

4.3.3 DSC analysis of PEG-*b*-PCL copolymers and polymer aggregate powders

A Discovery differential scanning calorimeter (DSC) from TA Instruments (Newcastle, USA) was used for determination and measurement of the thermal characteristic of the polymers. The polymers were precisely weighed into an aluminum pan and sealed with a lid. All the experiments were conducted under nitrogen (flow rate 50 mL/min) in order to prevent oxidative degradation. The polymer sample was first heated from −20 to 80 ºC with a ramp rate of 10 ºC/min, then cooled to −65 ºC (10 ºC/min). The sample heating and cooling cycle was then repeated for a second time.

4.3.4 WXRD analysis of PEG-*b*-PCL copolymers and aggregate powders

WXRD patterns were obtained using a MMA XRD diffractometer from Diffraction technology Ltd (Australia) with a CuKα radiation source. The samples were scanned through a range of 2θ angles in the angular range 15 to 25°, with a rate of 1° /min. The wavelength used was λ = 1.54060, with a voltage of 30.0 kV and current of 30.0 mA. Temperature-dependent WXRD patterns were recorded by placing the polymer sample on a temperature-controlled stage at 25 ºC, and the initial diffraction pattern was recorded.

The sample was then heated to 80 ºC, and the molten state diffraction pattern was recorded. Subsequently, the sample was cooled down at a rate of 10 ºC/min to the T_c and diffraction pattern was recorded once again.

4.4 References

1. Paclitaxel-loaded Pluronic P123/F127 mixed polymeric micelles: formulation, optimization and in vitro characterisation. *Int. J. Pharm.* **2009**, *376* (1-2), 176.

2. Adak, T.; Kumar, J.; Shakil, N. A.; Walia, S., Development of controlled release formulations of imidacloprid employing novel nano-ranged amphiphilic polymers. *J. Environ. Sci. Health B* **2012**, *47* (3), 217-25.

3. Cai, M.; Cao, J.; Wu, Z.; Cheng, F.; Chen, Y.; Luo, X., In vitro and in vivo anti-tumor efficiency comparison of phosphorylcholine micelles with PEG micelles. *Colloids Surf. B* **2017**, *157*, 268-279.

4. Gohy, J.-F., Block Copolymer Micelles. In *Block Copolymers II*, Abetz, V., Ed. Springer Berlin Heidelberg: Berlin, Heidelberg, 2005; pp 65-136.

5. Gong, J.; Chen, M.; Zheng, Y.; Wang, S.; Wang, Y., Polymeric micelles drug delivery system in oncology. *J Control. Release* **2012**, *159* (3), 312-323.

6. Gou, M.; Zheng, X.; Men, K.; Zhang, J.; Wang, B.; Lv, L.; Wang, X.; Zhao, Y.; Luo, F.; Chen, L.; Zhao, X.; Wei, Y.; Qian, Z., Self-Assembled hydrophobic Honokiol loaded MPEG-PCL diblock copolymer micelles. *Pharm. Res.* **2009**, *26* (9), 2164-2173.

7. Glavas, L.; Olsén, P.; Odelius, K.; Albertsson, A.-C., Achieving micelle control through core crystallinity. *Biomacromolecules* **2013**, *14* (11), 4150-4156.

8. Majumdar, R.; Alexander, K. S.; Riga, A. T., Physical characterisation of polyethylene glycols by thermal analytical technique and the effect of humidity and molecular weight. *Pharmazie* **2010**, *65* (5), 343-7.

9. Sánchez-Soto, P. J.; Ginés, J. M.; Arias, M. J.; Novák, C.; Ruiz-Conde, A., Effect of molecular mass on the melting temperature, enthalpy and entropy of hydroxy-terminated PEO. *J. Therm. Anal. Calorim.* **2002**, *67* (1), 189-197.

10. Pielichowski, K.; Flejtuch, K., Differential scanning calorimetry studies on poly(ethylene glycol) with different molecular weights for thermal energy storage materials. *Polym. Adv. Technol* **2002**, *13* (10-12), 690-696.

11. Eldridge, J. E., Effect of the thermal history of polymers on their dynamic mechanical properties. *J. Appl. Polym. Sci.* **1967**, *11* (7), 1199-1207.

12. Kawai, T., Melting points of polyethylene crystals and the relation between molecular length and chain folding. *Kolloid-Zeitschrift und Zeitschrift für Polymere* **1965**, *201* (1), 15-20.

13. An, J. H.; Kim, H. S.; Chung, D. J.; Lee, D. S.; Kim, S., Thermal behaviour of poly(ε-caprolactone)-poly(ethyleneglycol)-poly(ε-caprolactone) tri-block copolymers. *J. Mater. Sci.* **2001**, *36* (3), 715-722.

14. Lemstra, P. J.; Kooistra, T.; Challa, G., Melting behavior of isotactic polystyrene. *J Polym. Sci. Pol. Phys.* **1972**, *10* (5), 823-833.

15. Holdsworth, P. J.; Turner-Jones, A., The melting behaviour of heat crystallised poly(ethylene terephthalate). *Polymer* **1971**, *12* (3), 195-208.

16. Wu, T.; Zhang, X.; Yang, G., Comparison of crystallisation behaviors of poly(ε-caprolactone) in confined environment with that in bulk. *J. Appl. Polym. Sci.* **2008**, *107* (6), 3796-3803.

17. Luo, C.; Chen, W.; Gao, Y., Fractional crystallisation behavior of PCL and PEG in blends. *Polym. Sci. Ser. A* **2016**, *58* (2), 196-205.

18. Douglas, P.; Albadarin, A. B.; Sajjia, M.; Mangwandi, C.; Kuhs, M.; Collins, M. N.; Walker, G. M., Effect of polyethylene glycol on the mechanical and thermal properties of bioactive poly(ε-caprolactone) melt extrudates for pharmaceutical applications. *Int. J. Pharm.* **2016**, *500* (1), 179-186.

19. Nojima, S.; Ono, M.; Ashida, T., Crystallisation of block copolymers II. Morphological study of poly(ethyleneglycol)-poly(ε-caprolactone) block copolymers. *Polym. J.* **1992**, *24*, 1271.

20. Cerrai, P.; Tricoli, M.; Andruzzi, F.; Paci, M.; Paci, M., Polyether-polyester block copolymers by non-catalysed polymerization of ε-caprolactone with poly(ethylene glycol). *Polymer* **1989**, *30* (2), 338-343.

21. Lauritzen, J. I.; Hoffman, J. D., Extension of theory of growth of chain-folded polymer crystals to large undercoolings. *J. Appl. Phy.* **1973**, *44* (10), 4340-4352.

22. Painter, P. C.; Coleman, M. M., Essentials of polymer science and engineering. DEStech Publications, Incorporated: 2008.

23. He, C.; Sun, J.; Deng, C.; Zhao, T.; Deng, M.; Chen, X.; Jing, X., Study of the synthesis, crystallisation, and morphology of poly(ethylene glycol)−poly(ε-caprolactone) diblock copolymers. *Biomacromolecules* **2004**, *5* (5), 2042-2047.

24. Hu, S.-R.; Kyu, T.; Stein, R. S., Characterisation and properties of polyethylene blends I. Linear low-density polyethylene with high-density polyethylene. *J. Polym Sci, Part B: Polym. Phys.* **1987**, *25* (1), 71-87.

25. Cheng, S. Z. D.; Chen, J.; Barley, J. S.; Zhang, A.; Habenschuss, A.; Zschack, P. R., Isothermal thickening and thinning processes in low molecular-weight poly(ethylene oxide) fractions crystallised from the melt. 3. molecular weight dependence. *Macromolecules* **1992**, *25* (5), 1453-1460.

26. Glover, A. L.; Nikles, S. M.; Nikles, J. A.; Brazel, C. S.; Nikles, D. E., Polymer micelles with crystalline cores for thermally triggered release. *Langmuir : the ACS journal of surfaces and colloids* **2012**, *28* (29), 10653-10660.

27. Xu, J.-T.; Fairclough, J. P. A.; Mai, S.-M.; Ryan, A. J., The effect of architecture on the morphology and crystallisation of oxyethylene/oxybutylene block copolymers from micelles in n-hexane. *J. Mater. Chem.* **2003**, *13* (11), 2740-2748.

28. Mihut, A. M.; Chiche, A.; Drechsler, M.; Schmalz, H.; Di Cola, E.; Krausch, G.; Ballauff, M., Crystallisation-induced switching of the morphology of poly(ethylene oxide)-block-polybutadiene micelles. *Soft Matter* **2009**, *5* (1), 208-213.

29. Reiter, G., Some unique features of polymer crystallisation. *Chem. Soc. Rev.* **2014**, *43* (7), 2055-2065.

30. Ooi, L., Principles of X-ray Crystallography. OUP Oxford: 2010.

Chapter 5

Application of NMR spectroscopy for studying the formation of drug-loaded aggregates from poly(ethylene glycol-*b*-caprolactone) copolymers

Chapter overview

Nanoscale polymeric DDSs prepared via the self-assembly of amphiphilic copolymers have significant advantages over conventional drug administration. These include high drug loading capacities, enhanced drug accumulation at the target site, improved solution concentrations, *in vivo* stability, prolonged blood circulation times, controlled and site-specific drug release, high cell penetration, and reduced systemic toxicity.[1] This chapter aimed to investigate the effect of copolymer microstructure and drug characteristics on the self-assembly process. The effect of drug characteristics on the self-assembly of amphiphilic block copolymers is not well explored or understood. In this chapter, PEG-*b*-PCL block copolymers were used to encapsulate two different drugs in polymeric aggregates; gossypol (hydrophobic; logP = 6.9) and phloretin (less hydrophobic; logP = 2.6). This provided information about the drug-polymer interactions and their effect on the self-assembly of PEG-*b*-PCL. For the first time, PGSTE NMR spectroscopy was used to investigate the diffusivity of the polymers in the drug-loaded aggregates. The PGSTE NMR data was then translated to provide a *D* distribution of PEG and PCL in aggregates present in core and corona, and insights into the mechanism of aggregate formation. In addition, analysis of the interaction between the aqueous phase and aggregate core was investigated using NMR spectroscopy.

5.1 Results and Discussion

5.1.1 Synthesis and characterisation of PEG-*b*-PCL copolymers

The synthesis and characterisation of PEG-*b*-PCL copolymers are outlined in detail in Chapter 2.

5.1.2 Synthesis of drug-loaded polymeric aggregates from PEG-*b*-PCL copolymers

Dialysis or solvent evaporation techniques commonly used to prepare drug-loaded polymeric aggregates.[2–4] The latter approach provided optimal drug loading and stability and was, therefore, the technique of choice in this study.[5] An aggregate solution free from sedimentation was the evidence of successful aggregation and drug encapsulation. However, it is difficult to remove all organic solvent from the solution. Therefore, an additional evaporation step was introduced by placing the aggregate solution under high vacuum to remove traces of organic solvent completely (as described in **Chapter 3**).

To prepare drug-loaded polymeric aggregates, the drug and polymer were dissolved completely in acetone, followed by the dropwise addition of an equal volume of D_2O. The acetone was then evaporated at 60 °C. Subsequently, the solution was placed under high vacuum (0.1 mbar) for 1 h, and then additional D_2O was added as required to ensure that the desired concentration of aggregates was produced. Initially, drug-loaded aggregates were synthesised using the PEG_5PCL_y copolymer series with PCL:PEG ratios of 0.1, 0.5:1, 1:1 and 2:1 to study the effect of copolymer structure on aggregate formation. Two drugs, gossypol (Gp) and phloretin (Ph), were separately loaded into the aggregates at 10 and 20 wt% of the total formulation, to allow the effect of the drug characteristics and loading to be studied. Gp loaded aggregate solutions were found to be yellow in colour due to the colour of Gp, whereas Ph loaded aggregates formed colourless solutions.

The drug-loaded aggregate solutions were then centrifuged to separate any free drug in the solution. The supernatant was carefully collected and used to analyse the aggregates, and any precipitated drug was then dissolved in ethanol to analyse loading efficiency (discussed in details in Section 5.3.4). The amount of un-encapsulated drug was quantified using UV-visible spectrophotometry using standard calibration curves for the drugs (**Table 5.1**).

Table 5:1: Drug loading efficiency of aggregates prepared using from the PEG_5PCL_y copolymers series.

Polymer	PCL:PEG ratio	Gp loading efficiency (%)		Ph loading efficiency (%)	
		10 wt% loading[a]	20 wt% loading[b]	10 wt% loading[a]	20 wt% loading[b]
$PEG_5PCL_{0.6}$	0.1:1	85.3 ± 1.2	86.1 ± 0.93	85.3 ± 2.2	88.5 ± 0.46
$PEG_5PCL_{2.3}$	0.5:1	93.6 ± 0.80	92.7 ± 0.54	96.4 ± 0.35	93.3 ± 0.54
$PEG_5PCL_{4.2}$	1:1	95.6 ± 0.04	95.8 ± 0.90	93.3 ± 0.01	93.5 ± 0.85
$PEG_5PCL_{9.4}$	2:1	92.6 ± 0.11	93.3 ± 0.35	95.8 ± 1.5	59.2 ± 11

[a] 10 wt% loading refers to the amount of drug being equal to 10wt% of the total aggregate formulation.
[b] 20 wt% loading refers to the amount of drug being equal to 20wt% of the total aggregate formulation.

For Gp-loaded aggregates, the drug loading efficiency did not significantly change with regards to polymer microstructure or the loading amount. For Ph-loaded aggregates at 10 wt% loading, the drug loading efficiency was ~ 90% for all of the copolymers. Similarly, this was also observed for a 20 wt% drug loading with the exception of the $PEG_5PCL_{9.4}$ copolymer, whereby a significant decrease was noted for Ph. Gp is hydrophobic and is expected to interact favourably with the large PCL block during aggregate formation. As a result, Gp is encapsulated in the aggregate core, and the drug loading efficacy is higher than for Ph. Relatively, Ph is more hydrophilic, and as a result, it interacts to a lesser extent with the large PCL block. Therefore, as Ph is not incorporated into the aggregate core and has poor water solubility, it aggregates and precipitates from solution.

5.1.3 Factors affecting the self-assembly behaviour of PEG-*b*-PCL copolymers in the presence of drugs

Self-assembly of polymer is a complex process regulated by different factors and their interplay with each other. For example, analysis of PGSTE NMR spectroscopy results (**Chapter 3**) indicated that as the PCL:PEG ratio and PEG molecular weight changed, so did the aggregate diffusivity of the aggregate and dispersity of the system. Therefore, it is anticipated that the presence of a small molecule drug during aggregation will increase the complexity of the existing model. To simplify the study of this complex system, three factors have been considered; the polymer microstructure, the physical characteristics of the drug, and the drug loading. The physical characteristics of the drug mainly imply its hydrophobic character in this case. In this study, Gp and Ph have been considered as model drugs, whereby Gp (logP = 6.9) is more hydrophobic than Ph (logP = 2.6) on the basis of their logP values.[6,7]

The amount of drug used (drug loading) during aggregate formation may also influence the self-assembly and drug encapsulation process. As in **Chapter 3**, the *D* value and its distribution were measured by PGSTE NMR spectroscopy and used to interrogate the effect of these factors on drug-loaded aggregate formation. The ^{1}H NMR spectra of drug-loaded solutions compared to blank aggregates revealed some interesting characteristics about the aggregate core (**Figure 5.1**).

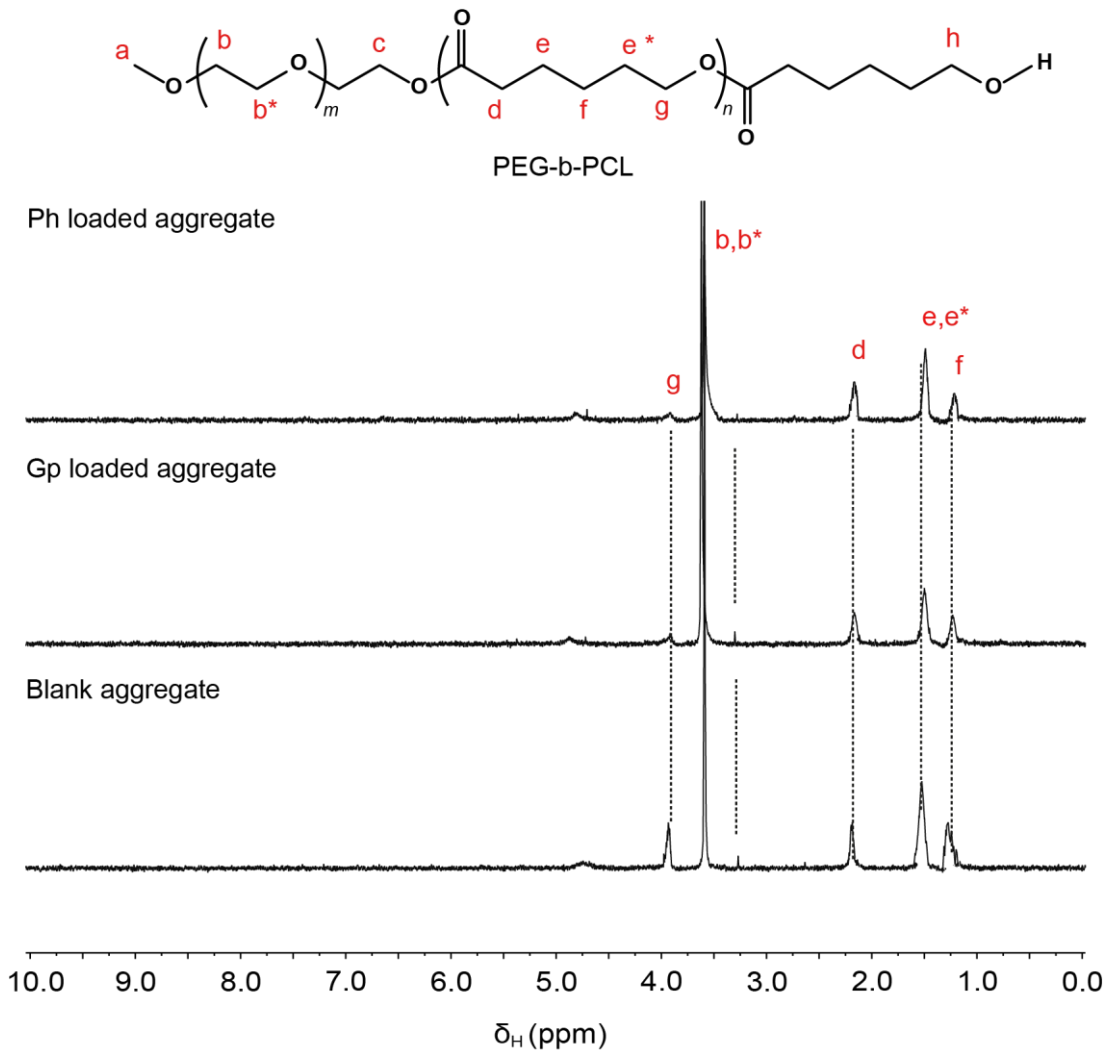


Figure 5.1: ^{1}H NMR spectra (D_2O, at 298 K) of blank and drug-loaded (10 wt%) aggregates prepared from the $PEG_5PCL_{9.4}$ copolymer at a concentration of 1 mg/mL. Characteristic peaks corresponding to the PCL block in the aggregates confirm NMR detection of a part of the aggregate core.

As observed previously (**Chapter 3**), the ^{1}H NMR spectra of the aggregates revealed characteristic resonances corresponding to the PEG and PCL blocks. The fact that PCL resonances can be observed indicates that water molecules can penetrate to some extent into the aggregate core. Therefore, it can be concluded there is a boundary layer or outer core that is partially hydrated. The characteristic proton resonances from the hydrophobic block of amphiphilic polymers prepared as aggregates have also been reported in previous studies,[4–9] which supports our hypothesis about aggregate structure presented in **Chapter 3**.

For the Ph-loaded aggregates (**Figure 5.1**), there are no characteristic Ph aromatic resonances at δ_H ~ 7 ppm visible in the spectrum (**Figure 5.2**). In the case of Gp, the characteristic methyl group resonances at 2.1 and 3.5 ppm (**Figure 5.3**) would overlap with resonances from the PCL block; however, Gp also has aromatic proton resonances at δ_H ~ 7 ppm, which are clearly absent in the aggregate spectrum (**Figure 5.1**). The fact that neither Ph or Gp characteristic signals are observed for the aggregate solutions also indicates that drugs are not present in the boundary layer or outer shell. This could be due to the solubility of the drug in water being below the NMR detection threshold and that the drug forms a cluster in the aggregate core in the presence of copolymers.

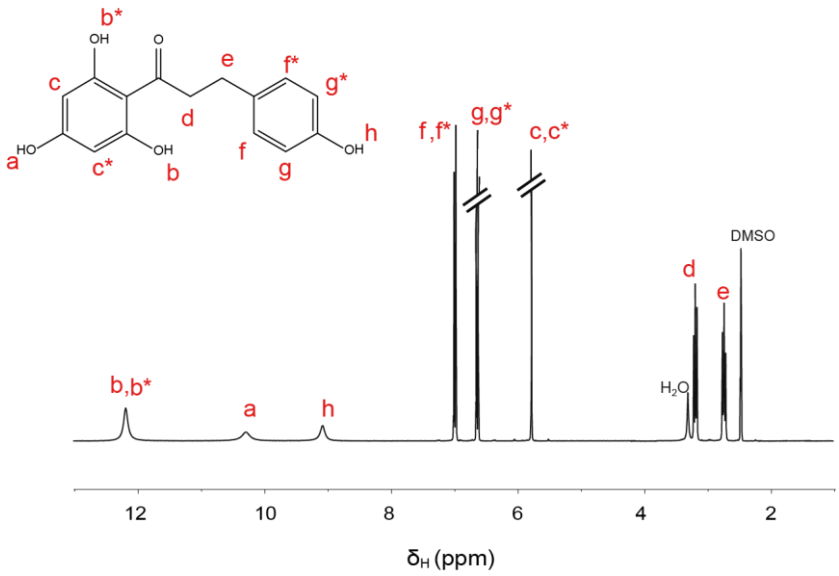


Figure 5.2: ^{1}H NMR spectrum (DMSO-d_6, at 298 K) of Ph.

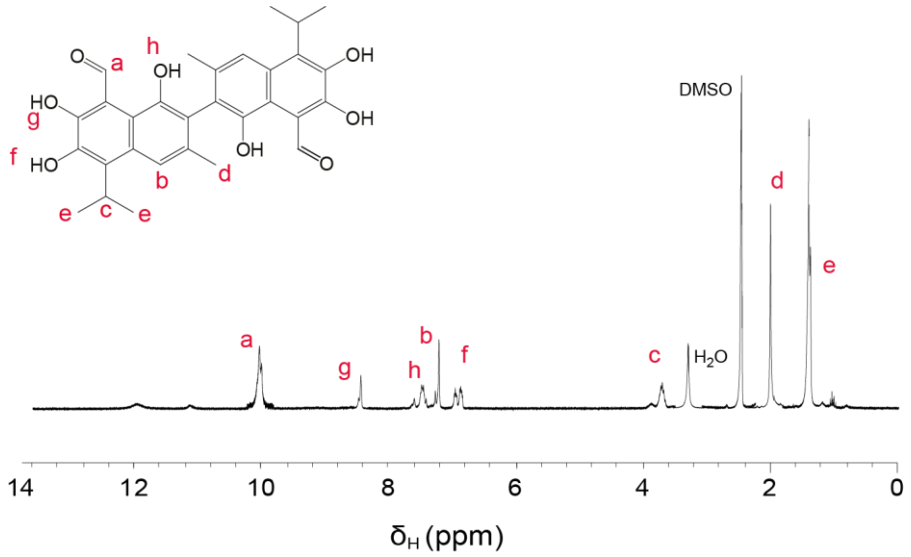


Figure 5.3: ^{1}H NMR spectrum (DMSO-d_6, at 298 K) of Gp.

In **Chapter 3**, an aggregate structure was hypothesised that consisted of five distinct regions (**Figure 5.4**): (i) the outer corona which is completely hydrated by the solvent; (ii) the inner corona which is well hydrated and adjacent to the boundary layer; (iii) the boundary layer, where the core and corona meet and is partially hydrated (the movement of polymer here is restricted); (iv) outer core which is adjacent to the boundary layer, and; (v) the deep core which is totally segregated from the solvent and the aqueous surroundings.

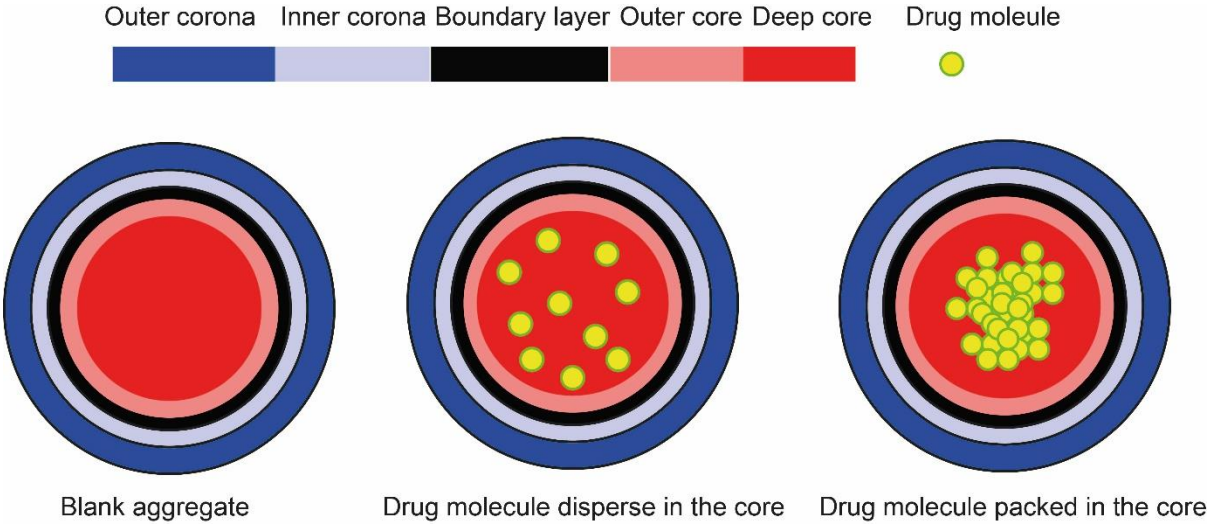


Figure 5.4: Illustration of possible drug distribution in the core of drug-loaded aggregates, showing two potential configurations whereby the drug is either molecularly dispersed within the polymer core, or forms a discretely packed mass within the core.

As discussed in **Chapter 3**, the analysis of the NMR signal decay profile in PGSTE NMR experiment can provide important information about the diffusivity of the polymers in the aggregate structure and indications of aggregates system dispersity and stability. In this chapter, the same protocol was used to conduct PGSTE experiments on drug-loaded aggregates as described in **Chapter 3**. A comparison between the signal decay profiles of the PEG resonance from the corona of the blank and drug-loaded aggregates prepared from different PEG-*b*-PCL copolymers was expected to provide information about how the drug loading changes the size of the aggregate (**Figure 5.5**).

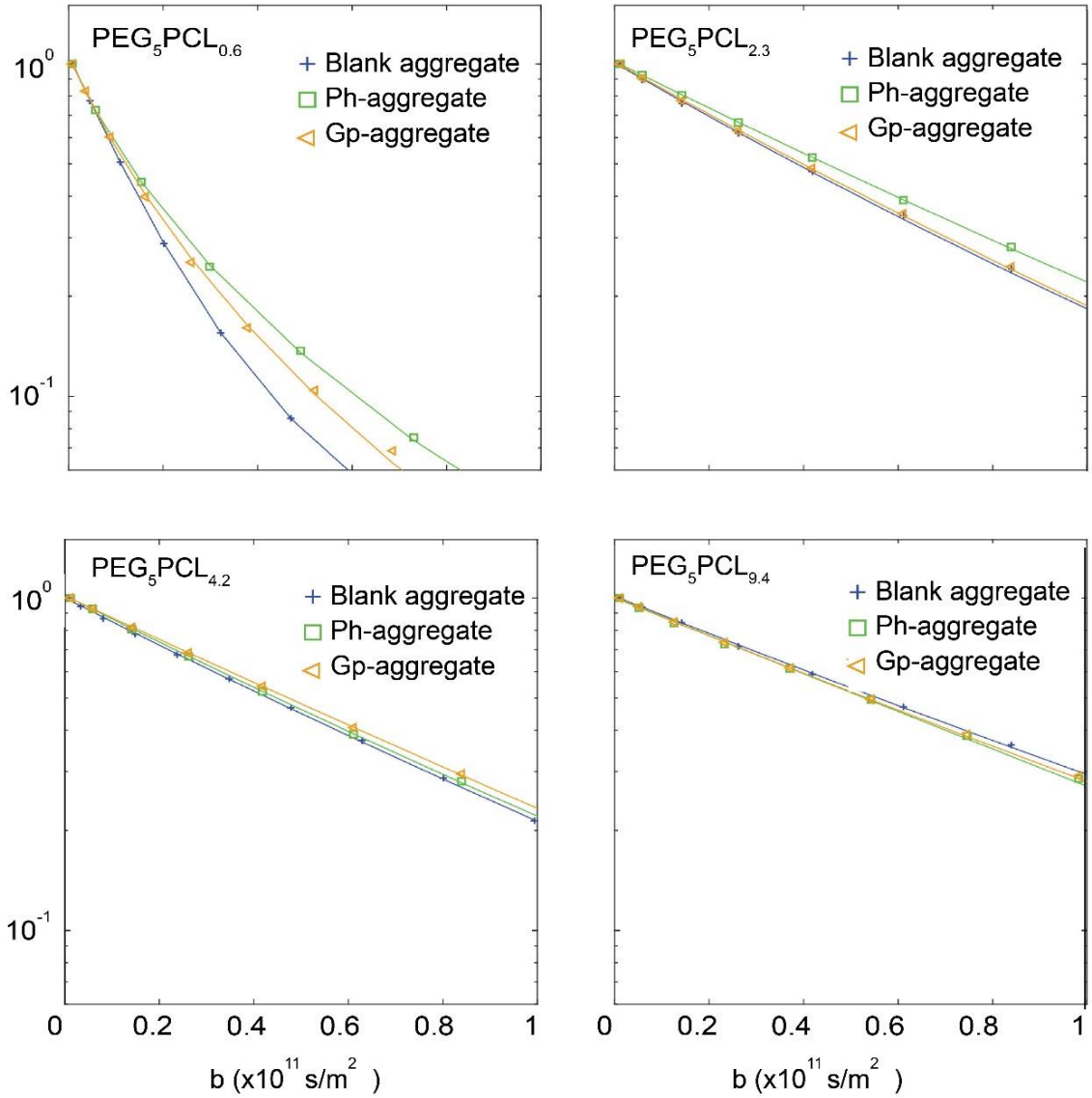


Figure 5.5: PGSTE NMR signal intensity decay profiles of the PEG methylene proton resonance of blank and drug-loaded aggregate synthesised from the PEG_5PCL_y copolymers series in D_2O (acquired at 25 ºC).

The effect of drug loading on the intensity decay profiles was found to be more prominent for copolymers with a lower PCL:PEG molecular weight ratio of 0.1:1 ($PEG_5PCL_{0.6}$) and 0.5:1 ($PEG_5PCL_{2.3}$) (**Figure 5.5**). In addition, the results indicate that the characteristics of the drug may also influence aggregate formation. For $PEG_5PCL_{0.6}$ (PCL:PEG 0.1:1) and $PEG_5PCL_{2.3}$ (PCL:PEG 0.5:1) the decay profiles show that the PEG signal in Ph-loaded aggregates decays more slowly compared to Gp-loaded and blank aggregates. Therefore, it can be assumed that the more hydrophilic Ph results in an increase in aggregate size, whereas the more hydrophobic Gp leads to smaller aggregates. Previous studies have also found that hydrophobic drugs contribute towards a more compact core, thus producing smaller sized aggregates.[10] For copolymers with higher PCL:PEG ratios, drug incorporation does not appear to significantly influence the decay profile as compared to blank aggregates (**Figure 5.5**). These results indicate that aggregate formation could involve a two-way interaction dependent on the polymer microstructure and characteristics of the drug.

The mechanism for drug incorporation/encapsulation in polymeric aggregates is not well defined. However, previous studies have suggested that polymer-drug compatibility controls aggregate formation in the presence of drugs.[11] Li *et al.* conducted a simulation study to understand the mechanism of drug loading in the aggregate core, and suggested that it depends on the interaction between the core forming block and the drug: initially the drug and polymer interact, which results in coaggregate formation, followed by aggregation**.**[11] However, this simulation does not provide information regarding the effect of the polymer microstructure (e.g. length of the blocks), and aggregate formation was pH trigged. A simulation study conducted by Woodhead *et al.* investigated drug-polymer interactions on aggregate formation.[27] In this study, two important factors were also considered: the polymer volume fraction (amount of polymer in the system) and packing fraction (density of the system). The system consists of three beads (as it is a simulation); solvent, solute, and polymer. The polymer volume fraction is the ratio between the number of polymer beads and the total number of beads (solute + solvent + polymer). In this simulation, the polymer volume fraction is constant. They concluded that five different aggregate systems could emerge in the presence of solute molecules (e.g. drugs) on the basis of the strength of the interaction between the hydrophobic block and solute molecules (**Figure 5.6**).[12]

The first scenario involves unimers in the presence of drug clusters (**Figure 5.6a**), which may occur when the packing fraction is high (high amount of solvent beads in the simulation) and drug-polymer interactions are low. This facilitates hydrophilic-hydrophilic interactions between the polymers and water, and thus the polymer remains in a unimer form, whereas the drug forms clusters as drug-solvent interaction are not favoured. In the second scenario, a reduction in the packing fraction leads to the aggregate formation as hydrophilic-hydrophilic interactions are reduced, but due to poor drug-polymer interactions, drugs form clusters (**Figure 5.6b**). In the third scenario, a further reduction in the system concentration leads to dispersion of the drug, but the dispersed solute is a nano-aggregate of solute. (**Figure 5.6c**).[12] An increase in drug-polymer interactions leads to a fourth scenario whereby the aggregates begin to encapsulate the drug (**Figure 5.6d**). When the drug-polymer interaction crosses a threshold level, then aggregates are formed with encapsulated and dispersed drugs in the core, which is the fifth scenario (**Figure 5.6e**). This behaviour can also be represented on a phase diagram of system concentration versus drug-polymer interaction (**Figure 5.7**).[12]

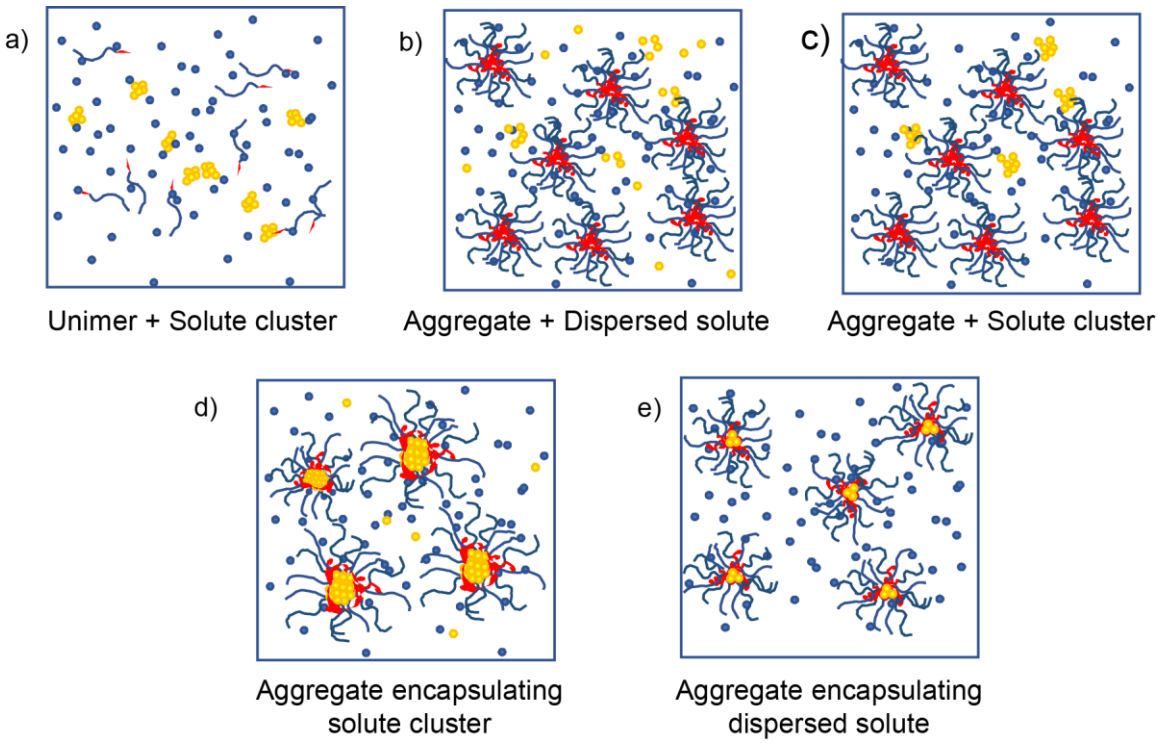


Figure 5.6: Illustration of different types of drug-aggregate systems adapted from Woodhead *et al.*[27] Hydrophobic and hydrophilic blocks are shown in red and blue, respectively, whereas drug molecules are yellow and blue dots represent water molecules.

In **Chapter 3**, the $PEG_5PCL_{0.6}$ copolymer was shown to form loose molecular aggregates (gel-like network, SAXS analysis), whereas the slower decay profiles for the PEG signal of the drug-loaded aggregates would imply that larger aggregates are formed. As the PCL block is very short in the $PEG_5PCL_{0.6}$ copolymer, drug-polymer interactions may initially be unfavourable compared to drug-drug interactions, leading to the formation of drug clusters that are subsequently stabilised through interactions with the polymer resulting in a scenario akin to the aggregate + solute clusters in the simulation (**Figure 5.7**).

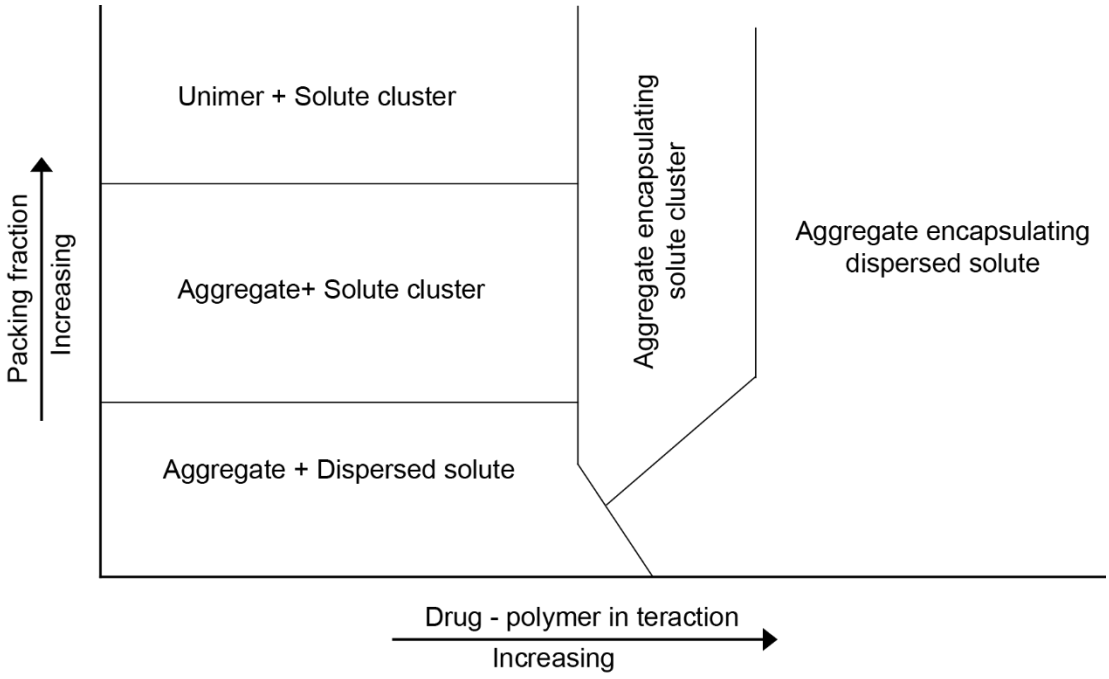


Figure 5.7: Phase behaviour of solute (e.g. drug)-copolymer-solvent system adapted from Woodhead *et al.*[27] The packing fraction is the total amount of solvent, solute and polymer divided by the volume of the simulation block; in this study solute and polymer amount is constant. A constant polymer amount was used in the simulations, and therefore, the polymer concentration decreases as the packing fraction increases.

Calculation of the mean D ($\langle D \rangle$) values for the drug-loaded aggregates prepared from the $PEG_5PCL_{0.6}$ copolymer revealed that the $\langle D \rangle$ for aggregates prepared with Ph was lower than those prepared with Gp (**Figure 5.8**), implying that Ph-loaded aggregates are larger in size. A possible explanation for this is that Ph is less hydrophobic than Gp, and therefore, the Ph clusters grow larger before they are stabilised through interactions with the polymer.

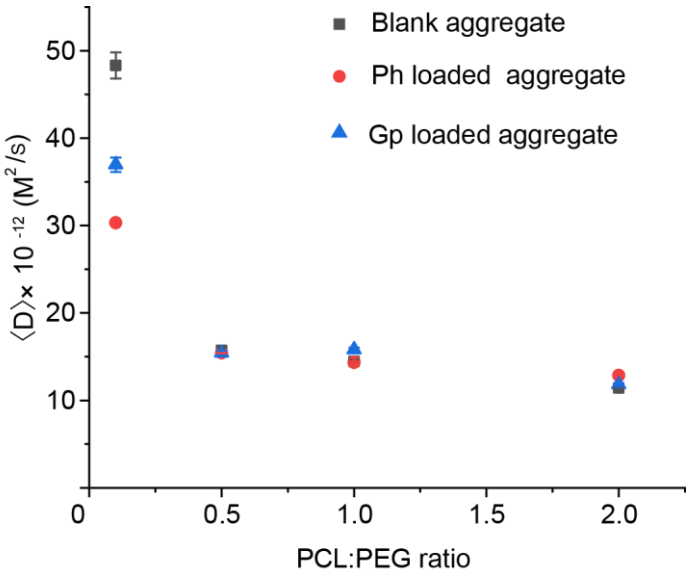


Figure 5.8: Mean (marker) and standard deviation (error bars) of $\langle D \rangle$ measured on three separate self-assembled samples for each PEG_5PCL_y copolymer, plotted against PCL:PEG molecular weight ratio. The black square, red circle and blue triangle symbols correspond to the blank, phloretin and gossypol loaded aggregate, respectively.

The PEG_5PCL_y copolymers with PCL:PEG molecular weight ratios > 1:1 were found to form drug-loaded aggregates with very similar $\langle D \rangle$ values to their respective blank aggregates (**Figure 5.8**), indicating a constant aggregate size. Furthermore, the nature of the drug did not appear to impact the $\langle D \rangle$. Hence, when PCL is longer in length (PCL:PEG ratio increased), the formation of drug-loaded aggregates appears to be controlled by the polymer structure. Therefore, the mechanism of drug loading changes depending on the PCL to PEG molecular weight ratio. At lower ratios, it appears to be drug-dependent, and at higher ratios, it appears to be polymer controlled.

In the absence of drugs, thermodynamic models predict that self-assembly of amphiphilic block copolymers will affect the conformation of blocks (relative to their solvated state),[45] which was shown by the PGSTE NMR experiments conducted in **Chapter 3**. However, when drugs are present, it is not known what further effect they will have on the conformation of the blocks. The D distribution was determined for both components in the blank, and drug-loaded aggregates synthesised from the PEG_5PCL_y copolymer series provide information about the stability and dispersity of the drug-loaded aggregate system (**Figure 5.9** and **Figure 5.11**).

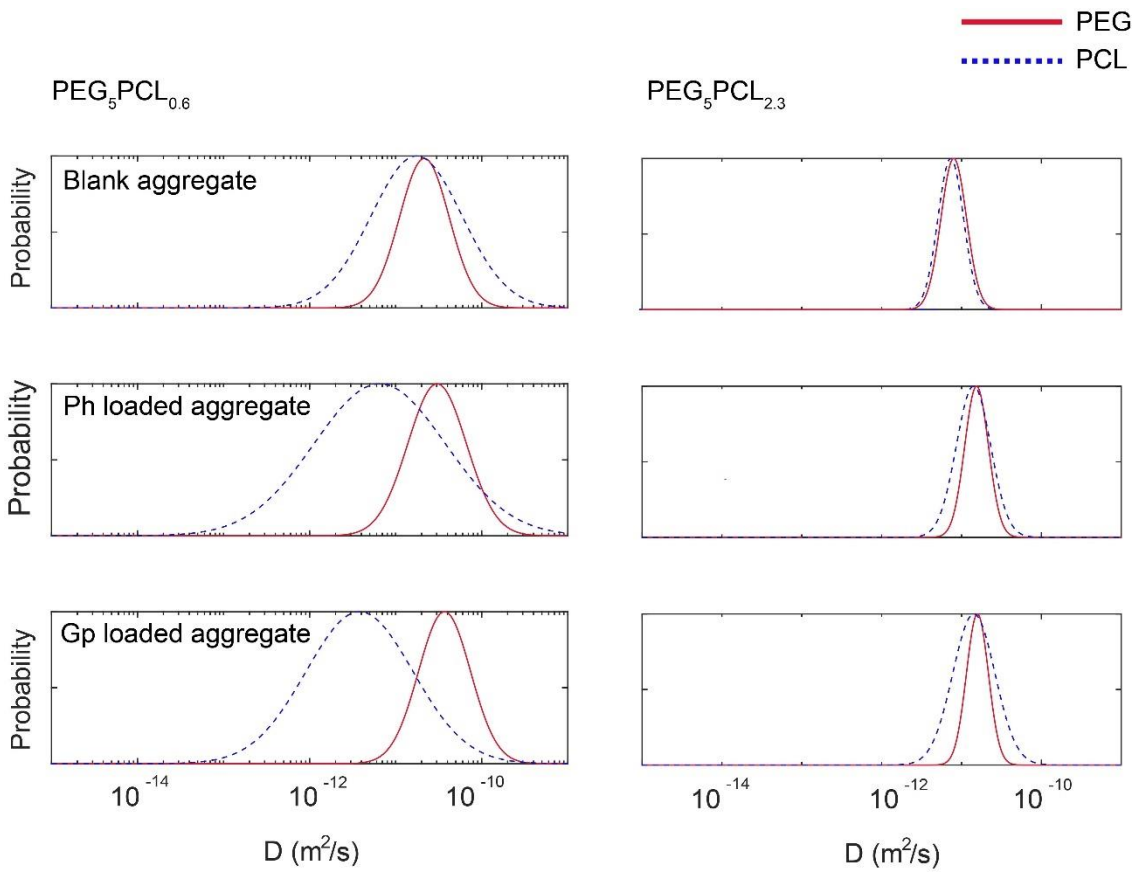


Figure 5.9: *D* distribution profile determined from PGSTE NMR diffusion of the blank and drug-loaded (10 wt%) self-assemblies, synthesised from $PEG_5PCL_{0.6}$ and $PEG_5PCL_{2.3}$ block copolymers.

For the blank $PEG_5PCL_{0.6}$ copolymer aggregate, the PEG and PCL components display broad *D* distribution aligned with one another. The SAXS analysis indicated that this might be a gel-like polymer network, where polymer aggregate interconnected with polymer chain (**Chapter 3**). However, in the presence of drugs, the PCL in the boundary layer becomes less diffusive as the distribution shifts towards a lower *D* value and broadens (**Figure 5.9**). This indicates that there might be an accumulation of drug on those polymer aggregate, which results in the PCL in a more compact and immobile state. Therefore, from the simulation the study conducted by Woohead *et al.*[12] and experimental data, it can be hypothesised that for the $PEG_5PCL_{0.6}$ copolymer, drug-polymer aggregates form to solubilise the drug, rather than discrete aggregate (i.e. a corona-core structure).

DLS analysis of the $PEG_5PCL_{0.6}$ copolymer without drug revealed multimodal distributions in the intensity and volume PSD, suggesting the presence of polydisperse aggregates. In the presence of the drugs, monomodal distributions were obtained. However, the size of the aggregates is unusually large. (**Figure 5.10**).

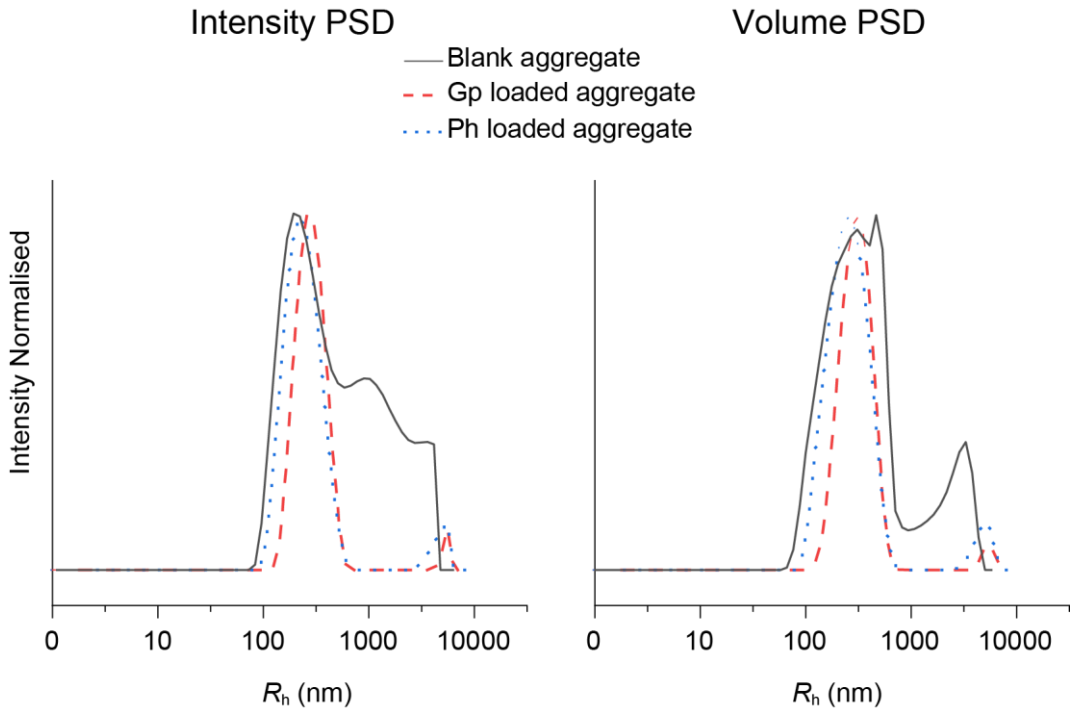


Figure 5.10: DLS analysis of blank and drug-loaded (10 wt%) aggregates showing intensity and volume particle size distributions (PSD), prepared using the $PEG_5PCL_{0.6}$ (PCL:PEG 0.1:1) copolymer.

As the molecular weight of the PCL block is increased (PCL:PEG 0.5:1, 1:1, 2:1) for the PEG_5PCL_y copolymer series, the interaction between PCL and drug is also expected to increase, which according to the simulation would lead to an aggregate encapsulating dispersed solute.[12] Examination of *D* distribution data for the $PEG_5PCL_{2.3}$, $PEG_5PCL_{4.2}$ and $PEG_5PCL_{9.4}$ aggregates with and without drugs revealed that the PEG and PCL *D* distributions become narrower and superimposed (**Figure 5.11**), indicating the formation of more defined aggregates, possibly as a result of a more controlled self-assembly process.

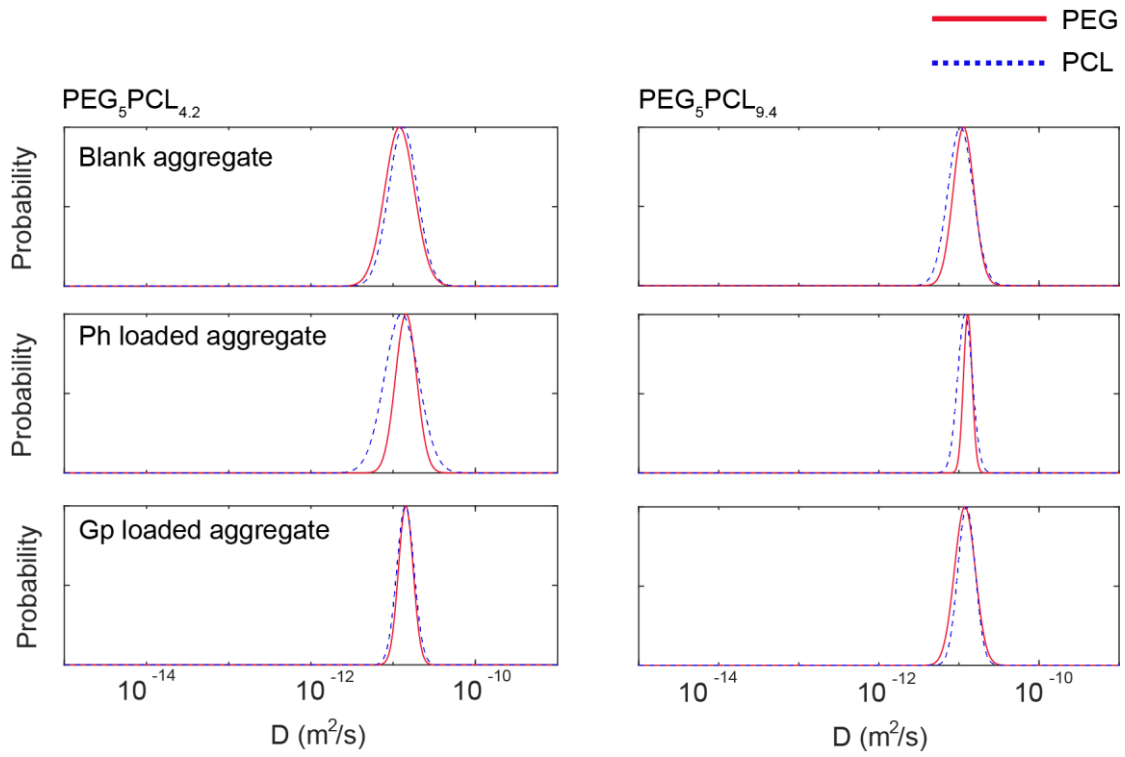


Figure 5.11: *D* distribution profile determined by PGSTE NMR diffusion spectroscopy of drug-loaded (10 wt%) aggregates synthesised from the $PEG_5PCL_{4.2}$ and $PEG_5PCL_{9.4}$ block copolymers.

As discussed previously, the main driving force behind aggregate formation is the deformation of the hydrophobic block into the aggregate core and the interfacial tension between the core and the aqueous environment.[13] The addition of a solute (e.g., drug) is expected to modify these parameters, with a hydrophobic solute increasing the interaction between the core-forming blocks. In thermodynamical terms, the drug increases the hydrophobic-hydrophobic interactions in the system; this facilitates aggregate formation by lowering the energy needed to transfer the hydrophobic polymer into the aggregate core and to increase the interfacial tension leading to higher aggregate stability.[14] Therefore, aggregate formation is favoured in the presence of hydrophobic drugs as compared to the copolymer alone, resulting in more stable and uniform aggregates with narrower *D* distributions (**Figure 5.11**).

DLS analysis also supports the trends observed in the PGSTE NMR diffusion studies, with narrow volume-based PSD for copolymers with larger molecular weight PCL blocks (**Figure 5.12**).

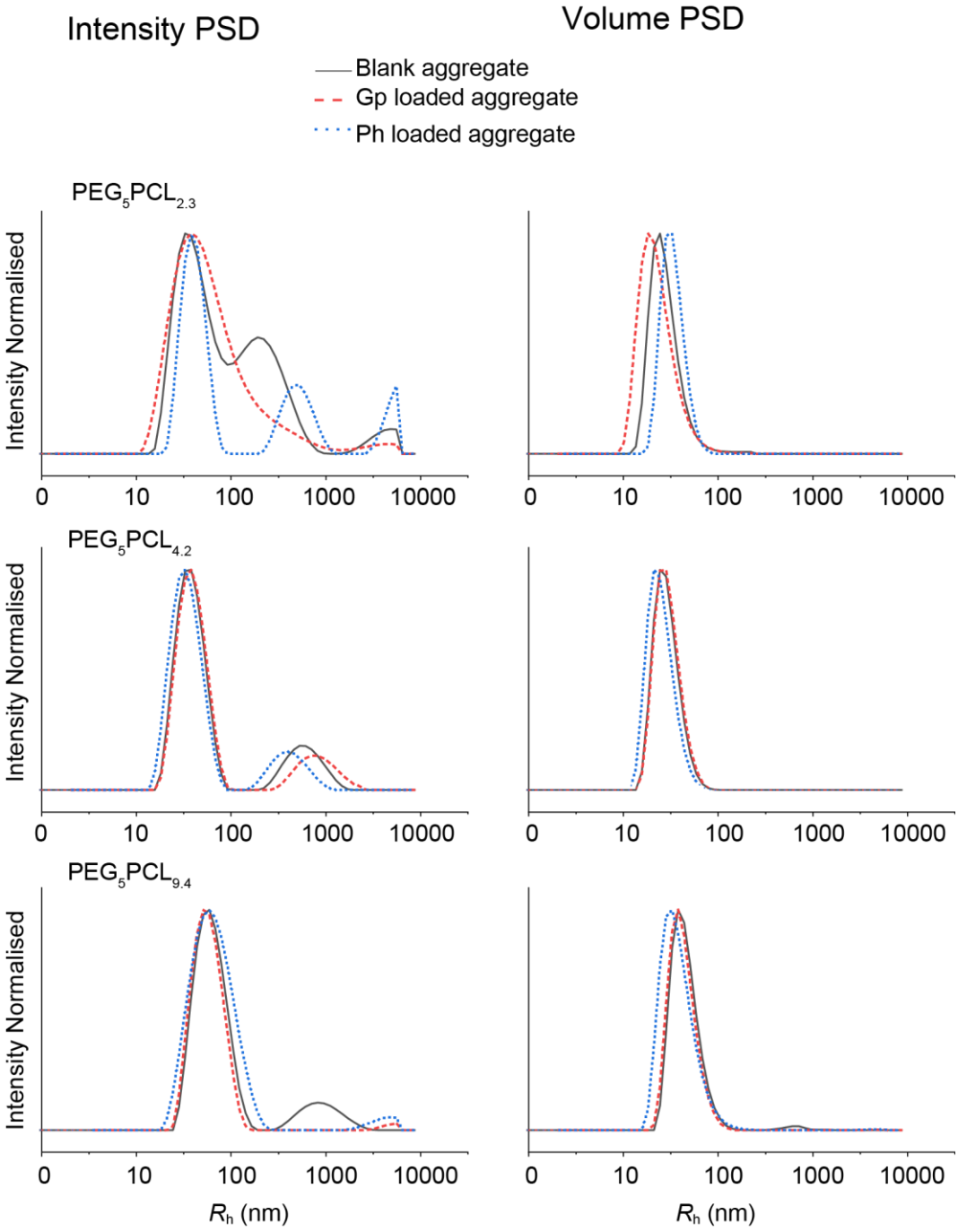


Figure 5.12: DLS analysis of blank and drug-loaded (10 wt%) aggregates showing intensity and volume PSD, prepared using the $PEG_5PCL_{2.3}$, $PEG_5PCL_{4.2}$, and $PEG_5PCL_{9.4}$ copolymers.

It should be noted that although the intensity PSD indicates the presence of larger particles, their absence from the volume PSD confirms that they are very small in number. The presence of small populations of large particles in aggregate solutions is a common phenomenon and is generally caused by the secondary aggregation to form loose aggregate clusters. The NMR spectroscopy and DLS results indicate that aggregate formation is limited by a threshold PCL:PCL molecular weight ratio, which explains the slight increase in aggregate size across the PEG_5PCL_y copolymer series.

Effect of drug loading on aggregate formation for the $PEG_2PCL_{0.4}$ copolymer

The PGSTE NMR experiments on the drug-loaded aggregates synthesised from the PEG_5PCL_y copolymers series can provide guidance to predict the behaviour of other copolymers. For instance, at a low PCL molecular weight, the aggregation will be dominated by the drug, whereas increasing PCL molecular weight will lead to an increasingly polymer driven self-assembly. Drug-loaded aggregates were synthesised from $PEG_2PCL_{0.4}$ (PCL:PEG 0.25:1) and analysed via PGSTE NMR diffusion spectroscopy to obtain the *D* distribution of PEG and PCL to test this hypothesis. (**Figure 5.13**).

Interestingly, the *D* distribution for the PEG and PCL components was found to change significantly when the drug was introduced drug into the system; however, the change was different to that previously noted for the $PEG_5PCL_{0.6}$ copolymer aggregates. In the absence of drugs, the $PEG_2PCL_{0.4}$ block copolymer remains as a unimer in solution (**Chapter 3**). In the presence of drugs, the *D* distribution of PEG was very similar to the PEG_2 homopolymer. Therefore, the $PEG_2PCL_{0.4}$ (PCL:PEG 0.25:1) copolymer may form a unimer+drug cluster system (**Figure 5.6a**). The deviation in the *D* distribution of PCL relative to the PEG signal may result from PCL interactions with the solvent, drug and itself, which generates different environments with different diffusivities. It can also be predicted based on the SAXS and PGSTE NMR data of $PEG_5PCL_{0.6}$ copolymer blank aggregates that in the presence of drug $PEG_2PCL_{0.4}$ polymer might exhibit a gel-like morphology. In this system, the drug cluster act as the nucleus to form drug-polymer aggregate, which might be interconnected by the polymer. This support previous prediction that at lower PCL:PEG ratio aggregation formation is regulated by the drug.

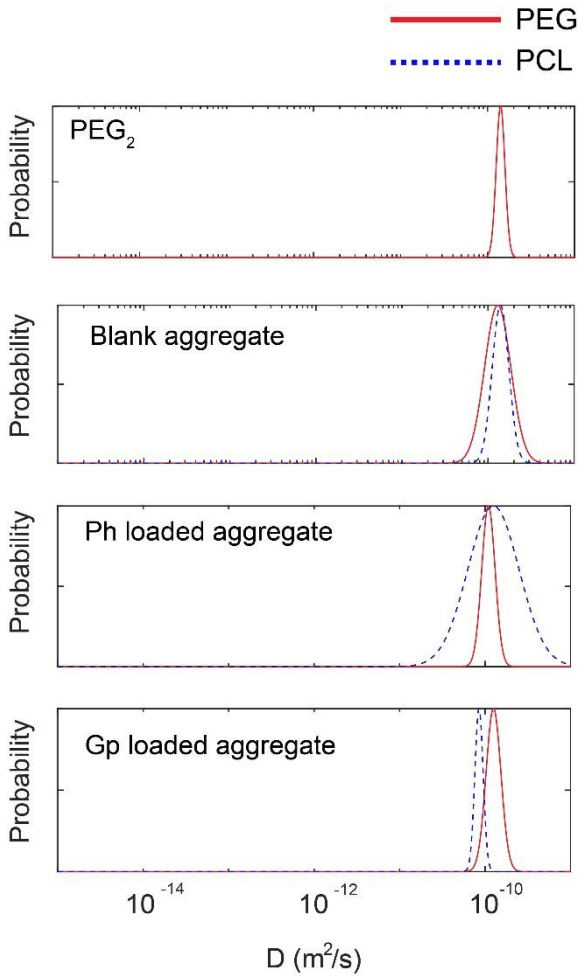


Figure 5.13: *D* distribution profile determined by PGSTE NMR diffusion studies of the PEG_2 homopolymer, and blank and drug-loaded aggregates prepared using the $PEG_2PCL_{0.4}$ copolymer.

Effect of drugs on aggregate formation from the $PEG_{10}PCL_{10.7}$ copolymer

Drug-loaded aggregates were also prepared using the $PEG_{10}PCL_{10.7}$ (PCL:PEG 1:1) copolymer and analysed via PGSTE NMR spectroscopy to obtain the *D* distribution of PEG and PCL (**Figure 5.14**). The blank and drug-loaded aggregates displayed narrow and nearly identical *D* distribution for both the PEG and PCL components, indicating that the drug does not affect the aggregate formation and that formation is most likely driven and controlled by the polymer, which is the same at that observed for the PEG_5PCL_y copoplymers series at higher PCL molecular weights. DLS analysis also revealed monomodal and narrow volume PSDs consistent with the PGSTE NMR diffusion spectroscopy results and indicative of uniform aggregates (**Figure 5.15**).

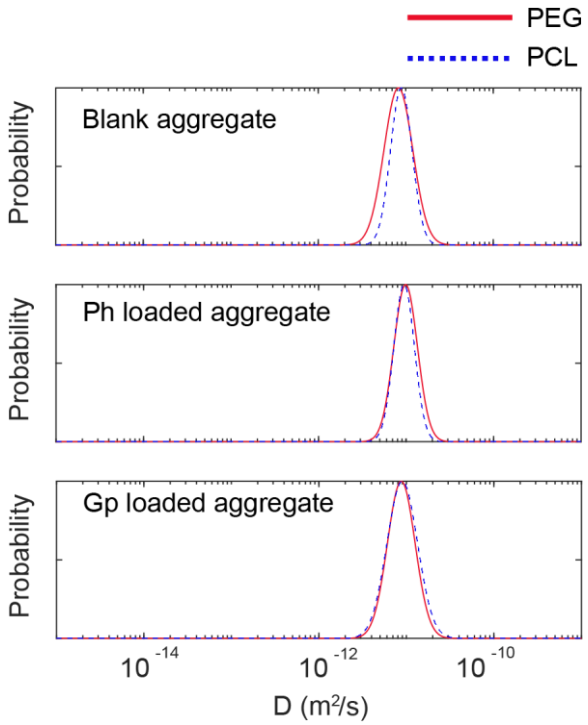


Figure 5.14: *D* distribution profile determined by PGSTE NMR diffusion studies of drug-loaded aggregates (10 wt%) prepared using the $PEG_{10}PCL_{10.7}$ copolymer.

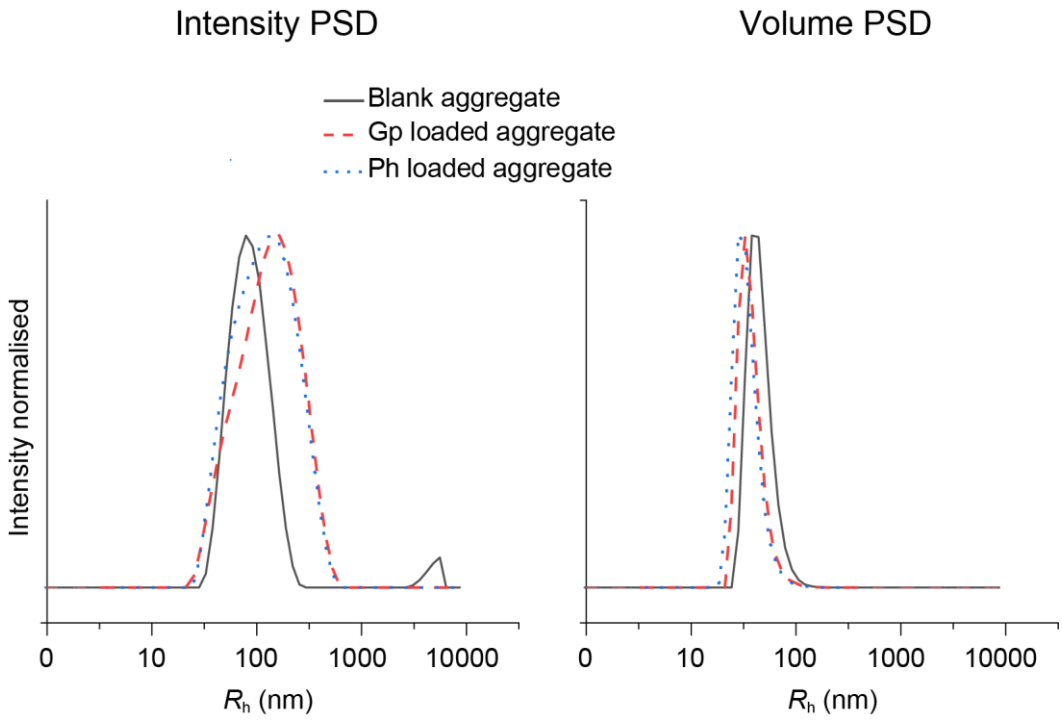


Figure 5.15: DLS analysis of blank and drug-loaded aggregates (10 wt%) showing intensity and volume PSD, prepared using the $PEG_{10}PCL_{10.7}$ (PCL:PEG 1:1) copolymer.

Effect of drug loading on aggregate formation

As discussed previously, drug-loaded aggregates were prepared from the PEG_5PCL_y copolymers series with Gp and Ph loadings of 10 and 20 wt%. The encapsulation efficiency at a loading of 20 wt% was found to be very similar to that at 10 wt% for all copolymers, with the exception of Ph and the $PEG_5PCL_{9.4}$ copolymer (**Table 5.1**). Therefore, the effect of drug-loading on aggregate formation and structure was investigated for the $PEG_5PCL_{9.4}$ copolymer using ^{1}H NMR spectroscopy and PGSTE NMR spectroscopy. As with the 10 wt% drug-loaded aggregates, ^{1}H NMR spectra of the 20 wt% drug-loaded aggregates did not contain any signals from the drugs, however, the characteristic signals from the PCL component were also absent (**Figures 5.16**).

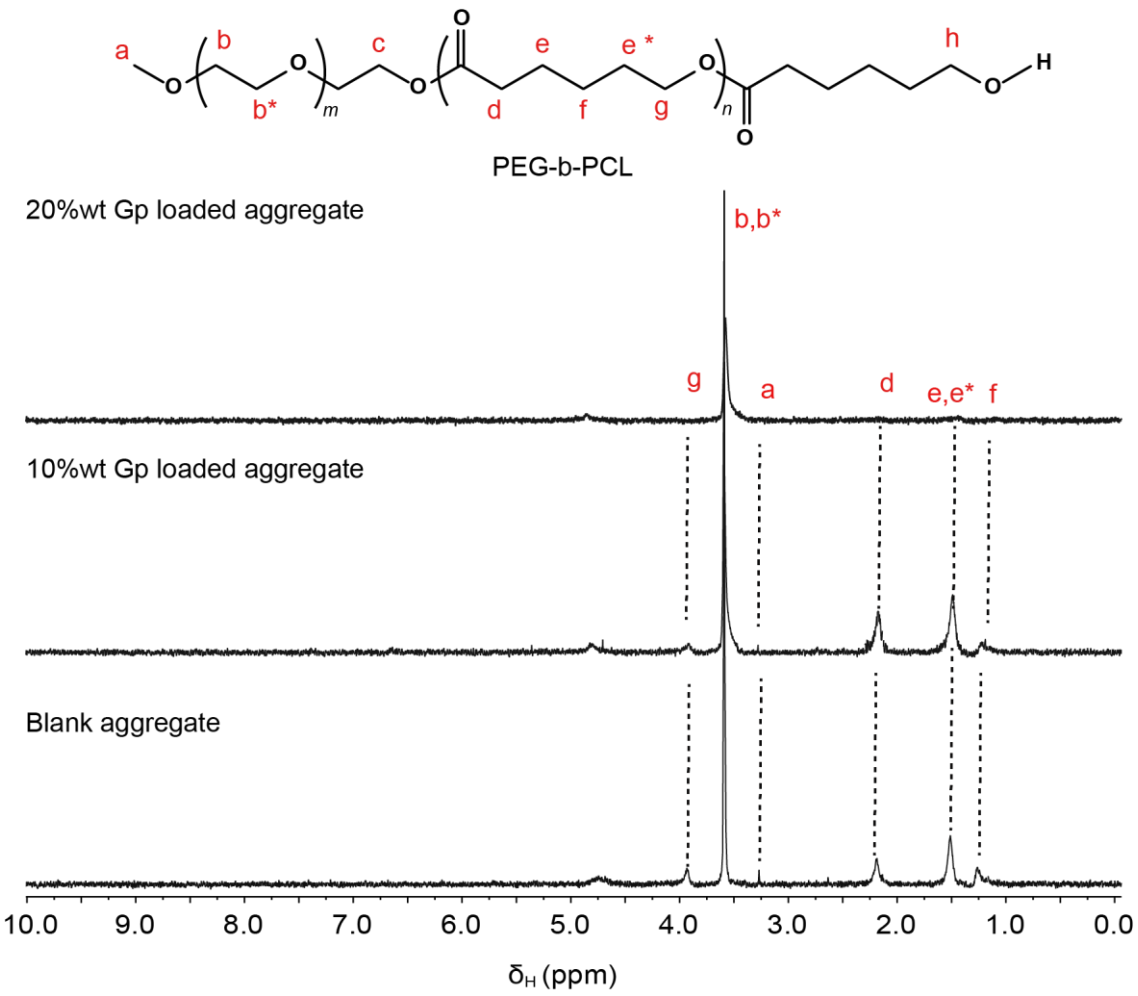


Figure 5.16: ^{1}H NMR spectra (D_2O, 298 K) of blank and Gp-loaded aggregates prepared from the $PEG_5PCL_{9.4}$ copolymer.

Previously it was postulated that the PCL signal observed in the ^{1}H NMR spectroscopy results originate from a boundary region between the PEG corona and PCL core. For blank aggregates, hydration of the boundary layer allows observation of the PCL signal, however, increasing the drug loading may also change the hydration state of the boundary layer, resulting in loss of the PCL signal (**Figure 5.17**). Another possible explanation is that the higher drug loadings might increase the drug-polymer interaction and reduce the boundary layer thickness as well as PCL mobility, causing a loss of PCL signal.[15]

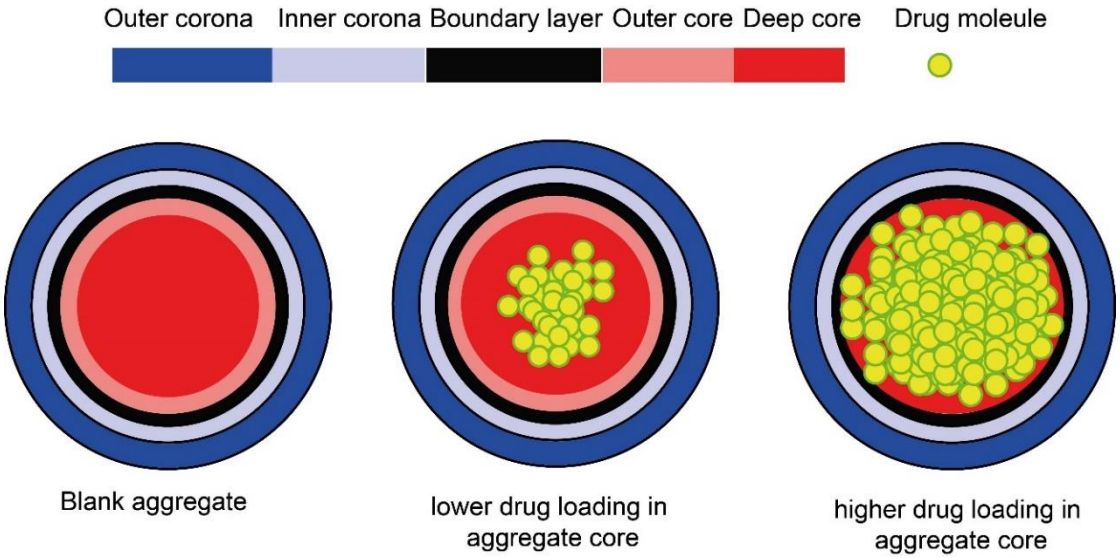


Figure 5.17: Effect of drug-loading on the aggregate structure. An absence of outer core region in aggregate with higher drug loading.

Long *et al*. provided evidence that aggregates can form very compact cores, which are completely dehydrated, although a peripheral portion of the core remains in contact with water.[16] Using Raman-multivariate curve resolution (MCR) analysis of aggregates formed from surfactants, they found peaks related to non-hydrogen bonding hydroxyl groups, which indicated that there was a small population of water in the core (core-corona interface).[16] The increase in the core compactness due to drug loading has also been observed in both simulations and experimental studies.[10,11]

The decay analysis of the PEG signal from the aggregate corona (as PCL signals were not visible), revealed the effect of the drug loading on the aggregate (**Figure 5.18**). For 20wt% Gp-loaded aggregates, *D* distribution is broad, to the 10 wt% Gp-loaded aggregate or blank aggregate. These results indicate the formation of a polydisperse aggregate system.

For the Ph-loaded aggregates at a higher loading (20 wt%), the PEG signal decay is slower, leading to a shift in the *D* distribution to lower value. Although it still remains narrow, this indicates the formation of larger, well-defined aggregates. The lower encapsulation efficiency of Ph at 20 wt% (~ 60%) (**Table 5.1**) suggests that the interaction between the PCL block and the Ph is weaker (as compared to Gp), which results in poor encapsulation efficiency. At a lower Ph loading of 10 wt% the encapsulation efficiency is higher, indicating the formation of smaller Ph clusters that are encapsulated in aggregates before it precipitates. Therefore, it can be rationalised that there is a certain limit of drug loading, which is dependent on the drug characteristics and drug-polymer interactions. From a thermodynamic point of view, drug-loaded aggregate formation is governed by solvent-solvent, solvent-drug, drug-polymer, drug-drug and polymer-polymer interactions.[14] At higher drug concentrations, drug-drug interactions might dominate over drug-polymer interactions, leading to the formation of large drug clusters that precipitate from solution and reduce the encapsulation efficiency.[12,17]

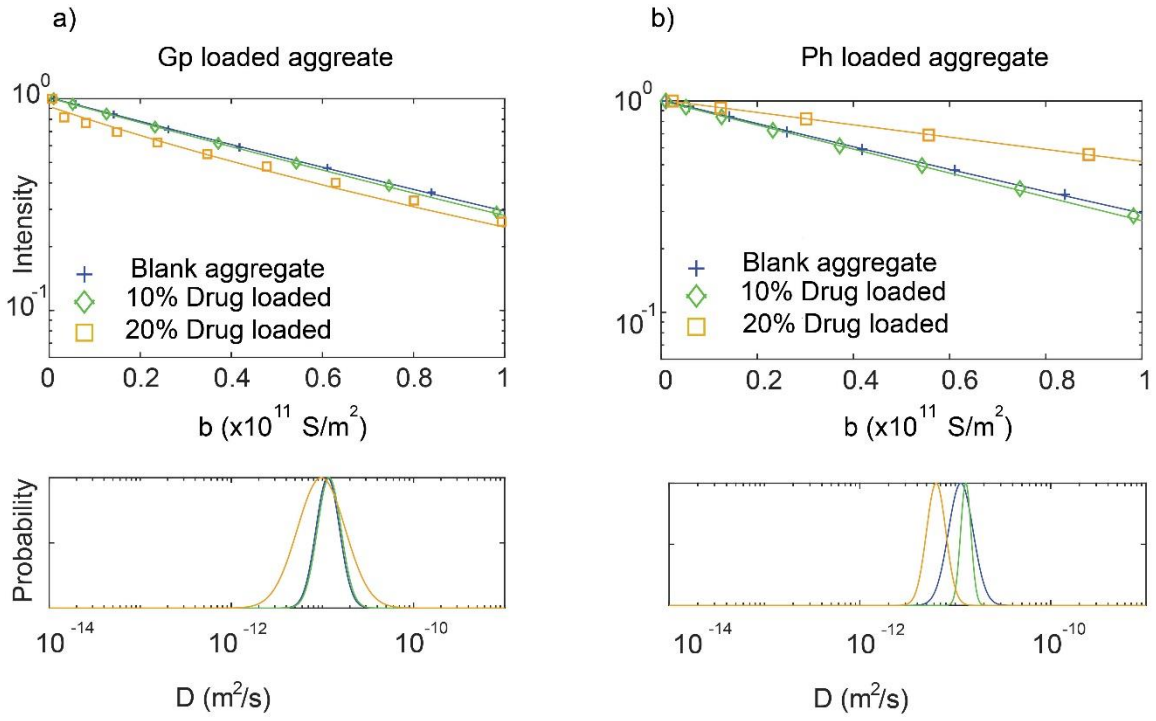


Figure 5.18: *D* distribution profiles determined by PGSTE NMR studies of the drug-loaded aggregates synthesised from $PEG_5CL_{9.4}$ with different drug loadings; a) GP-loaded aggregates, b) Ph-loaded aggregates.

DLS analysis of the 20 wt% drug-loaded aggregates supports the NMR spectroscopy results (**Figure 5.19**). For the 20 wt% Gp-loaded aggregates, a slight increase in the broadness of PSD intensity peak is observed, whereas the 20 wt% Ph-loaded aggregates display a clear increase in size with a shift of the PSD intensity peak. Thus, it would appear that the hydrophobicity of the drug and drug-polymer interactions play a crucial role in controlling drug loading.

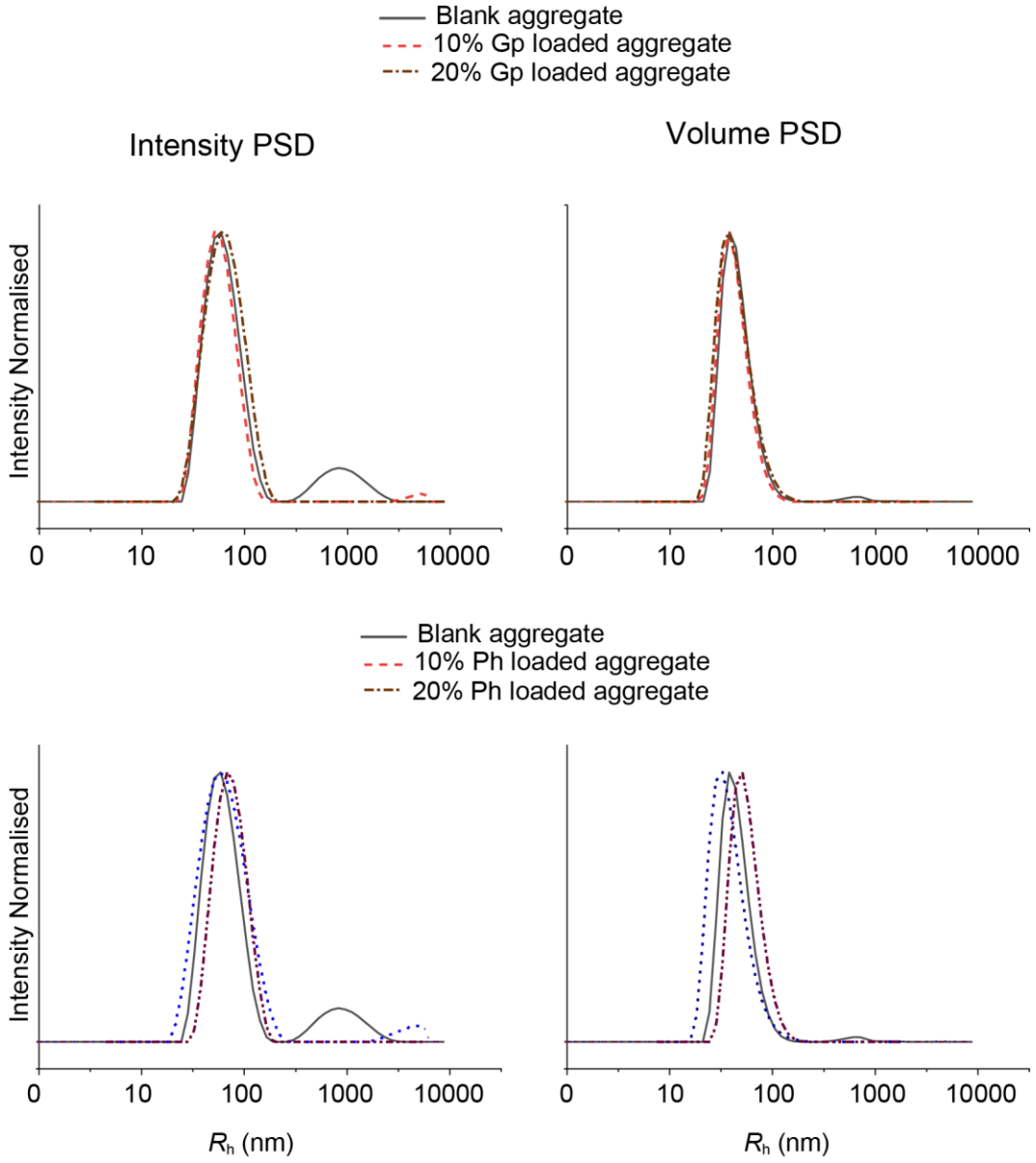


Figure 5.19: DLS analysis of blank and drug-loaded aggregate showing intensity and volume PSD, prepared using the $PEG_5PCL_{9.4}$ copolymer and drug-loadings of 10 and 20 wt%.

A mechanistic overview of drug-loaded aggregate formation

In this study, a solvent evaporation technique was used to prepare the aggregates. This technique involves dissolving the drug and polymer in an organic solvent (acetone), adding water, and then removing the organic solvent through gradual evaporation. The relative ratio between water and acetone marks different stages of drug-loaded aggregate formation. Therefore, when proposing the mechanistic pathways, four different compositions of acetone:water (3:5, 1:2, 1:4, and 1:100) were considered. In this study, two different mechanisms of drug-loaded aggregate formation have been proposed. First, let us consider the formation of drug-loaded aggregates from copolymers with a short PCL block, whereby the aggregation of the drugs would be expected to occur prior to the aggregation of the block copolymer (**Figure 5.20**).

In this scenario, a nucleation-type mechanism would be expected, with the drugs forming clusters (i.e. nuclei) onto which the copolymer adsorbs through weak interactions. At high acetone content (acetone:water 3:5), the copolymer and drug remain solvated. As acetone evaporates (e.g., acetone:water 1:2) the copolymer remains solvated. The critical aggregation concentration (CAC) (CAC is a specific concentration where a component of the system start aggregating) for the drug in that solvent mixture is surpassed, leading to drug aggregation and cluster formation. For the more polar Ph, it would resist cluster formation longer or might form a small cluster that poorly interacts with the PCL blocks due to its more polar nature. With a further decrease in the acetone (acetone:water 1:4), the CAC for the copolymer is also surpassed, and the PCL block of the polymer starts to interact with the previously formed Gp-drug clusters. For Ph, larger clusters are formed due to the weak interaction with the copolymer preventing stabilisation of cluster growth. Thus, differences in the CAC of the drugs and copolymer regulate the aggregation pathway.

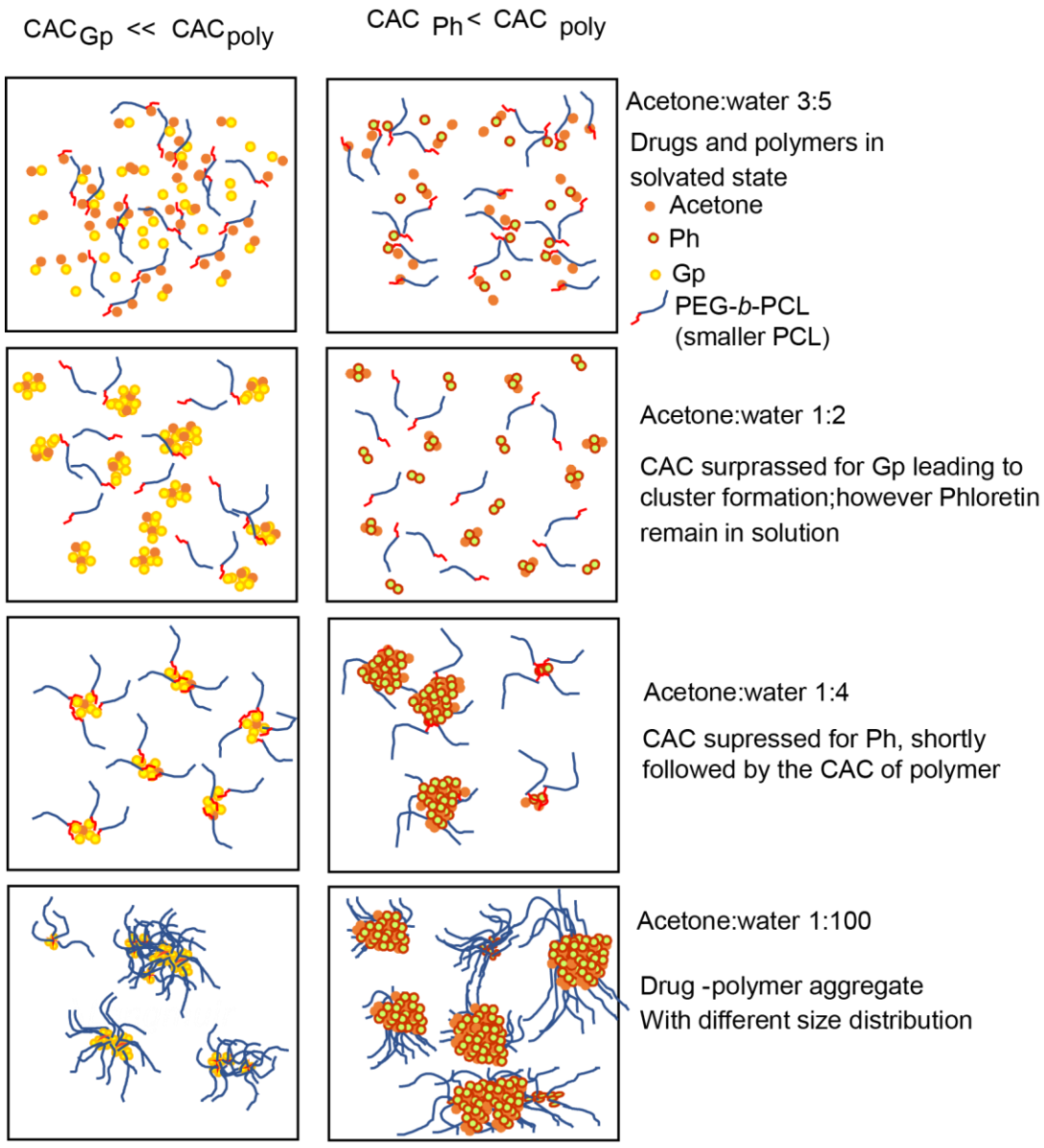


Figure 5.20: Proposed nucleation-type mechanism of aggregate formation at different acetone to water ratios. Water has been omitted for clarity.

As the PCL to PEG ratio increases, the CAC of the drug and polymer become more similar, which could lead to a coaggregation-type mechanism (**Figure 5.21**). In this mechanism, a decrease in acetone concentration causes the CAC of the drugs and polymer to be surpassed at approximately the same solvent composition, resulting in coaggregation and the formation of a dispersed drug-polymer core. It is also possible that the CAC of the drug may be affected by the CAC of the polymer (or vice-versa), particularly when there is competition for solvation by acetone.

For example, when the PCL block is large, a significant portion of the acetone may be involved in interactions with the PCL block, decreasing the effective concentration of acetone so that aggregation of the drug occurs sooner.

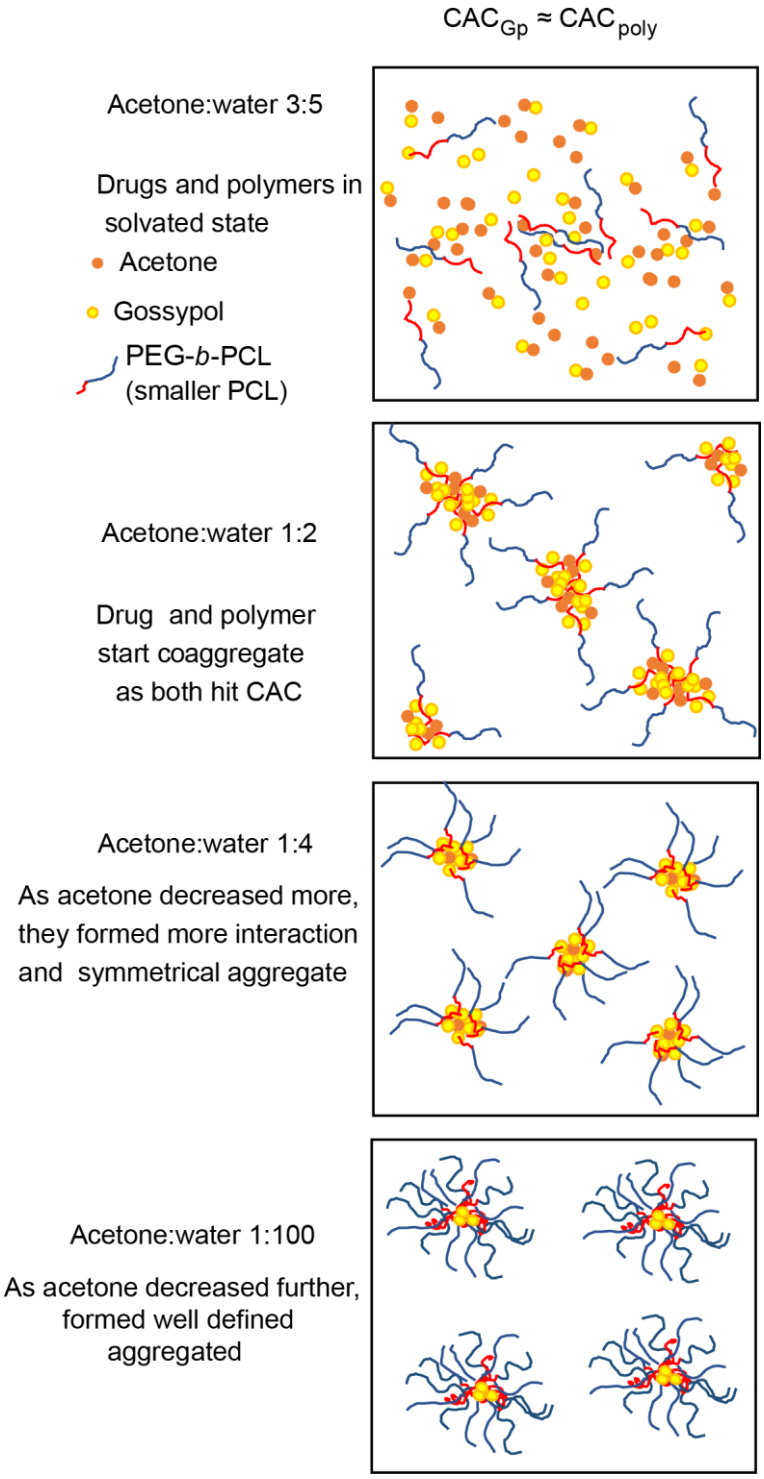


Figure 5.21: Proposed coaggregation-type mechanism of aggregation at different acetone to water ratios. Water has been omitted for clarity.

In addition, the reverse could also be true, whereby a hydrophobic drug has a stronger interaction with acetone that the copolymer, effectively decreasing the CAC of the polymer. For these scenarios, it can be hypothesised that there will be competition between the nucleation and coaggregation mechanisms (mixed model), with both occurring simultaneously (**Figure 5.22**).

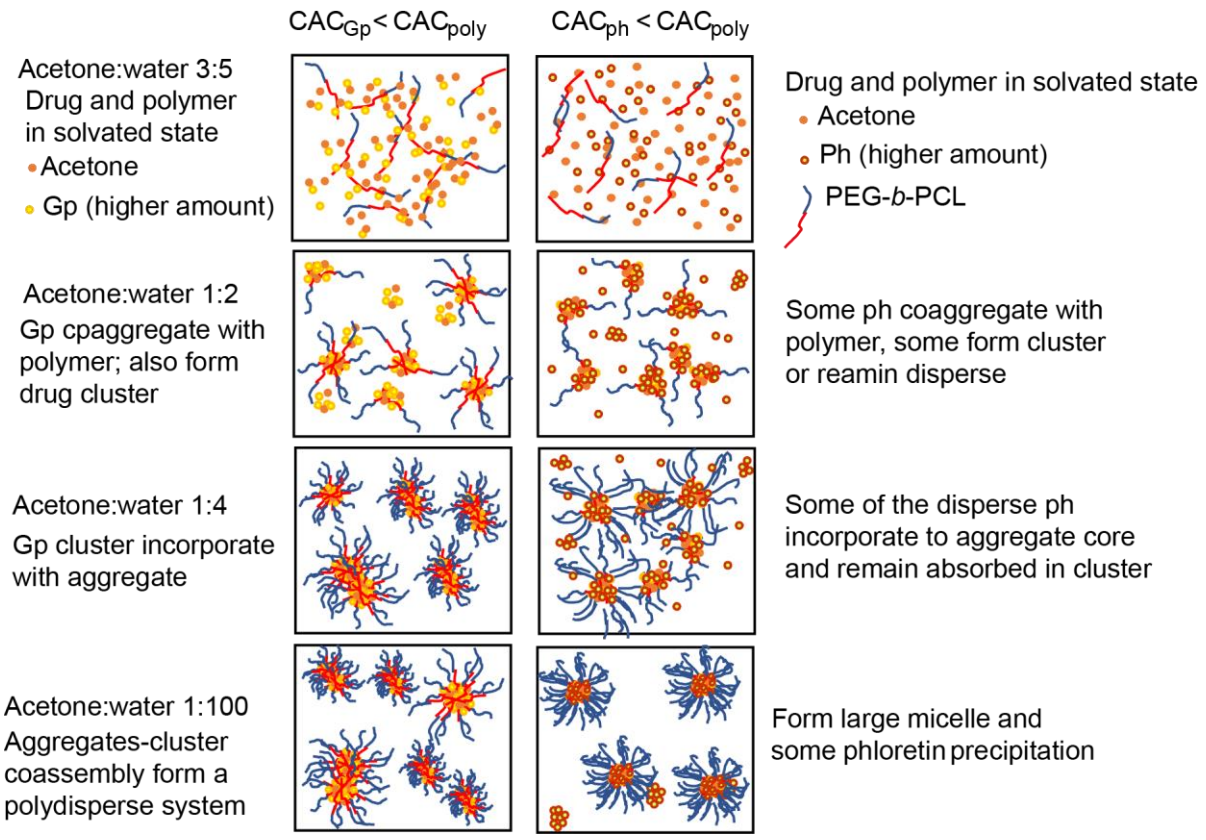


Figure 5.22: Mixed model of aggregate formation, at higher drug loading (20 wt%). Water molecules omitted for clarity.

This mixed model may help explain the behaviour observed at higher drug loadings for Gp. As the acetone is evaporated, the more hydrophobic Gp starts to form drug clusters, as well as drug-polymer aggregates (coaggregates) due to favourable interactions with PCL. Over time, the drug clusters act as nucleation sites for copolymer adsorption, or coaggregate with previously formed drug-polymer aggregates, leading to a more disperse range of aggregates responsible for the broad *D* distribution observed in the PGSTE NMR studies (**Figure 5.19**). In the case of the more polar Ph, some Ph might coaggregate with copolymer, some form clusters and some remain dispersed.

Over time, as the acetone is reduced, some of the dispersed drug molecules might add to the clusters, causing an increase in cluster size and precipitation from the solution. This explains the poor encapsulation efficacy at higher Ph loadings. Some portion of the dispersed drug might get incorporated into the coaggerates, which would cause an increase in aggregate size and explains the shift in the *D* distribution observed in the PGSTE NMR diffusion studies.

5.2 Conclusion

In this chapter, the underlying factors regulating aggregate formation in the presence of drug molecules have been explored using a combination of PGSTE NMR spectroscopy and DLS. As for blank aggregates, aggregate formation in the presence of drugs appears to be highly dependent on the size of the hydrophobic PCL component of the copolymer. At higher PCL to PEG molecular weight ratios, aggregation is favoured and polymer mediated, although it appears to be aided by the presence of drugs when the PCL to PEG molecular weight ratio is smaller. It can be hypothesised that this drug-polymer interaction leads to different aggregate formation mechanisms, which are consistent with previous simulation studies. At lower PCL content, aggregation occurs via nucleation of drug clusters, which is regulated by the hydrophobic characteristics of the drug. As the ratio increases, aggregation becomes more polymer driven, leading to a coaggregation mechanism. Furthermore, drug loading also plays a role in the formulation of aggregates and higher drug loadings may contribute to both mechanisms occurring simultaneously. The results also suggest that drug loading affects the internal structure of the aggregates. PGSTE NMR spectroscopy was used to probe the stability of the aggregate system, and that it provides complementary results to DLS. Nevertheless, further studies are required to fully understand the complex mechanisms at play during aggregate formation, and it is recommended that PGSTE NMR studies be conducted at various stages of the solvent evaporation technique to gain further insight into the processes at each step. In addition, the data collected in this study and hypotheses drawn are solely related to the PEG-*b*-PCL copolymer system and may not be applicable to other copolymer or polymer-drug systems. However, this study provides a general approach to analyse drug-loaded aggregate systems using PGSTE NMR studies. With further studies, it might be possible to generate a universal model of drug encapsulation in aggregate systems, which could provide guidance for the development of DDSs.

5.3 Experimental

5.3.1.Material

Acetone and ethanol (AR grade) were purchased from Chem-Supply. Deuterium oxide (D_2O, 99.9% deuterated) was purchased from Sigma-Aldrich. Gossypol (Gp) and phloretin (Ph) were purchased from Shaanxi Ciyuan Biotech Co., Ltd. All reagents were used as received.

5.3.2 Synthesis and characterisation of PEG-*b*-PCL copolymers

PEG-*b*-PCL was synthesised via ring-opening polymerisation of ε-caprolactone using methoxy PEG as the macroinitiator and stannous octoate as the catalyst at 120 °C. Details of the polymer synthesis, purification and characterisation are provided in **Chapter 2.**

5.3.3 Formulation of drug-loaded aggregates from PEG-*b*-PCL copolymers

Aggregates were synthesised using a solvent evaporation technique. Separately, the PEG-*b*-PCL polymer and the drug (Gp or Ph) were dissolved in acetone at a concentration of 1 mg/mL. The calculated volume of polymer and drug solution were then combined in a vial (4 mL) to give a total solution volume of 1 mL (**Table 5.2**). D_2O (1 mL) was then added dropwise and the vial was placed in a pre-heated dry-block heater at 60 °C. The solvent level was checked periodically and the vial was removed from the dry-block heater when the volume was ~1 mL (~ 4 h). The vial was then placed in a vacuum desiccator (0.1 mbar, 1 h) to remove the residual organic solvent and the volume was corrected, if necessary, by the addition of D_2O to give a total of 1 mL.

Table 5.2: Description of aggregate formulation used in the study.

Polymer	PCL:PEG	10% drug loading			20% drug loading		
		Polymer amount (mg)	Drug amount (mg)	Conc. (mg/mL)	Polymer amount (mg)	Drug amount (mg)	Total conc. (mg/mL)
$PEG_5PCL_{0.6}$	0.1:1	0.9	0.1	1	0.8	0.2	1
$PEG_5PCL_{2.3}$	0.5:1	0.9	0.1	1	0.8	0.2	1
$PEG_5PCL_{4.2}$	1:1	0.9	0.1	1	0.8	0.2	1
$PEG_5PCL_{9.4}$	2:1	0.9	0.1	1	0.8	0.2	1
$PEG_2PCL_{0.4}$	0.25:1	0.9	0.1	1	-	-	-
$PEG_{10}PCL_{10.7}$	1:1	0.9	0.1	1	-	-	-

5.3.4 Determination of drug loading efficiency in the polymeric aggregates

The aggregate solution (1 mL) was placed in a microcentrifuge tube (1.5 mL) and centrifuged for 30 min at 16000 rpm to sediment any precipitate; i.e., the free drug which was not encapsulated in the aggregates. The supernatant was collected carefully without disturbing the pelletised precipitate, the precipitate was dissolved in ethanol, and the amount of drug was quantified via UV-visible spectroscopy via appropriate calibration curves (Appendix 5.1). The drug loading efficiency was subsequently calculated by subtracting the amount of drug determined in the precipitate from the total drug used in the formulation. The drug loading efficiency was calculated using the following equation (5.1):

$$drug\ loading\ \text{efficiency}(\%) = \frac{Mass\ of\ drug\ in\ micelle}{Mass\ of\ drug\ used\ in\ formulation} \times 100 \qquad (\mathbf{5.1})$$

The supernatant solution used to determine aggregate properties using NMR spectroscopy and DLS.

5.3.5 Analysis of the drug-loaded aggregates using PGSTE NMR spectroscopy

PGSTE NMR spectroscopy experiments were performed on a 600 MHz Bruker Avance III HD spectrometer with PEG and PEG-*b*-PCL copolymer solutions (1 mg/mL, 500 µL) in D_2O, using standard 5 mm NMR tubes. The details are discussed in **Chapter 3.**

5.3.6 DLS analysis of the polymer of aggregates solution

The aggregate solutions were analysed using a Malvern Zetasizer, NANO ZS (Malvern Instruments Limited, U.K.) equipped with a 4 mW He–Ne laser operating at a wavelength of 633 nm. The sample were analysed at an angle of 173 ° using a quartz cuvette. All measurements were repeated three times in order to check their reproducibility.

5.4 References

1. Panyam, J.; Labhasetwar, V., Biodegradable nanoparticles for drug and gene delivery to cells and tissue. *Adv. Drug. Del. Rev.* **2003**, *55* (3), 329-347.

2. Allen, C.; Han, J.; Yu, Y.; Maysinger, D.; Eisenberg, A., Polycaprolactone-b-poly(ethylene oxide) copolymer micelles as a delivery vehicle for dihydrotestosterone. *J. Control. Release.***2000**, *63* (3), 275-286.

3. Jette, K. K.; Law, D.; Schmitt, E. A.; Kwon, G. S., Preparation and drug loading of poly(ethylene glycol)-block-poly(ε-caprolactone) micelles through the evaporation of a cosolvent azeotrope. *Pharm. Res.* **2004**, *21* (7), 1184-1191.

4. Shuai, X.; Ai, H.; Nasongkla, N.; Kim, S.; Gao, J., Micellar carriers based on block copolymers of poly(ε-caprolactone) and poly(ethylene glycol) for doxorubicin delivery. *J. Control. Release.***2004**, *98* (3), 415-426.

5. Aliabadi, H. M.; Elhasi, S.; Mahmud, A.; Gulamhusein, R.; Mahdipoor, P.; Lavasanifar, A., Encapsulation of hydrophobic drugs in polymeric micelles through co-solvent evaporation: The effect of solvent composition on micellar properties and drug loading. *Int. J. Pharm.* **2007**, *329* (1), 158-165.

6. National Center for Biotechnology Information. PubChem Database. Gossypol, CID=3503, https://pubchem.ncbi.nlm.nih.gov/compound/Gossypol (accessed on Mar. 28, 2019)

7. National Center for Biotechnology Information. PubChem Database. Phloretin, CID=4788, https://pubchem.ncbi.nlm.nih.gov/compound/Phloretin (accessed on Mar. 28, 2019)

8. Shuai, X.; Merdan, T.; Schaper, A. K.; Xi, F.; Kissel, T., Core-cross-linked polymeric micelles as paclitaxel carriers. *Bioconjug. Chem.* **2004**, *15* (3), 441-448.

9. Nusselder, J. J. H.; Engberts, J. B. F. N., A proton NMR study of the order and alkyl chain packing in the core of spherical micelles formed from 1-methyl-4-alkylpyridinium iodide surfactants. *J. Chem. Phys.* **1989**, *93* (16), 6142-6145.

10. Cheng, F.; Guan, X.; Cao, H.; Su, T.; Cao, J.; Chen, Y.; Cai, M.; He, B.; Gu, Z.; Luo, X., Characteristic of core materials in polymeric micelles effect on their micellar properties studied by experimental and dpd simulation methods. *Int. J. Pharm.* **2015**, *492* (1), 152-160.

11. Li, Q.; Yao, W.; Yu, X.; Zhang, B.; Dong, J.; Jin, Y., Drug-loaded pH-responsive polymeric micelles: Simulations and experiments of micelle formation, drug loading and drug release. *Colloid. Surface. B.* **2017**, *158*, 709-716.

12. Woodhead, J. L.; Hall, C. K., Simulation of micelle formation in the presence of solutes. *Langmuir* **2010**, *26* (19), 15135-15141.

13. Cui, W.; Li, J.; Decher, G., Self-assembled smart nanocarriers for targeted drug delivery. *Adv. Mater.* **2016**, *28* (6), 1302-1311.

14. Woodhead, J. L.; Hall, C. K., Encapsulation efficiency and micellar structure of solute-carrying block copolymer nanoparticles. *Macromolecules* **2011**, *44* (13), 5443-5451.

15. Zubkov, M.; Dennis, G. R.; Stait-Gardner, T.; Torres, A. M.; Willis, S. A.; Zheng, G.; Price, W. S., Physical characterisation using diffusion NMR spectroscopy. *Magn. Reson. Chem.* **2017**, *55* (5), 414-424.

16. Long, J. A.; Rankin, B. M.; Ben-Amotz, D., Micelle structure and hydrophobic hydration. *J. Am. Chem. Soc.* **2015**, *137* (33), 10809-10815.

17. Li, Z.; Hall, C. K., Parametric Studies of interaction strengths in polymer/CO_2 systems: Discontinuous molecular dynamics simulations. *Langmuir* **2005**, *21* (16), 7579-7587.

Chapter 6

Conclusions and Future work

Polymeric aggregates or micelles have great potential to provide the next generation of drug-delivery systems due to their ability to encapsulate hydrophobic therapeutics, leading to improved apparent drug solubility, longer circulation times and more targeted delivery. The formation of polymeric aggregates relies on the self-assembly of amphiphilic polymers, which in turn is controlled by the microstructural properties of the polymer (e.g., composition, sequence, molecular weight and architecture). Furthermore, the successful encapsulation of therapeutics and stability of aggregates relies on favourable polymer-drug interactions. Understanding the relationship between the polymer microstructure and the self-assembly behaviour of a polymeric aggregate in aqueous systems is, therefore, key to unlocking the full potential of polymeric drug delivery systems. Determination of the parameters that control polymeric aggregation and drug encapsulation will allow the establishment of design rules that could provide a more targeted approach to the formulation of polymeric drug delivery systems. Whilst much work has been conducted showing the potential benefits of polymeric aggregate for the delivery of drugs, there are still gaps in our understanding of the mechanisms of self-assembly and the parameters that govern aggregation of polymer, particularly in the presence of drugs.

In this body of work was aimed to provide a deeper understanding of aggregate formation from PEG-*b*-PCL block copolymers with different block lengths, and in particular, assess the potential suitability of new analytical tools approaches for this task, namely PGSRTE NMR spectroscopy. In this study, the effect of the polymer microstructure and drug encapsulation on the self-assembly process was investigated by studying the diffusion behaviour of the aggregate. This study has revealed information about the self-assembly behaviour and mechanism of PEG-*b*-PCL block copolymers. To achieve this goal, it was necessary to initially prepare a series of well-defined PEG-*b*-PCL copolymers so that there were no complicating factors caused by impurities.

PEG-*b*-PCL is a very well-studied polymer in polymeric drug delivery applications; however, in most cases, the polymers used have broad molecular weight distributions suggesting that they are not particularly well-defined in structure. Therefore, in **Chapter 2** the synthesis of PEG-*b*-PCL copolymers has been investigated. Using conventional ROP procedures reported

in much literature, PCL has been polymerised in the presence of PEG macroinitiators in anhydrous toluene and found that this approach only provides polymers with broad *Đ*, mainly due to transesterification side-reactions. To avoid this problem, ROP was conducted in bulk (solvent-free environment) and with a large excess of monomer, which provided access to PEG-*b*-PCL polymers with very narrow *Đ* (~1.02-1.12). Using this new approach, a series of PEG-*b*-PCL copolymers with different molecular weights and PCL:PEG ratios were synthesised. In addition, a precipitation technique has been developed based on the solubility of PEG and PCL in different solvents. A binary mixture of diethyl ether and ethyl acetate 30% (v/v) was found to effectively remove PCL impurities from the desired products.

Generally, the polymeric aggregate systems are analysed by scattering techniques (DLS or SAXS), however, in this study, PGSTE NMR spectroscopy was used and compared to scattering techniques to validate it's use as a novel approach to characterising polymeric aggregates. In **Chapter 3**, the diffusion behaviour of the micelles was studied by considering the self-diffusion coefficients (*D*) and their distribution patterns. From distribution analysis, it was evident that the PCL:PEG ratio greatly determines the dispersity of the aggregate system. Four different types of aggregate system have been identified within this study by analysing the *D* distribution and PDI values (DLS); unimer, unimer + aggregate, metastable and stable system. The polymer transforms from unimer to a stable aggregate system as PCL:PEG ratio increases. However, the molecular weight of PEG also plays a critical role in the aggregation behaviour of the system. As the molecular weight of PEG increases, aggregates become more stable, with a defined core and corona structure. The aggregate shape transforms from cylindrical to ellipsoid shape as PCL:PEG ratio increases in PEG_5PCL_y and $PEG_{10}PCL_y$ series. The shape also depends on PEG molecular weight as PEG_2PCL_y series forms mostly cylindrical aggregate but aggregates in $PEG_{10}PCL_y$ are ellipsoid in shape. Interestingly the core radius of the aggregate does not significantly change with alterations in the PCL:PEG ratio; hence, it was hypothesised that this could result from packing of PCL into the aggregate core.

Since polymeric aggregate can be considered as a nano-phase separated system with core and corona composed of different blocks, it was hypothesised that a phase-separated structure would affect the basic properties of the polymers, such as their thermal characteristics and crystallinity comparing to its homopolymer and bulk (non-aggregated polymer) form. The crystallinity of the core is also important for understanding drug encapsulation and release.

Therefore, in **Chapter 4**, the effects of aggregation on the polymer morphology and thermal characteristic have been investigated using DSC and WXRD. In addition, it was evident from a literature survey that a systemic study correlating PEG-*b*-PCL microstructure to thermal behaviour had not previously been conducted. As might be expected, covalent tethering between PEG and PCL significantly alters thermal characteristics (e.g., depression of melting point and crystallisation temperature) of the PEG and PCL blocks in bulk compared to that of the respective homopolymer. A significant melting point depression (≈ 10 °C) is observed in all PEG-*b*-PCL copolymers compared with the PEG homopolymer, which attributed to the imperfect crystal formation under the influence of PCL. The change in the DSC thermogram and depression of melting enthalpy also point towards imperfect crystal formation. In addition, the PCL:PEG ratio plays a critical role in the order of crystallisation. Temperature controlled WXRD analysis revealed that in the PEG_5PCL_y copolymers series as the PCL:PEG ratio increases, the PCL component dominates the crystallisation process. However, for the $PEG_{10}PCL_y$ copolymers series crystallisation is dominated by the PEG component even when the PCL block is very large.

The effect of aggregation does not significantly affect the melting temperature of PEG-*b*-PCL copolymers comparing to its non-aggregated form. However, the appearance of the DSC thermogram is different compared to its non-aggregated form. The appearance of melting peaks in the DSC thermograms indicated that the core of the aggregate is crystallised, and in some cases double melting peaks were observed, which indicates different foldings and lamella thickness in the polymer crystallites. However, without further investigation, it is difficult to comments which block crystallised in the aggregate. Although in **Chapter 3**, the SAXS analysis does not represent any crystalline behaviour of the aggregate core. So it can be concluded that the crystallisation occurs during the freeze-drying process. It could be an interesting topic to be persued to understand how lyophilisation changes the aggregate crystallinity and its rehydration in water.

Self-assembly of polymer is a complex process; however, in the presence of drug molecules, it becomes even more complicated. In the literature, the fundamental interpretation of drug-loaded polymeric aggregate systems is not well studied. Therefore, in **Chapter 5**, the relationship between polymer microstructure and drug characteristics has been explored in regulating the aggregation process. In this body of work, PGSTE NMR spectroscopy has been used to probe the structure of the polymeric aggregate, which provided compelling evidence that this technique could be useful for the analysis of the aggregate structure.

NMR spectroscopy shows PCL characteristic proton peak, which confirms some portion of the core is penetrable to water, which supports the prediction of the boundary layer in the aggregate. Interestingly as drug loading content increased from 10 to 20%; the PCL characteristic peak become weak, this indicates the change of core characteristic (packing of PCL in the core) due to interaction between PCL and the drug. This nature of drug-loaded aggregate has never been reported before. The *D* distribution of PEG and PCL has been investigated to probe the effect of polymer microstructure and drug interaction. At PCL:PEG ratio < 1:1, the aggregate system shows a broad *D* distribution, which indicates a disperse nature of the system; this could be unfavourable interaction between PCL and drug, due to short PCL chain. As the ratio increases, the *D* distribution narrowed, which ensures the formation of stable aggregates. It was hypothesised that self-assembly of polymer in the presence of drug follows three pathways. Firstly, the nucleation pathway, where the drug acts as a nucleus of aggregation; this happens when PCL:PEG ratio is low as a result of poor PCL-drug interaction which leads to the formation of drug clusters which act as the nucleus of aggregation. Secondly, the coaggregation pathway, wherein, as PCL ratio increases (>1), drug-polymer interactions are favoured, resulting in coaggregation leading to polymeric aggregation that is regulated by the PCL self-assembly. The narrow *D* distribution (NMR) and lower PDI value (DLS) supports this hypothesis. Thirdly, the mixed mechanism pathway, wherein aggregation in the presence of higher drug content occurs through a combination of nucleation and coaggregation; This is resultant of high drug concentration facilitating drug-drug interactions which lead to the formation of a drug composite nucleus. It should be noted, however, that in this instance a portion of the drug also coaggregates with the polymer. This is a characteristic of a disperse system, the broad distribution of PEG *D* at 20% gossypol loading supported the presence of a disperse system resulting from the mixed mechanism pathway.

In this study, the fundamental aspects of the PEG-*b*-PCL block copolymer and its self-assembly system have been investigated. Yet through this work several questions have been identified that will require further investigation in further studies. For instance, although PEG-*b*-PCL is a well-studied polymer; there is a lack of synthetic procedures for the synthesis of well-defined PEG-*b*-PCL polymers of narrow *Đ* in high purity. In this study a technique has been proposed; however, copolymers have been synthesised with a moderate length of PCL, which needs to be tested to see if it can be used to efficiently synthesise higher molecular weight PCL. Polymeric aggregate systems are prominent candidates for the next generation of drug delivery system, but more attention should be given to investigating their fundamental properties.

In this study, the effect of polymer microstructure and drug type on self-assembly has been investigated, but there are other factors such as the method of preparation (e.g., solvent evaporation, dialysis), polymer concentration, and the selection of organic solvent that likely also affect the self-assembly process, and should be explored in future studies.

A new perspective on the analysis of polymeric aggregate in solution has been introduced by conducting in-depth PGSTE NMR spectroscopy experiments. However, there are many aspects yet to be addressed, particularly the reason for and origin of characteristic the PCL peaks which were observed within the core of PEG-*b*-PCL aggregate. In addition, the effect of drug nature on the self-assembly of polymer is not well studied. This study investigated what effect the hydrophobic nature of drug has on polymer aggregation. Further work may be directed toward evaluating other drug-related factors which impact the self-assembly of the polymer. For example, the structure of the drug likely impacts drug-polymer interactions, which is a key regulator of the self-assembly process. In addition, the stability of drug delivery systems plays a vital role in the real-life application of these systems. Within this work, an investigation of the thermal characteristics of the polymeric aggregate as a lyophilised powder was conducted and could provide grounds for exploring the nature and stability of aggregate as lyophilised powders in more detail. This could also be related to dispersibility and long term stability of these systems. Polymeric drug delivery systems have the potential to provide much needed drug delivery solutions; however, in conclusion, more systematic studies are required to further elucidate the fundamental aspect which underpins the behaviour and structural attributes of these systems.

Appendices

Chapter 3

Fitting parameters from the SASView models of the recorded SAXS data for the self-assembled PEG_2PCL_y block copolymers series in water

a) $PEG_2PCL_{0.4}$ (PCL:PEG 0.2:1) copolymer aggregate

Model = power law + monGussiCoil

Parameters:
scale = $2.754 \times 10^{-6} \pm 1.611 \times 10^{-7}$
background = 0.0003 (fixed)
power law = 2.37 ± 0.26
i zero = 0.463 ± 0.33
R_g = 269.1 ± 34.63 Å
χ^2/N = 0.334

b) $PEG_2PCL_{1.1}$ (PCL:PEG 0.5:1) copolymer aggregate

Model = power law + cylinder

Parameters:
scale = 0.0032 (fixed)
power law = 3.1 (fixed)
background = 0.001 (fixed)
sld = 9 (fixed)
sld solvent = 9.47 (fixed)
radius = 47.203 ± 0.246 Å
length = 440.23 ± 20.04 Å
χ^2/N = 0.21406

c) $PEG_2PCL_{1.8}$ (PCL:PEG 0.9:1) copolymer aggregate

Model = flexible cylinder
Parameters:
scale = 1.0885 (fixed)
background = 0.001 (fixed)
sld = 9.35 (fixed)
sld solvent = 9.4
radius =71.5 ± 0.11 Å
Kuhn length = 499.89 Å (fixed)
length = 10000 Å (fixed)
polydispersity = radius (0.2) (fixed)
χ^2/N = 1.1488

d) $PEG_2PCL_{3.9}$ (PCL:PEG 2:1) copolymer aggregate

Model = power law + cylinder
Parameters:
scale = 0.054833 (fixed)
background = 0.001 (fixed)
sld = 9.33 (fixed)
sld solvent = 9.4 (fixed)
radius =64.58 ± 0.152 Å
length = 11087 Å (fixed)
χ^2/N = 0.27473

Fitting parameters from the SASView models of the recorded SAXS data for the self-assembled PEG_5PCL_y block copolymers series in water

a) $PEG_5PCL_{0.6}$ (PCL:PEG 0.1:1) copolymer aggregate

Model = power law + gel fit

Parameters:

scale = 1.29×10^{-6} (fixed)
background = 0.001 (fixed)
power law = 2.5382 ± 0.13799
Guninier scale = 0.684 (fixed)
Lorentz Scale = 0.0364 (fixed)
Fractal dimension = 3.6577 ± 0.5802
R_g = 433.33 ± 16.39 Å
Core length = 36.341 Å
χ^2/N = 0.2240

b) $PEG_5PCL_{1.3}$ (PCL:PEG 0.25:1) copolymer aggregate

Model = power law + cylinder

Parameters:

scale = 8×10^{-4} (fixed)
background = 0.001 (fixed)
sld = 9.4 (fixed)
sld solvent = 9.47 (fixed)
radius =59.74 ± 0.1235 Å
length = 315.35 Å (fixed)
χ^2/N = 0.28046

c) $PEG_5PCL_{2.4}$ (PCL:PEG 0.5:1) copolymer aggregate

Model = cylinder

Parameters:
scale = 3×10^{-4} (fixed)
background = 0.002 (fixed)
sld = 11 (fixed)
sld solvent = 9.4 (fixed)
radius = 64.61 ± 0.3743 Å
length = 982.43 Å (fixed)
$\chi^2/N = 0.419$

d) $PEG_5PCL_{4.2}$(PCL:PEG 1:1) copolymer aggregate

Model = power law + ellipsoid

Parameters:
scale = 0.890 ± 0.02693
background = 0.001 (fixed)
power law = 2.95 (fixed)
sld = 9.4 (fixed)
sld solvent = 9.4 (fixed)
radius equatorial =125.54 ± 1.00Å
radius polar = 65.96 ± 1.30 Å
$\chi^2/N = 0.20307$

e) $PEG_5PCL_{9.4}$ (PCL:PEG 1:1) copolymer aggregate

Model = power law + ellipsoid

Parameters:
scale = 1.33 ±0.0069
background = 0.002
power law = 2.7
sld = 9.38
sld solvent = 9.4
radius equatorial = 186.7 ± 1.57 Å
radius polar = 87.624 ± 0.9225 Å
$\chi^2/N = 0.21201$

Fitting parameters from the SASView models of the recorded SAXS data for the self-assembled $PEG_{10}PCL_y$ block copolymers series in water

a) $PEG_{10}PCL_{3.1}$ (PCL:PEG 0.3:1) copolymer aggregate

Model = get fit

Parameters:

scale = 1.51 (fixed)

background = 0.001 (fixed)

Guninier scale = 32.186 ± 3.06

Lorentz Scale = 4.552 ± 0.1343

Fractal dimension = 2.6895 ± 0.013524

R_g = 904.95 ± 18.24 Å

Core length = 189.34 ± 3.8683 Å

χ^2/N = 0.6532

b) $PEG_{10}PCL_{7.8}$ (PCL:PEG 0.8:1) copolymer aggregate

Model = power law + cylinder

Parameters:

scale = 0.4966 ± 0.0075

background = 0.001 (fixed)

power law = 2.13 ± 0.0057

sld = 9.4 (fixed)

sld solvent = 9.4 (fixed)

radius = 93.918 ± 0.84513 Å

length = 349.8 Å (fixed)

χ^2/N = 0.5663

c) $PEG_{10}PCL_{10.7}$ (PCL:PEG 1:1) copolymer aggregate

Model = ellipsoid

Parameters:

scale = 4.6 (fixed)

background = 0.002 (fixed)

power sld = 9.38 (fixed)

sld solvent = 9.4 (fixed)

radius equatorial = 219.65 ± 2.06 Å

radius polar = 62.939 ± .6041 Å.

$\chi^2/N = 0.30475$

d) $PEG_{10}PCL_{14.7}$ (PCL:PEG 1.5:1) copolymer aggregate

Model = power law + ellipsoid

Parameters:

scale = 0.387 ± 0.00305

background = 0.001 (fixed)

power law = 3.6 ± 0.02304

sld = 9.38 (fixed)

sld solvent = 9.4 (fixed)

radius equatorial = 138.4 ± 1.63210Å

radius polar = 63.40 ± 0.97108 Å

$\chi^2/N = 0.21201$

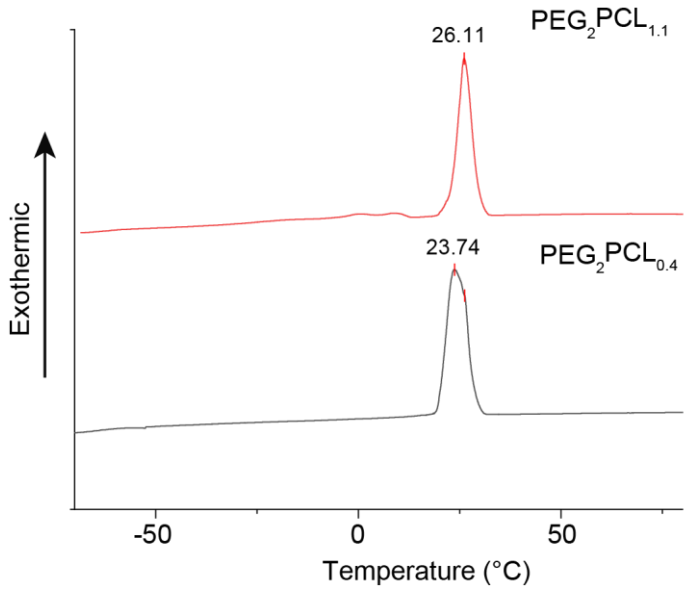


Figure A.4.1: DSC crystallization curve of polymer from $PEG_2PCL_{0.4}$ and $PEG_2PCL_{1.1}$ after the first heating cycle. The absence of a second melting peak confirms the presence of single-crystal species in the copolymer.

The standard curve of gossypol and phloretin used for quantification of drug encapsulated in the aggregates. The stock drug solution was made at a concentration of 1 mg/mL in ethanol. The stock was diluted to appropriate concentrations and then the UV-visable spectra were collected to calculated standard curves (**Figure A 5.1**).

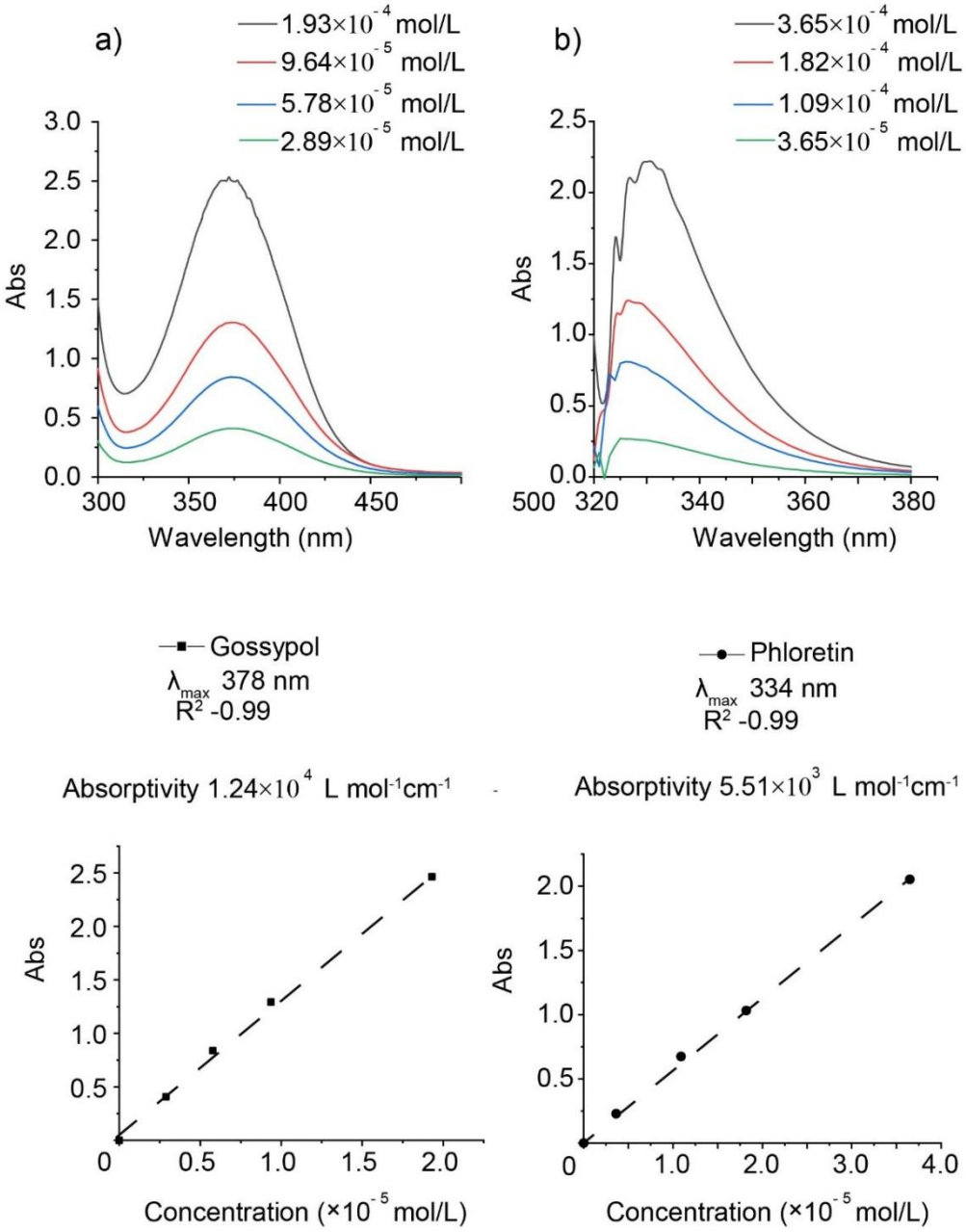


Figure A5.1: UV-visible spectra and standard curves for a) gossypol and b) phloretin in ethanol.

The drug amount was calculated from the equation provided from the standard curves. An example of the calculations is provided in **Table A5.1**.

Table A 5.1: Drug loading efficiency calculation from Uv-spectrometry

Polymer	**Drug loading (%)**	**Drug amount (mg)**	**Uv-Abs**		**Drug in precipitation (mg)**		**Drug in micelle (mg)**		**Drug loading efficacy**		**Average Drug loading efficacy**
			Sample1	Sample 2	Sample1	Sample 2	Sample1	Sample 2	Sample1	Sample 2	
$PEG_5PCL_{0.6}$	10%	0.103	0.476	0.419	0.013	0.016	0.086	0.089	84.18	86.48	85.33 ± 1.15
$PEG_5PCL_{2.3}$	10%		0.264	0.224	0.007	0.005	0.095	0.097	92.79	94.39	93.59 ± 0.8
$PEG_5PCL_{4.2}$	10%		0.195	0.193	0.004	0.004	0.098	0.098	95.56	95.64	95.6 ± 0.04
$PEG_5PCL_{9.4}$	10%		0.271	0.265	0.007	0.007	0.095	0.095	92.49	92.71	92.6 ± 0.11